Evaluation of Cellulosic Materials for the Enzymatic Production of Bioplastics

Calum C.J. Birch

Submitted in accordance with the requirements for the degree of Doctor of Philosophy

School of Chemical and Process Engineering

May 2021

The candidate confirms that work submitted in his/her own, except where work has formed part of jointly-authored publications has been included. The contribution of the candidate and other authors to this work has been explicitly indicated below. The candidate confirms that appropriate credit has been given within the thesis where reference has been made to the work of others.

This copy has been supplied on the understanding that is its copyright material and no quotation from the thesis may be published without proper acknowledgement.

© 2021 The University of Leeds and Calum C.J. Birch

“You’re only young once, but you can be immature forever”

Germaine Greer

Acknowledgments

I would firstly like to thank my supervisor John Blacker for the opportunity to work on such an exciting and multidisciplinary project. Although I found difficulty in understanding the complex chemical engineering and biochemistry, John was always available, with a profound patience and depth of knowledge. Irrespective of results John continued to push me, helping me strive for excellence when I could not see it. I would also like to thank my co-supervisor Andrew Ross, whose biochemical and life-cycle assessment knowledge proved invaluable throughout the project. A special thanks also to Nikil Kapur, who provided throughout my fourth chapter. I would like to thank all the people I had the pleasure of collaborating with throughout this project. The team at Biome (Krisztina, Paul, Paul and Pierre) who assisted me in my first two years. The academics at the University of Liverpool (Andrew and Chris) who made me feel welcome and taught me the basics of microbiology during my one-month placement. The Bioenergy CDT for giving me this wonderful opportunity. Mark Howard for his NMR expertise.

All present and past members of the iPRD, especially Alistair Baker who always made time to give me feedback and advice. Everyone else in the lab who made my days in the basement brighter than the sun ever could: Mary, Adam, Chris, Connor, Micaela, Alvaro, Luke, Brendan, Ricardo, Jamie, Ollie, Becky, Ilias, Matt, Sarah, Tom, Rosie, Sam, Alison, Nisha.

Thank you to all the members of Leeds Dancesport for providing me with an assortment of brilliant distractions (Richard, Alice, Natalie, Imogen, Matt and Sarah). You guys made my time at Leeds my most memorable and I am forever grateful. Thank you to all my online friends, who were always up for an adventure (Kienan, John, Alex, Tiff, Dave, Jack and Nathan). Thank you to all my family (Linda, Ashley and Kai), your continued support helped me more than you know. I love you all dearly. A final thanks to food, without its delicious qualities' life wouldn't be the same.

Abstract

There is an increasing awareness of the benefits that continuous flow processes provide for the synthesis of platform chemicals, using the biorefinery approach. Continuous flow bio-oxidations offer advantages over traditional chemical batch oxidations through faster rates, higher selectivity, green oxidants and cascade reactions. This thesis explores different methods for continuous flow bio-oxidation of hydroxymethylfurfural (HMF) a sugar-derived building block that has potential use in bioplastics. To evidence improved sustainability, life-cycle analysis (LCA) techniques that look at the impact of production on the environment are essential in determining whether the new processes will be beneficial in the long-term.

The objectives of this thesis were: to improve upon existing bio-oxidative techniques and then apply them to continuous flow to further bridge the gap between academic and industrial research. This includes: introducing continuous oxidations for furan-based intermediates; developing reactors for foam production and transport of solid particulate; and analysing the techniques for their environmental impact. To establish a green route for the synthesis of FDCA from HMF, a variety of green oxidisers were tested. CAL-B lipase gave the highest yield and was developed further into a continuous flow bio-oxidation. Production of the precursor DFF in continuous flow required resolving common solubility issues. Protein-stabilised aqueous foams were able to transport insoluble particulate out of a reactor, whilst air could generate the foam and simultaneously supply the oxidation. To determine the feasibility of each developed process, a life-cycle assessment was conducted. A cradle-to-gate approach was used and compared to both a platinum catalysed synthesis of FDCA and petroleum derived terephthalic acid. Although the environmental impacts for the two FDCA processes are similar, significant improvement is needed to compete with the petroleum industry. The liquid foam reactor looks promising for up-scaling production but requires further evaluation of the DFF to FDCA setup before a full telescoped process can be developed.

Table of Contents

List of Figures

List of Tables

List of Abbreviations

1HPDCA	1H-pyrrole-2,5-dicarboxylic acid
ACR	Agitate cell reactor
AcOH	Acetic acid
AcOOH	Peroxyacetic acid
AMF	5-acetoxymethylfurfural
AP	Acidification potential
Aq	Aqueous
Asp	Aspartate
AU	Units per milligram of protein
BPR	Back pressure regulator
BMF	5-butoxymethylfurfural
BsPAD	*Bacillus subtillis* enzyme
CAL-B	*Candida antarctica* Lipase B
$CDCl_3$	Deuterated chloroform
CFE	Cell-free extract
CFC	Chloroflurocarbons
cm	Centimetre
CO_2	Carbon dioxide
COD	Chemical oxygen demand
CSTR	Continuous stirred tank reactor
CTA	Carbon transfer agent
d	Doublet
DABCO	1,4-diazabicyclo[2,2,2]octane
DCM	Dichloromethane
DEHU	4-dehoxy-L-erythor-5-hexoseulose urinate
DES	Deep eutectic solvent
DE	Deutschland (Germany)
DFF	Diformylfuran
DHG	2-dehydro-3-deoxy gluconate

DOC	Dissolved organic carbon
DMF	Dimethylformamide
DMSO-d^6	Deuterated dimethyl sulfoxide
EMF	5-ethoxymethylfurfural
EP	Eutrophication potential
Equiv	Equivalents
Et	Ethyl
EtOAc	Ethyl acetate
EtOH	Ethanol
EU-28	Europe's 28 member countries
FAD/FADH	Flavin adenine dinucleotide
FAME	Fatty-acid methyl esters
FD	Fossil depletion
FDCA	2,5-furandicarboxylic acid
FFCA	2-formyl-5-furancarboxylic acid
g	Gram
$GOase_{M3-5}$	Galactose oxidase M_{3-5} mutant
GHG	Greenhouse gases
GWP	Global warming potential
HDPE	High-density polyethylene
HFCS	High fructose corn syrup
HCFC	Hydrochlorofluorocarbons
His	Histidine
HMF	5-hydroxymethyfurfural
HmfH	5-hydroxymethfyfurfural oxidase
HMFCA	5-hydroxymethyl-2-furancarboxylic acid
HPLC	High performance liquid chromatography
HRP	Horseradish peroxidase
hrs	Hours
HT	High temperature
Hz	Hertz

ID	Inner diameter
IGEPAL-CA720	Polyoxyethylene-(12)-isooctylphenyl ether
IR	Infrared
IS	Internal Standard
ISO	International organisation for standardisation
J	Coupling constant
k	Rate constant
Kg	Kilogram
K_M	Michaelis-Menton constant
Kpi	Potassium phosphate
KWh	Kilowatt hours
L	Litre
LCA	Life-cycle assessment
LCIA	Life cycle inventory analysis
LCI	Life cycle inventory
LLE	Liquid-liquid extraction
m	Metre or multiplet
mCPBA	Meta-chloroperoxybenzoic acid
Me	Methyl
MeCN	Acetonitrile
MFDCA	2,5-furandicarboxylate salt
MFR	Mixed-flow reactor
mg	Milligram
min	Minute
MJ	Megajoules
mL	Millilitre
mm	Millimetre
mM	Millimolar
MMF	Methoxymethfylfurfural
mmol	Millimoles
mol	Moles

MPa	Mega pascals
MPIR	Multi-point injection reactor
n	Number of moles or repeating units
NMP	N-methyl-2-pyrrolodone
NMR	Nuclear magnetic resonance
ODP	Ozone depletion potential
Org	Organic
OVAT	One variable-at-a-time
Oxone™	Potassium peroxymonosulfate
P	Pressure
PaoABC	Periplasmic aldehyde oxidoreductase
PAT	Process analytical technologies
PEF	Polyethylene furanoate
PET	Polyethylene terephthalate
PD/C	Palladium on carbon catalyst
PFR	Plug-flow reactor
Ph	Phenyl
PLA	Polylactic acid
PS	Polystyrene
PSi	Pounds per square inch
PTFE	Polytetrafluoroethylene
Pt/C	Platinum on carbon catalyst
PTC	Phase-transfer catalyst (Q^+)
RBF	Round-bottomed flask
RER	Rest of Europe region
RHL	*Rhizomucor miehei* lipase
RoW	Rest-of-world
rpm	Revolutions per minute
RTD	Residence time distribution
Rv	Reactor volume
s	Second or singlet

SDBS	Sodium dodecylbenzene sulfonate
Ser	Serine
SM	Starting material
SPAN 80	Sorbitane monooleate
T	Temperature
t	Triplet
t-BuOH	Tert-butanol
TFA	Trifluoroacetic acid
THF	Tetrahydrofuran
T_g	Glass transition temperature
T_m	Melt temperature
TMP	Trimethylphosphate
TOC	Total organic carbon
TON	Turnover number
t_{res}	Residence time
TWEEN 80	Polyethylene glycol sorbitane monooleate
UHP	Urea-hydrogen peroxide
UPR	Unit process requirement
UV-Vis	Ultra-violet visible
$U.L^{-1}$	Enzyme activity
V	Volume
WARF	Wisconsin Alumni Research Foundation
[*E*]	Enzyme
[*ES*]	Enzyme-substrate transition state
[*P*]	Product
[*S*]	Substrate
µL	Microlitre
µM	Micromolar
v	Volumetric flow rate

Chapter 1 - Introduction

Our planet's population is continually growing with mankind's expansion seemingly infinite; the majority of resources on the planet however are finite. With the population set to increase to 9.8 billion by 2050, a 31% increase from today's 7.5 billion population, establishing a greener society for the next generation is essential.[1] Energy, food and materials are of primary importance, with populations demanding more each year as nations develop, resulting in an exponential growth of CO_2 emissions. Global warming has already reached a critical stage, with many experts believing we are past the "point of no return". The human race must adapt to the planet's changing environment, preventing the onset of mass natural disasters.

Recent trends in scientific and industrial research have moved towards the development of sustainable alternatives for energy, resources and power production.[2] As the world's fossil fuels reserves are continually depleted, oil prices rise, unfortunately crude oil is the source of most commercially available chemicals. Although the supply of food is of the utmost importance, there are other areas of modern society that require the development of renewable alternatives. Modern day plastics are derived from petroleum; a main by-product of oil refineries. Green alternative chemicals vary dependent upon their application, from intermediary drug chemicals, to renewable polymers and pesticides.[3]

All products rely on a source of aromatic compounds from crude oil, an unsustainable source that will eventually run out. Nature provides one known sustainable source of aromatics; lignocellulose, through the utilisation of lignin and cellulose; the breakdown of which can be used to produce platform chemicals. Polymers such as polyethylene terephthalate (PET) have been targeted first due to their high volumes of production, with corporations like Coca Cola attempting to produce a renewable plastic bottle.[4] Successful substitution for a sustainable polymer requires the acquisition of renewable feedstock monomers.

Production of intermediary and platform chemicals from biological sources requires harsh conditions, solvents and expensive catalysts. Biological approaches are now being adopted and developed as a greener technique.[5] Enzymes have long been used in biochemistry, particularly fermentation, to produce vast quantities of a product with little environmental impact; aside from the CO_2 produced. However, initial industrial adoption of enzymes is slow, requiring the artificial optimisation of wild-type enzymes.[6] For the process to be economically viable, allowing it to compete with PET, production of platform chemicals must be improved.

Renewably produced polymers aren't the only interest, with biodegradable plastics set to take a substantial portion of the market. A staggering 79% of all plastic produced ends up in landfill or the ocean, with roughly 5-13 million tonnes of plastic entering the ocean each year. This extreme level of global pollution has seen the shift in research interest to naturally degrading polymers, some from natural resources, others petroleum sourced.

The American Department of Energy listed its "Top 10" high-value added chemicals in the coming years, of note are 5-hydroxymethylfurfural (HMF) and 2,5-furandicarboxylic acid (FDCA).[7] FDCA has notable interest as a monomer, replacing terephthalic acid in the ever growing PET polymerisation industry, set to be worth $60billion by the end of the year.[8–10] The aliphatic nature of FDCA is the centre furan ring, this can be substituted with a pyrrole ring for potentially interesting innovations; the possibility of biodegradation.

FDCA based polymer blends can be manufactured to provide some biodegradation but only in specific environments.[8–10] The properties however have distinct improvements over their petroleum-based counterparts. Avantium is currently the main producer of HMF, sold as both a crude liquid (88%) and pure solid (99%). [11] HMF is manufactured from the dehydrogenation of lignocellulose derived fructose and glucose.

1.1 Process Chemistry

Continuous flow chemistry has been hailed as a suitable approach to increasing throughput whilst decreasing cost. Nonetheless development surrounding the combination of enzymes in flow is limited; a major issue requires the catalyst (enzyme) to be immobilised onto a surface, rather than separation and recycling. Without immobilisation the enzyme is free in solution and must be separated out from the product. As with most chemical processes, separation and purification can dramatically increase the cost and time of manufacture.

Flow reactions can further be applied to polymerisations, a process that has long been undertaken in batch settings. Polymerisation in flow poses extensive problems, with the majority of reactions forming a solid as a product, the biphasic mixture can necessitate complex machinery to complete. They do offer a high degree of control for temperature and mixing, granting a highly reproducible and pure product. Successful optimisation of the process provides a platform for the economically viable production of a bio-based and biodegradable polymer. For the procedure to be competitive with PET, the process must be both intense and efficient, a difficult task with an aqueous processing medium. Production and replacement of which would help low carbon emissions and provide a biodegradable alternative, that can lower the impact form landfill and plastic pollution.

1.2 FDCA: A Platform Chemical

FDCA is furan derivative containing two carboxylic acid groups at the 2 and 5 positions on the ring. It has been identified as a key intermediate for numerous pharmaceuticals and a precursor for polyethylene furanoate (PEF); a bio renewable alternative to polyethylene terephthalate (PET). Current synthetic routes for FDCA use harsh solvent conditions, metal catalysts and slow reaction rates, suffering from relying on oxygen mass transfer in solution.

HMF is typically used as the starting material, derived from the dehydration of fructose, it acts as renewable feedstock, enabling a shift away from petrochemical sources. Metal catalysis has dominated the research and patents developed for conversion of HMF, many focusing around variations of the commercially available Pt/C catalysts.

Oxygen is the oxidant with a weak base or simply water as the solvent, with temperature and pressure varying dependent upon the type of Pt/C catalyst used. A notable advantage of these reactions is the high yield quoted by most to be >98%,[12] in some instances close to 100% yield.[13] A simplified reaction scheme below indicates the three different products that can be formed, owing to a lack of chemoselectivity using this technique.

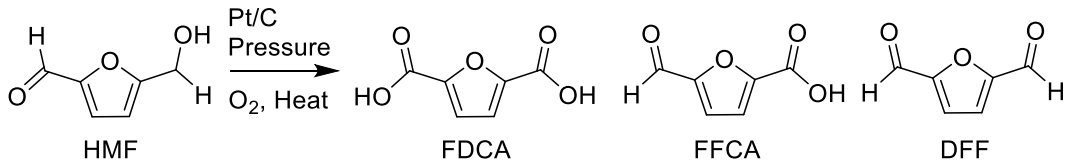

Figure 1 - Reaction scheme for the Pt/C catalysed reaction of HMF to FDCA/FFCA/DFF.[12]

Other metal catalysts include: $CuO\text{-}AgO/Al_2O_3$, Amberlyst $15/CrCl_3$ with Au_8Pd2/HT.[14,15] These processes fall more in-line with traditional oxidation chemistry, employing a solvent extraction purification. The Cu based catalyst is used in a trickle-bed reactor for an initial ambient air oxidation, followed by an ethyl acetate wash to remove NMP initially yielding 74% FDCA.[14] A secondary oxidation uses the aforementioned Pt/C catalyst providing a yield of 94% FDCA and 5% HMFCA.

Amberlyst is used in the oxidation step of a one-pot conversion from sugar to FDCA (glucose requires isomerisation to fructose). A complex phasic reactor is used to chemically separate the sugar reactions and the intermediates shown in Figure 3.

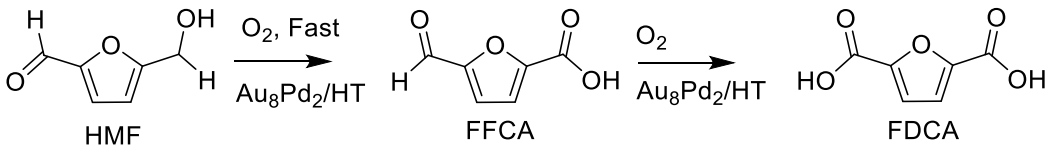

Figure 2 - Oxidation of HMF to FDCA in the presence of Au_8Pd_2 catalyst.[15]

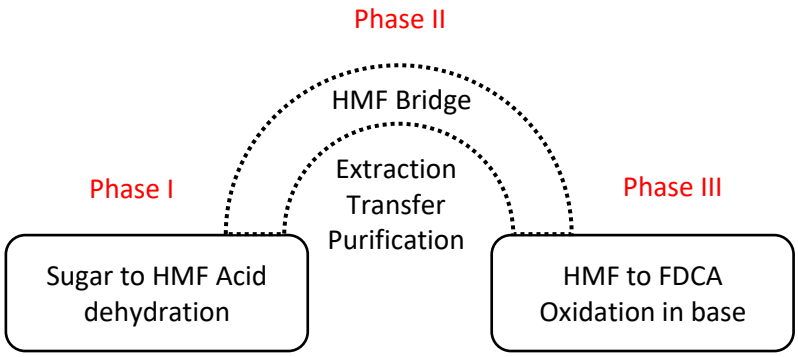

Figure 3 - Phasic reactor used to separate out the sugars and intermediates allowing for the dehydration of sugars such as fructose into HMF (phase I), with the continual mass transfer of HMF using the bridge (phase II) to a oxidative reactor (phase III).[15]

Acid catalysis can form FDCA via a dehydration reaction, starting with glucaric acid rather than HMF.[16–18] A HBr/H_2O/sulfolane system is operated at 100°C, sulfolane being an optimal solvent for the dehydration. DEHU, also known as 4-dehoxy-L-erythor-5-hexoseulose urinate, is converted to FFCA then FDCA at 80% yield. The 1st step is acid catalysed using hydrochloric acid, whilst the 2nd step uses a Pt/C oxidation with ambient air providing the necessary equivalences of oxygen.

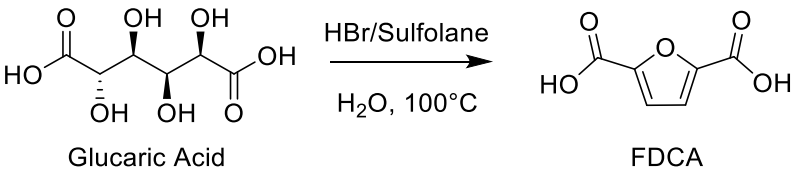

Figure 4 - Dehydration of glucaric acid to form FDCA using HBr/H2O/sulfolane in an acid catalysis.[16]

A Lewis acid catalysed process has been developed by Wisconsin Alumni Research Foundation (WARF) for the conversion of HMF to FDCA at 62% yield.[19] With the oxidation reaction of HMF to FDCA using a Pt/C catalyst at 100 °C, however the novelty of the patent is not derived from this common HMF oxidation technique. Instead, the patent uses a Lewis and Bronsted acid to convert a portion of glucose to HMF.

A process developed by Braskem produces FDCA at 15% yield by disproportionation of potassium furoate, proceeding secondly by a metal catalysis reaction using Cd, Zn or Fe at elevated temperatures.[20] Petrobras uses supercritical water in a novel technique to convert glucose to HMF, then a noble metal catalysed oxidation of HMF to FDCA with a 97% yield.[21] Both techniques employ a 2-step procedure, with their novelty attributed to HMF production rather than FDCA.

A notable catalyst trio is Co/Mn/Br. Together they're capable of oxidising HMF, 5-ethoxymethylfurfural (EMF), 5-acetoxymethylfurfural (AMF), 5-methoxymethylfurfural (MMF) and/or 5-butoxymethylfurfural (BMF) in the presence of air and acetic acid, producing 48% FDCA and 52% 5-formyl-2-furancarboxylic acid (FFCA).[22–31] The mixture is subjected to a liquid displacement treatment followed by a secondary oxidation step designed to maximise FFCA oxidation.[22–24] The process requires several purification steps (a total of 4), as well as high pressure and high temperature. Further variation of the catalyst produces DFF or ester derivatives that can be hydrogenated to yield FDCA.[25,28,29]

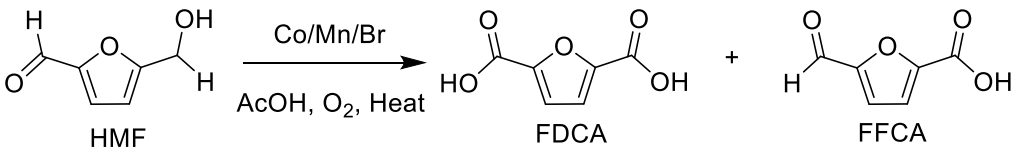

Figure 5 - General synthesis of FDCA from HMF using a Co/Mn/Br catalyst.[22]

1.3 Overview of Enzyme Kinetics

In an enzyme catalysed reaction substrate (S) with enzyme (E) proceeds through transition state (SE) to product (P); each reaction has its own respective rate.

$$[\boldsymbol{S}] + [\boldsymbol{E}] \underset{-1}{\overset{1}{\rightleftharpoons}} [\boldsymbol{ES}] \underset{-2}{\overset{2}{\rightleftharpoons}} [\boldsymbol{P}] + [\boldsymbol{E}] \qquad \text{Eqn. 1}$$

$$\text{Rate}_1 = K_1\,[E][S]$$

$$\text{Rate}_2 = K_2\,[ES]$$

$$\text{Rate}_{-1} = K_{-1}\,[ES]$$

$$\text{Rate}_{-2} = K_{-2}\,[P][E]$$

$$\boldsymbol{Rate_1 + Rate_{-2} = Rate_{-1} + Rate_2} \qquad \text{Eqn. 2}$$

Assumptions are that must be noted; (1) solutions behave ideally, having two distinct steps: binding of substrate and transition to product; (2) the two constants of the reaction remain constant: enzyme concentration (no degradation) and the rate constant, that are unchanged by external factors like temperature; (3) the formation of product without enzyme occurs at a negligible rate, such that product formation only occurs in the presence of the enzyme.

The steady-state assumption considers the formation of the intermediate $[ES]$ to be equivalent to the loss of $[ES]$. However, the reverse reaction (shown in equation 2 and 3 as Rate_{-2}), is considered to be negligible due to the product being more thermodynamically stable.

$$\boldsymbol{K_1[E][S] = K_{-1}[ES] + K_2[ES]} \qquad \text{Eqn. 3}$$

With the assumption that the total amount of enzyme $[E]_T$ never changes:

$$[\boldsymbol{E}]_{\boldsymbol{T}} = [\boldsymbol{E}] + [\boldsymbol{ES}] \quad \text{Eqn. 4}$$

By combining the two equations and rearranging results in the equation below, which can be further simplified by assigning the value of K_M to all the equal rate constants.

$$[\boldsymbol{E}]_{\boldsymbol{T}}[\boldsymbol{S}] - [\boldsymbol{ES}][\boldsymbol{S}] = [\boldsymbol{ES}]\left(\frac{\boldsymbol{K_{-1} + K_2}}{\boldsymbol{K_1}}\right) \quad \text{Eqn. 5}$$

$$\boldsymbol{K_M} = \left(\frac{\boldsymbol{K_{-1} + K_2}}{\boldsymbol{K_1}}\right) \quad \text{Eqn. 6}$$

Substitution of K_M into equation 6, and rearrangement to make $[ES]$ the subject.

$$[\boldsymbol{ES}] = \frac{[\boldsymbol{E}]_{\boldsymbol{T}}[\boldsymbol{S}]}{\boldsymbol{K_M}[\boldsymbol{S}]} \quad \text{Eqn. 7}$$

The rate of reaction can be given by V_0 as the change in product over time.

$$\boldsymbol{V_0} = \frac{\Delta[\boldsymbol{P}]}{\Delta \boldsymbol{t}} = \boldsymbol{Rate_2} = \boldsymbol{K_2}[\boldsymbol{ES}] \quad \text{Eqn. 8}$$

Inclusion of the rate limiting rate constant K_2 to both sides:

$$\boldsymbol{K_2}[\boldsymbol{ES}] = \frac{\boldsymbol{K_2}[\boldsymbol{E}]_{\boldsymbol{T}}[\boldsymbol{S}]}{\boldsymbol{K_M}[\boldsymbol{S}]} \quad \text{Eqn. 9}$$

If the reaction is at the maximum speed, where $V_0 = V_{max}$ at very high substrate concentration, then the total enzyme concentration $[E]_T$ is going to be equal to$[ES]$. In this case the enzyme is completely saturated with substrate leaving no free enzyme left.

$$\boldsymbol{K_2}[\boldsymbol{E}]_{\boldsymbol{T}} = \boldsymbol{V_{max}} \quad \text{Eqn. 10}$$

Combining the expressions produces the Michaelis-Menton equation.

$$\boldsymbol{V_0 = \frac{V_{max}[S]}{K_M[S]}} \qquad \text{Eqn. 11}$$

If the Michaelis-Menton constant K_M is equal to the substrate concentration then:

$$\boldsymbol{V_0 = \frac{V_{max}}{2}} \qquad \text{Eqn. 12}$$

The model predicts the rate of reaction, when the substrate concentration $[S]$ exceeds the Michaelis constant K_M the reaction velocity is at a maximum $V_0 = V_{max}$ and a zero-order reaction is observed. Michaelis constant is equivalent to the substrate concentration at half the maximum reaction rate; for most enzymes the value lies between 10^{-1} – 10^{-7} M. Environmental conditions can alter the value of K_M, such as the temperature, ionic strength and pH. A plot of the reaction velocity as a function of the substrate concentration is a common approach to determine the V_{max}.[32] Simplified, the lower an enzymes K_M value the better it performs at lower substrate concentrations. The Michaelis-Menton constant can be used to quantify an enzyme's ability to catalyse reactions. Known as the catalytic efficiency, this is derived from an enzymes Turnover Number (TON) defined below.

$$\boldsymbol{K_{cat} = \frac{V_{max}}{[E]_T}} \qquad \text{Eqn. 13}$$

Turnover Number refers to how much substrate is converted to product using enzyme, in one second at its maximum speed, give in units of sec^{-1}. For an enzyme to be catalytically efficient it must have either a high K_{cat} or a low K_M value. The catalytic efficiency can be defined as:

$$\boldsymbol{Catalytic\ Efficiency = \frac{K_{cat}}{K_M}} \qquad \text{Eqn. 14}$$

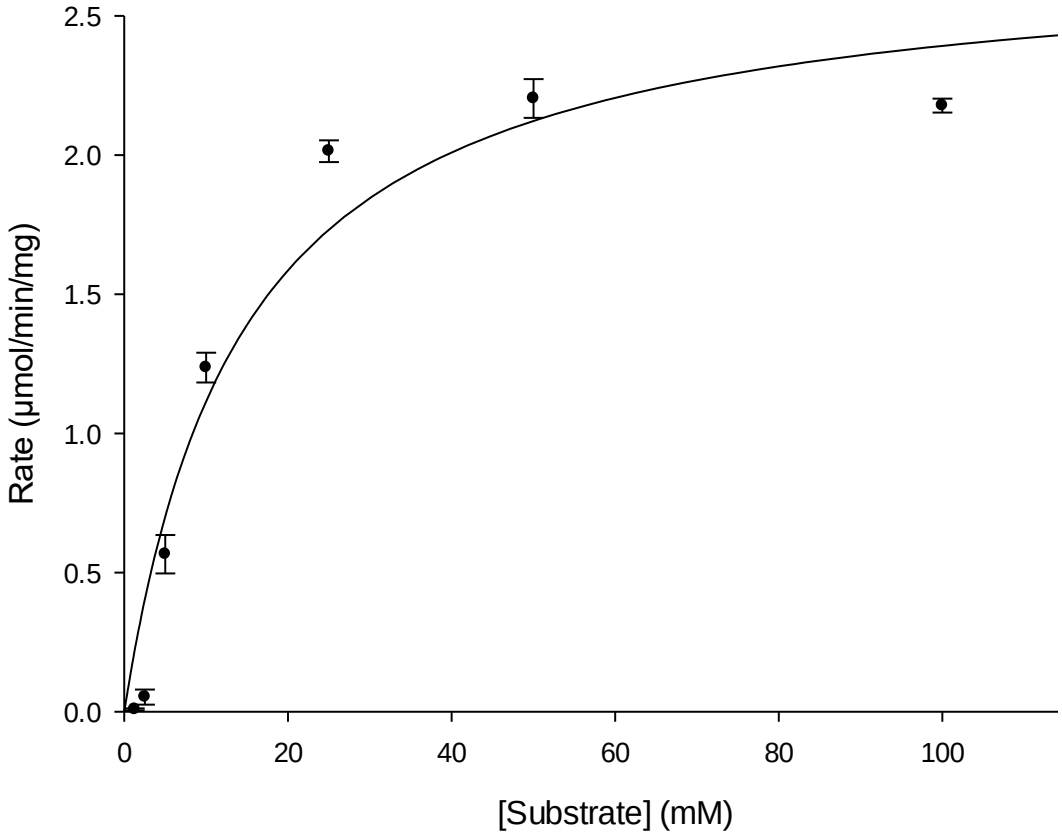

Vmax = 2.7
Km = 14.5

kcat = 189 s^{-1}

kcat/Km = 13 s^{-1} mM^{-1}

Figure 6 - Michaelis-Menton kinetics plot of $GOase_{M3\text{-}5}$ for determining the Michaelis constant (KM).

1.4 Biocatalytic Oxidation of HMF

Novel work was undertaken by Carnell *et al.*[33] in combination with Turner *et al.*[34], culminating in an enzymatic cascade synthesis for the oxidation of HMF to FDCA. The scheme uses two major oxidative enzymes, galactose Oxidase$_{M3-5}$ mutant (GOase$_{M3-5}$),[35] and Periplasmic aldehyde oxidoreductase (PaoABC).[36] Wild-type GOase has limited substrate specificity, accepting glucose poly saccharides and certain primary alcohols. Broadening this selectivity requires mutation of the enzyme by mutagenesis, giving increased activity to specific substrates. A notably interesting variant is the M_{3-5} mutant; it can selectively oxidise enantiomers of secondary alcohols to their corresponding ketones.[35]

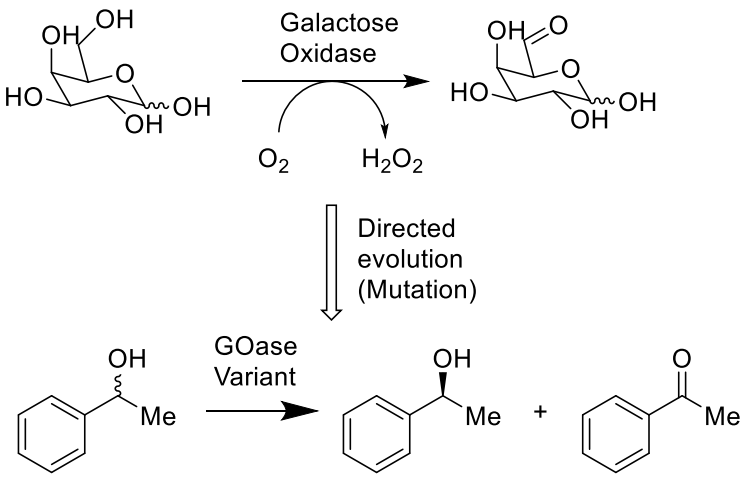

Figure 7 - Mutation of galactose oxidase to produce a mutant capable of selectively oxidising a racemic mixture of 1-phenylethanol to the corresponding aldehyde.[35]

The process follows the reaction scheme shown in

Figure 8 with the reaction taking two routes dependent upon which enzyme is initially reacted with HMF. The ideal route using GOase$_{M3-5}$ initially to form DFF, avoiding the slow oxidation of HMFCA to FFCA. Galactose oxidase$_{M3-5}$ mutant requires a chelated metal in the active site of enzyme to function, copper being used for the former and molybdenum for PaoABC.

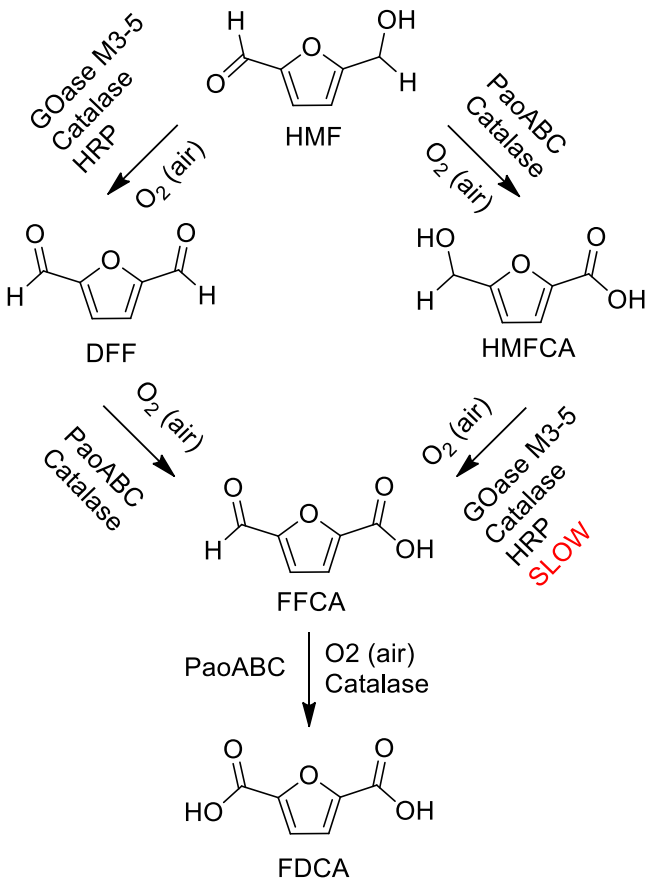

Figure 8 - Enzymatic bio-catalysis synthesis for FDCA from HMF, via the DFF and HMFCA reaction intermediates.[33,37]

A by-product of the oxidation process, produced by the enzymes is hydrogen peroxide, this oxidant degrades the enzymes, requiring swift removal.[38] A second enzyme, catalase, is therefore added to both enzyme catalysed reactions, converting the peroxide into half an equivalent of oxygen (a substrate to both enzymes).[39]

The reaction scheme for galactose oxidase catalysed oxidation is shown in Figure 9. This demonstrates the requirement of oxygen for the enzyme, whilst producing half an equivalent as a by-product from catalase decomposition of hydrogen peroxide.

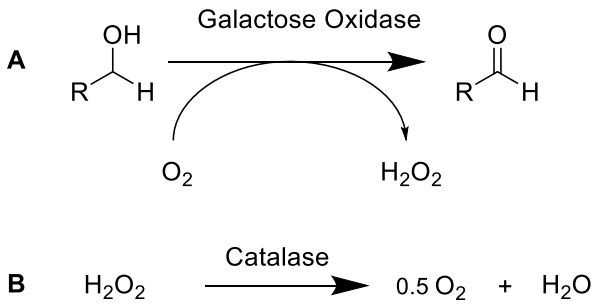

Figure 9: A) Reaction scheme for the oxidation of a primary alcohol to a secondary alcohol using galactose oxidase; B) conversion of hydrogen peroxide into half an equivalent of oxygen by the enzyme catalase.

A secondary additive is required for $GOase_{M3-5}$, a single electron oxidant to oxidise the now reduced copper ions back to their 2+ state.[40] Peroxidase from horseradish (HRP) is a suitable oxidant for the cofactor ions, with the optimum concentration shown to be 40 $U.L^{-1}$.[38] A certain amount of copper ions must be present in the reaction to achieve full activity, typically this is 15 µM for 100 mg of $CFE.L^{-1}$. The quantity of HRP and Cu^{2+} ions required differs dependent upon if purified enzyme of its cell-extracted alternative (cell-free extract – CFE) is used.

A buffer system is necessary to ensure the aqueous environment remains at the ideal pH (7.4). Potassium phosphate buffer (KPi) increases the enzyme activity of GOase, originating from the free OH^- ions interacting with the copper in the active site as suggested by Saysell *et al.*[41] The conversion of HMF to FDCA requires an enzyme that can selectively oxidise the alcohol & aldehyde both to carboxylic acids; whether this be several in a cascade reaction, or a single enzyme performing both oxidations.

A recent patent by Purac Biochem BV uses a HMF oxidoreductase known as HmfH to selectively oxidise the reaction of HMF to FDCA.[42] The enzyme is left within the cell (whole-cell) allowing it to be free or immobilised onto a substrate. The whole-cell enzyme used contains host-indigenous dehydrogenases that assist in the oxidation steps forming HMFCA, with a 2nd oxidation forming the diacid product. The process produces FDCA from HMF with one enzyme, at low temperatures and with a wide pH range tolerance. The reaction forms a furan-2,5-dicarboxylate salt (MFDCA) that can be precipitated out as FDCA through the addition of HCl, with a simple solid-liquid filtration step providing the separation from the reaction medium.[43]

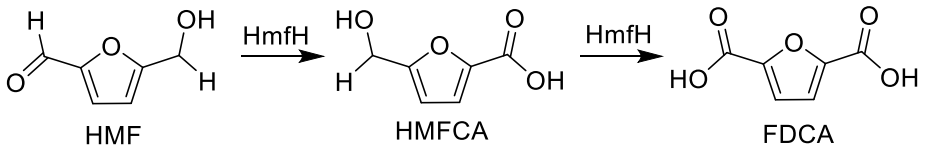

Figure 10 - Selective oxidation of HMF to HMFCA then FDCA using the enzyme HmfH.[42,43]

Another industrial development patented by Synthetic Genomics Inc. uses a cocktail of enzymes produce DHG (2-dehydro-3-deoxy gluconate) from glucose, with the choice to produce FDCA.[44] These enzymes include: pSGI-433, 434, 476, 353 and catalase. Catalase indicates the necessity to remove H_2O_2 from the reaction, with the enzymes being oxidative in nature. The first reaction of DHG is a dehydration requiring a catalyst, which can be a polymeric material or copolymer of polystyrene with divinylbenzene or a zeolite. It can produce a variety of DHG ester derivatives such as 2KGA and 5KGA (2-ketogluconic acid and 5-ketogluconic acid respectively).

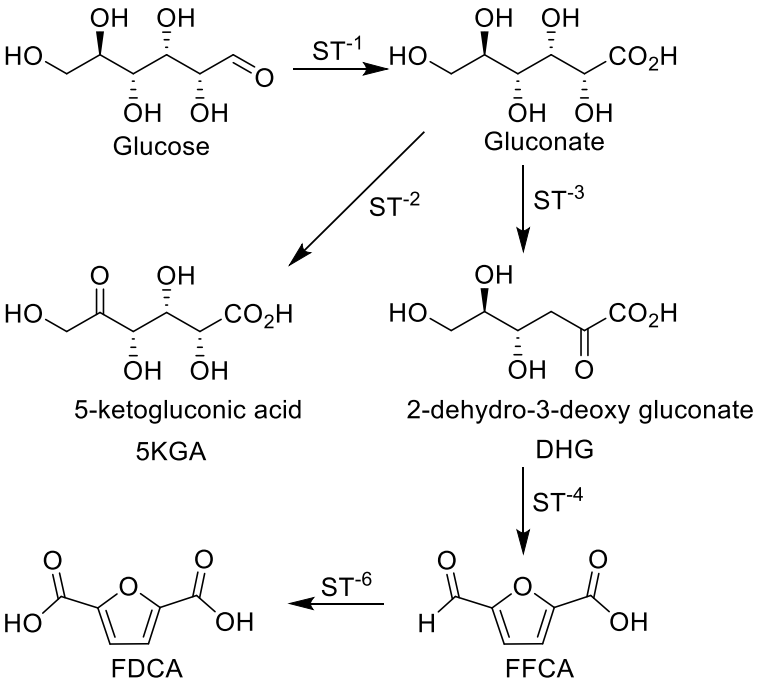

Figure 11 - Conversion of glucose to DHG and then to FDCA through various reaction intermediates by the enzyme catalysed oxidation reactions using pSGI based enzymes.[44]

1.5 Chemo-Enzymatic Oxidation of HMF to FDCA

The first biocatalytic oxidation of HMF was reported by Sheldon *et al.*[45] using chloroperoxidases to yield DFF and HMFCA as a by-product, affording a selective yield of 60-74%. Since then numerous enzymes have been employed to oxidise alcohols and aldehydes, notably HmfH, galactose oxidase and lipases.[46]

Lipase enzymes are used primarily in the body to catalyse the hydrolysis of fats but have seen significant use in industry for transesterification reactions, converting vegetable oil into fatty acid methyl esters (FAME), known industrially as biodiesel. Similar to most enzymes, lipases are particularly sensitive to changes in pH, solvent and temperature, making their application to large-scale manufacturing a challenge. However, the ease of immobilisation, lack of co-factor requirements and reaction stereo selectivity necessitate their continued interest in research.

CAL-B lipase from yeast (*Candida antarctica*) has seen the most success in process development of hydrolases; the Lipase A variant having far less activity.[47] Its active site consists of 'the catalytic triad'. The triad contains a nucleophilic serine, activated by a hydrogen bond from a histidine and aspartate (glutamate). Unlike some enzymes the binding site for a hydrophobic substrate is exposed to the solvent.[48] Aqueous or organic media can be used with the enzyme, with aqueous environments showing slightly higher activity levels.

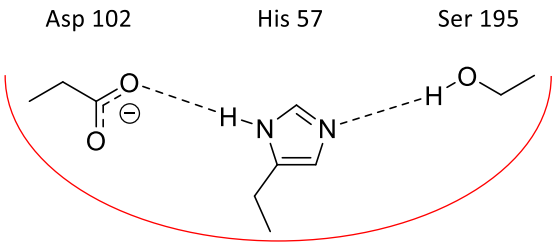

Figure 12 – Catalytic triad found in CAL-B lipase. The active site (contained in the red semicircle) consists of the eponymous Serine (Ser) residue, Histidine (His) and an Aspartate (Asp) residue.[48]

Mechanisms vary dependent upon on the enzyme substrate in the catalysis reaction. Initial attack however comes from the lone-pair of electrons located on the serine oxygen, typically into a carbonyl. The triad's major role is to function as a charge relay system with partial charges moving throughout the structure.[49]

Fernández *et al.* used the lipase CAL-B to catalyse the epoxidation of cylcohexane, with urea-hydrogen peroxide (UHP) as the oxidiser, in an acetonitrile media.[50] Urea-hydrogen peroxide was used a safer, anhydrous alternative to hydrogen peroxide. Having a longer shelf-life and the potential of controlled release avoids the slow and continual addition of hydrogen peroxide. Original work on epoxidations was undertaken by Björkling *et al.* which used gradual addition of peroxide to prevent deactivation of the lipase, use of UHP negated this complication.[51]

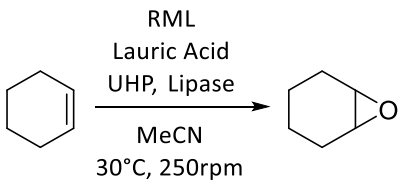

Figure 13 – Epoxidation of cyclohexane using: Rhizomucor miehei lipase (RHL); lauric acid and urea-hydrogen peroxide in acetonitrile at 30 °C and 250 rpm, as undertaken by Fernández et al.[50]

Reasonable conversion was seen at higher reaction times, in excess of 24 hrs. As stated in other reports, the enzymatic formation of peroxyacetic acid is relatively fast, however the oxidation (epoxidation in this instance), is slow by comparison. Particularly so, with increased quantities of lipase having little impact on the overall conversion.[50] Furthermore, their scheme suffered poor enzyme recycling, with activity reduction observed after each recycle, and no activity present after a third reprocessing. Again, an issue associated with prolonged exposure to hydrogen peroxide, something RML may be more susceptible to.

1.6 Chemo-Catalytic Oxidation of HMF to FDCA

Although numerous routes exist for the chemo-catalytic oxidation of a primary alcohol to a secondary alcohol, the routes explored in this work were those of significant industrial feasibility and in aqueous, green solvent systems. Firstly, the Noyori reaction using sodium tungstate dihydrate as a catalyst for a peroxide-based oxidation, secondly potassium peroxymonosulfate (Oxone™) as the oxidiser.

Sodium tungstate dihydrate has been used extensively for the epoxidation of alkenes and the oxidation of primary and secondary alcohols to the corresponding aldehyde and ketone.[52,53] As an inorganic catalyst in most reactions, the compound is typically dissolved in aqueous solutions and recovered downstream. Flow systems using the tungstate are limited, requiring immobilisation of the catalyst onto glass beads or other suitable surfaces.

Oxidation reactions use the in-situ formation of a pertungstate to undertake the oxidative process, this is initiated by an oxidiser, usually hydrogen peroxide. A phase-transfer catalyst (PTC) is required to initiate transfer of the pertungstate from the aqueous phase, where peroxide is converted to water, to the organic phase for the desired reaction to occur. Methyltrioctylammonium hydrogensuflate (Q^+) is a noteworthy PTC used in the procedure; providing a secondary benefit of increased hydrogen peroxide stability at elevated reaction temperatures.[54] Dehydrogenation of alcohols to their corresponding carbonyl compounds is undertaken at 90 °C preventing any unproductive decomposition of H_2O_2. The quaternary ammonium salt (PTC – shown in Figure 14 as Q^+) splits into a lipohilic Q^+ cation and HSO_4^- anion; the former aiding in phase-transfer, the latter inhibiting breakdown of peroxide.[54] The system is highly dependent upon aqueous-organic phase transfer as well as the acidity of the reaction medium. Product formation favours pH's lower than 2, a pH of 4 or above shows weak oxidative activity due to the pKa of the intermediate species A, with compound B being dominant in a pH range of 0.3-4.

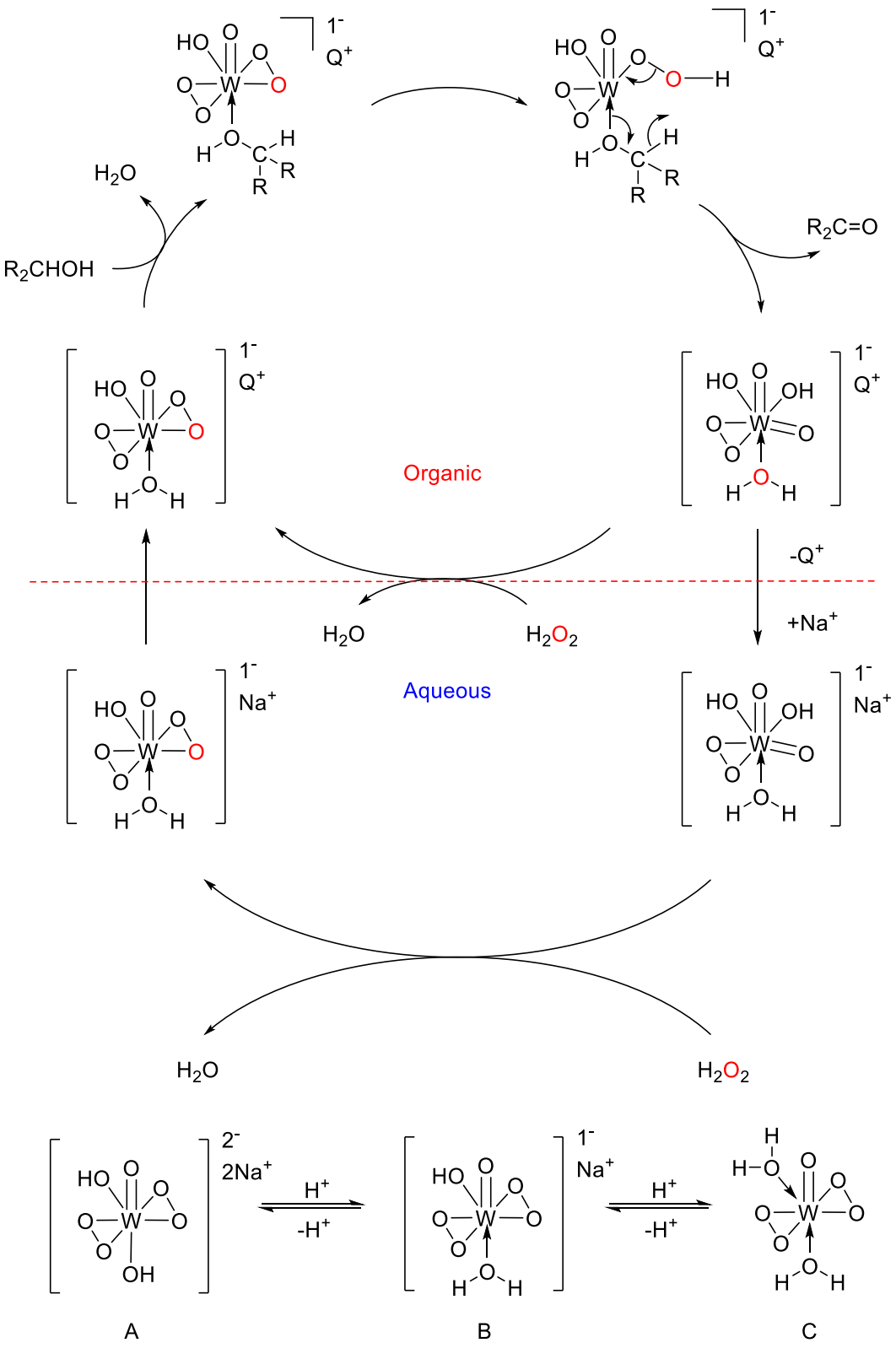

Figure 14 – Catalytic cycle for the sodium tungstate catalysed oxidation of an alcohol to aldehyde. System using a biphasic mixture with a phase-transfer catalyst (PTC) for the required oxidation in the organic phase. Hydrogen peroxide is used to form the perhydrate in-situ.[54]

Research on sodium tungstate dihydrate has seen it used in non-oxidative reactions as a catalyst to form pyrano[2,3-c]coumarins. A three-component system was employed by S. Khodabakhshi *et al*.[55] to synthesise the compound from a mixture of 4-hydroxycoumarin, malonitrile and various aromatic aldehydes. These compounds are of synthetic importance for medical and biological research, yet current methods have numerous drawbacks: low yield, long reaction times and harsh conditions.

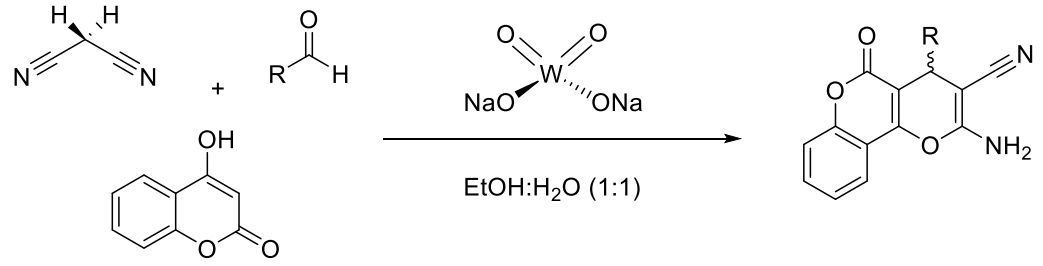

Figure 15 – Synthesis of a pyranocoumarin using a three-component, one-pot, and sodium tungstate dihydrate catalysed reaction to yield the product. Work done by Khodabakshi et al. used an aqueous solvent system to yield 90% of the product in 20 minutes.[55]

Their system used a range of protic and aprotic solvents, culminating in a mixture of ethanol and water for the highest conversion, with polar solvents affording a greater yield. Temperature was taken into consideration with reactions undertaken at room temperature and requiring longer reaction times.[55] Throughout the majority of aforementioned chemo catalytic reactions, the pH of a system is generally not of concern, however with recent work into the Cannizzaro reaction, this will likely change. Original work was done by Stanislao Cannizzaro *et al.*[56] looking at the base disproportionation of two non-enolizable aldehydes, forming a primary alcohol and a carboxylic acid.

With the majority of intermediates present in HMF oxidation to FDCA (
Figure 8) containing either an alcohol or aldehyde group, conversion by the Cannizzaro reaction in alkali media is a considerable likelihood. The redox process reduces one aldehyde molecule whilst simultaneously oxidising another, with each reaction occurring at the stage of hydride transfer.

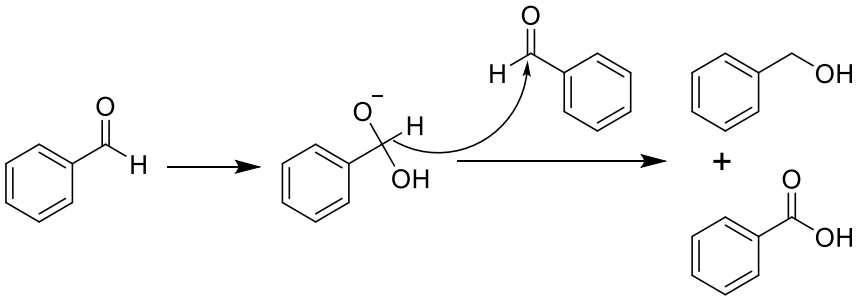

Figure 16 – Base disproportionation of benzaldehyde in alkali conditions, forming both benzoic acid and benzyl alcohol, known as the Cannizzaro reaction.

Several attempts have been made to selectively produce one product of the Cannizzaro over another, with most exploring a range of bases or metal catalysts. Saeed *et* al.[57] have shown success converting aldehydes to their respective alcohols and carboxylic acids at 85% formation. The workup procedure was altered to use methanol instead of water, for more convenient fractionation. This resulted in the respective methyl esters of the starting aldehydes along with equivalent quantities of their analogous alcohols.

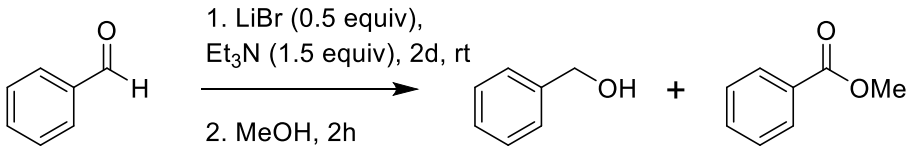

Figure 17 – Cannizzaro reaction for the conversion of benzaldehyde to benzyl alcohol and methyl benzoate using methanol with LiBr/Et_3N acting as the necessary bases.[57]

1.7 Polymerisation & Biopolymers

Polymerisation involves the linking together of small monomer molecules to form a long-chain polymer molecule, known as a macromolecule. With polymers growing typically by either chain-growth or step-growth: In chain growth, addition takes place at the ends of each molecule (or both), with three distinct sub stages: initiation, propagation and termination. In step-growth polymerisation monomers react to form dimers, then trimers, oligomers and eventually long chain polymers. Polyurethane polymerisation is a type of step-growth without condensation known as addition polymerisation. The reaction can be seen in Figure 18. With such a wide array of product capabilities, PET is the most widely produced plastic in the world.[58,59] PET is polymerised from the condensation reaction between ethane-1,2-diol (ethylene glycol) and benzene-1,4-dicarboxylic acid (terephthalic acid) monomer units, with the resultant polymer extruded or moulded as a pellet into desired shapes (Figure 19).

Since the discovery of plastics in the 1950's over 9 billion tons have been produced, yet as of 2015, only 9% of that plastic waste was recycled, and 12% incinerated.[60] With the remaining 79% building up in landfills, regions of the ocean, beaches and unofficial disposal sites.[60] A rough estimate places 5-13 million tons of plastic entering the ocean every year, with plastic remnants being found in every major ocean basin in the world.[60] The consequences of this are the destruction of fish, ocean habitats, livelihoods and the pollution of our oceans and seas. This has become a major driving force to produce biodegradable polymers. Bio-degradable polymers are expected to naturally decompose by the action of living organisms; this is different to compostable polymers that are expected to turn into hummus.[61] Bio-renewable plastics may take several years to breakdown, but are sourced from renewable sources. A notable example that aligns with both is polylactic acid (type of polyester); derived from corn starch or sugarcane.[62] This polymer degrades into lactic acid over the period of 6 months to 2 years depending on how the structure is modified with additives.[62]

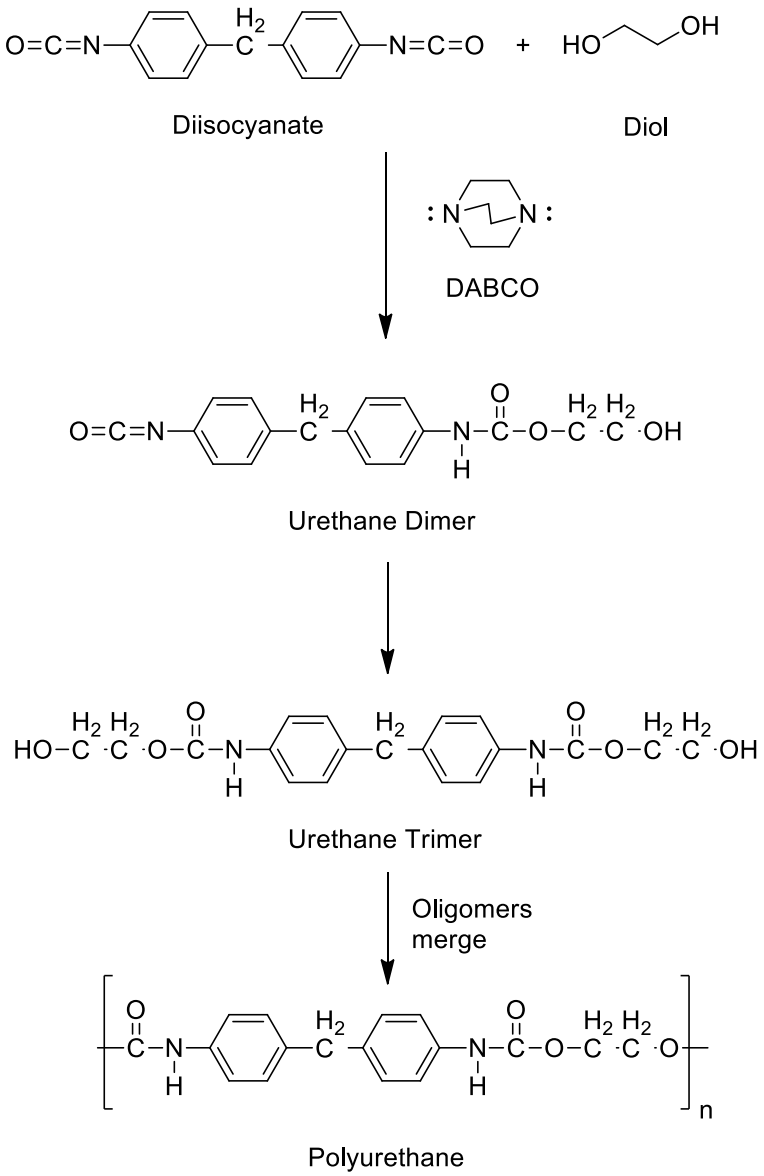

Figure 18 - Step-growth polymerisation of an isocyanate and a diol to form polyurethane. The strong nucleophile DABCO initiates the reaction by binding (through hydrogen bonding) to a hydrogen of the alcohol group. The process produces oligomers of varying sizes (dimers, trimers) that then merge forming the high molecular weight polymer.[63]

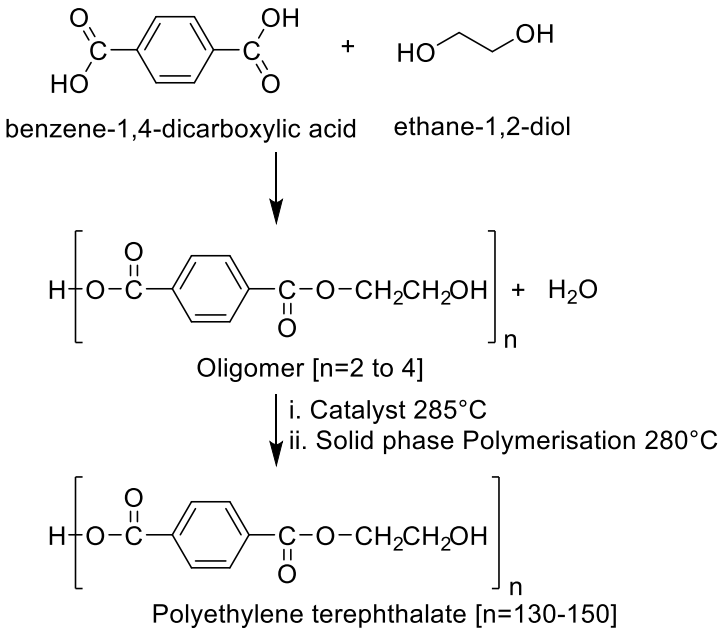

Figure 19 - *General reaction scheme for the condensation polymerisation of Terephthalic acid and ethylene glycol to produce polyethylene terephthalate (PET).*[64]

The thermoplastic polylactic acid is usually synthesised from the product of microbial fermentation, lactic acid. The polymer forms by either condensation (low molecular weight) or ring-opening (high-molecular weight), with the lower molecular weight polymer more susceptible to microbial attack and therefore improved biodegradability.

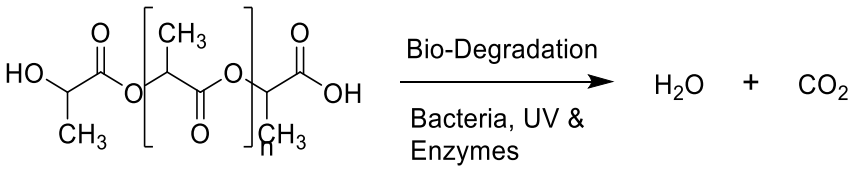

Figure 20 - Polylactic acid formed from the condensation reaction between lactic acid and lactide degrading by natural means (enzymatic reactions, sunlight and bacteria) to form water and carbon dioxide.

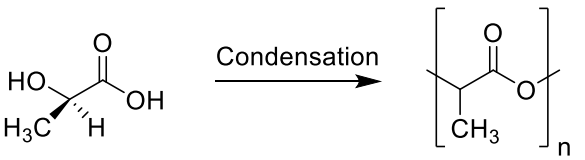

D-lactic acid Polylactic acid

Figure 21 – Condensation of lactic acid to form low molecular weight Polylactic acid (PLA). Has a high susceptibility to biodegradation, hence its use in single-use, disposable items.

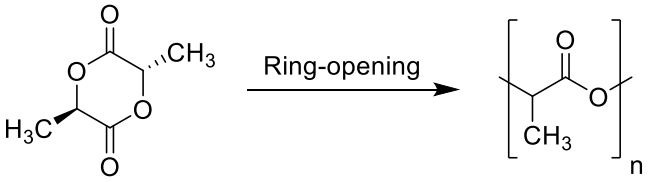

Meso Lactide Polylactic acid

Figure 22 – Ring-opening polymerisation of a dimer of lactic acid, meso lactide (two others can exist, the L and D forms). Produces a high molecular weight polymer with decreased susceptibility to biodegradation.

It is important to distinguish between a biodegradable plastic like polycaprolactone (PCL) that is derived from petroleum sources and bio-based PEF, a biopolymer derived from fructose that isn't biodegradable. For a polymer to be bio-degradable it must degrade from the action of living organisms, notably microorganisms and fungi. A biopolymer on the other hand is manufactured from renewable or natural resource, this includes bio-based polymers that are extracted from biomass; rubber being the most notable example.

Natural polymers are produced by living organisms, being essential to their survival. They can be extracted, refined and modified, if necessary, for commercial use. Rubber, polysaccharides, starch, cellulose and chitin are all common examples of natural polymers.[65] All require processing before use, with vulcanisation of rubber necessary to create the cross-linked structure necessary for a tough tyre.[66]

Bio-based polymers are derived from biomass, generating the monomers from renewable sources, as substitutes for petroleum building blocks. Fatty acids have been used extensively for the production of polyesters, polyurethanes and polyamides via triglycerides. Vegetable oils are polymerised through a selection of techniques tailored to yield a polymer of desired properties.

Biopolymers are not without their disadvantages. With the use of 1st and 2nd generation feedstock's for production, competition with both the biofuel's industry and animal feed industry increases production costs.[67] Many plastics being developed as bio-degradable have been shown to decompose into harmful by-products, shifting the plastic littering problem from a physical form to chemical pollution. There is considerable potential for success, with many new polymers being hailed as carbon neutral. The development of polymers from 3rd generation feedstock's (algae) being of considerable interest.[68]

Cellulose in particular has been hailed as a feedstock with unlimited potential. As nature's most abundant biopolymer and the largest carbon source on earth, interest in the compounds future has seen the rapid research and development of the bio-refinery concept.[69,70] Cellulose content in plants can vary from roughly 45% in wood up to 90% in cotton with a structure consisting of D-anhydroglucose repeating units linked by ether linkages, making it a highly hydrophilic linear polymer.[71]

Cellulose is not the lone biopolymer found in plants, hemicellulose and lignin are present in mixed amounts dependent upon the species and environmental conditions. Hemicellulose is composed up of multiple five and six membered ring polysaccharides, lignin on the other hand is a highly complex, branched and cross-linked structure with both aliphatic and aromatic constituents. Lignin is the limiting step in plant fibre degradation with a limited number of fungi able to degrade it.[72]

Degradation of cellulose to form glucose is one-step towards producing a bio-renewable platform chemical that can be used for biofuels, pharmaceuticals and polymers alike. Cellulase is an enzyme employed for the conversion of cellulose to glucose, a secondary dehydration reaction can then convert glucose to 5-hydroxymethylfurfural (HMF).[73] A major platform chemical as identified by the American Department of Renewable Energy.[7]

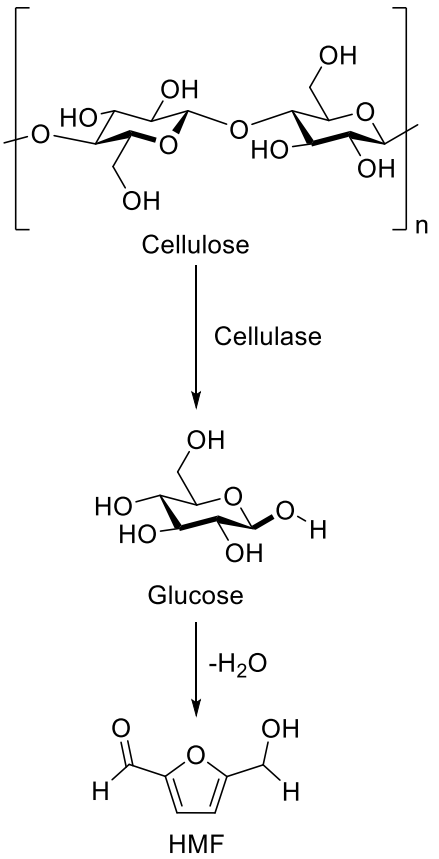

Figure 23 – Initial structure of cellulose repeating unit before enzymatic degradation to glucose and further conversion by dehydration to produce 5-hydroxymethylfurfural.

Once oxidised to 2,5-furandicarboxylic acid, the compound can be used as bio-renewable substitute for terephthalic acid in polyethylene terephthalate (PET) production, instead forming polyethylene furanoate (PEF).[11] A bio-polymer with enhanced properties over its fossil-fuel counterpart. FDCA is a bi-functional carboxylic acid containing a furan ring, arising to its notable use as a polymer building block substitute; with several companies dedicating manufacturing time to this monomer.[74]

Growth in furan-based polymers originally began with difuran diacids prepared from 2-subsituted furans, until a surge in HMF interest saw FDCA appear on the scene. Extensive studies have been carried out on the PET homologue PEF, with its highly comparable properties to the leading polyester. The first report of its synthesis from Gandini *et al.*[75] by polytransesterification, shown in Figure 24.

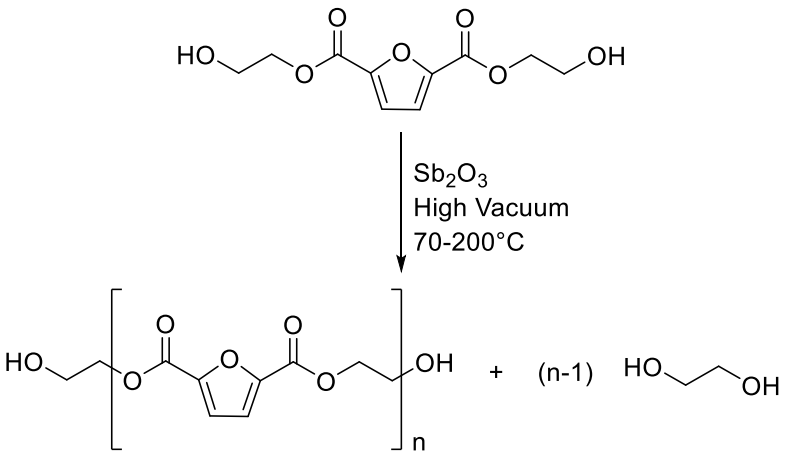

Figure 24 – Synthesis of polyethylenefuranoate (PEF) by transesterification between esterified 2,5-furandicarboxylic acid esters and ethylene glycol.[75]

Characterisation of PEF's thermal and physical properties has been thorough, including detailed sorption studies with water, carbon dioxide and oxygen.[76] A range of suitable diols have been examined for co-polymerisation with, along with their associated glass transition temperature (Tg), melt temperature (Tm) and degradation studies.[76]

In addition to the interest shown by academic research, the potential of biopolymers has been recognised by industrial concerns. Two of the biggest plastic polluters; Coca Cola recently being named the world's No.1, and PespiCo No.3,[77] have invested in the development of a bio-renewable bottle.[4] However, both companies have taken the aforementioned bio-renewable approach, since a bottle requires a shelf-life of several years before decomposition. The polymer may be produced from renewable feedstocks; however, it does not fix the pollution problem. Creating a greener future of plastics also requires biodegradability.

1.8 Continuous Flow Chemistry

In chemical engineering ideal reactor models can be used as a tool for predicting the performance of a reactor. Three ideal reactors types that exist are: batch, plug-flow (PFR) and continuous stirred tank reactors (CSTR) also known as a mixed-flow reactor (MFR). Reactor modelling is typically done around of the three types. Each have distinct concentration profiles with respect to both time and space and are classified as such (Figure 25). A batch reaction changes its composition over time, rather than space, hence it is termed transient. Plug-flow and Mixed-flow are continuous processes reaching steady-state after a period of transient flow.

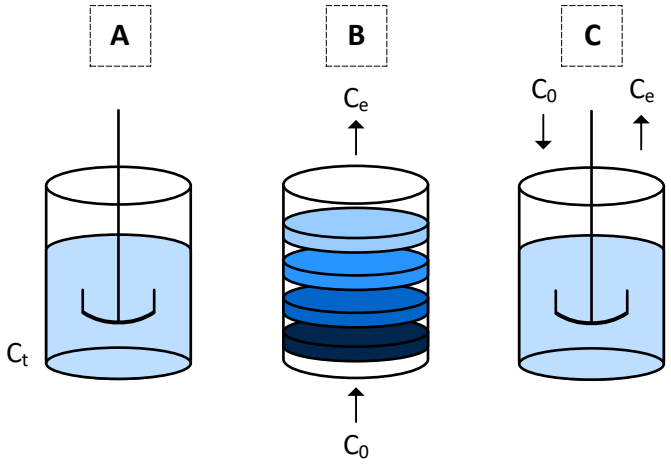

Figure 25 – The three ideal reactor types: (A) Batch - composition changing over time; (B) Plug-flow - Composition changes in space; (C) Mixed-flow reactor - Composition changes over space and time.

The time a species spends in a flow reactor is defined as the residence time. The residence time distribution (RTD) defines the distribution of times a molecule spends in a flow reactor. A mean value can be given to this, t_m, the mean residence time. For monophasic systems a singular RTD describes the flow, whereas multiphasic have a separate RTD for each phase. A RTD profile can be used to characterise reactor mixing, allowing for comparison against a model. By using ideal models to compare with, a reactors performance can be assessed, providing a method of identifying problems.

The residence time distribution function $E(t)$ also known as the exit age distribution. A plot of $E(t)$ against time (known as an E curve) gives the unity; the area under the curve. The RTD function can therefore be defined as:

$$\int_0^\infty \boldsymbol{E(t)dt = 1} \qquad \text{Eqn. 15}$$

With the fraction of the fluid that spends a given time, t in the reactor the value of:

$$\boldsymbol{E(t)dt} \qquad \text{Eqn. 16}$$

The fraction of fluid that exits the reactors with an age (time) less than t_1 is given by the value of $F(t)$. Referred to as the cumulative distribution. [78] This is obtained through integration of the area under the E curve between the limits of t_1 and 0.

$$\boldsymbol{F(t_1) = \int_0^{t_1} E(t)dt} \qquad \text{Eqn. 17}$$

The mean residence time t_m being a distribution function, is equal to the first moment of the function: the area under the curve of a graph of $tE(t)$ against t.

$$\boldsymbol{t_m = \frac{\int_0^\infty tE(t)}{\int_0^\infty E(t)dt}} \qquad \text{Eqn. 18}$$

$$t_m = \int_0^\infty tE(t)dt$$

Following on from the first moment of the function, the second moment allows for determination of the distribution from the mean. The variance term σ^2 can be used to compare different reactors without the need for a complete residence time distribution comparison.

$$\boldsymbol{\sigma^2 = \int_0^\infty (t - t_m)^2 E(t) dt}$$ Eqn. 19

The two other moments; third and fourth indicate the skewness and the Kurtosis (peakedness) of the RTD respectively. The residence time distribution function does have a substantial drawback. It can only be applied to the same reactors, preventing reliable comparison between differing reactor types. To solve this the function can be normalised to $E(\theta)$.

$$\boldsymbol{E(\theta) = \frac{E(t)}{\tau}}$$ Eqn. 20

Where τ is the space-time (residence time), calculated from division of the area by the flow rate in a reactor. In an ideal reactor containing no dead or stagnant regions the space-time is equivalent to the mean residence time t_m.

$$\boldsymbol{\tau = \frac{Reactor\ Area}{Flow\ rate}}$$ Eqn. 21

Calculation of these values is done experimentally. One method known as the Pulse experiment, injects a small volume of concentrated tracer into the reactor inlet. The mass of tracer, M, introduced to the vessel of volume, V, will have a residence time of τ. A dimensionless residence time distribution can be generated from the transformation of a $C(t)$ curve, using the following relation:

$$\boldsymbol{E(t) = \frac{\nu C(t)}{N_0}}$$

$$N_0 = \int_0^\infty \nu C(t) dt$$ Eqn. 22

Where $C(t), N_0, \nu$ indicate the concentration of the tracer measured at the outlet (with residing time $= t$), the total amount of tracer and volumetric flow rate respectively.

$$\boldsymbol{E(t) = \frac{C(t)}{\int_0^\infty C(t)dt}}$$ Eqn. 23

An ideal CSTR on the other hand assumes that all flow at the inlet undergoes complete and instant mixing. With the fluid in the reactor and exiting having identical, homogenous compositions. Ideal CSTR's therefore have an exponential residence time distribution. In reality this level of instantaneous mixing is not possible, with industrial reactors ranging vastly in size. Within reactors there will be a finite delay before a maximum $E(t)$ is reached, the length indicating the efficiency of mass transfer within the reactor. For CSTR's the function can be normalised allowing a direct comparison of different flow reactors.

$$\boldsymbol{E(t) = \frac{1}{\tau} e^{-\frac{1}{\tau}}}$$ Eqn. 24

$$\boldsymbol{E(\theta) = \tau E(t)}$$ Eqn. 25

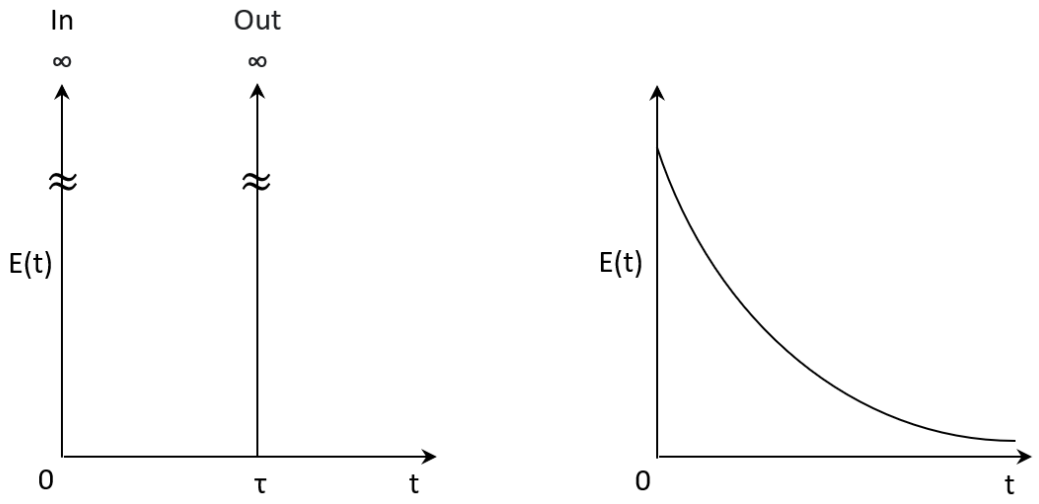

Figure 26 - Left curve is the theoretically determined E(t) curve from a pulse trace experiment for a PFR showing a single spike of infinite height and zero width. Right is the experimentally determined E(t) curve for an ideal CSTR, an exponential decay of RTD as time proceeds.

Reactors in reailty will deviate from these ideals. With common failures arising from by-passing or dead volume. In bypassing a quantity of the material passes straight through the reactor whilst dead-voulme refers to areas of the reactor vessel that are stagnant. For a bypassing system the velocity, v of the non-bypassing material is lower giving rise to a residence time greater than τ. For a CSTR this results in the slower exponential decay of $E(t)$. A PFR on the other hand would have a distinct spike near the origin representing the material that passed straight through. Dead-volume in a PFR can be represented by residence time lower than τ, as the volume of the reactor is also reduced. A spike is observed less than τ, but not at the origin. For a CSTR the exponential decay is of $E(t)$ is significantly faster (Figure 27).

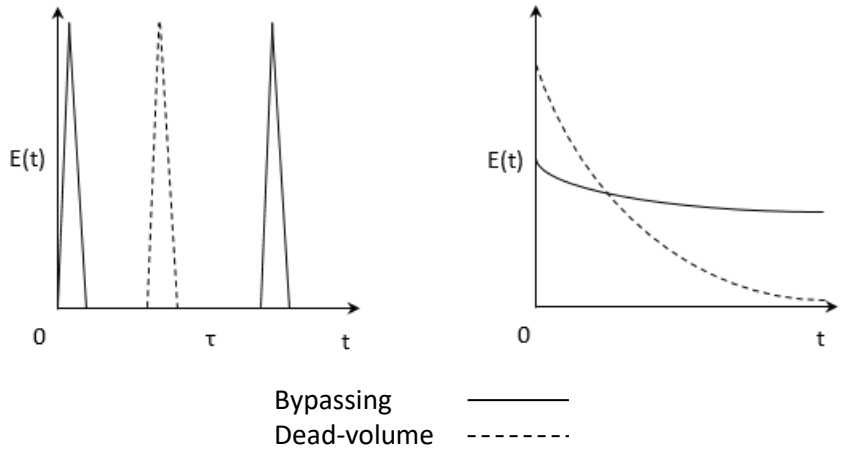

Figure 27 - RTD of a PFR and CSTR deviating from the ideals: (A) RTD curve for a PFR with bypassing $(\boldsymbol{t > \tau})$ *and dead-volume* $(\boldsymbol{t < \tau})$*; (B) RTD curve for a CSTR with bypassing (slower exponential decay, shown by the bold line) and dead-volume (fast exponential decay, shown by the dotted line).*

Plug-flow gives rise to Taylor flow, with discrete reaction plugs throughout the tubular vessel. Therefore, no axial mixing is observed in a PFR, giving rise to an infinite number of discrete reaction plugs. The composition of these plugs changes as a function of the distance travelled through the reactor, with the concentration of starting material decreasing, forming a gradient along the tube. CSTR's and batch reactors are assumed to exhibit uniform mixing, resulting in a uniform composition throughout the reactor.

As with most gas-liquid interfaces, insufficient mixing leads to a stoichiometric excess of gas within the reaction, prolonging the reaction.[79] A phenomena known as Taylor flow,[80] caused by the creation of a thin film of flow between the channel walls and the gas slug, reduces mixing path lengths in order of 2-3 magnitudes.[80]

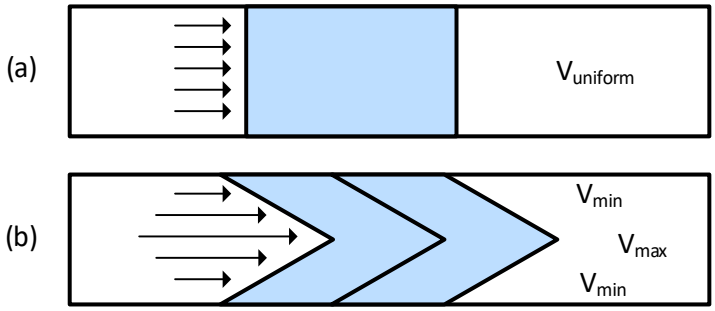

Figure 28 - Slug-flow of a gas through a tube: (a) ideal plug-flow exhibiting no axial dispersion; (b) Taylor flow produced when the flow velocity is non-uniform, resulting in a parabolic profile.

Slug flow of a gas through a channel can increase passive mixing when in excess; yet a gas's solubility in the fluid medium is critical to both flow,[81] and in the current reaction scenario, essential for the oxidation process. The reactions do not occur in the gaseous stage, instead any oxidation reactions occur using soluble oxygen, therefore the solubility of oxygen in the solution can be a rate determining factor.[82] Efficient phase mixing is therefore essential. Micro reactors alone have poor mixing capabilities, necessitating the use of an agitator; however, at the risk of denaturing the enzyme. A stable fluid distribution and mixing throughout the channel can be a significant challenge, particularly upon the introduction of tertiary and quaternary reaction feeds.[83]

Of significance to this project is continuous stirred tank reactors (CSTR's).[84] There are a number of other flow systems available: photochemistry,[85] electrochemistry,[86] and catalytic chemistry,[87] with noteworthy reactor developments currently in fluidised bed reactors,[88] microwave reactors [89] and packed bed reactors.[90]

1.9 Enzymatic Catalysis in Continuous Flow

Catalysis in flow can be both biological, chemical or a combination of the two; various work has been published in both areas [91], with chemo catalysed reactions being of prominence. [92] A non-biological homogeneous approach relies on small reactors volumes and laminar flow to establish a uniform environment in which to react in; thereby enhancing the catalyst to reagent ratio, surpassing the conversion present in batch processes.[93]

A biological system can employ whole-cell enzyme through the reactor as a feed, requiring a constant source of food for survival (usually sucrose), accumulating in numerous product separation issues. Enzyme immobilisation is a critical step in providing flow reactors for enzymatic synthesis approaches. Using continuous flow grants refined control over temperature and mass transfer: affording superior protection for highly temperature dependent enzymes.

Biocatalysis has been approached in the past, with enzymes like lipases being of prominence. However, the cost of the enzymes makes their use in an industrial setting unviable, consequently immobilisation has become the functional choice. Lipases, particularly *Candida antarctica* B have been used for years in industry, supplied as immobilised enzyme on methyl methacrylate beads.

CAL-B can be used to convert vegetable oils into useful biodiesel as stated by Sugihara *et al*. Triglycerides were converted to their corresponding methyl esters, through a three-step methanolysis, avoiding enzyme deactivation by methanol.[94] The enzyme was stable for 70 cycles with no noticeable decrease in conversion (95%). Initial work used a CSTR, with the standard conversion of a batch reactor, however results indicated destruction of the enzyme beads by the impellor. The process was then further improved by Royon *et.al.* using a single fixed-bed continuous reactor, showing no appreciable decrease in ester yields after 500 hours runtime.[95]

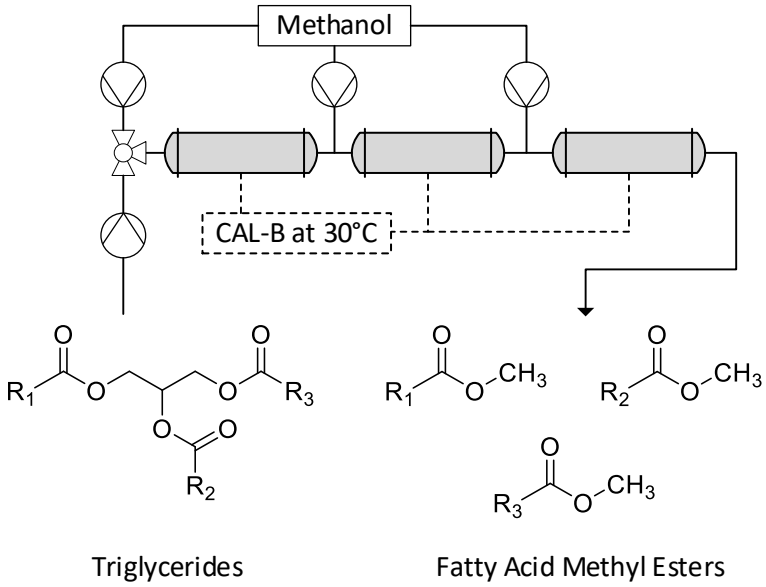

Figure 29 – Three step methanolysis of triglycerides into their corresponding fatty acid methyl esters (FAMEs) also known as biodiesel. Using a CAL-B (immobilised Candida antarctica B) catalyst in a packed-bed column at 30 °C (3g per column). At each stage glycerol was removed by settlement, the concentration of methanol decreased from a 1:3 to a 2:3 ratio (substrate to methanol), by the final tubular reactor.

Another example using enzymatic catalysis for the synthesis of esters is by Adarme *et al.*[96] They describe the importance of monoterpenic esters as both flavour enhancers and fragrances, and the current difficulties associated with manufacture and downstream purification. The process is environmentally unfriendly, using strong acids or bases in catalysis, hence a drive to develop cleaner strategies for production. The reaction occurs in a packed-bed reactor, with a 2.4 ml internal volume. The system (Figure 30) contained three distinct steps: (1) the reaction; (2) downstream processing and (3) liquid-liquid phase separation.

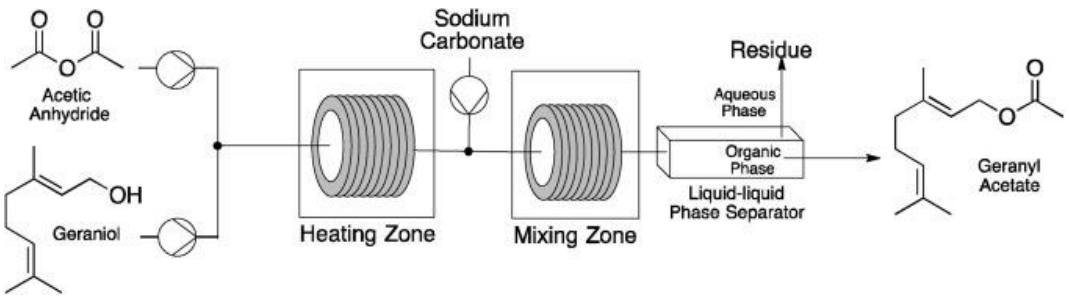

Figure 30 – Enzymatic-chemo catalysed production of Geranyl acetate in continuous flow from Geraniol and acetic anhydride.[96]

The process proved a success, producing geranyl acetate in continuous flow using the enzyme catalyst system. The reaction was undertaken at low temperatures with short residence times, exceeding the efficiency of a batch process. Downstream processing showed considerable promise with 94.1% product purity. However, for industrial sale of fragrances and flavour enhancers that enter the body, a higher purity is necessary.

Work by Grabner *et al.*[97] has combined both enzymatic and chemo-catalytic reactions in flow. Although work of this nature has been undertaken previously (see Yuryev *et al.*[98]), the group have separated out the two steps creating a tandem synthesis system. *Bacillus subtillis* (BsPAD) enzyme is stored in alginate beads by encapsulation immobilisation. The initial packed-bed column performs an enzymatic decarboxylation, the product of which serves as a substrate for a Pd-catalysed cross coupling with an aryl halide in the second column.

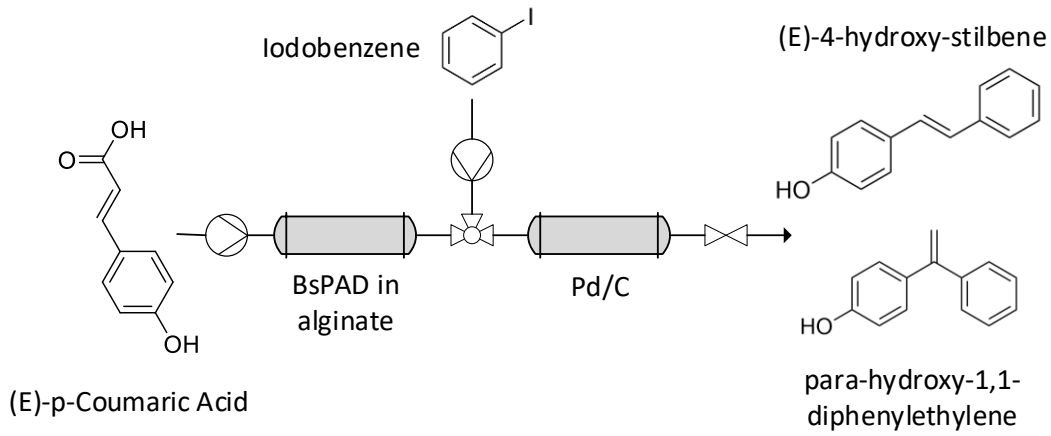

Figure 31 – Reaction scheme for the enzymatic decarboxylation of (E)-p-courmaric acid by a phenolic decarboxylase from Bacillus subtilis (BsPAD). The product, 4-vinylphenol is then the substrate for the Pd-catalysed cross-coupling reaction with iodobenzene, resulting in a mixture of the two products shown above, the para-hydroxy-1,1-diphenylethylene being the side product.[97]

The novel approach used a mixture of water and a non-conventional deep eutectic solvent (DES). Use of a biphasic system enabled them to overcome solubility barriers present in water systems. A reduction in substrate concentration was necessary for continuous flow, however long-term use of the catalyst and uninterrupted synthesis provide improved production and efficiency. Nonetheless product formation was less than ideal, with a number of side reactions occurring, reducing product yield considerably.

Work undertaken by Tamborini *et al.* sought to alleviate regio-selective problems present in chemo-catalysed reactions.[99] Using Novozym 435 (commercially available immobilised CAL-B) they were able to kinetically racemise flurbiprofen, an anti-inflammatory drug. The (S)-enantiomer of the compound is responsible for providing relief from inflammation: the (R)-enantiomer on the other hand, has anticancer capabilities. Hence both enantiomers are of significant importance.

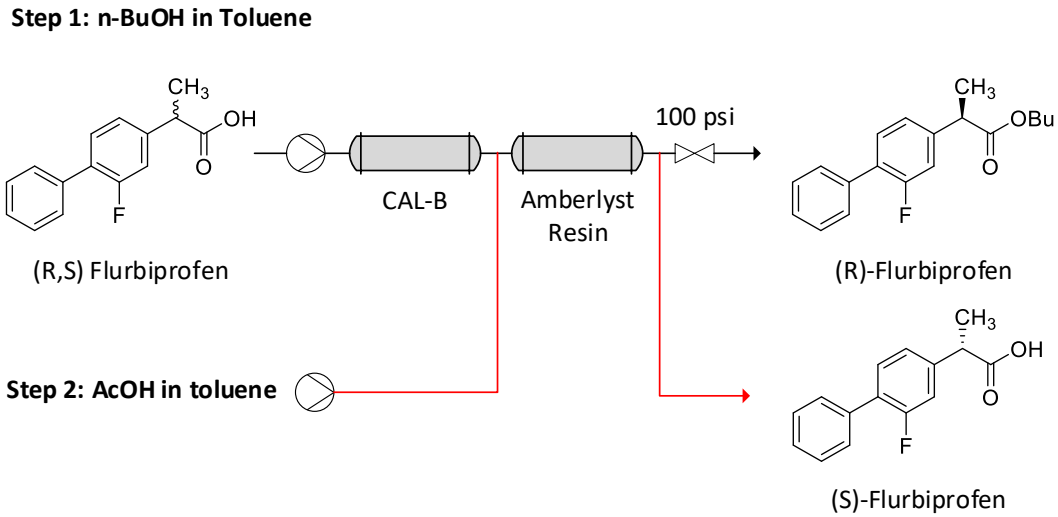

Figure 32 – Reaction scheme for the resolution and purification of (R) and (S) enantiomers of flurbiprofen from a mixture of the two. Using CAL-B lipase and Amberlyst resin to chemo-selectively react and produce the (R) enantiomer at 98% purity. The same process, without enzyme can be applied to produce (S)-flurbiprofen at 98% chemical purity and an enantiomeric excess of 92%.[99]

For the purpose of their work the (R)-enantiomer was the desired product from a (R,S)-flurbiprofen mixture. CAL-B has an enantiopreference towards the R-enantiomer, through esterification of the mixture catalysed by butanol. Although an enantiomeric excess (ee) of 90% was achieved, flow rates and overall productivity were extremely low at mere 72 µmol.min^{-1} g; this is however 10x more than the current batch process. Conditions were fairly mild, running in toluene at 60 °C, allowing for a molar conversion at a maximum of 40%. The most notable improvement was a reduction in reaction time from batch to flow. Six hours in batch down to 15-60 mins in flow, dependent on the degree of conversion desired.

Biphasic mixtures in batch can suffer from inconsistent mixing, with dead spots present in non-baffled vessels. Flow reactors have seen many developments in reactor design focusing on improving the blending of phases. This has also been applied to gas-liquid reactions, particularly biocatalytic oxidations, where oxygen solubility in water is relatively low.

Research done by Jones *et al.* explored the use of a Coflore™ agitated Cell reactor (ACR), a dynamically mixed plug flow reactor, for the biocatalytic resolution of DL-analine.[100] The reaction is highly sensitive to mixing due to the transfer of oxygen in the system and has seen difficulties with industrial scale-up. Using an ACR the group avoided the problems of centrifugal separation when materials of different density are present. They recorded uniformly sized and dispersed gas bubbles throughout the system, affording them a reduction of several hours reaction time to reach the maximum conversion.

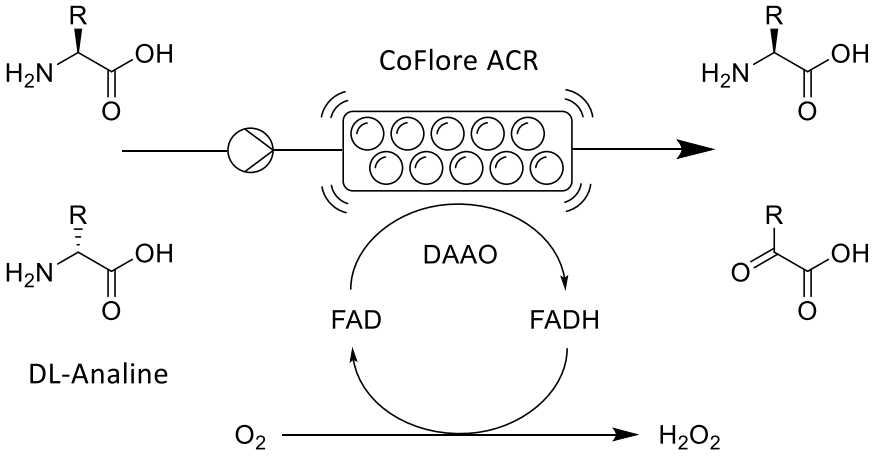

Figure 33 – Use of a Coflore™ agitated cell reactor (ACR) for the biocatalytic resolution of DL-analine using D-amino oxidase (DAAO). Oxygen is pumped into the reactor with the system uniformly distributing the bubbles throughout the biphasic mixture. FADH is a redox-active coenzyme that selectively oxidises and reduces to produce molecular oxygen.[100]

By transferring the process to a continuous ACR setup, reaction times were drastically reduced, whilst keeping enzyme loading and oxygen input comparable. A substantial improvement for production efficiency. Despite the observed improvements only one-scale-up reaction in flow was undertaken, from a 0.1 L to 1 L reactor tube. Although overall conversion reached the maximum, the time to reach steady-state (5 hrs) was longer than the 0.1 L reactor at (2.5 hrs). Oxygen solubility and transfer throughout the system is the likely cause. Larger scale columns suffer from decreased mass transfer and oxygen uptake, with gas-liquid uniformity from efficient mixing being critical.[100,101]

1.10 Aqueous Foams

Foams are defined as a gas-in-liquid dispersion.[102] Similar to an emulsion the dispersed continuous phases in foams are immiscible. For foaming to occur a stabilisation agent is necessary to prevent foam collapse. A stabilising agent can be surfactant, particle, protein and various other alternatives.[103] Destabilisation occurs when the lamellae film ruptures (coalescence) or by disproportionation; the merging of different sized bubbles (Ostwald ripening).

Foam structure varies over time, initially having a relatively low volume of gas in the form of small spherical bubbles, known as a sphere foam kugelshaum. The bubbles are enclosed by a layer of viscous liquid known as the lamella. In a surfactant stabilised foam the lamellae bond with one another, allowing the surfactants to align on this new lamella layer; stabilisation by adsorption enthalpy.[104] Over time the bubbles change to a 3D polyhedral shape, as the film thickens around the larger bubbles. Plateau borders (also known as nodes) are where 3 or more faces intersect. The film here is considerably thicker as the interfacial curvature lowers the pressure at these points. Connected plateau borders form a network for liquids to drain from the foam. After significant drainage the film begins to thin and the structure is referred to as a polyedershaum.[105]

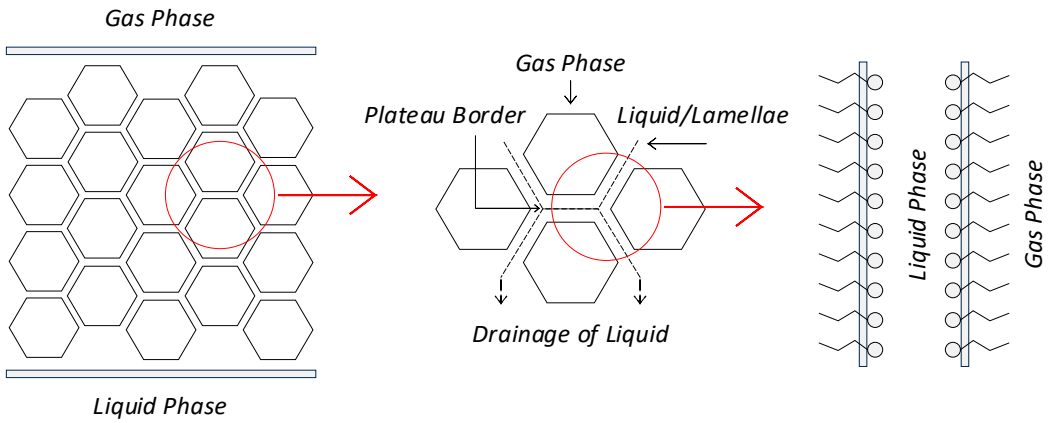

Figure 34 – Structure of a foam with a surfactant. Hydrophilic heads align towards the liquid, whilst hydrophobic tails face inwards to the gas (similar to a micelle).[103]

Foam collapse will usually occur by foam drainage; the irreversible flow through film membranes. Gravity and capillary pressure are the driving forces that drain the liquid from the lamellae. This results in a thinner film that is more susceptible to rupture. Rate of drainage can be decreased by increasing the bulk viscosity of the liquid, the surface viscosity or surface elasticity.[106] By increasing the surfactant concentration, these surface properties are altered favourably, producing strong cohesive and adhesive forces that stabilise the foam.

Foam stability can then be defined as either transient (lifetime of seconds) or metastable (lifetime of days). Transient foams are unable to withstand and ordinary disturbance whilst metastable are tolerant to thermal, static and some physical fluctuations, but will breakdown when introduced to irregular disturbances.[107] The metastable foam systems have a liquid volume fraction (ϕ). If this value is <0.05 the foam is considered dry, whilst a volume fraction >0.1 describes a wet foam (Plateau's Law).

$$Volume\ Fraction\ (\emptyset) = \frac{V_{liquid}}{V_{foam}} \qquad \text{Eqn. 26}$$

The shape of the foam can then be determined by the Young Laplace Law. [107]

$$\Delta P = \gamma\left(\frac{1}{R_1} + \frac{1}{R_2}\right) \qquad \text{Eqn. 27}$$

Where ΔP is the pressure difference across the fluid interface, γ the surface tension and R_1 & R_2 are the principal radii of curvature. The law dictates the function of surface tension is to flatten the surface of the bubbles. This is related to the pressure difference between the sides of the bubble, hence is influenced by many factors.

Surfactants are commonly used to produce foams, with the hydrophilic heads and hydrophobic tails arranging themselves similar to a micelle.[108] Mechanical agitation can be used to form a foam, however for improved control, pressurised air is used. A third, less used method is the *in-situ* generation of gas. The nucleation of gas in the liquid produces a supersaturated solution enabling rapid foam formation. Surfactants can then be used to reduce the surface tension, helping prevent rupture. When charged surfactants are used, a combination of Van der Waals attraction and the repulsion of adjacent interfaces balance the film and improves stability. [109] It is essential that the Critical Micelle Concentration (CMC) is lower than the concentration of surfactant for the optimum stability.

Protein stabilised foams have a desired foamability that remains stable under a range of dynamic conditions, including mechanical and thermal. Collapse is usually caused by denaturation of the protein at the air/water interface through either absorption or conformational changes.[110] Unlike long-chain hydrocarbon-based surfactants, proteins have greater elasticity allowing the foam to adjust its surface tension based upon the infliction of stress. However, with less ionic nature and minimal electrostatic interaction, stabilisation comes from mainly the Gibbs-Marangoni effect.[108] Also known as mechanical dynamic surface elasticity, the effect restores thickness of the film to prevent thinning and is directly proportional to the compactness of the surface monolayer.

Particle stabilised foams contain small hydrophobic particles that act as stabilising agents, similar to Pickering emulsions.[111] The particles are absorbed at the air/water interface reducing the surface energy, however unlike proteins or surfactants they do not alter the surface tension. Instead their absorption results in firm and thick foams with improved bubble stability.[112] The contact angle in these systems is 90° rather than 120° present at normal plateau borders, producing a more rigid structure.

A study by Erasov *et al.* demonstrated that foams containing particles, not used as stabilisers, have similar viscosity properties to those without.[113] However, at high solids concentration foam drainage is halted resulting in a viscosity increase, similar to a slurry. A further study by Al Yousef *et al.* reported the flocculation of nanoparticles on a foam, increasing the viscosity and reducing the rate of foam drainage.[114] Their work suggests at higher solids concentrations a more stable foam is produced as less drainage occurs. The report analysed the effects of solids on a compressed air generated foam under pressure from a back-pressure regulator (BPR). With a range of non-ionic surfactants used to generate the foam. A simple shaking approach was used to generate the foam, with no comparison between passive and active mixing. The report observed in detail the reduction in foam quality at higher surfactant and solids concentrations, due to increased flocculation.

The addition of surface-active molecules (such as insoluble particulate) result in an immobile surface. A mobile surface is present at the gas-liquid interface; the boundary is tangentially mobile, whilst an immobile surface cannot move.[115] The layer of packed surfactants at the surface of the gas-liquid boundary inhibits the diffusion of gas, lowering the mass transfer of the system. In relatively fast oxidation reactions this becomes the rate limiting step. A foam containing no surfactant has between a 70-200% increase in mass transfer compared to interfaces with surfactant.[115] Surfactants lower the surface tension at the gas-liquid boundary, reducing the driving force of gas diffusion into the liquid. The effect occurs in surfactant, protein and particle stabilised foam systems.

1.11 Life-Cycle Assessment (LCA)

Petrochemicals have been vital for the production of many important chemicals in the polymer, solvent, pharmaceutical and agricultural industries. With fossil fuel resources depleting biomass is the ideal, sustainable substitute. It is a source of carbon with large contents of carbohydrates, celluloses and fatty acids. Life-cycle assessment (LCA) is the industry chosen method to evaluate the environmental feasibility of biomass and waste conversions.

Numerous studies have shown the potential biomass has a feedstock replacement, ranging from production of biogas to the more novel biorefinery approach. For biomass conversion technologies to replace current fossil fuel products the systems need to be highly efficient, utilising all aspects of the biorefinery approach. Such a synergetic approach benefits from improved economics, reduced energy cost and most importantly a lower carbon footprint.

All inputs/outputs and external factors, such as transport, are taken into account to determine the environmental impact of a product. There are several approaches usually taken with the most common being: Cradle-to-Cradle, Cradle-to-Grave, Cradle-to-Gate and Gate-to-Gate. What each represents is summarised in the below diagram.

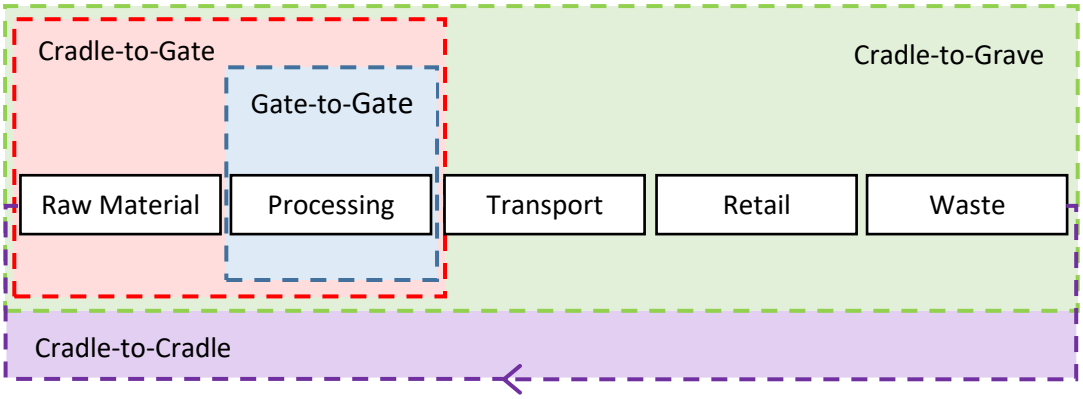

Figure 35 – Summary of life-cycle assessment approaches for a designated system. Cradle-to-cradle typically assumes the product is being recycled with minimal disposal to waste.

In accordance with ISO 14040/14044 assessments are conducted following a regime split into four distinct steps. Each phase depends on one another, with continuous assessment crucial to optimisation of the analysis as the process goes further in-depth. Each phase is listed below:

1. Goal & Scope
    - Define what is to be analysed and how deep the analysis will go.
2. Life-Cycle Inventory
    - Looks at the environmental inputs and outputs of the system.
3. Impact Assessment
    - Evaluate how significant each impact is.
4. Interpretation
    - Identify significant issues and evaluate the study.

The Goal and Scope serves three purposes: to define if it's a product or service being assessed; to determine what system it will be assessed in and to determine what will be excluded from the process. These enable a definition of the product life-cycle along with the choice of relevant impact categories. Importance is emphasised on the latter exclusion process, preventing the accumulation of non-relevant social and economic implications.

The second step quantifies the inputs and outputs. Measuring everything that enters and leaves the system defined in phase 1. This can include; raw materials, types of energy, water and emissions to air. This phase is typically the largest portion of work within an LCA. Data used is collected from professionals extensively trained in the standards that define an LCA, with industry averages used if data is unavailable.

Phase 3 selects indicators and models to precisely define the impact categories. With a variety to choose from, not all will be applicable, this depends on the goal and scope. Most of the impact categories are given as equivalents, typically CO_2-e (carbon dioxide equivalents). Several emissions can contribute to the same impact category; global warming potential (GWP) is also impacted by methane and nitrous oxide emissions, along with CO_2.

The fourth phase isn't necessarily the final one. Interpretation happens throughout the assessment and is used to identify issues in the LCA and LCIA (Life cycle Impact assessment), to evaluate the robustness of the study (it's completion, consistency and precision) and conclude with limitations and recommendations. Evaluation of correct measurement is key, otherwise recommendations lead to inaccurate assumptions.

Finally, all the emissions of the product or service can be identified, allowing comparisons to other products in a portfolio or industry. The completed LCA can be used to classify the largest impacts to the product for targeted reduction. This could be more efficient manufacturing or closer raw material acquisition for reduced transport time.

Considerable literature on the LCA of biorefineries has been undertaken in recent years, focusing heavily on the gate-to-gate and cradle-to-gate production of bioplastics.[116–120] Whilst bioplastics already in production have full cradle-to-grave or cradle-to-cradle LCA's.[121] The European commission produced a report in 2020 on the available and alternative feedstocks for production of currently non-renewable items, these include; beverage bottles, packaging film, mulch film, insulation board and automotive interior panels.[118] For PET beverage bottles several options are stated for a renewable alternative for ethylene glycol and terephthalic acid.

The cradle-to-grave production of a PET bottle has multiple routes listed, defining levels of bio-renewability based on the quantity of materials produced from renewable sources. The system boundary begins at the production from biomass cultivation (cradle) to the end-of-life (grave).[118] With grave options listed as; recycling, incineration, landfilling, composting and anaerobic digestion. The report focuses heavily on transport and recycling of each polymer with considerable assumptions on polymer production and intermediate synthesis. However, a detailed analysis of the cultivation and all end-of-life scenarios is completed for each dedicated route.

A report by Sadhukhan *et al.* studied the impact of five different biorefinery and process synthesis systems.[122] Notably the production of modified natural biopolymers; starch, cellulose and lignin composites. For each route a simple cradle-to-gate approach was taken, beginning at the crop. As seen prior, heavy focus was given to the end-of-life impacts, noting the importance of energy requirements to the system. Further study excluded the feedstock harvesting and focused on comparing gate-to-gate production of specific polymer blends. A functional unit of 1 kg was chosen in combination with a secondary functional requirement; each polymer must have a minimum tensile strength of 5 MPa. The life-cycle inventory assessment neglected synthesis information, including minimal information on water, glycerol and starch.[122]

Life-cycle assessments have limitations, not all information can be included in a report and numerous assumptions, estimations and calculations are made. A balance between available robust data and literature assumptions is necessary to produce a reliable assessment.

Chapter 2 - Comparison of oxidative techniques for the conversion of HMF, DFF and FFCA to FDCA

2.1 Introduction

The synthesis of 2,5-furandicarboxylic acid (FDCA) from its precursors; glucose, fructose and 5-hydroxymethylfurfural (HMF), use transition or noble metal catalysts to perform the oxidation, each method has its associated disadvantages (high cost, poor environmental credentials and lack of feasible manufacture). Recent work, mentioned in Chapter 1, has sought to address at least one of these problems by using enzymes as a greener alternative. When developing a cost-competitive process, to help determine the most suitable procedure for large-scale manufacture, it is important to consider a wide variety of synthesis techniques.

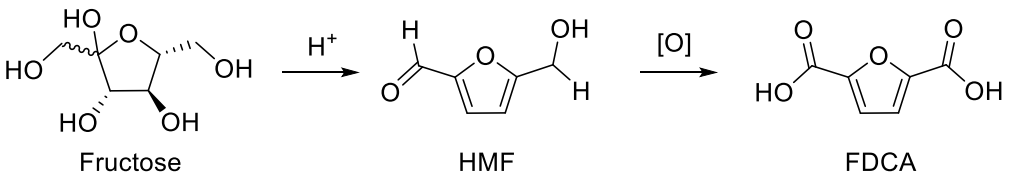

Figure 36 – 2,5-furandicarboxylic acid (FDCA) from its precursors; fructose and 5-hydoxymethylfurfural (HMF).

As with most oxidations using air as the oxygen source in either batch or continuous flow, the concentration of oxygen in solution, and its diffusion rate (mass transfer), is critical and typically rate determining. Chapman *et al.* sought to remedy this using hydrogen peroxide as an oxygen source.[123] The decomposition of hydrogen peroxide can be facilitated by chemo-catalysis, photo-activation and enzymatically. Chapman *et al.* selected the enzyme catalase, as it possessed high activity and the capability to generate oxygen at concentrations greater than the equilibrium solubility, resulting in significant increases in oxidation rates. As a result, residence times were suitably reduced for continuous flow.

Their initial experiments used several continuous stirred tank reactors (CSTR's) in series with hydrogen peroxide injected into each CSTR. Conversion of the substrate increased, but with the high turnover rate of catalase, super-saturation of oxygen in solution was too brief to sustain the required level of high productivity. Subsequently, to boost the continuous addition of hydrogen peroxide, a multi-point injector reactor (MPIR) was designed with 11 simultaneous injection points.

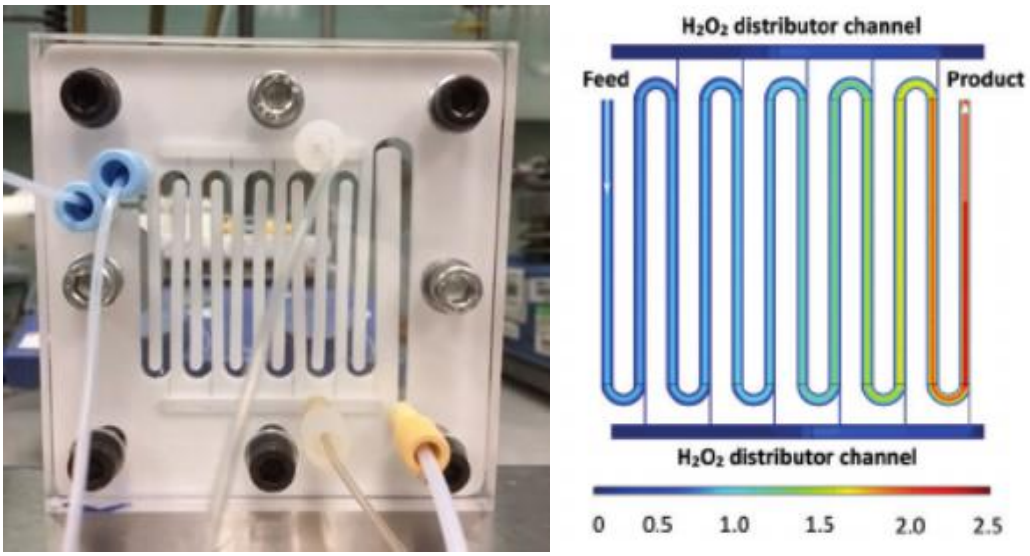

Figure 37: [left] Multi-point injection reactor (MPIR) developed by Chapman et al. for the continuous injection of hydrogen peroxide throughout a reactor; [right] flow velocities through the reactor channel (mm s^{-1}) with hydrogen peroxide added through 11 ports. Hydrogen peroxide is added at the most turbulent sections of the channel which are the 180° turns visible above.[123]

After optimising the reactor and chemical conditions, the substrate scope was expanded to 12 aryl alcohols and 3 heteroaryl alcohol substrates. All were oxidised selectively to aldehydes without over-oxidation to the carboxylic acid and resulted in good yields. Of note, is the oxidation of 5-hydroxymethylfurural (HMF) to 2,5-diformylfuran (DFF) using a modified galactose oxidase ($GOase_{M3-5}$). Using conditions similar to Carnell *et al.*, the substrate, a solution of horseradish peroxidase (HRP) and catalase were fed into the system to give 85% conversion of HMF to DFF.[33]

A low concentration of HMF was used as the product (DFF) suffered from poor aqueous solubility. This prevented the formation of solids that could cause blockages in the microreactor system, limiting the productivity. Unfortunately, the system used free enzyme, without the use of immobilisation. Having three enzymes present in solution can complicate downstream processing. The cost of single use enzymes and the use of buffer solutions is considerable, impacting the possibility of large-scale production.

The next sections examine the various reactions used to form FDCA from HMF, DFF and FFCA. A variety of pertinent oxidation reactions were chosen to apply to furan-based substrates, with the aim of finding a suitable synthesis for either batch or continuous flow production. A green process suitable for large-scale production was beneficial to the objectives of this research.

2.2 Oxidative reactions for the formation of FDCA from HMF

Figure 38 shows an oxidative route from HMF to FDCA through the partial oxidised DFF and FFCA. If oxidation of the HMF aldehyde occurs instead of the alcohol, another intermediate, 5-hydroxymethyl-2-furancarcarboxylic acid (HMFCA) is possible.

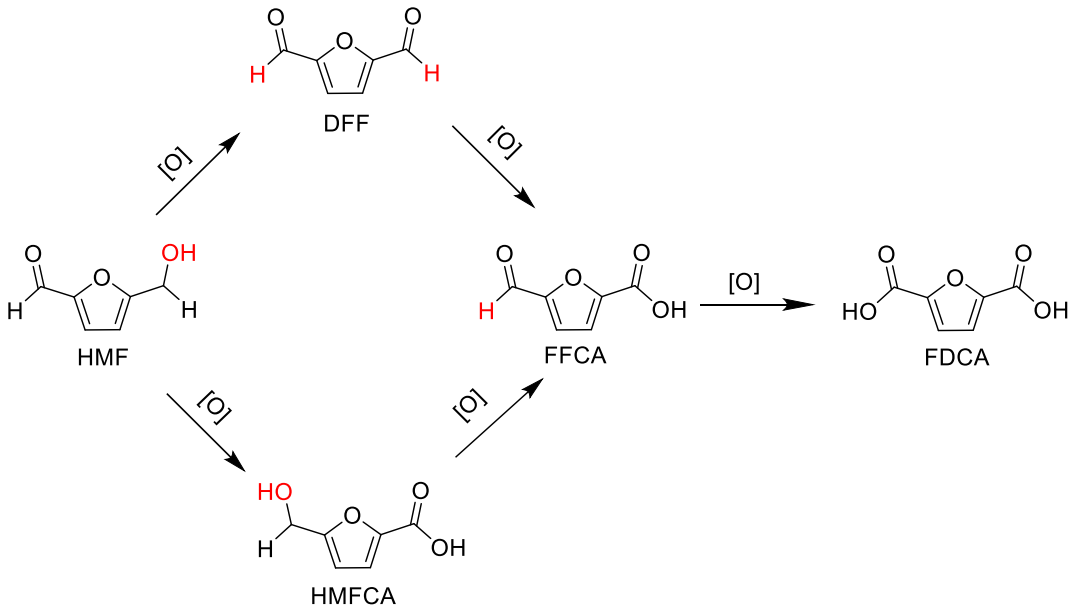

Figure 38 – General reaction scheme for the oxidation of 5-hydroxymehtylfurfural (HMF) through the intermediates diformylfuran (DFF) and 5-formyl-2-furancarboxlyic acid (FFCA) to the product 2,5-furandicarboxylic acid. Sites of oxidation have been highlighted in red.

A variety of oxidation techniques have been tested on HMF, DFF and FFCA. These include; sodium tungstate dihydrate (Noyori), Cannizzaro, CAL-B lipase and Oxone™.[54,124–126] The following sections explore the published reactions and apply them to the substrates of interest shown in Figure 38.

2.2.1 Noyori oxidation

Sodium tungstate dihydrate has been used extensively for the epoxidation of alkenes, and the oxidation of primary and secondary alcohols to the corresponding aldehyde and ketone.[52,55] Tungstate catalysts function in biphasic mixtures; facilitating oxidation in the organic fraction and dissolution in the aqueous phase for downstream recovery (as shown in Chapter one). This requires the *in-situ* formation of a pertungstate to undertake the oxidative process, initiated by an oxidiser, usually hydrogen peroxide. A phase-transfer catalyst (PTC) is required to transfer the pertungstate from the aqueous phase to the organic. Methyltrioctylammonium hydrogensulfate is a notable PTC used in the procedure; providing increased hydrogen peroxide stability at elevated temperatures.[53]

The first reported use of sodium tungstate for oxidations and epoxidations was reported by G.B. Payne and P. H. Williams,[52] which was further improved by Noyori *et al.*[54] The authors used hydrogen peroxide as an oxidiser to produce the pertungstate *in situ*. In addition to a PTC, their ternary system included aminomethylphosphonic acid due to its high activity toward olefin substrates, the resulting epoxidation affording 1,2-epoxydocecane from 1-dodecene.[53] Toluene and water provided the biphasic conditions ideal for the sodium tungstate system as shown in Figure 39.

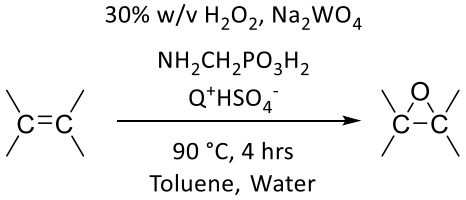

Figure 39 – Epoxidation of the olefin 1-dodecene to 1,2-epoxydocecane using 30% w/v hydrogen peroxide, olefin, sodium tungstate, (aminomethyl)phosphonic acid and methyltrioctlyammonium hydrogensulfate in a 150:100:2:1:1 molar ratio. Q refers to a lipophilic cation ($CH_3(n\text{-}C_8H_{17})_3N$).[53]

Reactions were carried out at 90 °C with all reagents combined in a flask; a significant risk considering the large volume of hydrogen peroxide at high temperature. The authors did not consider the use of a batch-fed or continuous flow system; a change that would reduce the equivalents of oxygen used, improve safety and lower conversion times.

Further work by Noyori *et al*. sought to improve on the oxidation of alcohols to aldehydes and carboxylic acids.[54] Again, a biphasic mixture was employed between octanal and hydrogen peroxide, forming the octanoic acid at 85% yield after 2 hours, shown in Figure 40. The reaction proceeds through the aldehyde intermediate and cannot be halted at this stage, continuing to oxidise further through to the carboxylic acid. The oxidation advances by formation of a hydrate with primary alcohols affording greater conversion than secondary or tertiary alcohols.

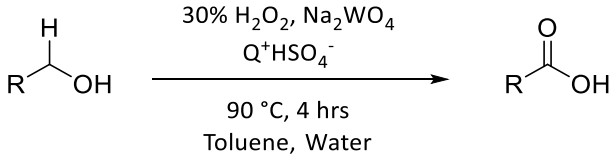

Figure 40 – Oxidation or primary alcohols using sodium tungstate dihydrate in combination with hydrogen peroxide and the phase-transfer catalyst, methyltrioctylammonium hydrogensulfate. Q refers to a lipophilic cation ($CH_3(n\text{-}C_8H_{17})_3N$).[54]

Based on the recent and suitable Noyori reactions in the literature, the process was applied to HMF, DFF and FFCA. The work recorded in this sub-section examines the results of numerous modifications to the published Noyori reactions.

- Altering solvent conditions (using both mono and biphasic mixtures).
- Temperatures (ranging between 25-90 °C).
- Removal of the phase-transfer catalyst (PTC).
- Reaction time (ranging between 60-240 mins).
- Equivalents of peroxide (4.7-23.0 equivalents).

Table 1 – Optimisation of sodium tungstate catalysed oxidation of HMF.

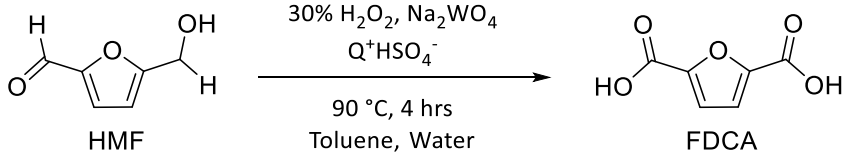

Entry	H_2O_2 equiv	Temp (°C)	Reaction time (mins)	Remaining (%) HMF [d]	Conversion (%) [d]				Mass Balance (%)
					HMFCA	DFF	FFCA	*FDCA*	
1[a]	4.7	90	240	0.0	0.5	0.0	0.3	4.6	-94.6
2[b]	4.7	90	240	15.1	1.1	0.0	0.2	2.9	-80.7
3[b]	4.7	50	240	3.9	0.9	0.0	0.1	4.0	-91.1
4[b]	4.7	25	240	38.0	0.2	0.0	0.1	0.8	-60.9
5[b]	23.0	25	240	1.3	0.2	0.0	0.0	2.2	-96.3
6[a]	1.0	90	240	21.8	1.8	0.0	0.3	1.4	-74.7
7[a]	4.7	90	120	1.3	0.8	0.0	0.1	2.7	-95.1
8[a]	4.7	90	60	0.5	1.0	0.0	0.0	3.0	-95.5
9[b,c]	23.0	90	240	0.0	0.0	0.0	0.0	0.9	-99.1

[a] reaction used a 1:1 mixture of toluene and water as solvents, [b] reaction used water a solvent with no toluene, [c] no phase transfer catalyst was included in the reaction and [d] determined by HPLC analysis. Equiv = molar equivalents of hydrogen peroxide compared to HMF, temp = temperature.

However, all these resulted in a similar outcome: up to 100% HMF conversion with a high of 4.6% FDCA. All the reactions showed formation of HMFCA with minimal FFCA and no DFF, indicating the oxidation was preferentially oxidising the HMF aldehyde rather than the alcohol. Only 16 mg of a compound was isolated from a reaction that started with 1 g of HMF. The ^{1}H NMR analysis of the compound determined it was impure. The main singlets at 8.30 and 2.34 ppm, with relative integrations of 1:1.74, fit generally with the di-keto symmetrical structure shown in Figure 41, and peaks on the baseline around 6.5 ppm may indicate the di-enol tautomer.

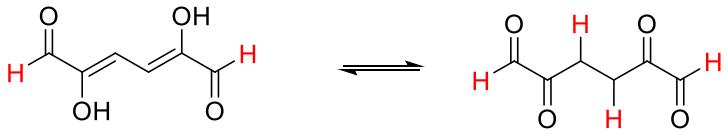

Figure 41 – Symmetrical dialdehyde-diketone compound synthesised from Noyori oxidation of HMF, tentatively identified from the below ^{1}H NMR spectra (Figure 43).

Unfortunately repeating the experiment did not produce the same product, and further characterisation of it was not possible. Related structures have been reported by Kappe *et al.* produced as a by-product from the photochemically catalysed oxidation of HMF.[127] The compound of interest is a postulated intermediate in the ring-opening of 5-hydroxy-5-(hydroxymethyl)-furan-2(5H)one (H^2HMF) to 5-hydroxy-4-keto-pentenoic acid (HKPA) (Figure 42). The structure of this compound would make it useful for further amelioration into new monomers however with little product formed using either HMF or DFF, it was decided to research other oxidative avenues.

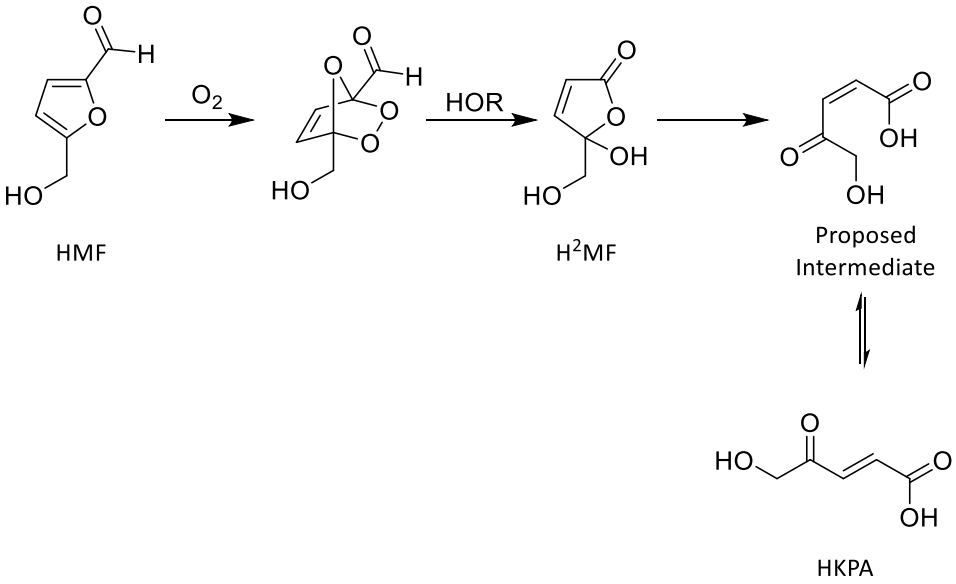

Figure 42 – Proposed mechanism for the formation of HKPA from H_2MF.[127]

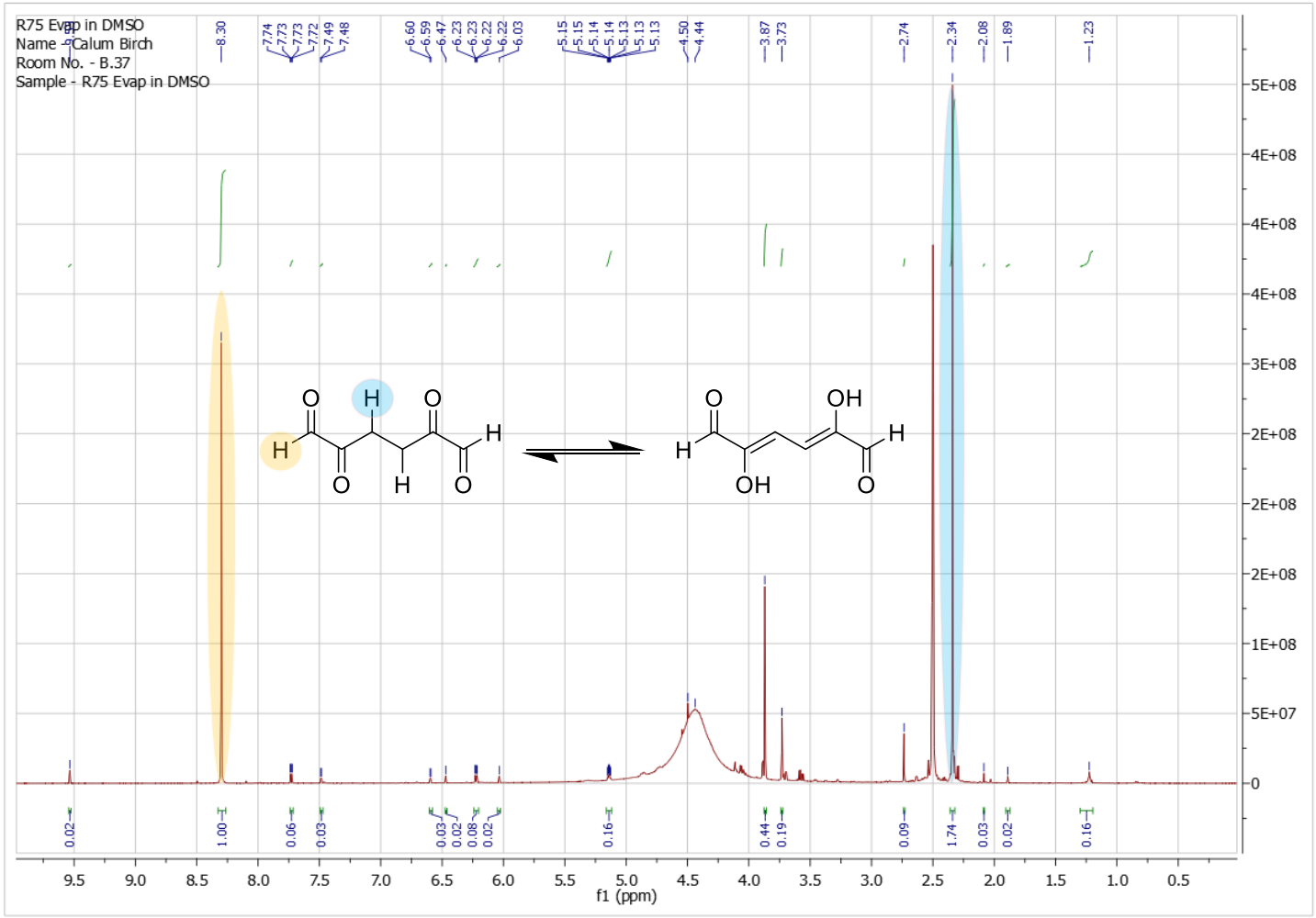

Figure 43 – ^{1}H NMR spectra obtained from an evaporated and extracted sample from the Noyori reaction with HMF, showing the dialdehyde-diketone.

2.2.2 Cannizzaro redox disproportionation reaction with HMF, DFF and FFCA

Work published by Zhang *et al.* used potassium hydroxide with hydrogen peroxide to synthesise completely oxidised FDCA in a reported 55% yield with 99% purity from HMF.[126] The system dosed in hydrogen peroxide at a maximum of 32 mmol in 20 ml of water, this provided sufficient oxygen to the reaction, shown in Figure 44.

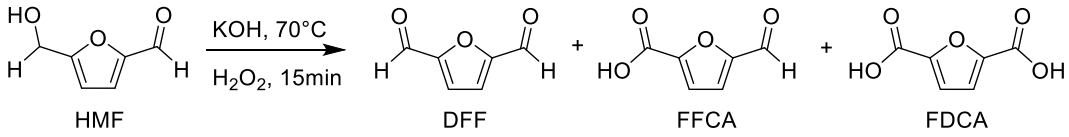

Figure 44 – Use of base and oxidant for the conversion of HMF to DFF, FFCA and FDCA by Zhang et al.[126]

Eight equivalents of hydrogen peroxide (160 mmol) were dosed manually into the alkaline solution of HMF (20 mmol) to provide enough oxidant, as it decomposes rapidly at 70 °C. Their results indicate a fast reaction that would be hazardous to scale-up. Although the results appear promising, evidence for the products is flawed. The ^{1}H NMR included as evidence of the product FDCA shows a single peak at 7.25 ppm purporting to be the aromatic protons on the furan-ring of FDCA. However, this peak also corresponds to the chemical shift of H-CCl_3 in the $CDCl_3$ NMR solvent used, since an authentic sample of FDCA has aromatic protons at 7.45 ppm.

We suspect the authors may have inadvertently used the Cannizzaro reaction. This involves the simultaneous transformation of two moles of aldehyde into a carboxylic acid and alcohol; it was discovered in 1853 by Stanislao Cannizzaro.[128] The general scheme is shown in Figure 45.

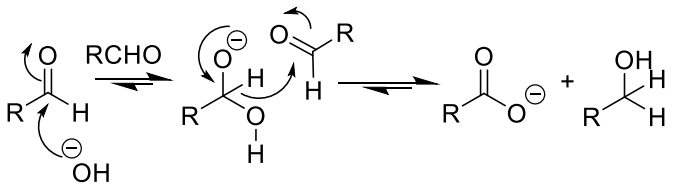

Figure 45 – General mechanism for the Cannizzaro reaction, a base disproportionation of an aldehyde to its corresponding alcohol and carboxylic acid.[128]

A hydroxide ion reacts with an aldehyde to form an acetal in which the reduction potential of the C-H proton is low enough to reduce the substrate aldehyde forming simultaneously a carboxylic acid and alkoxide. The products are stabilised when the acid protonates the alkoxide. Whilst the reaction is reversible, the equilibrium favours the carboxylate and is accelerated by a strong base and high substrate concentrations. The Cannizzaro reaction with furfural has been reported by Janczewski *et al.* to yield furan-2-carboxylic acid and furfuryl alcohol.[129] The reaction was microwave assisted, using Al_2O_3 as a catalyst for the reaction shown in Figure 46. The group ground the reagents beforehand in a mortar and pestle, increasing the yield to 35%, indicating surface activation of the alumina. Alterations were made to the conditions, to form the furfuryl alcohol, however without success.

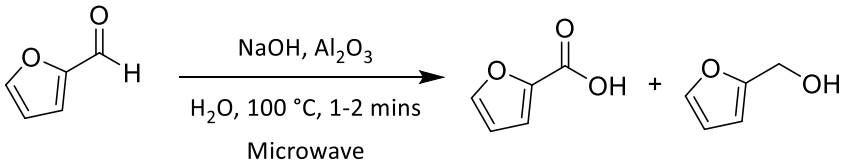

Figure 46 – Microwave assisted Cannizzaro reaction, using aluminium oxide as a catalyst for the base disproportionation of furfural aldehyde.[129]

For this project the reaction can provide conversion <20% to FDCA without the need for any catalysts, requiring a basic solution with hydrogen peroxide. The buffer system used for enzymatic oxidations is slightly basic (pH 7.4), and is a suitable environment for the process to occur, hence the need for further research.

Following on from the previous sub-section, the Cannizzaro reaction was tested with HMF, DFF and FFCA. Also tested, was a reaction mixture containing DFF in an aqueous buffer, produced by a galactose oxidase catalysed oxidation of HMF using hydrogen peroxide. Due to the nature of the base disproportionation reaction, it was important to analyse all furan-based intermediates, as shown in Figure 38. The results are shown below.

Table 2 – Optimisation of HMF reacting with aqueous KOH and hydrogen peroxide (160 mM).

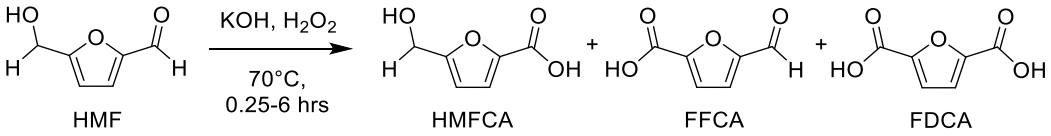

Entry	H_2O_2 equiv	Reaction time (hrs)	Remaining HMF (%) [a]	Conversion (%) [a]				Mass Balance (%)
				HMFCA	*DFF*	*FFCA*	*FDCA*	
1	8.0	0.25	1.4	0.0	0.0	11.4	0.4	-86.8
2	0.0	0.25	28.7	0.0	0.0	4.1	0.0	-67.2
3	8.0	6.00	0.0	0.0	1.0	20.0	0.0	-79.0
4	0.0	6.00	0.0	0.0	0.0	22.6	0.0	-77.4

[a] determined by HPLC analysis. Equiv = molar equivalents of hydrogen peroxide compared to HMF. Reactions used 20mM HMF. 80 mM KOH and 160 mM H_2O_2.

The addition of peroxide may have detrimental effect on the reaction, with low mass balance observed and little effect on the conversion to FFCA (Table 2). On the other hand, longer reaction times are beneficial, resulting in higher conversion and improved reproducibility. Regardless of peroxide addition, the product formed is FFCA, with minimal DFF and no HMFCA. The mechanism for this oxidation is therefore unclear, and may not involve peroxide. A problem with the reactions was the lack of mass balance. High conversion of HMF was seen without the corresponding formation of products as measured by HPLC. Insoluble solids were observed, suggesting the polymerisation of HMF into undesirable humins. Other side reactions may include peroxo-addition and ring-opened products.

To determine the effects of using a buffered system containing DFF the Cannizzaro reaction was tested using an aqueous buffered solution of GOase generated DFF. Importantly to test how much backwards conversion to HMF occurred. The results are shown below.

Table 3 - Optimisation of DFF and aqueous solution of DFF from a reaction of HMF catalysed by GOase, reacting with aqueous KOH and hydrogen peroxide.

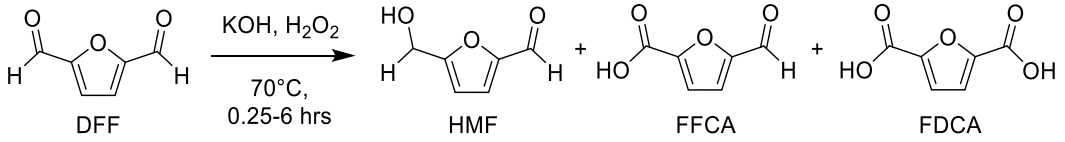

Entry	H_2O_2 equiv	Reaction time (hrs)	Remaining DFF (%) [c]	Conversion (%) [c]				Mass Balance (%)
				HMF	***HMFCA***	***FFCA***	***FDCA***	
1[a]	8.0	0.25	3.5	84.1	0.0	16.1	0.0	+3.7
2[a]	0.0	0.25	19.2	20.5	0.0	1.4	0.0	-58.9
3[a]	8.0	6.00	2.6	66.1	0.0	29.9	0.0	-1.4
4[a]	0.0	6.00	7.2	29.1	0.0	8.9	0.0	-54.8
5[b]	8.0	0.25	100.0	0.0	0.0	0.0	1.1	+1.1
6[b]	0.0	0.25	100.0	0.0	0.0	0.0	0.0	0.0
7[b]	8.0	6.00	100.0	0.0	0.0	0.0	1.1	+1.1
8[b]	0.0	6.00	53.7	0.0	0.0	0.0	0.0	-46.3

[a] used a solid sample of DFF, [b] aqueous buffered solution of DFF from a reaction of HMF catalysed by GOase, selectivity calculated from the average quantity of DFF/FFCA already present in the solution and [c] determined by HPLC analysis. Equiv = molar equivalents of hydrogen peroxide compared to DFF. Reactions used 20mM DFF. 80 mM KOH and 160 mM H_2O_2.

The major products formed in the reactions were HMF and FFCA, in varying quantities. Without peroxide more conversion is observed, with the majority as backwards progression to the HMF (Table 3). The mass balances are improved without peroxide, and Entry 3 shows a useful level of FFCA. In the reactions using the DFF solution, little conversion is observed, other than Entry 8 where peroxide addition converts 53% HMF, but with not corresponding product formation.

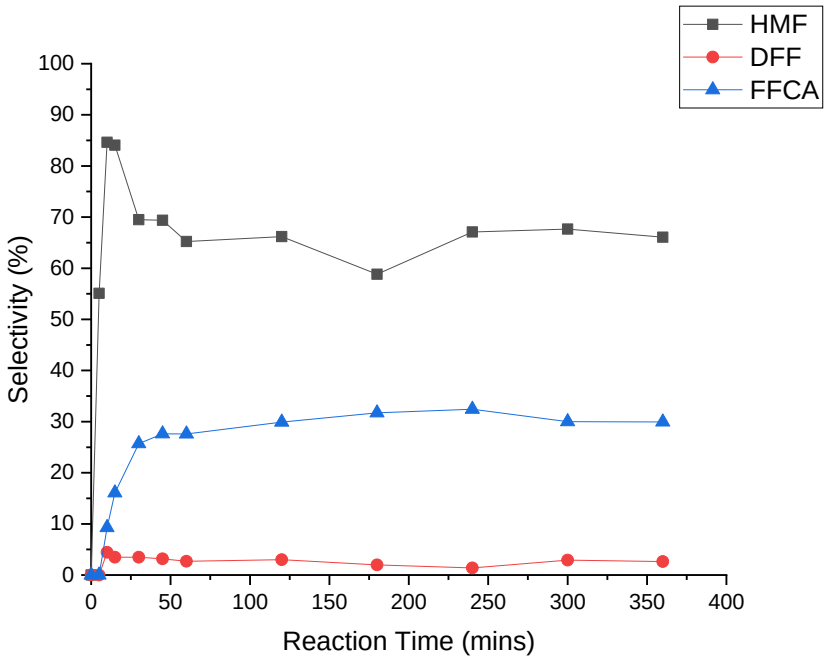

Figure 47 – DFF with potassium hydroxide and hydrogen peroxide over 6 hours, simulating the conditions described in Zhang et al. (Table 3, Entry 13).[126]

The peroxide was added over 15 minutes and was consumed in 30 minutes, Figure 47. The HMF concentration increases rapidly to 83% then decreases to 70%, remaining steady thereafter. FFCA starts to form after 15 minutes and slows after 30 minutes, which matches the peroxide levels. The formation of HMF from DFF is a reductive process, however the oxidative conditions contradict this mechanism.

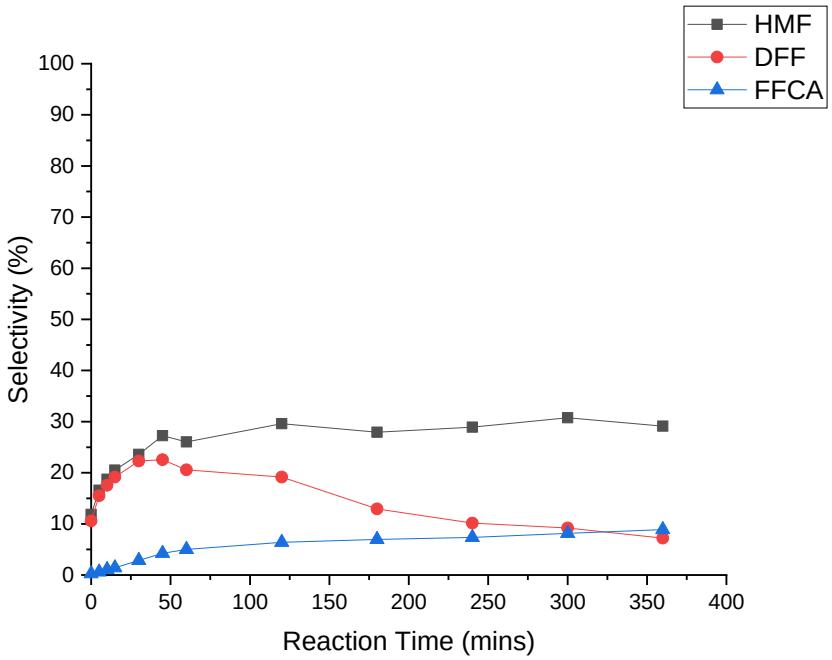

Figure 48 – DFF with potassium hydroxide over 6 hours and no hydrogen peroxide. Timepoint t=0 has been highlighted as an anomalous result. With undissolved DFF still present in the reactor (Table 3, Entry 4).

The profile for the reaction without hydrogen peroxide is different (Figure 48). The conversion to HMF is 30% after 50 minutes, the concentration of FFCA increases to 10% after 360 mins. The ratio of HMF to FFCA at the end of the experiment is 3:1. The rate of DFF conversion is half the rate of increase of FFCA and implies that FFCA is in equilibrium with some other product, which may be its acetal. Only 2% HMFCA was seen in this experiment.

The Cannizzarro reaction is a redox reaction, however the mechanism requires a 1:1 stoichiometry of HMF and FFCA, and less than half the expected FFCA is seen, likely forming another product. A complicating factor in these experiments is the reaction of hydroxide with aldehydes to form acetals, so HMF, DFF, and FFCA may all exist as either mono- or di-acetals that form rapidly and reversibly. FFCA may be in equilibrium with its acetal, this can be checked by altering the pH.

To further understand the reaction of hydroxide with DFF, ^{1}H NMR experiments were carried out at a pH range from 5-9 in deuterated water with either deuterated sulphuric acid or sodium deuteroxide. The compound undergoes a base induced disproportion, forming the compounds shown below, Figure 49. The protons on each species have been tentatively assigned, Figure 50. Five distinct peaks are visible at *ca.* 9 ppm representing aldehyde protons. The largest is DFF, the peak at 9.4 has been assigned to DFF-acetal (hydrate), the three small peaks may be HMF, FFCA and HMFCA.

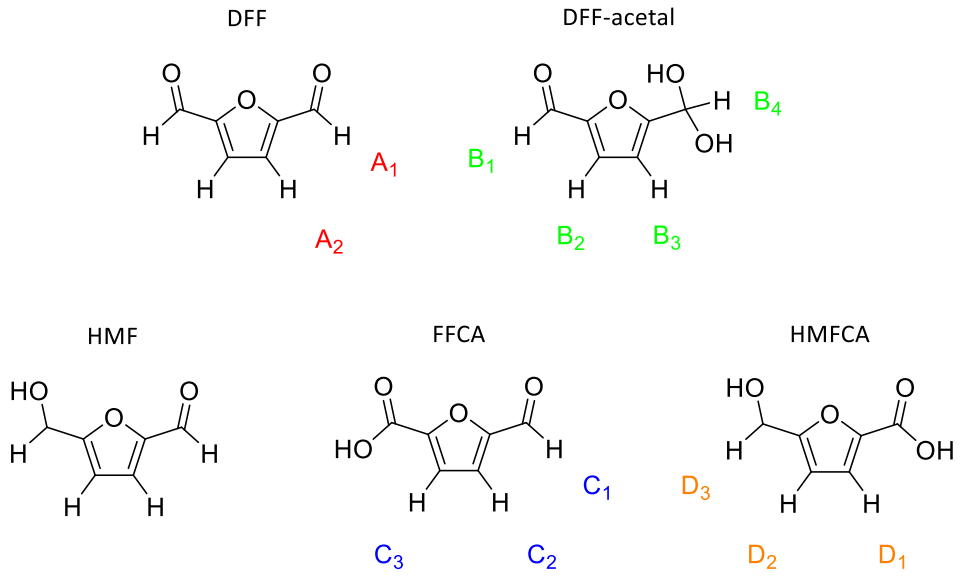

Figure 49 – ^{1}H NMR peak assignments for the compounds DFF, HMF, FFCA and HMFCA in sodium deuteroxide at pD 8(Figure 50).

Labelling off the protons in Figure 49 corresponds to their chemical shift on the 1H NMR in Figure 51. The ^{1}H NMR at pD 5 shows only the presence of DFF and its hydrate (H*). The ratio of both species is 0.74 to 0.26 and is similar to the ratio at pD 8. Only the sample at pD 8 shows formation of other species. The expected aldehyde proton peak for HMF at 9.6 ppm was not observed, indicating none present in the sample (Figure 49). Using these samples, the solubility of DFF was determined against an internal standard (Deuterated dimethyl sulfone) as 40 mg mL^{-1}.

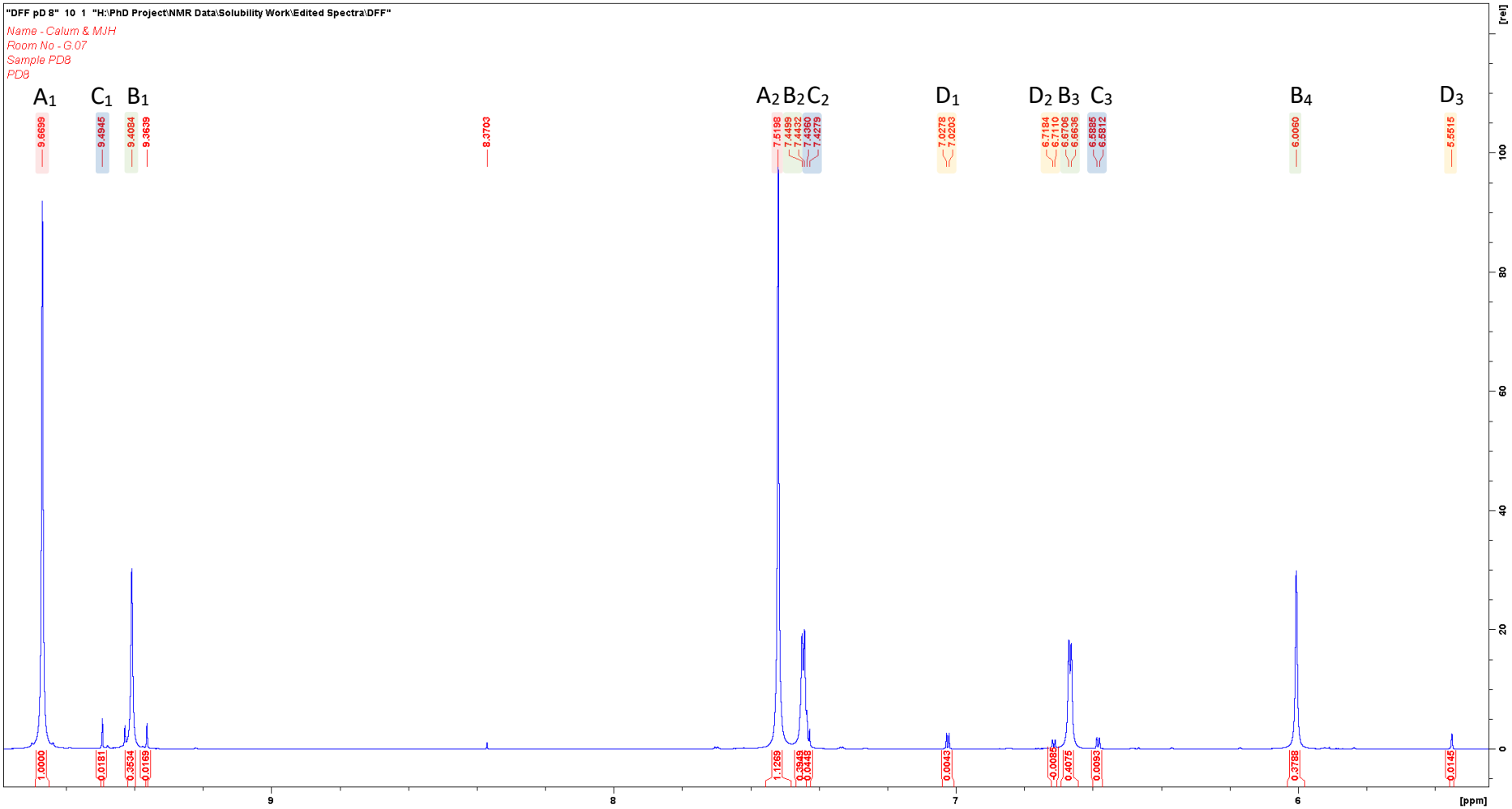

Figure 50 – ^{1}H NMR of DFF in sodium deuteroxide at pD 8.

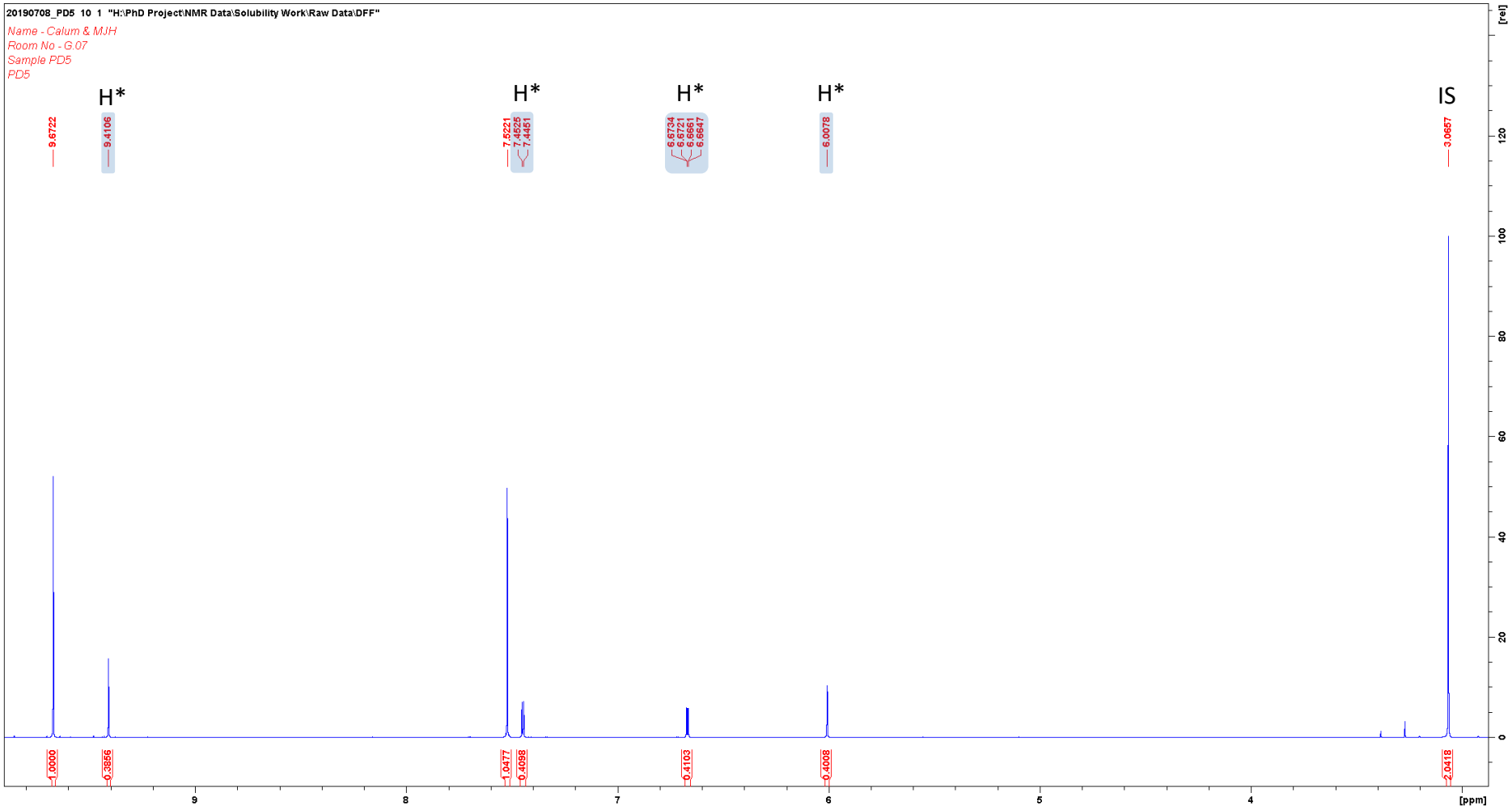

Figure 51 - ^{1}H NMR of DFF in deuterated sulphuric acid at pD 5. Spectrum indicates the presence of the DFF hydrate (H). With added Dimethyl sulfone IS.*

All intermediates required testing, including FFCA. As shown in Figure 50, FFCA is present in basic conditions when starting with DFF, hence conversion is possible in both directions. Producing FDCA forwards and the remaining intermediates backwards. The results are shown below.

Table 4 – Optimisation of FFCA reacting with aqueous KOH and hydrogen peroxide.

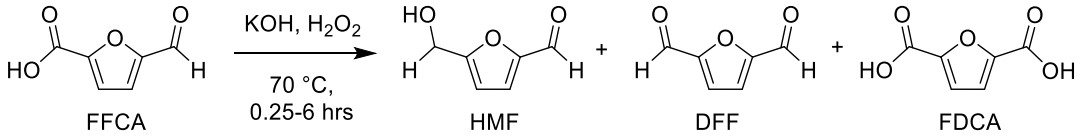

Entry	H_2O_2 equiv	Reaction time (hrs)	Remaining FFCA (%) [a]	Conversion (%) [a]				Mass Balance (%)
				HMF	*HMFCA*	*DFF*	*FDCA*	
1	8.0	0.25	44.6	0.0	0.0	0.0	4.8	-50.6
2	0.0	6.00	19.5	0.0	0.0	0.0	28.8	-51.7

[a] determined by HPLC analysis. Equiv = molar equivalents of hydrogen peroxide compared to FFCA. Reactions used 20mM FFCA. 80 mM KOH and 160 mM H_2O_2.

Addition of peroxide to FFCA produced FDCA at prolonged reaction times, suggesting the oxidation of FFCA to be slow compared to HMF and DFF (Table 4). The mass balances show a 50% loss, which isn't ideal. Notably no backwards conversion to HMF, HMFCA or DFF is observed, with the only product produced being FDCA.

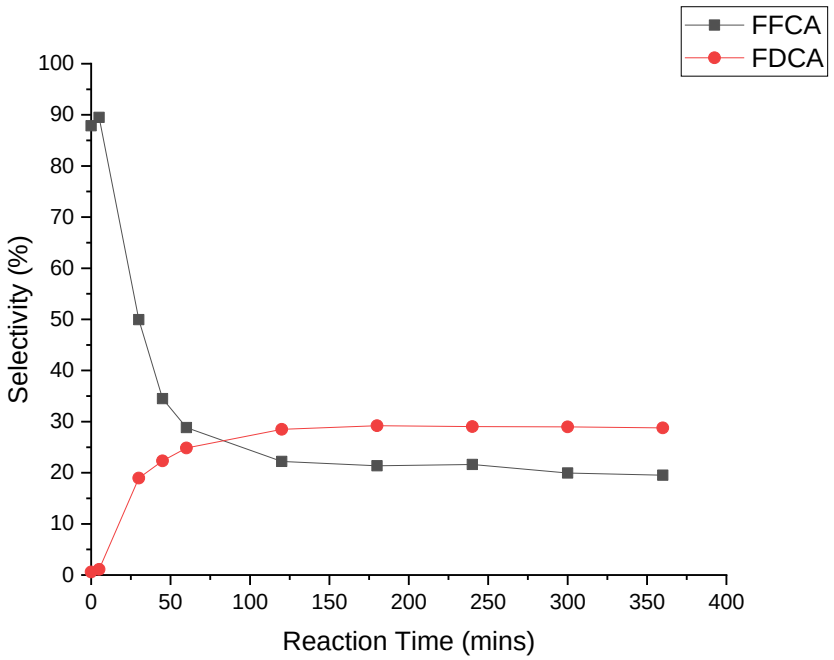

Figure 52 – FFCA with potassium hydroxide and hydrogen peroxide added over 6 hours (Table 4, Entry 2).

FFCA was reacted with hydroxide and peroxide. Figure 52 shows reaction of FFCA and formation of FDCA. The reactions tail-off at 125 minutes, at which point no peroxide remains (tested with starch paper), but the pH is still highly alkaline. Surprising is the lack of HMFCA that is the co-product in the Cannizzaro reaction. This might be oxidised or form an acetal that is undetected. The poor mass balance is a concern, and further work is required to understand this. The reaction would benefit from reduced temperatures, continuous addition of H_2O_2 and the short contact times available in a flow system.

2.2.3 Lipase catalysed oxidation of HMF, DFF and FFCA

Candida antarctica lipase (CAL-B) from yeast has been used successfully in many hydrolase processes because of its solvent and temperature stability, broad chemo- and high enantio- selectivity; the Lipase A variant has much less activity.[47] Furthermore, the immobilised form has benefited large-scale applications.[130] The engineered version, Novozym 435,[131] is a commercially available form of CAL-B immobilised on acrylic resin beads and has increased catalytic efficiency, higher temperature tolerance and can be repeatedly re-used, or in a fixed bed continuous flow. The enzyme functions in anhydrous environments, for example ethyl acetate, acetonitrile and tert-butanol (t-BuOH) solvents.

Despite CAL-B being a hydrolase, Ning *et al*. reported its use in the oxidation of DFF to FDCA.[132] They used a co-solvent system of 1:1 ethyl acetate and t-BuOH with hydrogen peroxide; the solvent composition was essential for activity. From their report it is unclear what the reaction mechanism is. One possibility is the catalysed hydrolysis of ethyl acetate to acetic acid, then an uncatalyzed reaction with peroxide to produce peroxyacetic acid, which then oxidises DFF, Figure 53.

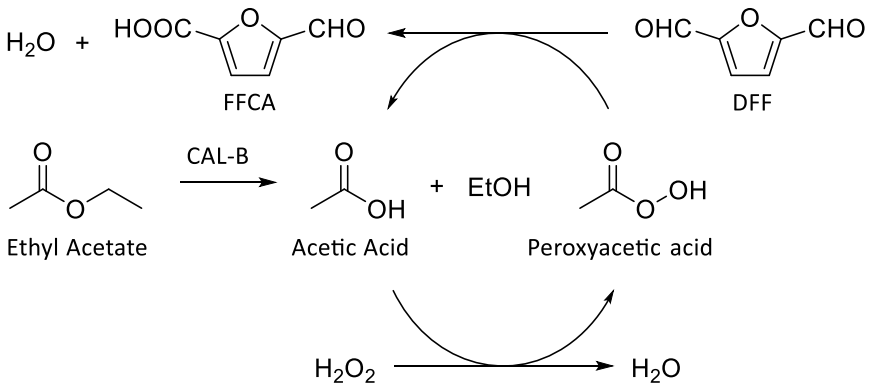

Figure 53 – Proposed mechanism of DFF oxidation with CAL-B forming acetic acid for in-situ formation of peroxyacetic acid.[125,133]

The lipase-peroxide oxidation was tested with an aqueous solution of DFF produced from galactose oxidase catalysed aerial oxidation of HMF, Figure 54.[38] Ning Li etal. extracted DFF from water using a deep eutectic solvent yielding 88-93% pure-product.[132] CAL-B then oxidised DFF to FDCA through addition of hydrogen peroxide. yielding near 95% conversion over a 24-hour period. The main problem with this system is the explosive danger of using peroxide in organic solvents which prevents scale-up.

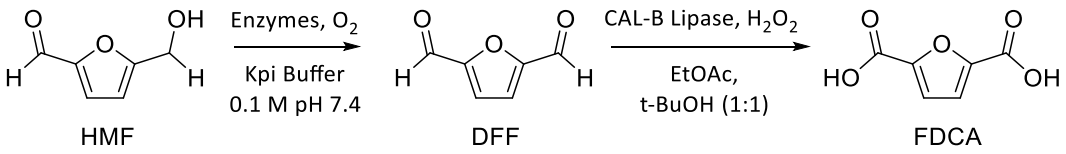

Figure 54 –Scheme for the conversion of HMF to DFF by GOase$_{M3-5}$, followed by the lipase catalysed oxidation to FDCA in an organic solvent system.[132] *Enzymes used are galactose oxidase (M_{3-5} mutant), catalase and horse radish peroxidase.*

Whilst some reports have focused on the use of *in-situ* peracid formation in epoxidation, amine oxidation and hydrolysis reactions, the problem of handling peroxides in organic solvents remains.[134,135] The explosivity problem could be overcome if peroxyacetic acid were used directly in fed-batch to an aqueous solution of DFF. Holtmann *et al*. discusses the importance of using peroxyacetic acid as a safe alternative to the current peracid formation techniques.[125,136] Industrial scale production of peroxyacetic acid is carried out by auto-oxidation of acetaldehyde, or the treatment of acetic acid with hydrogen peroxide and a strong acid catalyst.[125] The Holtmann group recently established a continuous method for the formation of peracids.[125] Although in the early stages of development, the process is noteworthy as it opens the possibility of FDCA production from DFF in continuous flow. Their system used a CSTR containing CAL-B with an inlet pump and an overflow acting as a passive outlet. A non-aqueous single-phase system was adopted in which ethyl acetate, saturated with hydrogen peroxide (20-430 mM), was pumped into the CSTR containing the immobilised and compartmentalised (with gauze) lipase, with the solution overflowing into a collection vessel.

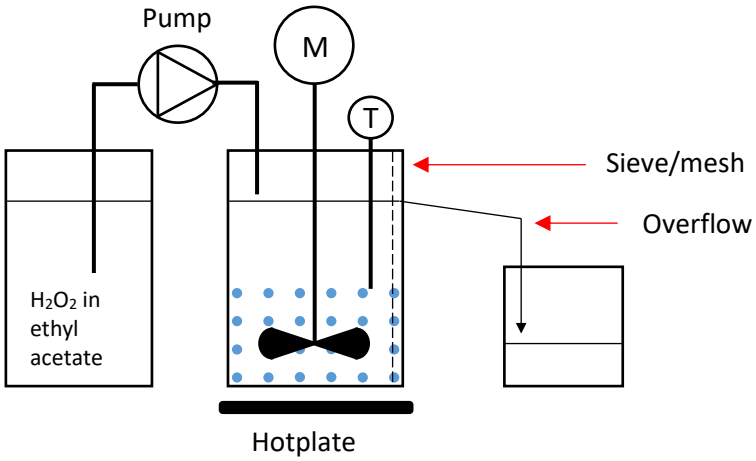

Figure 55 – Equipment used in the continuous formation of peracetic acid in a CSTR.[125] *CAL-B shown with blue circles. T = temperature probe, M = overhead stirrer.*

A one variable at a time (OVAT) experimental approach was used to test the variables. The highest reaction rates were achieved at high peroxide concentrations. Residence times of up to 45 mins were explored, with shorter times yielding faster reaction rates at the lower concentrations. Stability of the enzyme was shown to be intact over a 50 hour period, presenting an opportunity for application to the HMF process.[125] The ethyl acetate-peroxide setup still presents explosive dangers, nonetheless the details of the process are useful for developing a safer flow system.

This sub-section describes the application of CAL-B catalysed oxidations to HMF, DFF and FFCA. Furthermore, galactose oxidase synthesised aqueous buffered DFF (GOase DFF) was also tested as a possible substrate. The CAL-B oxidation reaction was selected for further study with potential for a continuous flow process. To begin, the published system was repeated at lab-scale behind a blast shield, using HMF and a 1:1 mixture of ethyl acetate and t-butanol, with the addition of hydrogen peroxide every hour over the first six hours, (Table 5, Entry 1).

Although the reported process for CAL-B catalysed oxidation used DFF it was necessary to determine if oxidation is possible with HMF. This included the use of safe solvent systems (acetic acid), providing a process that can be safely scaled-up and converted to continuous flow. The results are shown below.

Table 5 – Optimisation of CAL-B catalysed conversion of HMF with hydrogen peroxide and varying solvent systems.

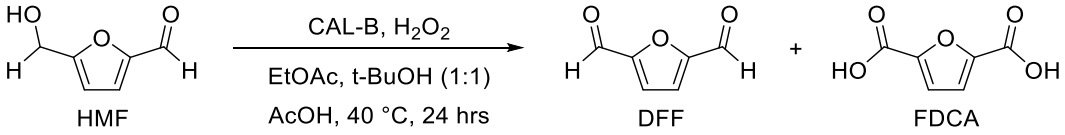

Entry	Solvent system	Remaining HMF (%) [c]	Conversion (%) [c]				Mass Balance (%)
			HMFCA	***DFF***	***FFCA***	***FDCA***	
1[a]	EtOAc, t-BuOH (1:1)	1.8	0.0	18.2	50.5	0.1	-29.4
2[a]	AcOH, t-BuOH (1:1)	0.0	0.0	26.1	2.1	0.0	-71.8
3[a]	AcOH	23.0	0.0	0.0	1.4	0.0	-75.6
4[b]	AcOH, t-BuOH (1:1)	12.5	0.0	0.0	0.0	0.0	-87.5
5[b]	AcOH	0.0	0.0	0.0	0.0	0.0	-100

[a] included immobilised CAL-B lipase beads, [b] no CAL-B beads were added, [c] determined by HPLC analysis. Total solvent volume remained the same at 2 ml for all entries. EtOAc = ethyl acetate, t-BuOH = tert-butanol, AcOH = acetic acid (96%). Reactions used 96 mg of CAL-B, 12mM HMF and 240 mM H_2O_2.

A 1:1 ethyl acetate/tert-butanol (v/v) solvent system provided the highest conversion of FFCA, substitution of the EtOAc with acetic acid (AcOH) produced less FFCA but more DFF indicating a slower reaction. Removal of CAL-B resulted in less conversion and reduced mass balance. No HMFCA or FDCA were produced.

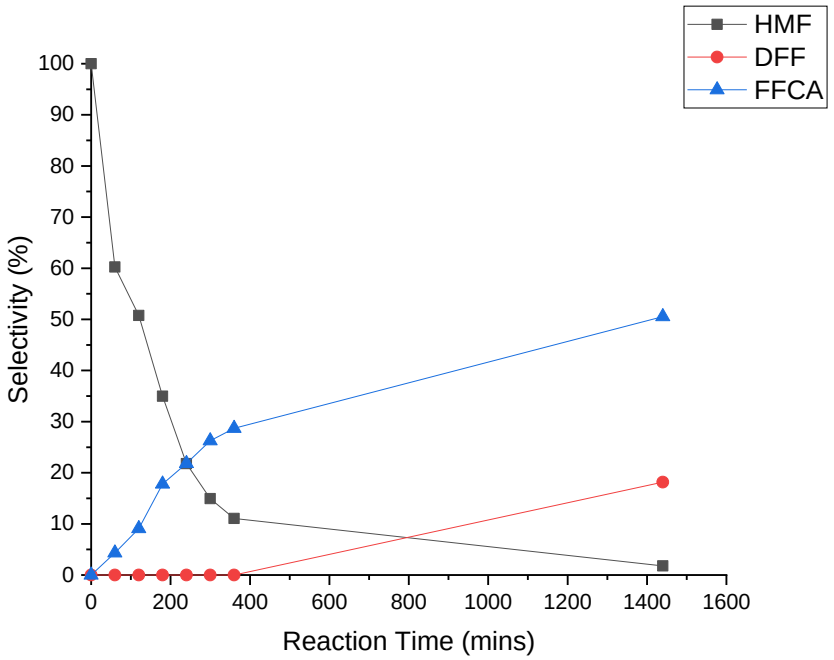

Figure 56 – HMF with H_2O_2 and CAL-B catalyst with ethyl acetate and t-butanol (1:1) (v/v) solvent system. Hydrogen peroxide was added from the start over 6 hours (Table 5, Entry 1).

Figure 56 shows the conversion of HMF with H_2O_2 and CAL-B. HMF is consumed at a faster rate than the formation of FFCA, and the missing mass was unidentified by HPLC. The formation of FFCA slows after hydrogen peroxide addition is stopped, but DFF is formed during the overnight period. At the end of the reaction 50% FFCA and 18% DFF are formed, with no FDCA observed.

Considerable success with HMF was observed, as such the reaction was replicated using DFF, adhering to the literature process. Safe solvents combined with removal of the enzyme were tested to determine the effect of gradual peroxyacetic acid production and subsequent oxidation. The results are shown in Table 6.

Table 6 – Optimisation of CAL-B catalysed conversion of DFF with hydrogen peroxide and varying solvent systems.

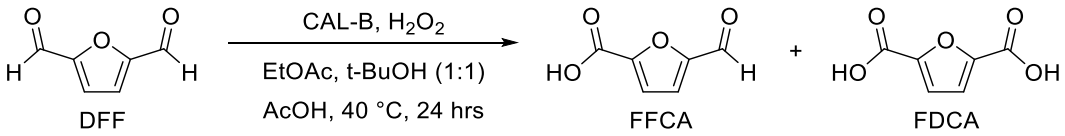

Entry	Solvent system	Remaining DFF (%) [e]	Conversion (%) [e]				Mass Balance (%)
			HMF	*HMFCA*	*FFCA*	*FDCA*	
1[a]	EtOAc, t-BuOH (1:1)	0.0	0.0	0.0	0.0	95.9	-4.1
2[a]	AcOH, t-BuOH (1:1)	0.0	0.0	0.0	0.0	77.2	-22.8
3[a]	AcOH	0.0	0.0	0.0	19.9	33.2	-46.9
4[a,b]	AcOH	1.7	0.0	0.0	34.6	42.8	-20.9
5[c]	AcOH, t-BuOH (1:1)	4.9	0.0	0.0	41.8	46.3	-7.0
6[c]	AcOH	0.0	0.0	0.0	21.3	28.5	-50.2
7[c,d]	AcOH	0.0	0.0	0.0	0.0	0.0	-100

[a] included immobilised CAL-B lipase beads, [b] reaction was sampled on a ChemSpeed, [c] no CAL-B beads were added, [d] reaction was run at 70 °C, [e] determined by HPLC analysis. Total solvent volume remained the same at 2 ml for all entries. EtOAc = ethyl acetate, t-BuOH = tert-butanol, AcOH = acetic acid (96%). Reactions used 96 mg of CAL-B, 12mM DFF and 240 mM H_2O_2.

Similar to HMF, a 1:1 ethyl acetate/tert-butanol (v/v) solvent system provided the highest conversion to FDCA, substitution of the EtOAc with acetic acid (AcOH) produced less FDCA but more FFCA with lower mass balance. Removal of CAL-B resulted in comparable mass balance, but with conversion split between FFCA and FDCA (Table 6, Entry 5). Acetic acid reactions were able to produce both FFCA and FDCA but at a slower rate with CAL-B seeming to have no effect. Increased temperature may have caused degradation with zero mass balance. No HMFCA or HMF were produced in the reactions. Other work in the group had developed a process to produce DFF, using the enzyme galactose oxidase ($M_{3\text{-}5}$ mutant). Table 7 shows the results using this DFF product to convert it to FDCA. Both the pure DFF solid (99.8%) generated, and an aqueous buffered solution were used. The purity differed as it decomposed in storage.

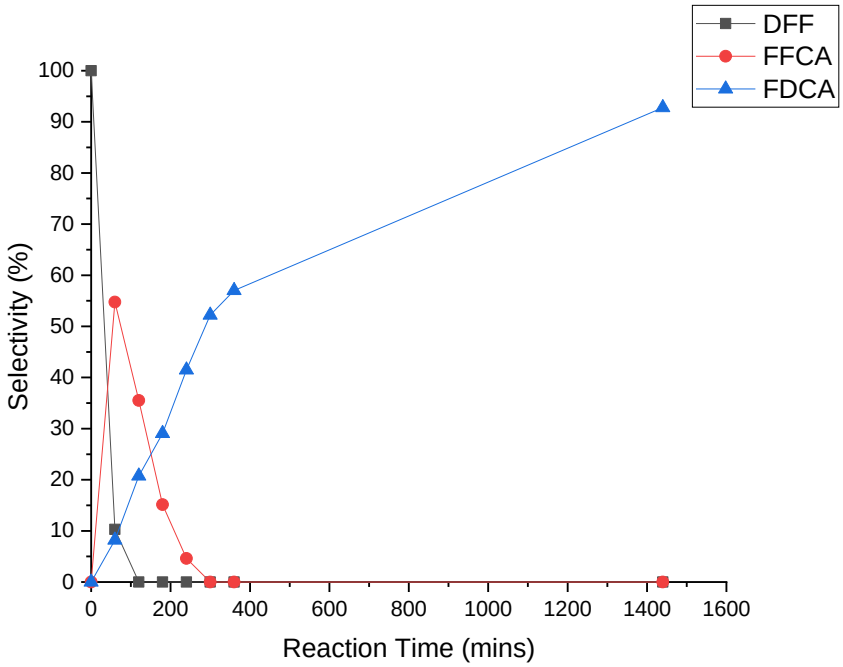

Figure 57 – DFF conversion with hydrogen peroxide in 1:1 ethyl acetate and t-butanol with CAL-B lipase. Hydrogen peroxide was added over the first 6 hours (Table 6, Entry 1).

Figure 57, shows the conversion of DFF to FDCA using CAL-B and ethyl acetate-t-butanol (Table 6, Entry 1). DFF is consumed over 120 minutes whilst 58% FFCA is formed. The FFCA is the consumed with formation of FDCA. There are some problems with the intermediate mass balance, but the outcome near quantitative conversion of HMF to FDCA. To avoid the explosive conditions ethyl acetate was replaced by acetic acid, so that peracetic acid could be produced *in-situ*. Retaining t-butanol, the reaction gave 77% FDCA (Table 6 ,Entry 2). Removal of t-BuOH dropped the conversion to 33% FDCA and 20% FFCA (Figure 58). Again, the formation of FFCA seems to stop after the peroxide is added and is incompletely converted to FDCA.

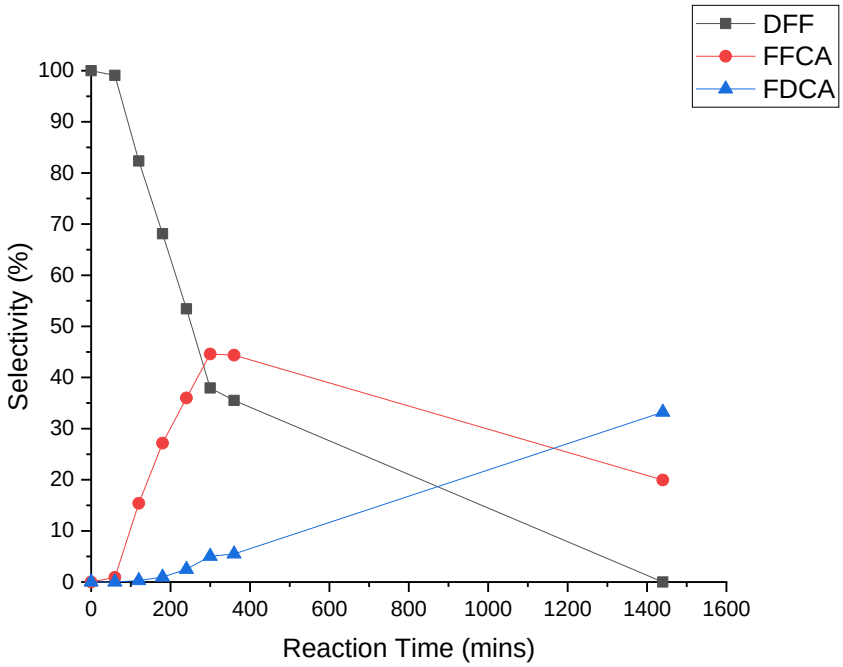

Figure 58 – DFF with acetic acid and hydrogen peroxide with CAL-B. H_2O_2 is added over the first 6 hours (Table 6, Entry 3).

In Figure 58 the reaction is slower in the acidic environment than with ethyl acetate. Loss of DFF is initially first order with formation of FFCA (19.9%) and the slow conversion to FDCA (33.2%). The oxidation of FDCA being the slower of the two oxidations. Further analysis over the full timeframe was essential and is demonstrated in Figure 59. Leaving the enzyme out of the reaction, but retaining t-butanol to solubilise the DFF, it still proceeded to give 33% FDCA and 20% FFCA (Table 6, Entry 5). Removal of t-butanol produced half the amount of each product over a similar timeframe. Nevertheless, this shows the enzyme may not be required for the reaction, and that it can be run under safer conditions.

An automated reactor system (ChemSpeed) was used to overcome the difficulty of sampling through the night. The instrument was able to add hydrogen peroxide every hour for the first 6 hours. Reactions were repeated for DFF in acetic acid with CAL-B, Figure 59.

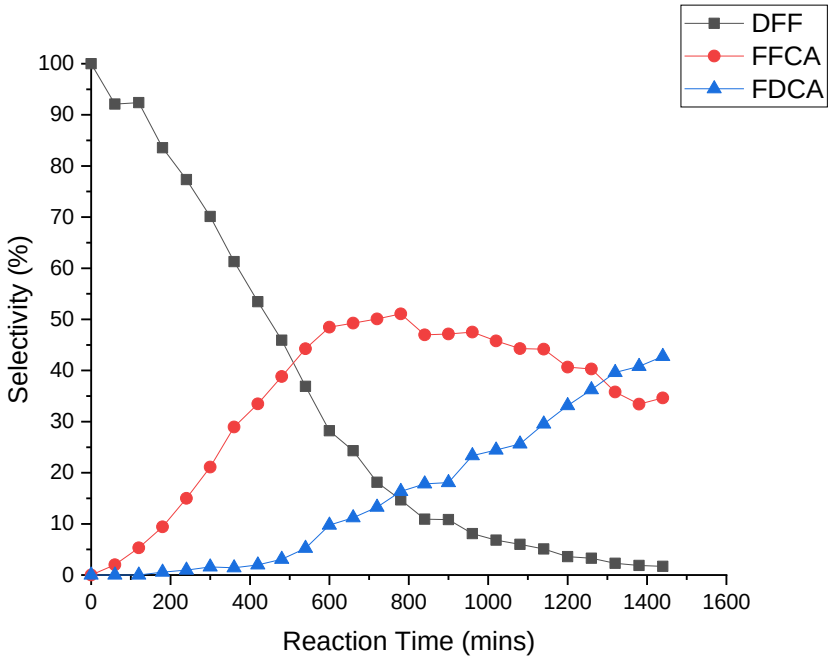

Figure 59 – DFF with acetic acid and hydrogen peroxide with CAL-B over 24 hours. Hydrogen peroxide added over the first 6 hours (Table 6, Entry 4).

Figure 59 is consistent with the previous result in Figure 58, and shows first order loss of DFF up to 700 minutes, and formation of first FFCA then FDCA. The mass balance is improved. For an industrial process to make FDCA, the starting material needs to be HMF not DFF. To this end the product of a GOase catalysed oxidation of HMF to DFF was tested for it's potential in a telescoped continuous flow process. The aqueous solution of DFF from the previous stage contained buffer, copper salts, catalase and peroxidase enzymes as well as small quantities of HMF, FFCA and FDCA (Table 7, Entries 1-6).

To determine the effects of a telescope reaction from galactose oxidase catalysed production, of DFF and the following CAL-B catalysed oxidation to FDCA; the reactions in were Table 7 completed. The solution used was an aqueous buffered solution of GOase generated DFF.

Table 7 – Optimisation of CAL-B catalysed conversion an aqueous solution of DFF from a reaction of HMF catalysed by GOase with hydrogen peroxide and varying solvent systems.

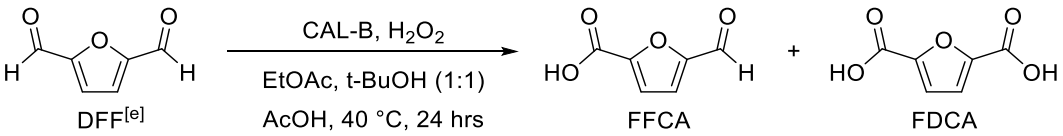

Entry	Solvent system	Remaining DFF (%) [d]	Conversion (%) [d]				Mass Balance (%)
			HMF	*HMFCA*	*FFCA*	*FDCA*	
1[a]	EtOAc, t-BuOH (1:1)	12.8	0.0	0.0	5.8	21.4	-60.0
2[a]	AcOH, t-BuOH (1:1)	34.9	0.0	0.0	0.4	17.6	-47.1
3[a]	AcOH	0.0	0.0	0.0	0.0	54.8	-45.2
4[b]	AcOH, t-BuOH (1:1)	41.9	1.2	0.0	30.9	23.8	-2.2
5[b]	AcOH	0.0	0.0	1.9	0.0	73.8	-26.2
6[b,c]	AcOH	0.0	0.0	80.6	0.0	0.0	-19.4

[a] included immobilised CAL-B lipase beads, [b] no CAL-B beads were added, [c] reaction was run at 70 °C, [d] determined by HPLC analysis, [e] aqueous buffered solution of DFF from a reaction of HMF catalysed by GOase, selectivity calculated from the average quantity of DFF/FFCA already present in the solution. Total solvent volume remained the same at 2 ml for all entries. EtOAc = ethyl acetate, t-BuOH = tert-butanol, AcOH = acetic acid (96%). Reactions used 96 mg of CAL-B, approx. 2 mg.mL^{-1} GOase DFF solution and 240 mM H_2O_2.

Unlike the pure DFF, an acetic acid solvent system provided the highest conversion to FDCA, however with a poor mass balance due to the loss of DFF (Table 7, Entry 5). The highest mass balance used a 1 : 1 acetic acid/t-butanol solvent system, with a mixture of DFF, FFCA and FDCA remaining. Addition or removal of CAL-B had little impact, with improved conversion observed without (Table 7, Entry 4). The solvent used had a greater impact, acetic acid (AcOH) producing more FDCA but with lower mass balance. Elevated temperatures reduced the DFF solution back to HMFCA (Table 7, Entry 6). No HMF was produced in these reactions. Overall oxidation gave less FFCA and FDCA product when compared to pure DFF, and might be interference of the residuals carried-over from the previous stage.

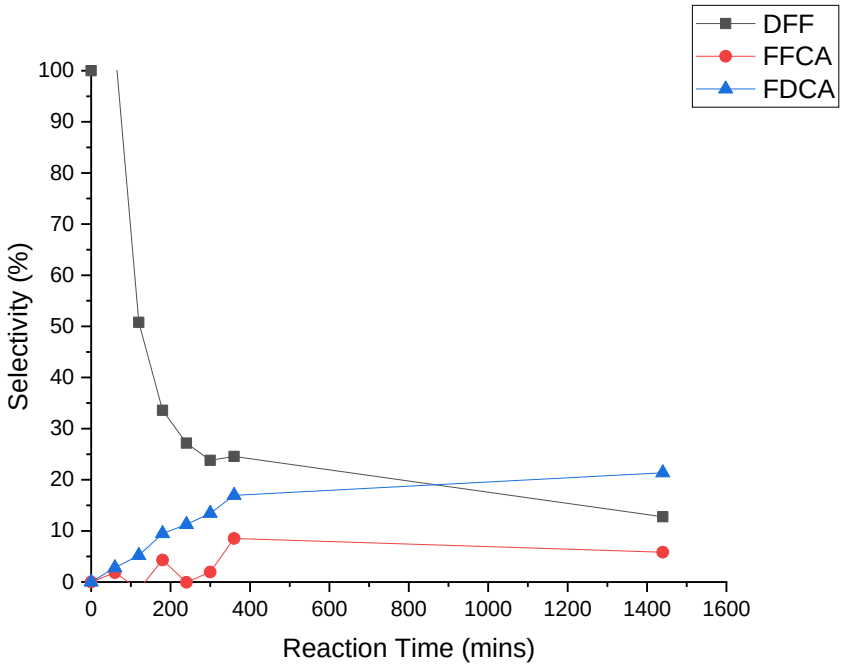

Figure 60 – GOase generated DFF with ethyl acetate/t-butanol with CAL-B. H_2O_2 is added over the first 6 hours (Table 7, Entry 1).

Steady-state is reached after roughly 6 hours, and is maintained for the remainder of the reaction. Initial conversion of DFF is fast, converting 75% in 4 hours, however a corresponding rate of conversion for FFCA or FDCA is not observed. FFCA forming at less than half the rate of DFF consumption.

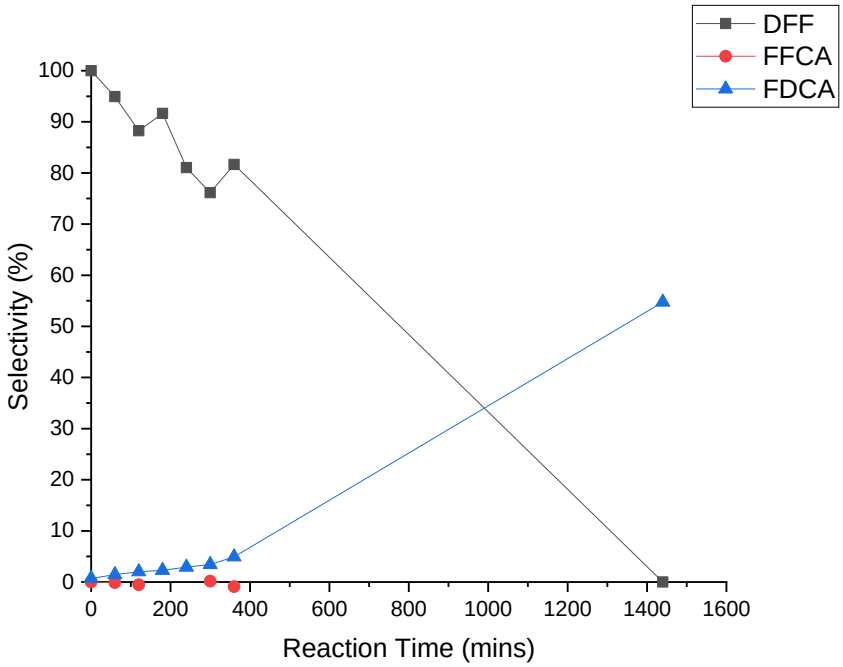

Figure 61 – GOase generated DFF using acetic acid and hydrogen peroxide with CAL-B. H_2O_2 is added over the first 6 hours (Table 7, Entry 2).

Instead of ethyl acetate, direct addition of acetic acid and peroxide appeared to overcome the effects of the buffer and catalase, and 54% FDCA was observed after 24 hrs. However little conversion is observed in the first 6 hours (maximum of 5% FDCA) and with a lack of data between 360 and 1440 minutes, an accurate estimate isn't possible. HMF conversion is slower than Figure 60 (Table 7, Entry 1), taking the entire reaction duration to reach an equivalent conversion of starting material.

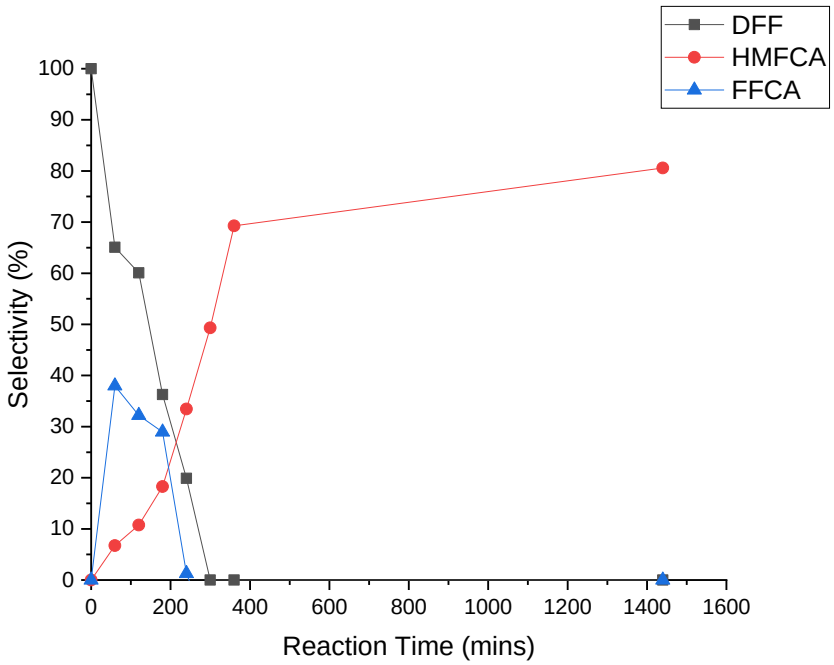

Figure 62 – DFF with acetic acid and hydrogen peroxide at 70 °C, without CAL-B. H_2O_2 is added over the first 6 hours (Table 7, Entry 6).

At 70 °C with excess H_2O_2 the reaction progresses in a sideways manner, with FFCA only an intermediate and HMFCA formed (Figure 62). This result implies a change in mechanism with the FFCA aldehyde being reduced to hydroxymethyl. The lifetime of hydrogen peroxide at 70 °C is short, it's rapid decomposition may cause the DFF to disproportionate to FFCA and HMF, and further to dihydroxymethylfurfural (DHMF) by the Cannizzaro reaction.

For most of the CAL-B catalysed oxidations the process slows considerably at FFCA, hence a standard reaction using the ethyl acetate and t-butanol (1:1) solvent system was undertaken to determine overall conversion in a 24-hour time period.

Table 8 – Optimisation of CAL-B catalysed conversion of FFCA with hydrogen peroxide.

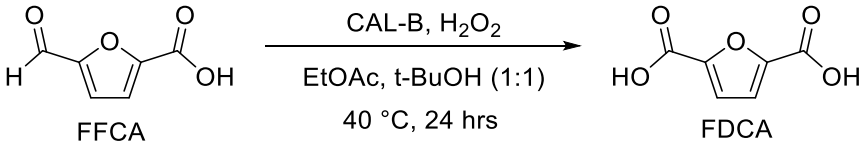

Entry	Solvent system	Remaining FFCA (%) [b]	Conversion (%) [b]				Mass Balance (%)
			HMF	***HMFCA***	***DFF***	***FDCA***	
1[a]	EtOAc, t-BuOH (1:1)	0.0	0.0	0.0	0.0	85.2	-14.8

[a] included immobilised CAL-B lipase beads, [b] determined by HPLC analysis. Total solvent volume remained the same at 2 ml for all entries. EtOAc = ethyl acetate, t-BuOH = tert-butanol, AcOH = acetic acid (96%). Reactions used 96 mg of CAL-B, 12mM FFCA and 240 mM H_2O_2.

Use of pure FFCA produced 85% FDCA with the remaining mass balance unknown. Further reactions using FFCA with an AcOH solvent system (with and without Cal-B) would be beneficial. Giving insight into CAL-B's importance and if FFCA is a slower to oxidise compound than DFF. As observed with DFF, the compound is poorly soluble in distilled water (pH 6), 2 $mg.mL^{-1}$ so reactions were run at 1.5 $mg.mL^{-1}$ (14 mM).

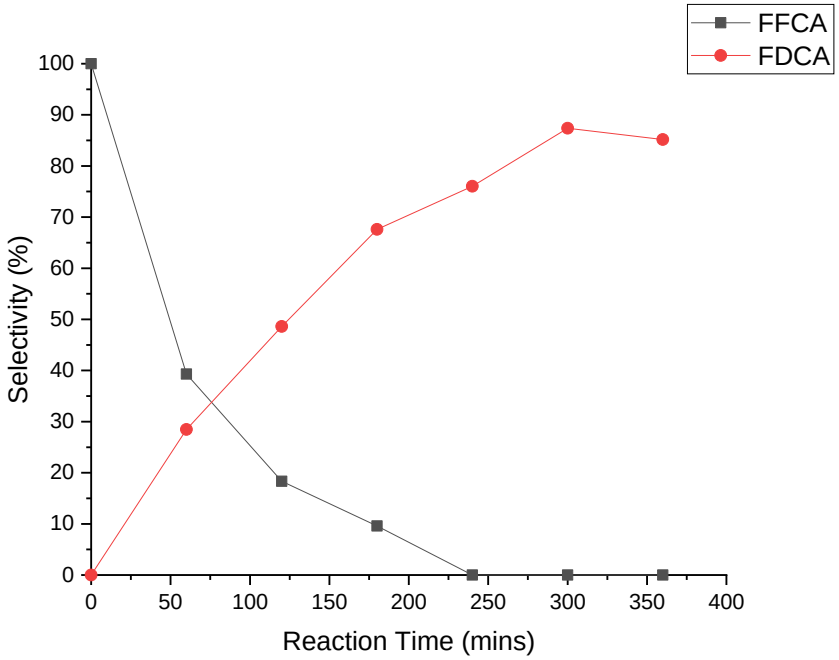

Figure 63 – FFCA with ethyl acetate/t-butanol, hydrogen peroxide and CAL-B. H_2O_2 is added over the first 6hrs (Table 8, Entry 1).

The rate of FDCA formation was similar to that observed for DFF, however there is a mis-match in the concentration of each species that indicates an unobserved intermediate that may lack a chromophore, making it undetectable by a UV-Vis. Conversion to FDCA is slower than DFF to FFCA reactions suggesting this to be a rate-determining step in the oxidation. A continuous flow setup with increased peroxide injections and mass transfer would accelerate the reaction.

To summarise, CAL-B was successful in converting both DFF and FFCA to FDCA at relatively high conversion (>85%). The peracetic acid formed *in-situ* was able to oxidise HMF to DFF and FFCA with considerable success, however this was notably slower than using the furan substrates. Maximum conversion to FDCA (95%) was observed using the ethyl acetate and t-butanol (1:1) solvent system (Table 6, Entry 1). Although a safe alternative using acetic acid was developed this gave reduced conversion. All reaction times were in excess over 6 hours, suggesting a continuous flow system may be of benefit.

2.2.4 Oxone™ catalysed oxidation of HMF, DFF and FFCA

Potassium peroxymonosulfate (Oxone™) is a common triple salt oxidant used primarily as an anti-bacterial agent in the cleaning solution Virkon. The compound is a white crystalline solid that readily and safely decomposes in water or air, supporting its widespread use in the medical field. The chemical can be classed as a green oxidant due to its relatively safe decomposition pathway.[137]

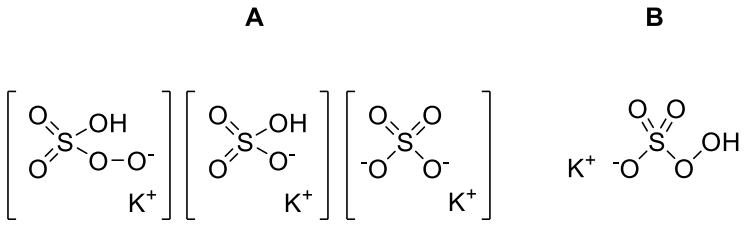

Figure 64: A) Triple salt Oxone™ exists as; B) the IUPAC structure for the three salts.

The compound oxidises alcohols to carboxylic acids, and esters are formed when an alcoholic solvent is used.[138] The reaction can be stopped at intermediary stages using fewer molar equivalents, for example in sulphide oxidation to sulfoxide or sulfone. The mechanism of Oxone oxidation is shown in Figure 65.

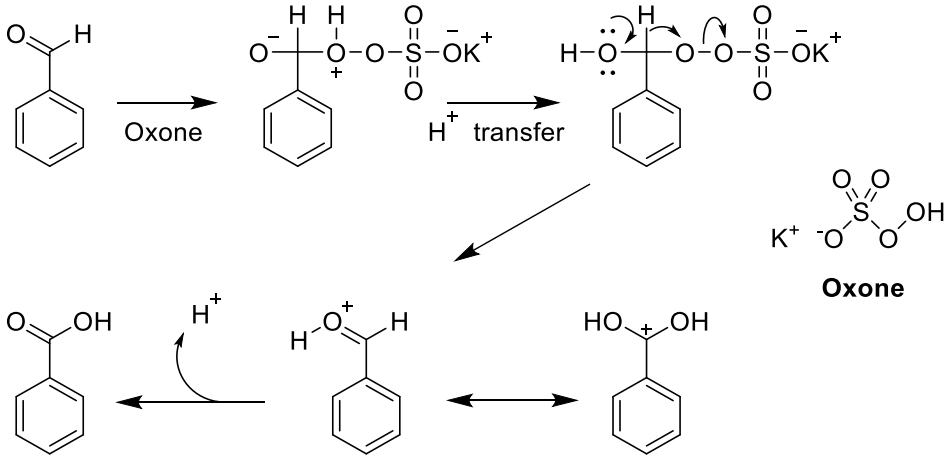

Figure 65 – Oxidation mechanism of benzaldehyde to benzoic acid by Oxone™.[124]

Industrial applications of Oxone have benefited from mixed solvent systems, such as ethanol and water 1:1 (v/v), ethanol acting a both substrate and solvent for ester formation. As with hydrogen peroxide, transition metals cause the rapid decomposition of Oxone, limiting its use.[138]

Kennedy *et al.* published work in the 1960's on the use of potassium monopersulfate, known then as peroxymonosulfuric acid salt, for the preparation of lactones from cyclic ketones.[139] Oxone™ is used as a single-oxygen donor, an environmentally safe alternative to common oxidants like Chromium (IV) oxide and potassium permanganate. In more recent years the compound has seen renewed interest in the oxidation of tri-substituted phenols, and their derivatives in combination with an iron-based catalyst. Fukushima *et al.* studied the effects of potassium peroxymonosulfates on dechlorination of chlorophenols, Figure 66.[140-141]

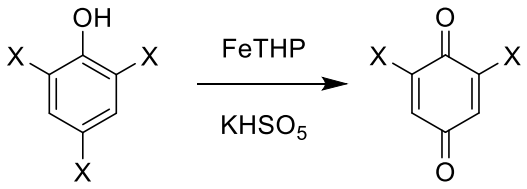

Figure 66 – Iron(III)-5,10,15,20-tetrakis(p-hydroxyphenyl) porphyrin (FeTHP) catalysed oxidative dechlorination of chlorophenols. Potassium peroxymonosulfate is used as an oxygen source rather than an oxidiser, an alternative being hydrogen peroxide.

Given its properties and low cost, Oxone™ was investigated for the oxidation of HMF, DFF, and FFCA in water. This would avoid expensive enzymes, additives and simplify work-up.

Table 9 – Optimisation of of; HMF, DFF, GOase generated DFF and FFCA with aqueous potassium peroxymonosulfate.

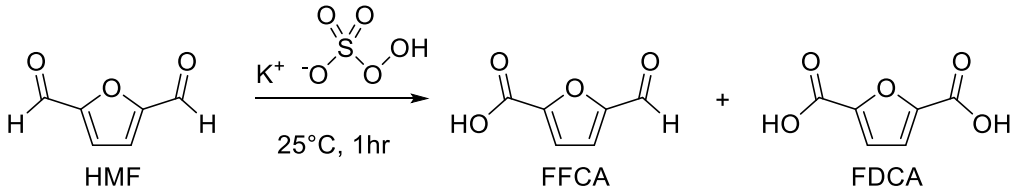

Entry	Starting Material [c]	Remaining SM (%) [d]	Conversion (%) [d]					Mass Balance (%)
			HMF	***HMFCA***	***DFF***	***FFCA***	***FDCA***	
1[a]	HMF	31.9	-	0.0	1.9	0.2	0.0	-66.0
2[a]	DFF	24.0	0.0	0.0	-	51.5	23.2	-1.3
3[b]	DFF[b]	0.0	0.0	0.0	-	2.7	7.1	-90.2
4[a]	FFCA	58.0	0.0	0.0	0.0	-	29.0	-13.0

[a] used dry standard material bought from a vendor, [b] aqueous buffered solution of DFF from a reaction of HMF catalysed by GOase$_{M3\text{-}5}$, selectivity calculated from the average quantity of DFF/FFCA already present in the solution, [c] starting material concentrations of 12mM, [d] determined by HPLC analysis. Reaction used 4 equivalents of Oxone™ at 25 °C for 1 hour. Measured using external HPLC calibration. SM = starting material.

Use of Oxone with HMF indicated little conversion with a large mass loss. However, with DFF, <50% was converted with 23% FDCA and an improved mass balance (Table 9, Entry 2). The aqueous buffered DFF had the lowest conversion and worst mass balance. With FFCA as the starting material considerable conversion to FDCA was observed but with a small mass balance, suggesting there isn't enough of the oxidant present to progress the reaction further. No HMFCA was observed in these reactions. Sequential addition to the reactions would be the next step in the process; determining if more oxidant is required to produce FDCA.

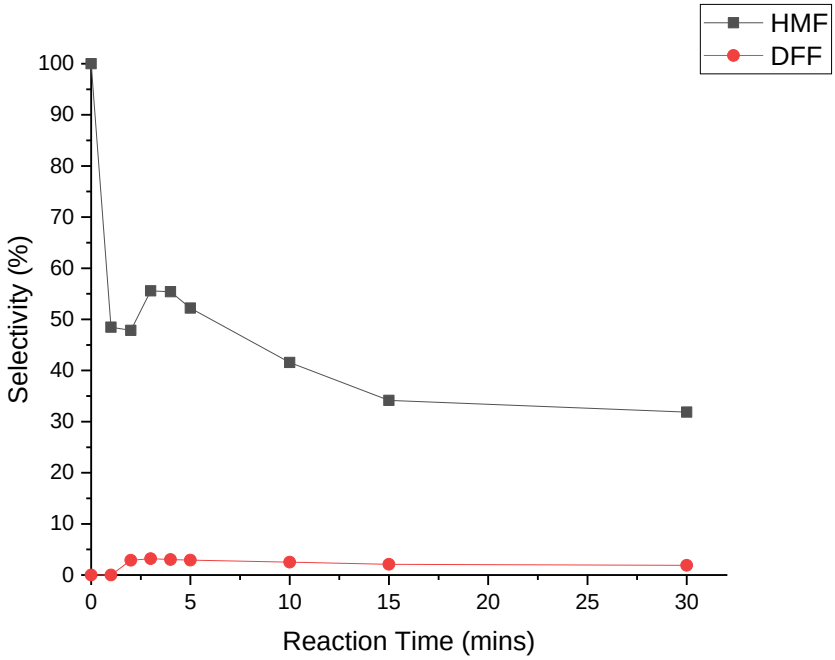

Figure 67 – HMF with Oxone™ in water over a 30-minute period. Oxone™ has been added in one aliquot at t=0 minutes (Table 9, Entry 1).

Oxone was added at the start in excess (5 equivalents) to compensate for its decomposition. Figure 67 shows HMF reacting within the first 15 minutes and then stalls. No products were observed, with uncharacterised peroxo- or sulphite adducts (bisulphite quench) likely forming. Minimal DFF was formed (2%) suggesting Oxone has difficulty oxidising the alcohols groups of HMF.

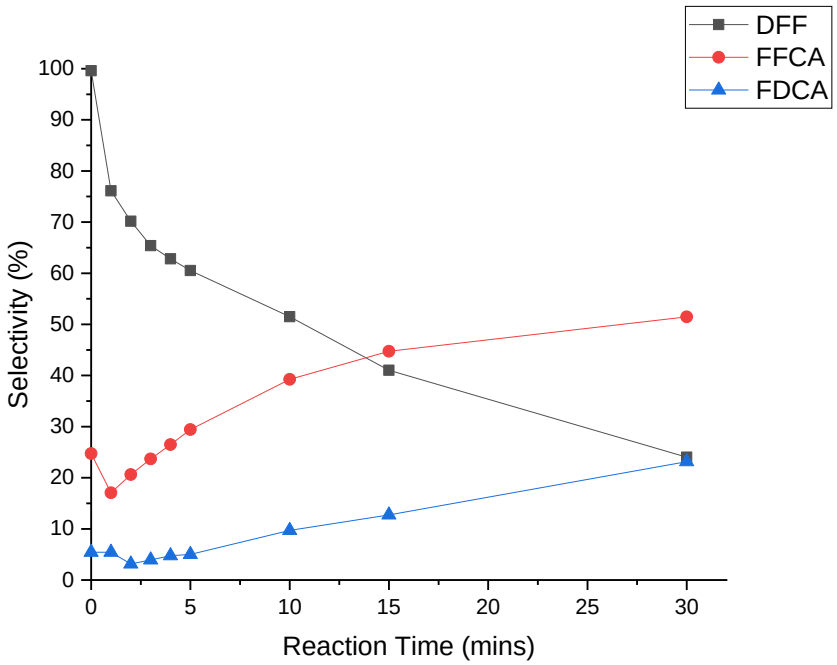

Figure 68 – DFF with Oxone™ in water over a 30-minute period. Oxone™ has been added in one aliquot at t=0 minutes (Table 9, Entry 2).

Hydrochloric acid was added at the end of reaction to hydrolyse any intermediates. The reaction produced 51% FFCA and 23% FDCA, with a negligible mass loss of 1.3%; 24% DFF remained in solution. Figure 68 shows the rapid consumption of Oxone and the reaction stalling. The reaction has yet to finish, with all intermediates showing a distinct and proportional rate of conversion. The rate slows significantly after 15 minutes suggesting the majority of oxidant has been used up. Further reactions would benefit for sequential addition of Oxone, providing a constant supply of oxidant.

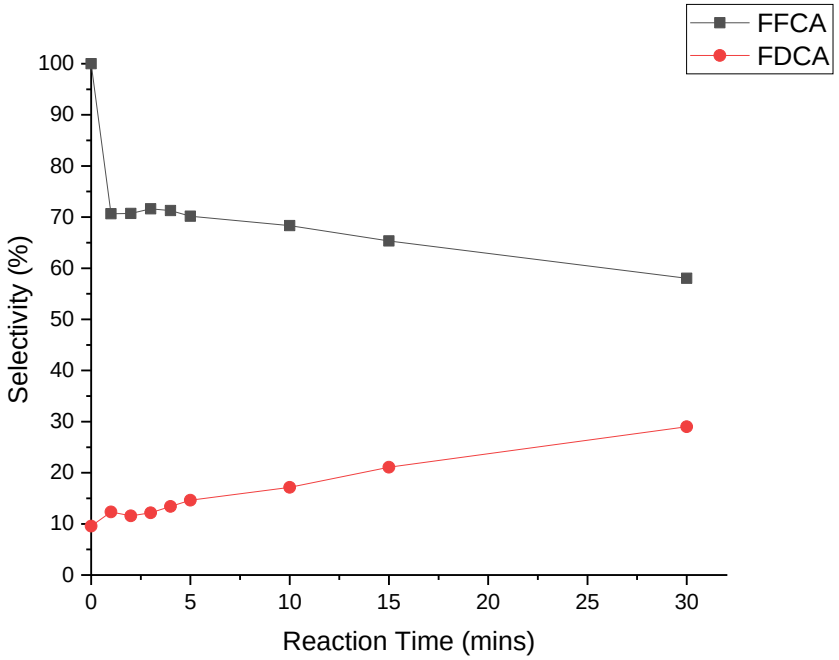

Figure 69 – FFCA with Oxone™ in water over a 30-minute period. Oxone™ has been added in one aliquot at t=0 minutes (Table 9, Entry 4).

An initial 10% conversion occurs rapidly between addition of the Oxone and sampling of the first timepoint. This rapid conversion lasts for a minute before the rate decreases. The slower rate of conversion steadily increases over the course of the reaction, peaking at 58% FFCA and 29% FDCA. As seen in previous experiments; the oxidation of FFCA is slow compared to DFF and the oxidant is consumed rapidly. Further addition of oxidant combined with a longer reaction may yield conversion in excess of 50% FDCA.

To summarise, Oxone proved a successful oxidant for oxidising DFF and FFCA, yielding a maximum of >50% conversion. Oxidation did not occur when using HMF and slowed considerably at FFCA, indicating this to be the slowest step. FDCA only formed when using DFF as a starting material, acetal formation of FFCA in water influencing this. Further addition of Oxone™ to DFF, by extrapolation of Figure 68, indicates a near 100% conversion to FDCA in a 2-hour reaction time.

2.3 DFF oxidation in continuous flow

Given the results using immobilised CAL-B lipase in batch, the system was considered useful to test in continuous flow. A preliminary experiment was undertaken to determine the reusability of the immobilised enzyme. Using DFF in ethyl acetate/ t-butanol, the reaction was run for 6 hrs. After separation of the enzyme, it was washed three times with ethyl acetate/t-butanol (1:1) (v/v) to remove insoluble DFF, and used in a second reaction. Figure 70, shows the results of this experiment with good conversion shown in the first run, but considerably reduced performance in the second run. Both experiments had similar pH values of 4 indicating the formation of acetic and peroxyacetic acid. Starch paper (colour purple) indicated peroxide remaining in the system for both runs; further conversion occurred when the reactions were left longer.

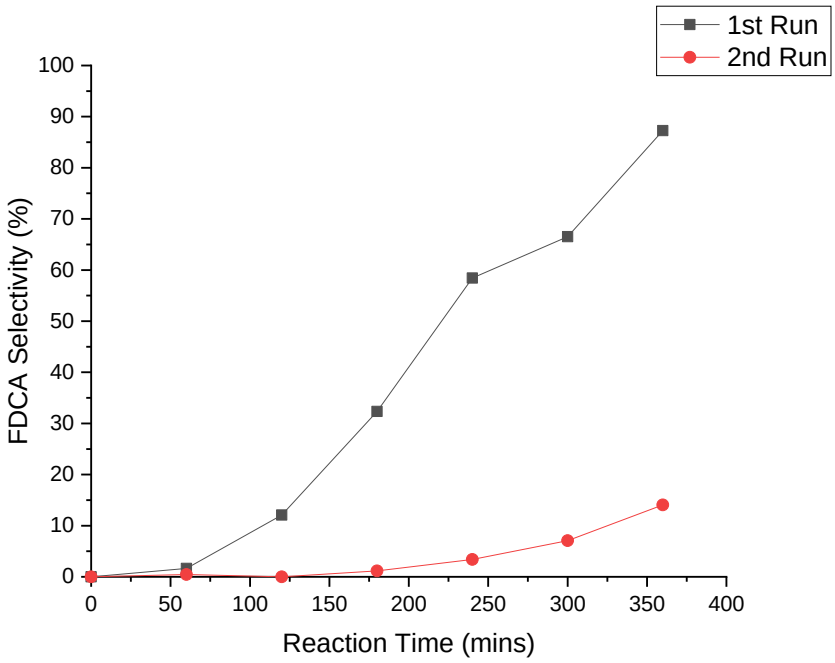

Figure 70 - lipase-catalysed oxidation of DFF with ethyl acetate/t-butanol and hydrogen peroxide. H_2O_2 is added over the first 6hrs. CAL-B beads are recycled and washed between the 1st and 2nd runs.

The cause of this may be the acidity of the system, as acetic acid is formed from ethyl acetate and may denature itself resulting in a significantly lower rate of conversion. Figure 71 shows the reactor set-up used. Hydrogen peroxide and acetic acid were fed into a fReactor to mix, DFF was introduced and mixed in a second fReactor. The solution travelled into a vertical CAL-B packed column, heated in a water bath to 37 °C, and on-line UV-Vis measurements were done before eluting through a 40 psi back-pressure regulator (BPR). The fixed-bed catalyst was made using CAL-B packed into an Omnifit column and the residence time distribution determined by a pulse-injection of red food dye at a flow rate of 2 mL.min^{-1} and 0.2 mL.min^{-1} and analysed by in-line UV-vis with measurements taken every second, Figure 72 and Figure 73.

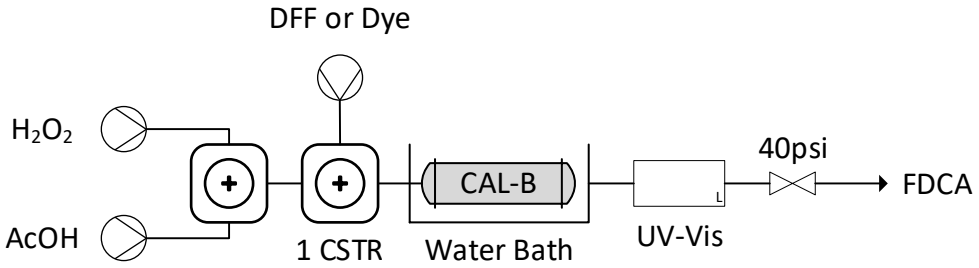

Figure 71 – Continuous flow reaction for the oxidation of DFF in acetic acid and hydrogen peroxide with CAL-B.

A pulse of 10% (v/v) red food dye was introduced into the 2nd CSTR using a port and syringe. The absorbance values were measured in-line (516 nm). The RTD function $E(t)$ was calculated by division of the absorbance at each residence time by the total normalised area under the absorbance curve. The average of the normalised area could then be taken, for 0.2 mL min^{-1} this was 54 seconds.

$$E(t)dt \qquad \text{Eqn. 28}$$

The fraction of fluid that exits the reactor with an age (time) less then t_1 is given by the value of $F(t)$, known as the cumulative distribution, Equation 2.

$$F(t_1) = \int_0^{t_1} E(t)dt \qquad \text{Eqn. 29}$$

The sum of which is used to produce an average area under the curve, residence time ($\boldsymbol{\tau}$). By rearrangement of the below equation to make the reactor volume the subject, the total volume of the CSTR and column can be determined.

$$\boldsymbol{\tau} = \frac{Reactor\ Volume}{Flow\ rate} \qquad \text{Eqn. 30}$$

For this setup the packed-bed had a volume of 0.31 ml when filled with 2 g of CAL-B methacrylate beads; piping used was estimated at 0.5 ml volume, a 0.1 ml volume UV-Vis flow cell and a 2 ml volume CSTR where the starting material or dye enters.

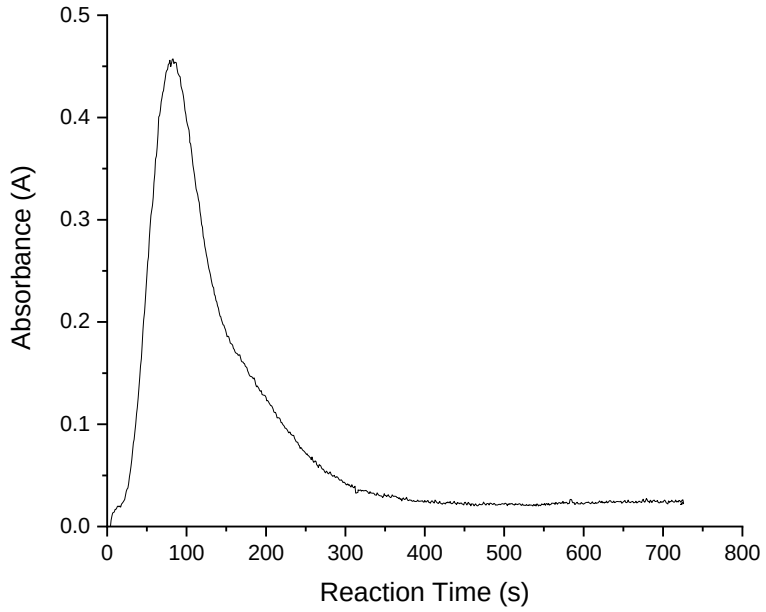

Figure 72 - Pulse injection experiment of the reaction shown in Figure 71 at 2 mL.min^{-1} with both the packed-bed column and CSTR included in the pulse.

Both runs show the pulse of dye running through the system with the expected tailing observed when using a CSTR. The tailing is fairly long and indicates back-mixing in the CSTR and packed-bed especially at the lower flow rate.

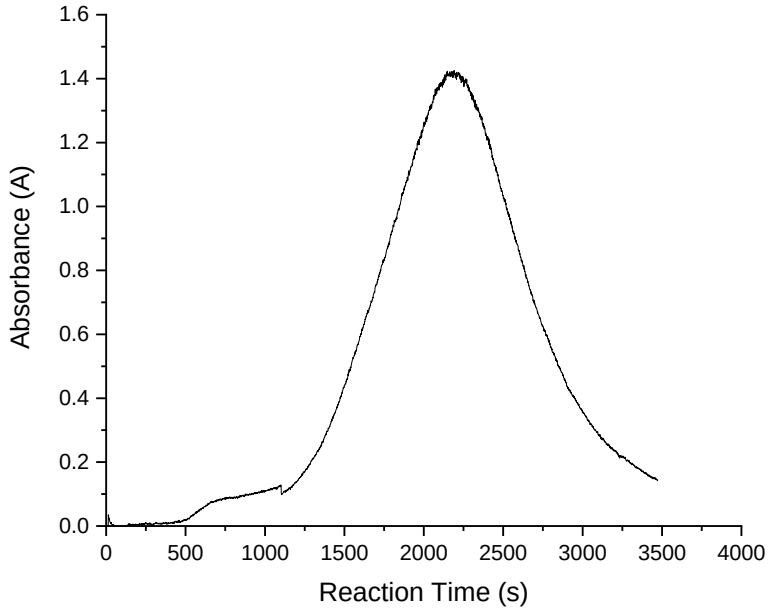

Figure 73 - Pulse injection experiment of the reaction shown in Figure 71 at 0.2 mL.min^{-1} with both the packed-bed column and CSTR included in the pulse.

Table 10 – Optimisation of CAL-B catalysed conversion of DFF with hydrogen peroxide in continuous flow.

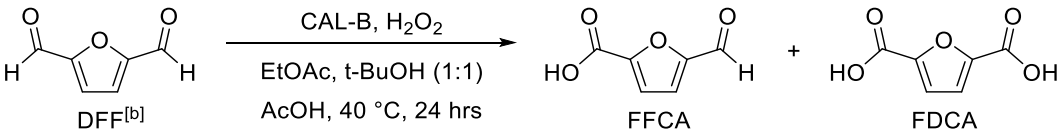

Entry	Residence time (mins)	Flow rate ($mL.min^{-1}$)	*Steady state (mins)*	Pump 1[a] flow rate ($mL.min^{-1}$)	Pump 2[b] flow rate ($mL.min^{-1}$)	Pump 3[c] flow rate ($mL.min^{-1}$)
1	1.0	2.81	3.0	1.183	0.813	0.813
2	2.0	1.14	6.0	0.592	0.407	0.407
3	4.0	0.70	12.0	0.296	0.203	0.203
4	6.0	0.47	18.0	0.197	0.136	0.136
5	8.0	0.35	24.0	0.148	0.102	0.102
6	10.0	0.28	30.0	0.118	0.081	0.081
7	16.0	0.18	48.0	0.074	0.051	0.051
8	20.0	0.14	60.0	0.059	0.041	0.041

[a] peroxide pump containing a solution of 5% (v/v) hydrogen peroxide in water, [b] enzyme pump containing aqueous buffered solution of DFF from a reaction of HMF catalysed by GOase, selectivity calculated from the average quantity of DFF/FFCA already present in the solution, [c] acetic acid pump containing a solution of 50% acetic acid. Reaction used 2000mg CAL-B, 12mM DFF and 240mM H_2O_2. Experimental residence times by varying flow rates used on the CSTR with a packed-bed, shown in Figure 71. Total volume of 2.81 ml without the UV-Vis. The process ran for 3 times the residence time to ensure steady state had been achieved.

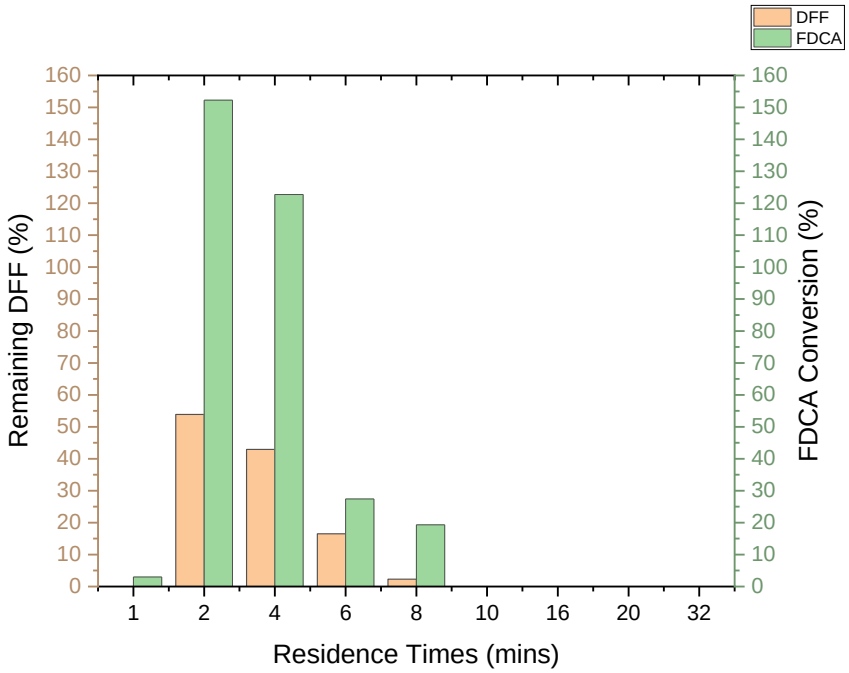

Figure 74 – Sequentially tested residence times for the CAL-B catalysed oxidation of DFF in continuous flow using EtOAc-t-BuOH 1:1 (v/v) solvents and addition of hydrogen peroxide. Variable flow rates as shown in Table 10.

A range of residence times were tested to determine the highest DFF conversion. The conversion shown above 100% is due to FDCA solubility with quantities remaining in the reactor and exiting in plugs as a result of back-mixing.

The continuous flow reaction was successful, forming FDCA product. A balance is required in the feeds to ensure complete reaction of peroxide and acetic acid before contact with the enzyme to prevent denaturation. Interestingly no FFCA is observed in any samples, with most being oxidised rapidly in the reactor. The reaction is an improvement over the batch process, going from 24 hours to 30 minutes whilst achieving similar concentrations of FDCA.

2.4 Conclusions

Production of large quantities of FDCA under 'green' conditions is highly challenging as multiple routes are available and need to be considered if they are to be cost-competitive. In this work multiple alternatives for the synthesis of FDCA from HMF, DFF and FFCA have been explored. The work has laid the foundations for a continuous process to produce FDCA from DFF. Initial analytical development resulted in an unusual dialdehyde diketone compound from a sodium tungstate catalysed reaction with HMF. The compound could be used in the formation of substituted pyrroles by a ring-closing reaction. However further replication proved unsuccessful. These Noyori modified reactions produced little FDCA with consistent loss of mass. Nevertheless, the use of hydrogen peroxide guided further oxidation studies under alkaline conditions.

The Cannizzaro reaction had varied success, with uncontrolled selectivity of the products. Both FDCA and FFCA were formed in reasonable amounts, peroxide seemingly hindering conversion. The alkaline conditions used however are ideal for the base disproportionation to react at roughly 20% conversion. Further analytical development enabled the determination of the Cannizzaro under ^{1}H NMR along with the solubility of DFF at varying pH. Implementation of this allows for the increased production and selectivity of FDCA in aqueous reactions. Further research into product selectivity in the Cannizzaro reaction would be beneficial. Use of CAL-B produced FDCA at quantities suitable for large scale- production or transfer to continuous flow. However due to safety concerns surrounding the solvent mixture, other options had to be explored. Substitution of ethyl acetate with acetic acid produced lower quantities of FDCA, yet provided a safer reaction for continuous flow. Hence additional screening of solvent systems and further optimisation of the residence time, may reduce mass loss and increase product formation.

Chapter 3 – Biocatalytic oxidation of 5-hydroxymethylfurfural to diformylfuran using liquid foam in continuous flow

3.1 Introduction

The majority of bio-based oxidations of 5-hydroxymethylfurfural (HMF) to 2,5-furandicarboxylic acid, and its precursor diformylfuran (DFF), use an aqueous solvent system. These suffer from poor product solubility and resultant precipitation of solid materials leading to reductions in the overall yield. Recent developments using deep-eutectic solvent systems or organic-aqueous solvent systems have been noted as possible solutions to inhibit the unfavourably low solubility.[97,132] However, these methods are often accompanied by hazardous solvents, poor selectivity and are expensive chemicals to produce FDCA in a high yield. A high product concentration and rapid reaction would be beneficial for the industrial scale manufacture of DFF, helping reduce solvent waste and giving high productivity.

Bio-oxidations usually use air as the oxygen source. Since the solubility of oxygen in water is low, 8 mg. L^{-1} (0.25 mM) at ambient temperature and pressure this is the rate limiting reactant. The Michaelis constant (K_M) for oxygen with galactose oxidase (GOase) is 3 mM, meaning the enzyme is turning-over well below its maximum. [142] Pressurised systems have been investigated using compressed air, and higher rates are observed, however, operating in this way is complex, with safety and capital cost issues.[143,144] The generation of oxygen by decomposition of hydrogen peroxide with catalase has been recently reported.[123] This system provides temporarily high (super-saturating) oxygen concentrations, accelerating $GOase_{M3\text{-}5}$ catalysed reactions to <10 minutes. During the reaction excess oxygen rapidly degasses to form bubbles and returns the concentration to the saturation level. To overcome this, a continuous flow system was developed in which the peroxide was metered into the stream by multi-point injection, providing intermittent pulses, to maintain a high oxygen concentration.

As this was carried out in a tubular reactor, the gas-liquid combination generates a slug-flow regime and the exit was found to produce a heavy and stable foam. The addition of anti-foam suppressed this and made the flow smoother and the product easier to separate.

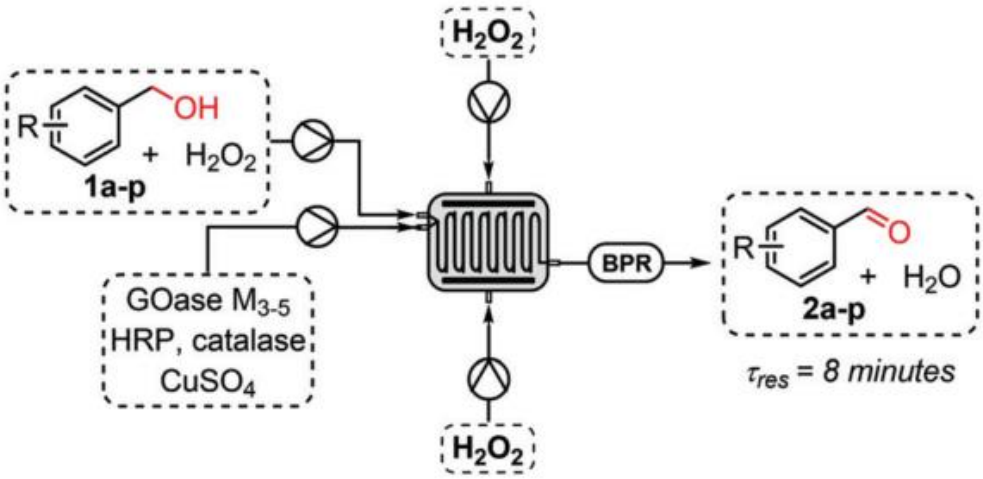

Figure 75 – Flow process for the galactose oxidase catalysed oxidation using a multi-point injection reactor.[123]

Biphasic reactions involving a gas and liquid can generate foam if a surfactant is present that stabilises the interface. The amphipathic nature of enzymes means they preferentially adsorb at the gas-liquid interface of a bubble. Their zwitterionic structure contains regions of hydrophilicity and hydrophobicity, these interact favourably with the water and gas respectively. Foam formation occurs in the presence of sufficient agitation or aeration, and is exacerbated at higher enzyme concentrations. Foam systems benefit from improved mass transfer by increasing the gas-liquid surface area. Interestingly, for this work, they also have the ability to transport solids. The gas-liquid mass transfer coefficient ($k_L a$) defines the rate of oxygen solubilisation and is a function of the surface area and concentration gradient. It is greatly affected by enzyme concentrations, buffer solutions and notably antifoaming agents. Lindeque *et.al* noted a 39% reduction in $k_L a$ upon the addition of antifoam, a value lower than that of pure buffer. The antifoam reduced the surface tension by interacting at the gas-liquid interface, resulting in coalescence and reduced foaming.[143]

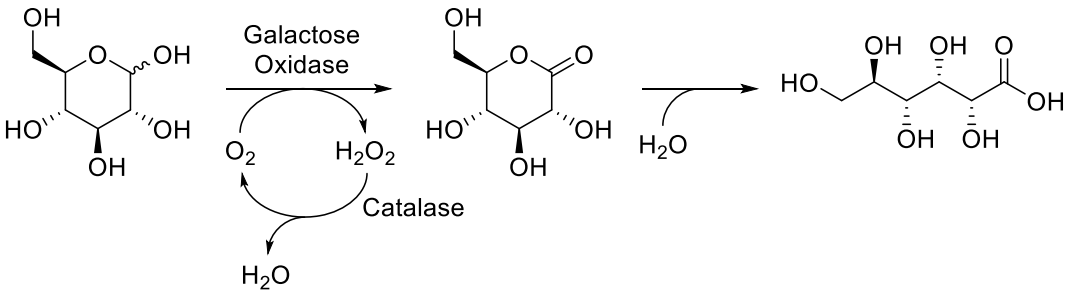

Figure 76 – Galactose oxidase catalysed conversion of D-glucose to D-glucono-δ-lactone, using catalase as a peroxide quench. Spontaneous hydrolysis forms the gluconic acid.[145]

Other findings by these workers reported a significant improvement in $k_L a$ by addition of GOase and catalase, both of which increased the oxidation by 12% and 33% respectively.[145] Bubbles were smaller, due to the increased surface tension, and were stabilised by the two amphiphilic proteins. The study focused on retrofitting a batch reactor to create a CSTR, rather than exploring other modes of carrying out continuous biocatalytic oxidations.[146] They previously noted the importance of enzyme immobilisation at larger scale, but opted not to use this technique in this study.[101]

The biocatalytic oxidation by Chapman *et.al* required low concentrations of starting material, due to poor product solubility. [123] At high substrate concentrations, product particulate caused blockages in flow tubing, necessitating the need for constant removal. Transport of solids through tubing is usually done by creating a slurry, or trapping the particle in a carrier. Liedtke *et.al* explored the flow of a gas-liquid-solid slurry for the hydrogenation of 3-methyl-1-pentyn-3-ol.[147] Solid homogeneous particle loading was used successfully up to 6 $g.L^{-1}$. The solid catalyst was transported as a suspension by means of internal vortices in the liquid portion of the segmented flow. Recent work by Peng *et.al* furthered the work on slurry Taylor-flow in microreactors, focusing on the flow characteristics, showing a larger proportion of particles in the liquid film as the gas velocity increases.[148] The work is applicable to T-junctions in microreactors, whilst different geometries have shown no correlation.

In triphasic foam systems, particles are not held at the gas-liquid boundary, these are carried by the foam through the system, in the same manner as a slurry. Solids have previously been transported by foams in the mining (mineral flotation) and construction (aerated concrete) industries, however our research shows no examples of liquid foams used with reactive systems to transport solids. A review on unreactive systems by Thonavadli *et al.* observed coal and sand particles transported in a foam, ranging up to 35 wt% solids, with no observable effect on the pressure drop across the beginning and end of the pipe.

The solid-carrying foam behaved similarly to the particle-free foam. Using a magnifying glass, they viewed the particles present at the plateau border (see Figure 77). Plateau borders are pockets within the foam, their contents have minimal effect on the gross flow characteristics. A similar study by Okpobiri *et.al* found that much larger particles of limestone or sandstone are unable to fit in the plateau border and therefore, have a considerable impact on the foam stability.[149] Unfortunately, the research used rudimentary measurements techniques and high particle size granulate, making comparison difficult.

Haffner *et.al* explored the trapping of particles in the plateau border, as shown by Figure 77.[150] The confinement parameter, λ, compares the size of particles contained in the plateau border (interstitial phase), to the size of the passage constrictions. Two mechanisms have been identified: (i) individual capture of the particles by the constrictions ($\lambda < 1$) and (ii) the collective trapping of the suspension ($\lambda > 1$). The particles trapped in the interstitial fluid can be trapped by constrictions or freely transported through the connected network of passages.

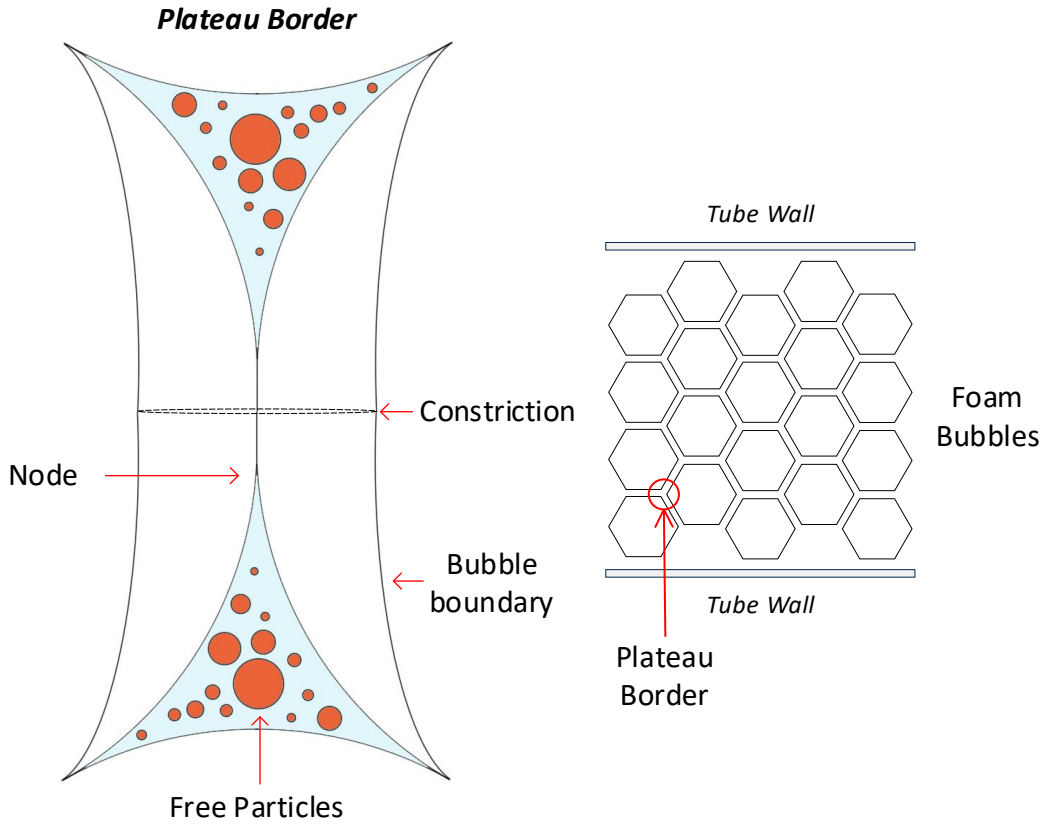

Figure 77: [left] Plateau border of a foam with particles suspended in the interstitial fluid between the nodes, allowing free movement or trapping by constrictions where the gap narrows[150]*; [right] foam structure travelling through a tube with the plateau border.*

As discussed in Chapter One, stabilisation of foams is important to ensure a long lifetime, stated as either transient (seconds) or metastable (days). Each technique used for foam generation changes the physical and rheological properties of a foam, an important variable for flow of a foam through a narrow tubing.

Solids can in some cases stabilise foams, this is analogous to micelles in liquid-liquid systems, known as Pickering emulsions.[151] Binks *et.al* noted the stabilisation of a foam by silica nanoparticles.[152] Adsorption of these to the interface did not change the interfacial tension but affected the contact angle between the bubbles, θ. This angle decreases with the hydrophobicity of the particle, at high contact angles particles prefer to stay in the air rather than the water.[143] For a hydrophobic solid, like DFF, in a foam , the particulate favours the air, reducing the concentration in the solution.

The rheology is critical for a continuously flowing foam process, and this can affect the process productivity. The shear force increases with flow rate and larger bubbles break, increasing the pressure on neighbouring bubbles.[153] A large pressure change alters the capillary stability, leading to further bubble collapse. Hence in high shear systems the bubble size will decrease over the time.[153] This results in a shear-thinning behaviour in most foams; their viscosity will decrease as a function of the shear rate.

Denkov *et.al* theorised that the surface tension was half the mechanical tension for the yield stress of a foam.[154,155] This was further explored by Yu *et.al* who demonstrated the reduction in bubble size of a surfactant stabilised foam upon the application of shear.[156]

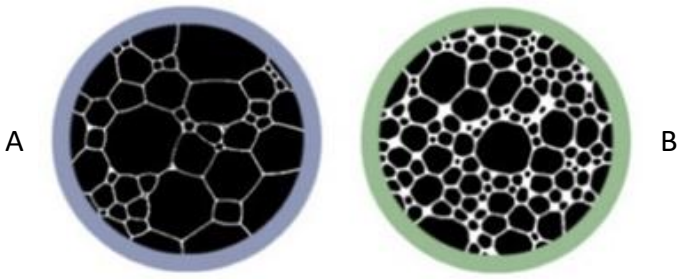

Figure 78 – Side-by-side comparison of a micrograph mask for fresh: (A) and post shear; (B) foam bubbles, indicating the decrease in average bubble size distribution.[156]

In continuous flow systems the shear rate can be controlled by the flow rate, but also the flow path, so sharp corners or tortuous paths are unfavourable. The flow of a foam in a tube has two regimes, known as high and low quality. The former is slug-flow, where a fine foam (small bubbles) are separated by a bulk gaseous phase.[157] Whereas low quality foam can be either plug-flow or segregated flow. The latter results in the separation of the gas and liquid, forming two distinct layers. For higher flow rates, plug-flow has the benefit of an increased liquid film that acts to lubricate the walls of the pipe. In segregated flow however, the separation results in greater liquid friction at the walls, increasing foam drainage.[157]

The following sections examine various methods used to form DFF from HMF using continuously flowing liquid foams. A variety of reactor types and foam generators were evaluated, with the aim of finding a suitable process for large-scale continuous production of DFF. Previous work in the group, using a trickle bed reactor design, had shown benefits in gas-liquid mixing to accelerate the oxidative reaction, and the use of immobilised enzyme, however the formation of DFF solid at concentrations greater than 16 mM caused fouling and blockage of the reactor and therefore limited the productivity. A viable, economic, process to produce a bioplastic monomer requires molar concentrations of product in minute reaction times. In this regard, the use of a continuously flowing liquid foam might provide both short reaction times and be able to process solid product, easily separated from soluble enzyme allowing it to be recycled.

3.2 Continuous foam oxidation of HMF to DFF

Figure 79 shows the oxidative route from HMF to DFF using the M_{3-5} mutant GOase enzyme, first produced by the Turner group and procured from Prozomix Ltd. [38,158] The liquid foam is formed by the addition of air through an air sparge, or generation of oxygen, by decomposition of hydrogen peroxide by catalase. The foam is stabilised by the three proteins present, and is sufficiently stable to carry DFF solid through the reactor.

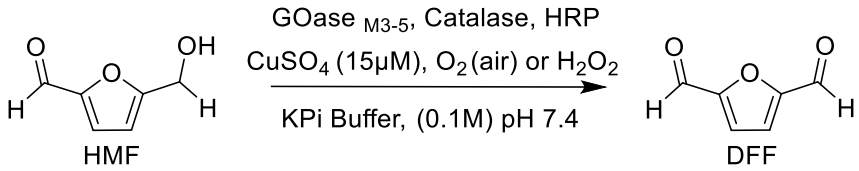

Figure 79 – General scheme for the oxidation of HMF to DFF. HRP = horse radish peroxidase, KPi = potassium phosphate. $CuSO_4$ is added to provide the necessary cofactor ions to the active site.

The reaction variables that have been examined include different physical and chemical conditions, and were evaluated with the aim of increasing both HMF conversion and DFF productivity (grams/litre/hour) of solid and solution. The following sections explore active or passive mixing methods used for foam generation, reactor modifications (tube length and diameter), foam flow rates (gas and liquid flow rates and ratio), residence times and distributions, and the activity of different $GOase_{M3-5}$ batches pre and post reaction.

Each reaction completed is described using a flow procedure and a table of results, including the relevant information on reactants; reactor dimensions and flow rates. Changes to the reactor setup or reactants have been stated where applicable.

3.2.1 Galactose oxidase batch activity (2017 & 2018)

Reactions were completed using the setup shown below. Initial experiments used a batch of $GOase_{M3-5}$ produced in 2017, whilst the latter half of experiments used enzyme produced in 2018. The later batch was of a larger quantity with less pure cell-free extract and lower activity. Figure 81 shows a continuous liquid foam flow reaction of HMF to DFF comparing GOase batches.

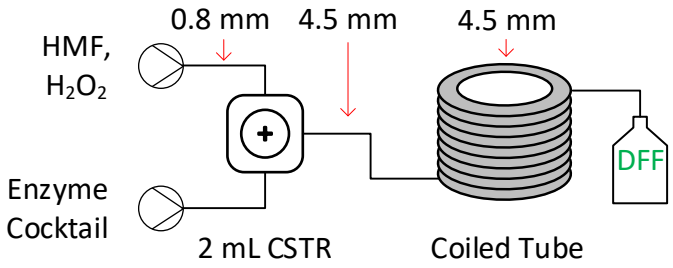

Figure 80 - Galactose oxidase catalysed oxidation in a continuous flow, using a 150 cm (4.5mm ID) coiled tube. A combined flow rate of 1 mL.min^{-1}. Enzyme cocktail contains $GOase_{M3-5}$, catalase, HRP and $CuSO_4$. HMF (200mM) in KPi buffer (0.1M) and 5% H_2O_2 (w/v).

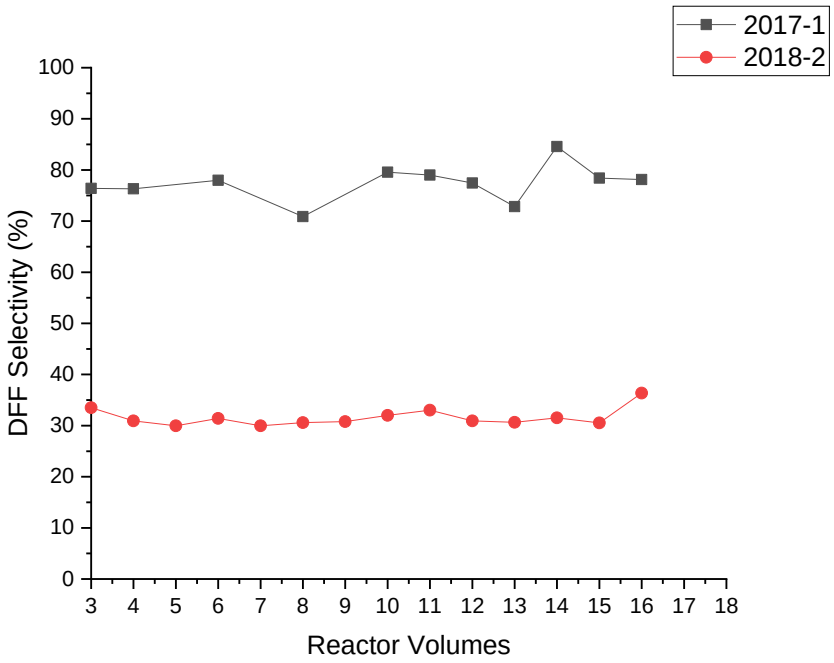

*Figure 81 - $GOase_{M3-5}$ LOT **2017-1** and LOT **2018-2** (Figure 82) catalysed oxidation of HMF to DFF in continuous flow.*

The crude preparation LOT **2018-2** shows around half the activity of LOT **2017-1** under the same conditions, with ~30% conversion at steady-state. Figure 82 and Figure 83 show the number of cellular debris in LOT **2018-2**, present as a fine solid, which was not observed for the earlier batch. Experiments using both batches have been used in the study and reference is made to the lot used.

*Figure 82 – [left] GOase$_{M3-5}$ CFE LOT **2017-1** from Prozomix [right] GOase$_{M3-5}$ CFE LOT **2018-2** from Prozomix.*

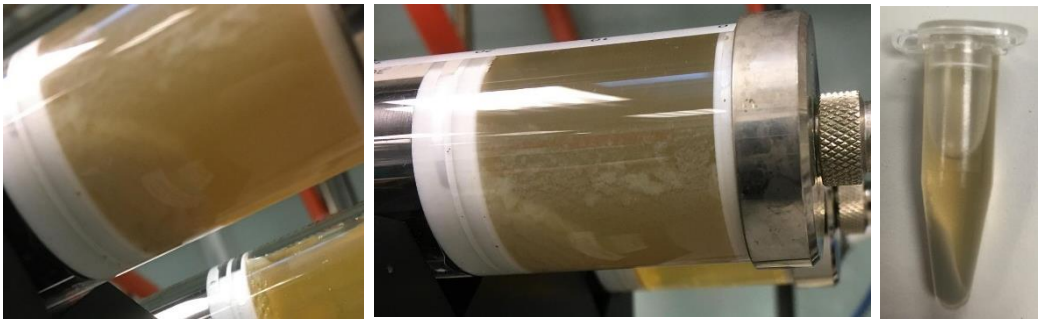

*Figure 83: [left & middle] GOase$_{M3-5}$ LOT **2018-2** enzyme precipitating out of solution in a syringe at RTP; [right] GOase$_{M3-5}$ LOT **2018-2** batch left to settle without centrifuging or denaturing the enzyme, showing most of the enzyme is unstable.*

3.2.2 Residence time of continuous foam flow

The residence time of a foam in a tubular continuous reactor is influenced by its volume that in turn is dependent upon the liquid and gas flow rates. The bubble size follows a distribution and its mean is affected by mixing intensity. For a foam generated by the decomposition of hydrogen peroxide with catalase, half an equivalent of oxygen gas is generated, equation 1, and the volume of this foam is dictated mainly by the molarity of the hydrogen peroxide, with the enzyme, substrate solution a minor fraction of this.

$$H_2O_2 \xrightarrow{\text{Catalase}} H_2O + \tfrac{1}{2}O_2 \qquad \text{Eqn. 31}$$

The quantity of oxygen evolved can be derived from equation 2.

$$V_o = \frac{C \times Q \times V}{2} \qquad \text{Eqn. 32}$$

Where:

V_o is the volume of evolved oxygen in $L.min^{-1}$

C is the concentration of H_2O_2 in $mol.L^{-1}$.

Q is the volumetric flow rate of liquid in $L.min^{-1}$.

V is the volume of an ideal gas at RTP (24 $L.mol^{-1}$).

All of the reactions tested used a standard, 0.49 $mol.L^{-1}$ (1% v/v), concentration of hydrogen peroxide, yielding an oxygen volume of 0.0059 $L.min^{-1}$. The foam volume could then be determined by the sum of the liquid and gas flow rates. The ratio of gas to liquid volume was varied around 20:1 The reactor volume was determined from the internal diameter and length of the tube, including any additional CSTR's used. From this the residence time was determined, equation 3.

$$t_{res} = \frac{(\pi r^2 l) + V_{CSTR}}{(Q_a + Q + V_o)}$$ Eqn. 33

Where:

t_{res} is the residence time in minutes.

r is the internal radius of the reactor tubing in cm

l is the length of the reactor/tubing in cm.

V_{CSTR} is the volume of a CSTR in mL.

Q_a is the gas flow rate in mL.min^{-1} (in air sparge experiments)

Q is the flow rate of liquid in mL.min^{-1}.

V_o is the volume of evolved oxygen in mL (in peroxide experiments).

The residence time distribution was measured using a pulse of 10% (v/v) red food dye introduced into the CSTR using a port and syringe, Figure 8. Separately, the peroxide was shown not to bleach the food dye, as the two components are only in contact for a short time before the peroxide is decomposed. A volume of foam was collected every 15 seconds, and the foam in each sample was acidified with 50 µL of 1 M HCl (to inactivate the enzyme) and collapsed to a liquid using the g-force in a lab centrifuge. The absorbance was measured off-line at 516 nm. The pulse-injection experiment produced a residence time distribution curve, Figure 85. The peak indicates the mean residence time of the reactor.

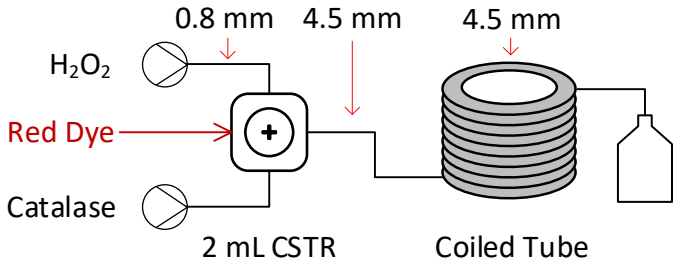

Figure 84 – Pulse injection reactor for the in in-situ generation of foam. A 150 cm (4.5 mm ID) coiled tube is connected to a 2 mL CSTR. Dye is pulsed in at a 10% (v/v) solution into the CSTR.

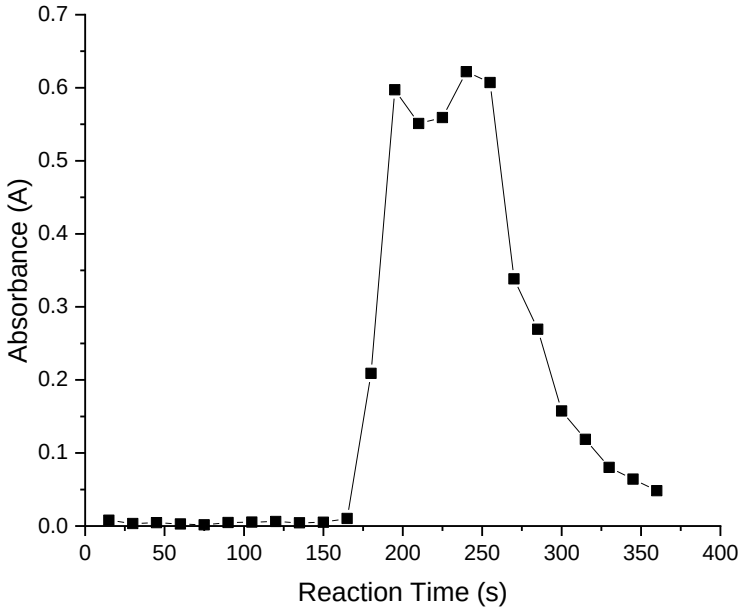

Figure 85 – Pulse injection experiment of a peroxide generated foam in a CSTR with 150 cm tubular reactor (4.5 mm ID) at 1 mL.min^{-1}. Absorbance measured at 516 nm. Reaction system used is shown in Figure 84.

Two distinct peaks are observed at the maximum (around 180 s and 250 s), indicating some back-mixing of the foam. However, the median is the same as the calculated residence time of 240 s (4 mins). Some tailing is observed with dye still present after half a reactor volume, taking >195 s to return to initial levels, and this may indicate a different flow regime at the vessel wall due to higher its frictional force. The result demonstrates that all the dyed foam formed during the reaction travels through the tubing, with minimal dead zones. When it comes to carrying solid, dead zones would retard the transport of particulates through the reactor and might cause the deposition of solid DFF on the inner walls of the tubing, known as fouling. The short residence time was ideal for fast biocatalytic oxidations, producing DFF in under 5 minutes.

With a theoretical and practical examination of the foam's residence time distribution, the study moved onto bio-oxidations using HMF as the substrate.

3.2.3 Continuous stirred tank reactor

A 2 mL continuous stirred tank reactor (CSTR) was used as a pre-mixer, installed before the reactor column. Its purpose was to efficiently mix the feed solutions to allow rapid formation of the foam, before it travelled through the pipe. The results of testing different HMF concentrations and residence times are shown in Table 11.

Table 11 – Optimisation of GOase catalysed oxidation of HMF to DFF in continuous flow, using a narrow-bore tube and a continuous stirred tank reactor.

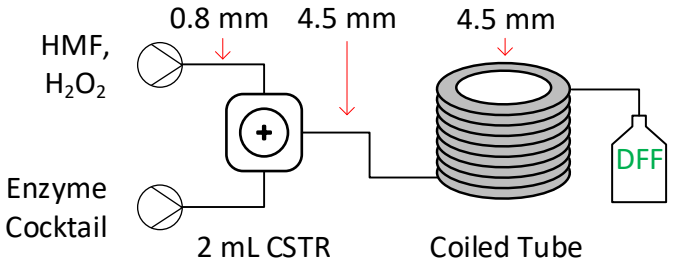

Entry	HMF (mM)	Tube Length (cm)	t_{res} (mins)	Remaining HMF (%) [c]	Conversion (%) [c]			Mass Balance (%)
					HMFCA	*DFF*	*FFCA*	
1 [a]	25	100	3.00	2.6	0.0	85.4	6.8	-5.2
2 [a]	125	100	3.00	26.8	0.1	36.4	0.3	-36.4
3 [a]	200	100	3.00	4.5	1.1	80.5	0.2	-13.7
4 [a]	200	150	4.00	5.8	0.9	71.8	0.5	-21.0
5 [a]	200	300	8.00	8.7	0.5	72.5	0.6	-17.7
6[b]	200	150	4.00	29.2	0.1	35.8	0.2	-34.7
7[b]	200	200	5.25	29.8	0.1	32.8	0.2	-37.1

*[a] reaction used batch $GOase_{M3\text{-}5}$ **(2017-1),** [b] reaction used batch $GOase_{M3\text{-}5}$ **(2018-2),** [c] determined by HPLC analysis at steady-state. Reactor tubing was a 100, 150, 200 or 300 cm (4.5 mm ID) coiled tube. Enzyme cocktail contains $GOase_{M3\text{-}5}$, catalase, horseradish peroxidase and copper sulphate. t_{res} = residence time.*

A significant and stable foam was formed in all the conditions used. The major product formed was DFF, with notable mass loss for all reactions. Although conversion is highest in Entry 1, the overall yield is greater in Entry 3, demonstrating the reaction can be completed at concentrations exceeding the DFF solubility limit of 16 mM (2 $g.L^{-1}$). The mass loss increases non-linearly with increasing HMF concentration, as seen in Entry 1 & 3. HMFCA and FFCA were always formed as by-products in minor quantities and no FDCA was observed in any of the samples. The residence time had a little impact as the reaction seemed faster than the minimum used, 3 minutes, Entries 1 & 5. The enzyme batch with lower activity led around 45% less DFF conversion, Entries 4 & 6.

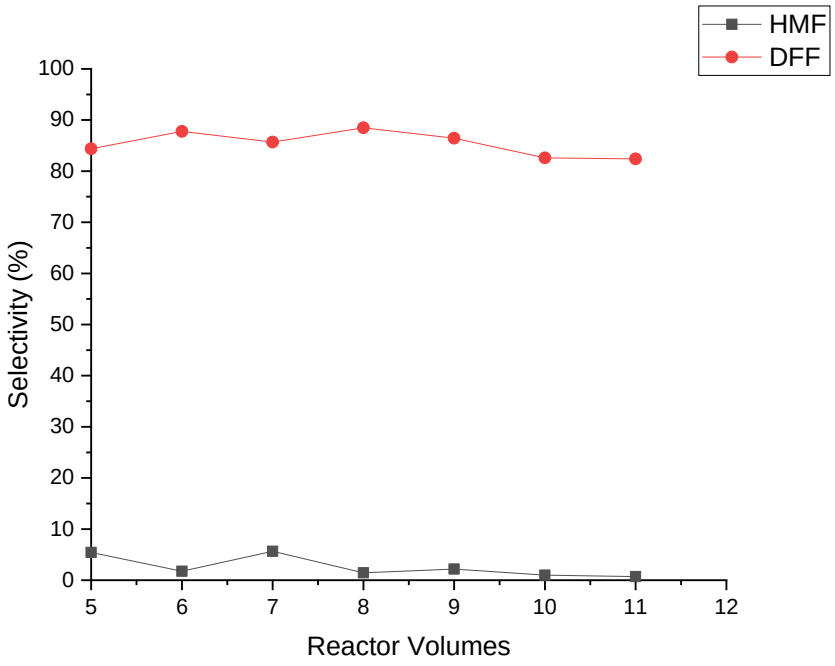

Figure 86 – $GOase_{M3-5}$ catalysed bio-oxidation of 25 mM HMF in continuous flow with a 100 cm 4.5 mm ID reactor (Table 11, Entry 1) and 2 mL pre-mixing CSTR shown in Table 11.

Figure 86 shows that steady-state is reached from 5 reactor volumes (RV), and remained consistent at ~85% conversion to the end of the experiment, 11 reactor volumes (30 minutes). There is up to 15% mass unaccounted for within the system (HMF compared to DFF and side-products), and this was later determined to be DFF solid collecting on the tube wall, but intermittently detaching in a slug.

There is potential for DFF to remain in the reactor as pockets of the foam dry-out during the pump refill, depositing the particulate at narrow tubing sections. Photographs of the foam are shown in Figure 87 and these illustrate both its mechanical and physical stability, retaining its shape over many hours.

Figure 87 – Foam "stalagmites" formed from the continual dripping of solution and foam out of the reactor, demonstrating the foams excellent stability.

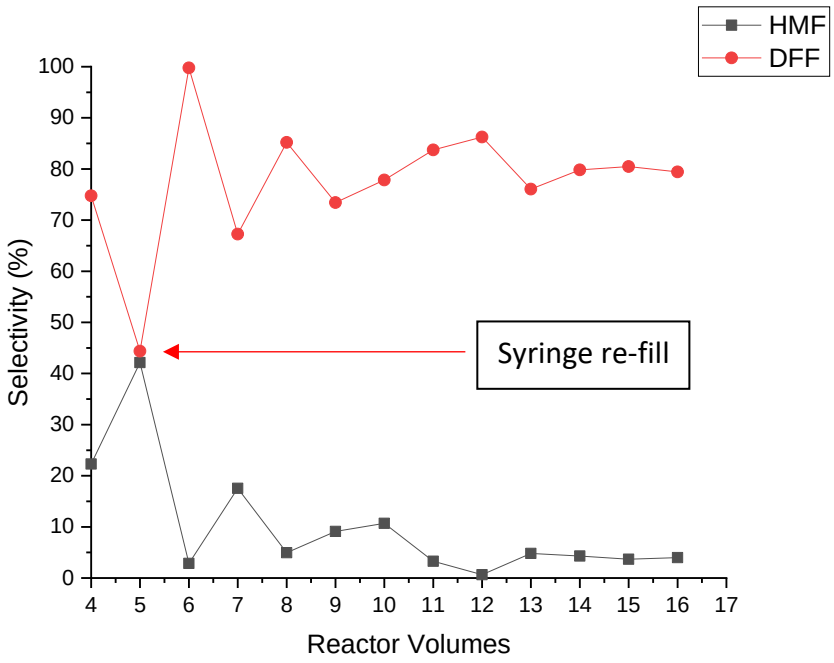

Figure 88 – GOase$_{M3-5}$ catalysed bio-oxidation of 200 mM HMF in continuous flow with a 100 cm 4.5 mm ID reactor (Table 11, Entry 3) and 2 mL pre-mixing CSTR.

Figure 88 shows the reaction of Table 1, Entry 3, in which 200 mM HMF was used. Whilst steady-state took longer to achieve, ~7 RV, though hindered by the syringe re-fill at 5 RV, ~85% conversion was also observed, with missing mass varying between 1 and 16% over the course of the reaction. Notable was the 100% conversion seen shortly after the syringe refill, with the reaction sitting stationary in the pipe for a period giving a longer reaction time. A longer residence time may provide a higher HMF conversion. The main result of this experiment was that large amount of DFF solid formed in the reaction could be successfully carried through the reactor, with calculated productivity 52 mM.min^{-1} or 6.4 g.L.$^{-1}$min^{-1}. This greatly exceeds the previous productivity of 0.18 g.L.$^{-1}$min^{-1}.[123] Furthermore, with reaction times <4 minutes the system is significantly better than the several hour batch process.

Figure 89 shows steady-state conversion data for three reactions separately carried out in reactor lengths of 100, 150 and 300 cm all at 200 mM HMF.

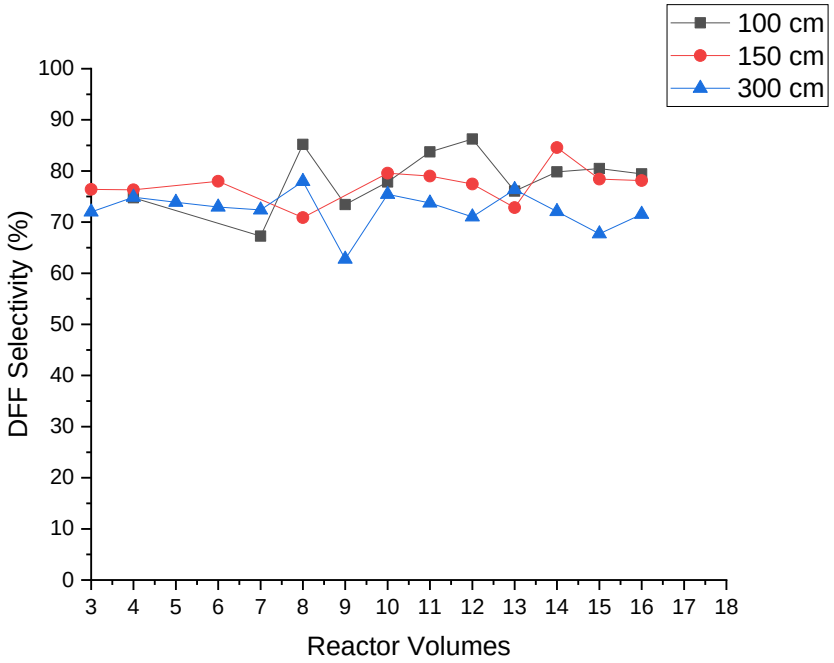

Figure 89 – GOase$_{M3-5}$ catalysed bio-oxidation of 200 mM HMF in continuous flow using reactors of differing length but equal diameter (4.5 mm ID) (Table 11, Entries 3, 4 & 5 respectively).

Varying the reactor length had no impact on the DFF conversion. With conversion similar between all three reactions, indicating all three residence times are sufficient for reaction completion. A fine foam was observed in all three systems, however slightly more particulate deposition was observed on the longer 300cm tubing. Containment and transport of DFF particulate within the foam plateau border may therefore last for a short duration of time. These lamellae can hold a finite amount of product, if this is reached then deposition on the inner walls of the tubing would occur. Although increased shear at longer tube lengths can lead to collapse of the foam, it has minimal impact on the three systems used here.

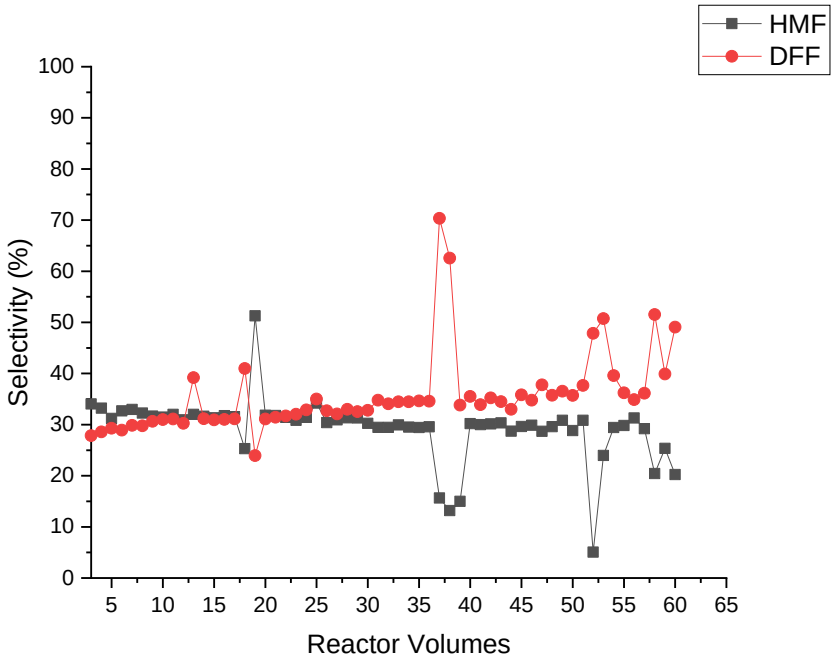

Figure 90 - GOase$_{M3-5}$ catalysed bio-oxidation of 200 mM HMF in continuous flow using a 150 cm 4.5 mm ID reactor (Table 11, Entry 6) over the course of 4 hours. GOase$_{M3-5}$ ***2018-2 LOT*** *was used for the reaction.*

Figure 90 shows a continuous flow reaction carried out over 4 hours using the less active GOase enzyme. A slow and small increase in DFF conversion is seen over 64 RV, going from ~30 to ~40%. Observation of the syringe pump revealed precipitation of the cell-free-extract debris, though it is likely that some of this is also carried with the foam, through the reaction. A continuous reaction is made possible by refilling the syringe with fresh enzyme solution kept on ice. The large peaks observed at RV's 8, 37 and 53 are caused by the refilling of the syringes. Once the pumps have been refilled, steady-state then resumes after 3 reactor volumes. Extraction of the reaction product into DCM, followed by an aqueous backwash yielded a sample of pure DFF with 78% recovered mass, based on an average of 36% DFF conversion (overall yield of 28% DFF from HMF). The ^{1}H NMR shown in *Figure* 91.

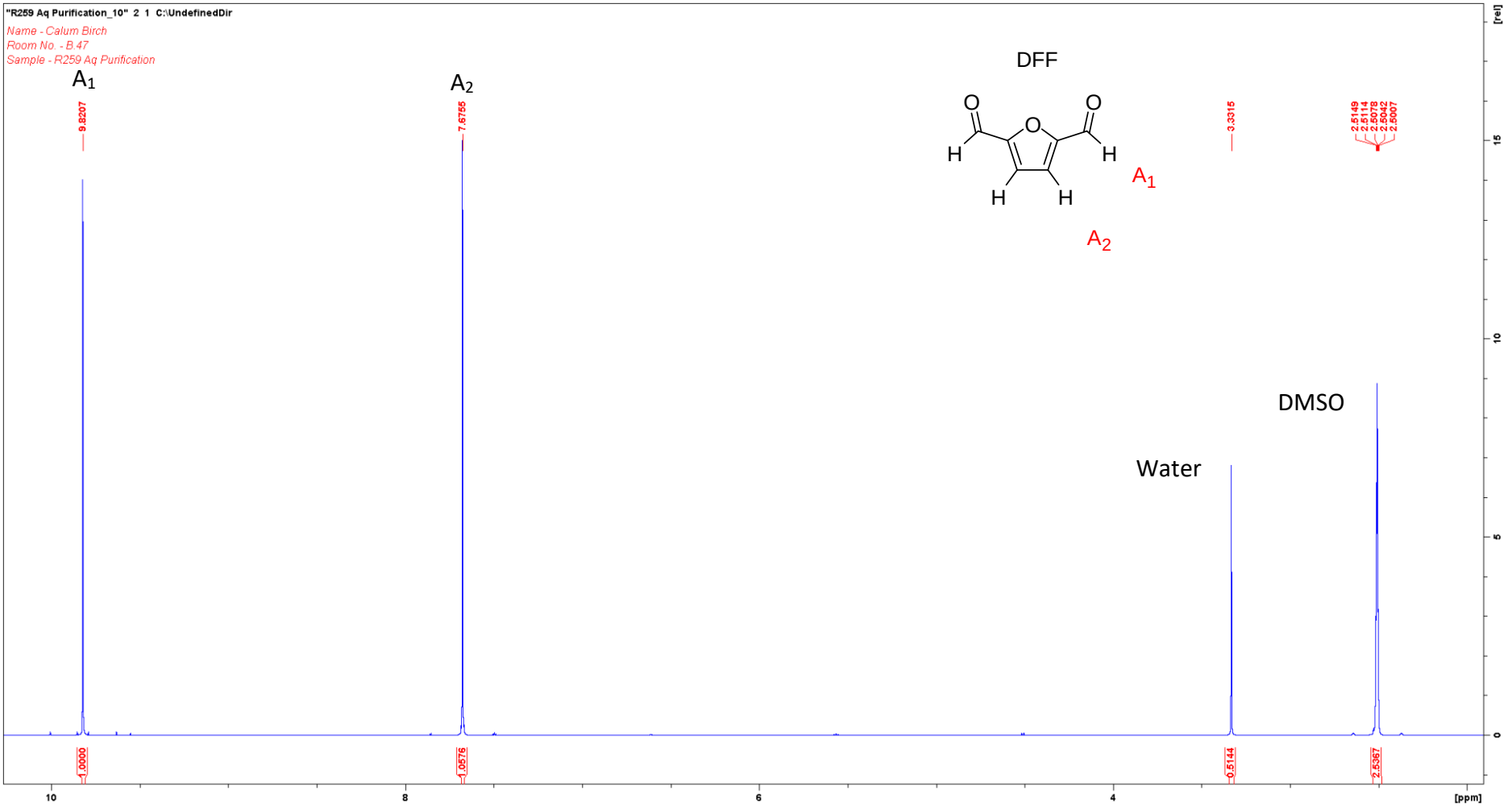

Figure 91 - ^{1}H NMR of purified DFF using DCM from Entry 10 in DMSO-d^{6}, peaks show pure DFF.

In an effort to increase and maintain conversion of >80% a second CSTR connected to a coiled tube was added on. At the second CSTR an additional feed of enzyme solution was pumped in to supply the system with fresh enzyme, negating the effect of denaturation that may occur in the tubing.

Table 12 - Optimisation of GOase catalysed oxidation of HMF to DFF incontinuous flow, using two coiled tubes and two continuous stirred tank reactors in series.

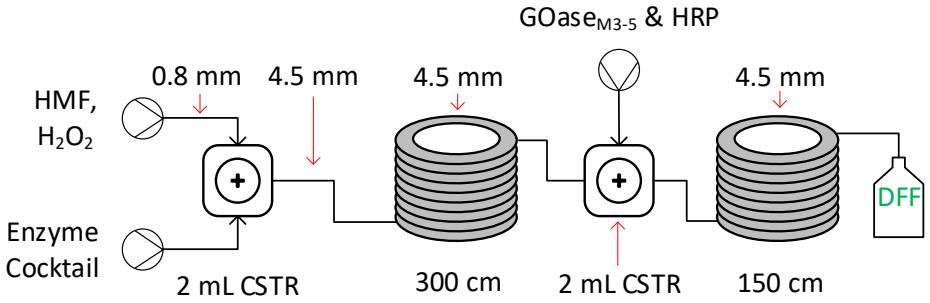

Entry	HMF (mM)	t_{res} (mins)	Remaining HMF (%) [a]	Conversion (%) [a]			Mass Balance (%)
				HMFCA	***DFF***	***FFCA***	
1	200	11.00	1.5	1.7	80.2	0.5	-16.1

*[a] determined by HPLC analysis at steady-state. Reactor tubing in order used; 1st coiled tube was 300 cm, 2nd coiled tube was 150cm, both with a 4.5 mm ID. Enzyme cocktail contains GOase$_{M3-5}$ (LOT **2017-1**), catalase, horseradish peroxidase and copper sulphate. A second enzyme pump containing GOase$_{M3-5}$ and HRP connects at the secondary CSTR. t_{res} = residence time.*

The reactor setup from Table 11 was extended to include an additional enzyme feed. Whilst this gave a temporary 95% HMF conversion, Figure 92, disappointingly, the steady-state was ~85%, more comparable to the shorter reactor (Table 11, Entry 3).

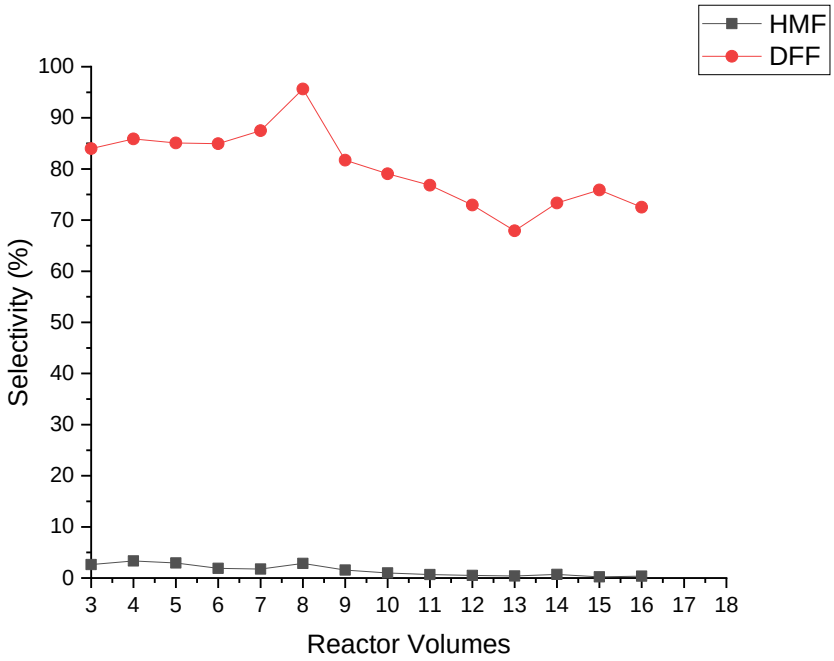

Figure 92 – GOase$_{M3-5}$ catalysed bio-oxidation of 200 mM HMF in continuous flow with a 300cm 4.5mm ID reactor, followed by a 2nd CSTR and 150 cm 4.5 mm ID reactor. A secondary enzyme pump fed into the 2nd CSTR, doubling the enzyme concentration (Table 12, Entry 1).

Addition of a second tubular coiled reactor increased the reactor volume by 66% from 50 mL to 75 mL, however the increased residence time did not translate into increased conversion. Furthermore, addition of a second dose of GOase/HRP failed to increase the conversion above 85%. It was speculated that GOase, HRP or catalase may be inactivated during the reaction, so their activity was assayed at the end of reaction. This was done by testing the outflow enzyme solution in a batch reaction, and gave further HMF conversion indicating all three enzymes were still active. Significant mass loss was also observed in the reaction, (Table 12, Entry 1) and visual observation showed signs of reactor fouling and solid deposition. The brown residue highlighted in (Figure 94) is present throughout the 2nd 150 cm reactor column. HPLC and ^{1}H NMR analysis confirmed the presence of DFF in this deposit, *Figure* 93. Prolonged exposure to peroxide combined with drying of the foam resulted in the enzyme denaturing, contributing to the reactor fouling and reduced conversion over time as solid built-up in the tubing.

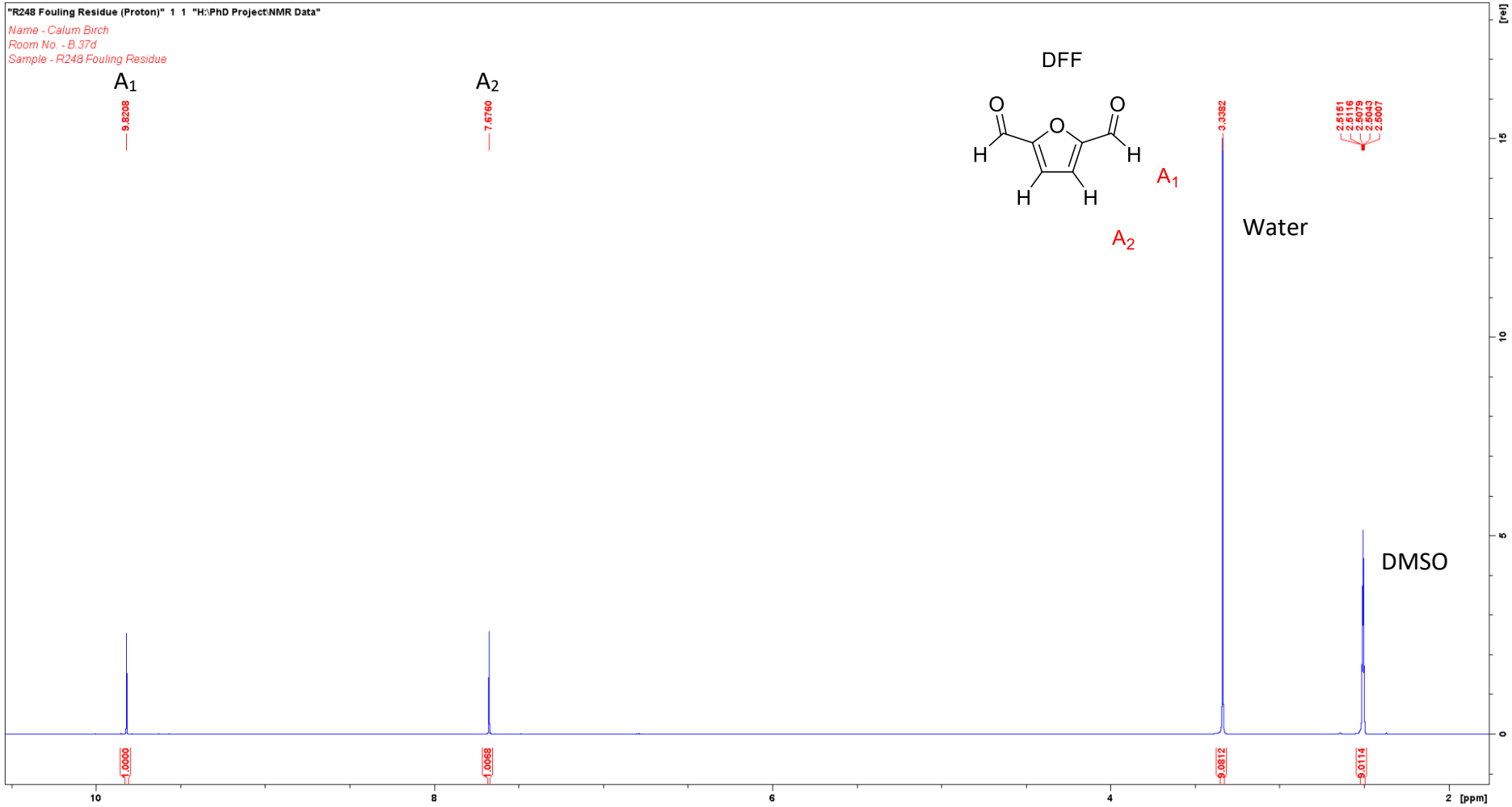

Figure 93 – ^{1}H NMR of fouling residue from Entry 6 in DMSO-d^{6}, peaks indicate the presence of DFF and water.

Figure 94 – Fouling residue observed in the 300 cm (4.5 mm ID) reactor (Table 12, Entry 8).

The ^{1}H NMR spectra of the residue in DMSO-d^{6} shows the presence of DFF (*Figure* 93), the two remaining peaks being that of water and the solvent. The ratio of the two further indicates a small concentration of DFF in a wet sample. A part of the residue was also enzyme. From activity assays against peroxide, 5-10% catalase is denatured when the foam is formed. Enzyme did not dissolve in the NMR solvent; visible as solid and filtered out before analysis. The residue was further dissolved in both ethyl acetate and water for HPLC analysis. The results indicated DFF with minimal quantities of HMF and FFCA.

The steady-state conversion fell when the syringe pumps were refilled (Rv 7), dropping to an average 75% DFF conversion. The time taken to refill three syringes impacted the recovery to steady-state. The DFF conversion is comparable with (Entry 3), suggesting the initial quantity of enzyme is sufficient, with excess having little impact. Removal of the residue by flushing the system through with water proved ineffective, physical contact was required to dislodge it from the inner walls. Further washing with ethyl acetate was able to partially remove the build-up, however some still remained and required removal using a pipe cleaner.

Table 13 shows the results of testing wider-bore tubing. This was felt important as the surface area of the wall affects both the foam flow (retarding it), and possibly its stability. The larger bore tubing was used to enhance foam generation, providing a larger formation area.

Table 13 – Optimisation of GOase catalysed oxidation of HMF to DFF in continuous flow, using a wide-bore reactor with a continuous stirred tank reactor.

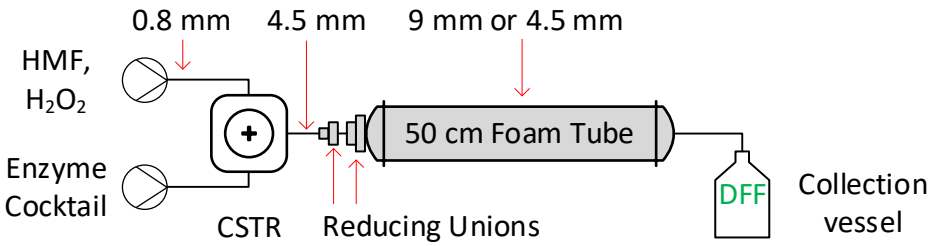

Entry	HMF (mM)	Tube ID (mm)	Tube Length (cm)	t_{res} (mins)	Remaining HMF (%) [c]	Conversion (%) [c]			Mass Balance (%)
						HMFCA	*DFF*	*FFCA*	
1[a]	200	9.0	50	5.25	7.6	0.7	73.1	0.4	-18.2
2[b]	200	4.5	200	5.25	29.8	0.1	32.8	0.2	-37.1
3[b]	200	4.5	50	1.25	41.4	0.1	12.9	0.1	-45.5
4[b]	200	9.0	50	5.25	36.1	0.1	30.1	0.2	-33.5

*[a] reaction used batch $GOase_{M3\text{-}5}$ (**2017-1**), [b] reaction used batch $GOase_{M3\text{-}5}$ (**2018-2**), [c] determined by HPLC analysis at steady-state. Reactor tubing was a 50 cm (9.0 mm ID) horizontal tube. Enzyme cocktail contains $GOase_{M3\text{-}5}$, catalase, horseradish peroxidase and copper sulphate. ID = internal diameter, t_{res} = residence time.*

Entry 1 shows the DFF conversion is 73% with the 9 mm ID tubing, in comparison to (Table 11, Entry 3) DFF conversion is reduced from 80%; the wider bore tubing results in increased foam drainage. Entries 3 & 4 investigate conversion at similar reactor lengths; a 40% reduction in DFF conversion is observed upon a 42% reduction in residence time. Another comparison can be made between two reactions with the same 50 cm tube length and 4.5- and 9-mm diameters, Figure 95 and Figure 96 respectively.

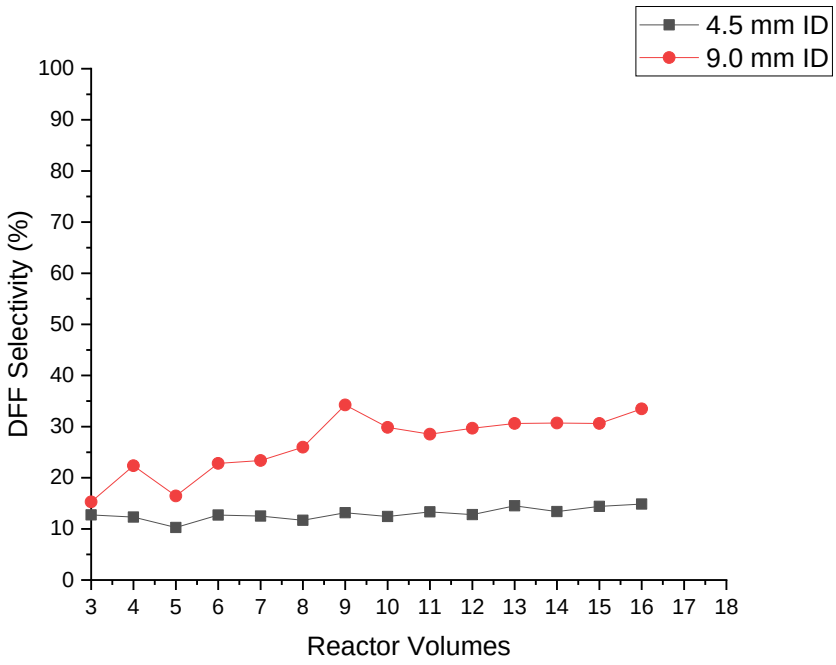

*Figure 95 – Goase$_{M3\text{-}5}$ catalysed bio-oxidation of 200 mM HMF in continuous flow using two 50 cm reactors of 9 mm ID (Table 13, Entry 4) and 4.5 mm ID (Table 13, Entry 3). GOase (LOT **2018-2**) was used for both reactions.*

For reactors of equal length (50 cm) but different diameter, the conversion favours the larger diameter tubing which can be attributed to the difference in residence times between the two systems. The larger tubing provides a residence time of 5.25 mins, the shorter of 1.25 mins, a factor of 4.2. If the correlation is linear then 8.0% conversion would be expected against 12% observed. The non-linearity probably relates to the difference in surface area (squared) to volume (cubed). The larger bore tubing has a further advantage of reducing the surface area of foam that comes into contact with the tube walls, helping reduce particulate deposition. The use of narrower tubing was explored but found infeasible, giving a residence time of <20 s so would require a much longer tube. To further explore the effect tube diameter has on the system, reactors of equivalent internal volume (36 mL) and therefore residence time, were built. Figure 96 shows two reactors of the same volume but different dimensions.

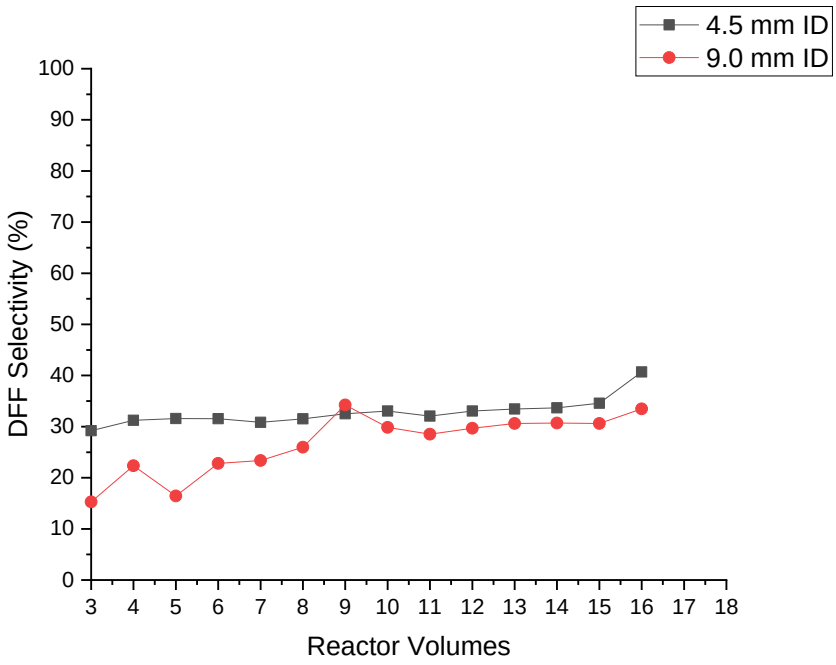

*Figure 96 – GOase$_{M3-5}$ catalysed bio-oxidation of 200 mM HMF in continuous flow using two 36 mL internal volume reactors of 4.5 mm ID (Table 13, Entry 2) and 9.0 mm ID (Table 13, Entry 4). These reactors had lengths of 200 cm and 50 cm respectively. GOase (**LOT 2018-2**) was used for both reactions.*

In this case the difference in DFF conversion was small. The narrower reactor has a more consistent steady-state, reached in less time, whilst the larger tube takes roughly 3 times longer to reach steady-state. Once this was reached, at ~9 RV, the systems were comparable. These systems may differ at higher HMF concentrations, where the transport and deposition of insoluble particulate are more prominent. The residence time of 5.25 minutes was sufficient for the reaction using the less active 2018 GOase$_{m3-5}$. A comparative batch test with this enzyme gave 40% DFF after 2 hours. But was much poorer than the (LOT **2017-1**) batch of GOase$_{M3-5}$ that gave >70% DFF conversion in 2 hours.

To determine the effects of passive mixing, for compressed air systems, a tube-in-tube mixer was constructed. This allowed for a direct comparison between active and passively mixed systems, for future development into using compressed air as the oxygen source.

3.2.4 Tube-in-tube pre-mixer

To test the effect of different pre-mixers in generating the foam, an impermeable tube-in-tube T-piece was used, installed before the reactor column, Table 4. In one of the experiments a fine steel mesh (wire wool) was incorporated into the pre-mixer as it was seen from other designs (fire extinguisher-type) this was useful in generating a fine foam. The T-mixer was used to generate the foam passively (rather than active mixing) at the opening to a larger aperture tubing. The mixing might also affect the enzyme stability. The foam was formed solely by the rapid catalase catalysed decomposition of hydrogen peroxide, to give gaseous oxygen. Length and diameter of the reactor were varied for a sufficient residence time.

Table 14 - Optimisation of GOase catalysed bio-oxidation of HMF to DFF in continuous flow, using a narrow-bore reactor with a tube-in-tube pre-mixer.

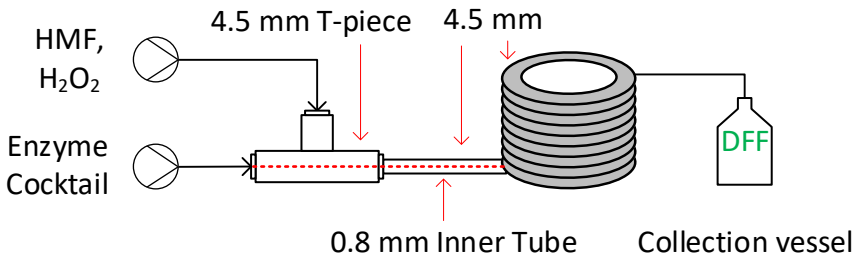

Entry	HMF (mM)	Tube Length (cm)	t_{Res} (mins)	Remaining HMF (%) [b]	Conversion (%) [b]			Mass balance (%)
					HMFCA	DFF	FFCA	
1	200	100	2.50	22.3	0.1	48.8	0.4	-28.4
2	200	150	3.67	11.2	0.4	69.3	0.5	-18.5
3	400	150	3.67	23.5	0.0	19.9	0.1	-56.5
4	200	300	7.50	29.0	0.2	55.5	0.6	-14.7
5[a]	200	150	2.50	42.6	0.0	11.1	0.1	-46.2

*[a] reaction setup incorporated a steel wire mesh packed tube before the reactor column, [b] determined by HPLC analysis at steady-state. Reactor tubing was a 100, 150 or 300 cm (4.5 mm ID) coiled tube. Enzyme cocktail contains $GOase_{M3\text{-}5}$ (LOT **2017-1**), catalase, horseradish peroxidase and copper sulphate. t_{res} = residence time.*

Most of the reactions in Table 4 produced DFF, though some had unreacted HMF remaining. The 100 cm reactor, with residence time of 2.5 minutes gave 49% DFF conversion at steady-state, Entry 1 and Figure 97, whilst the longer, 150 cm tube, with 3.7 minutes residence time, Entry 2 and Figure 98, gave a higher, 69%, conversion, and less mass loss. Increasing the residence time to 7.5 minutes using a 300 cm reactor, failed to improve the conversion further, and only 55% DFF was seen, though it provided the best mass balance. At 400 mM HMF concentration the conversion was less than half that expected, Entry 3, though it would have been useful to test the 300 cm reactor for increased residence time. Introducing the pre-mixer mesh at higher liquid flow rates, Entry 4, reduced the conversion compared to the equivalent system, Entry 1. Based on DFF conversion there is an optimum residence time between 2.5 minutes and 5.0 minutes, with 3.67 minutes producing the best result.

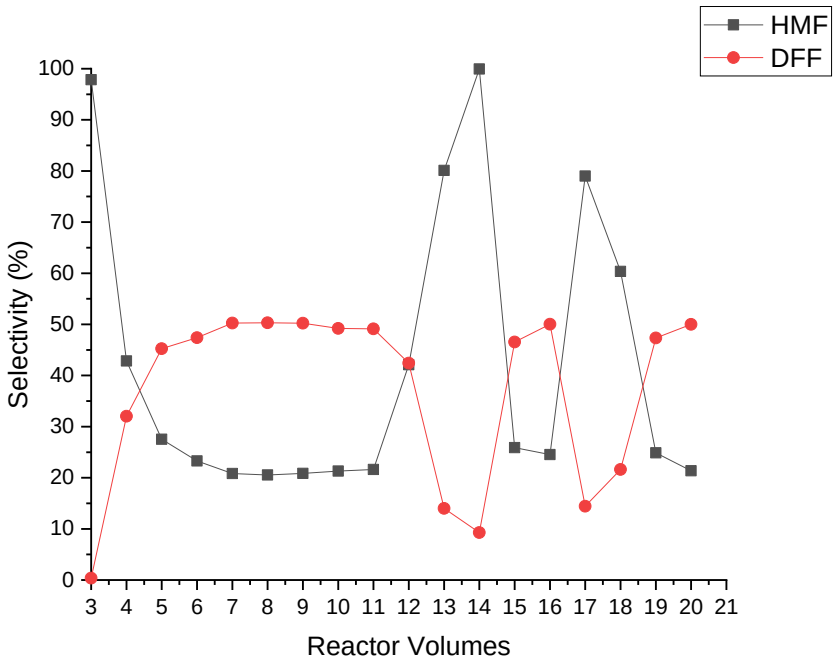

Figure 97 - GOase$_{M3-5}$ catalysed bio-oxidation of 200 mM HMF in continuous flow with a 100 cm (4.5 mm ID) reactor and a tube-in-tube pre-mixer (Table 14, Entry 1).

Figure 97 for the experiment in Table 14, Entry 1, shows that steady-state is achieved after six reactor volumes (totalling 18 minutes), less time than was required for the shorter but larger diameter reactor. The distinct peak changes observed initially at RV 12 and then RV 16 originate from pump issues. Once resolved and setup to run the conversion takes roughly 6-9 minutes (2-3 RV's) to reach steady-state again. Achieving a similar conversion at steady-state, prior to the pump failure, demonstrates the robustness of the process. As the enzyme pump fails and HMF returns to 100%, there is still DFF present (10%) in the system that gradually travels through the reactor. Overall DFF selectivity is maintained at 50%, indicating the residence time isn't long enough. Unlike the CSTR reactions, once the pumps are switched off DFF conversion drops. Indicating further conversion is a cause of the CSTR's active mixing rather than the limited mass transfer in the foam-filled tubing.

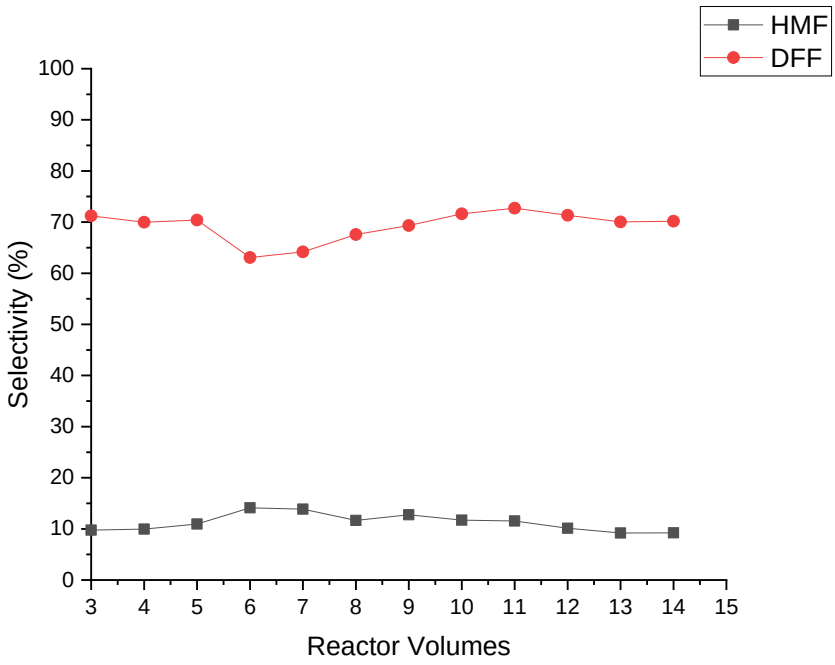

Figure 98 - GOase$_{M3-5}$ catalysed bio-oxidation of 200 mM HMF in continuous flow with a 150 cm (4.5 mm ID) reactor and a tube-in-tube pre-mixer (Table 14, Entry 2).

Figure 98 shows the steady-state data from experiment Table 14, Entry 2, and is achieved after 3 RV (11 minutes) and is maintained an hour. Conversion is higher in the longer 4.5 mm ID tubing than the shorter or wider counterparts. There is a particular balance between column length and tube diameter, this reaction lies closer to that optimum. The average conversion is 75% with 12% HMF remaining. Again, mass loss is observed, however it's on the lower end of values recorded for the tube-in-tube system. When compared to the CSTR system (Table 11, Entry 4) there is a 5% less conversion due to the lack of active mixing.

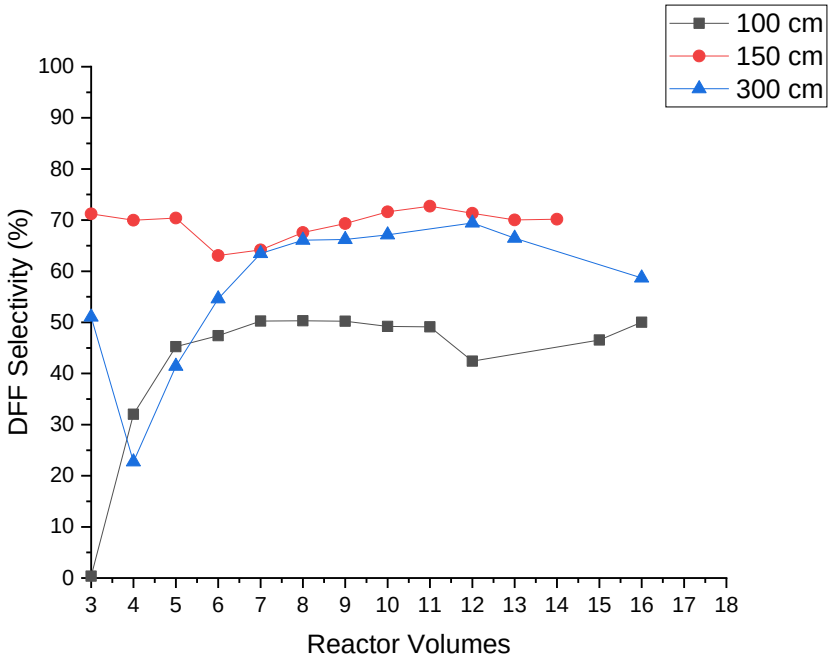

Figure 99 - GOase$_{M3\text{-}5}$ catalysed bio-oxidation of 200 mM HMF in continuous flow using three reactors of equivalent diameter (4.5 mm ID) but different lengths; 100 cm, 150 cm and 300 cm (Table 14, Entries 1, 2 & 4 respectively). Tube-in-tube pre-mixer used.

Figure 99 summarises the steady-state data from experiments in Table 14, Entries 1, 2 & 4 with three different reactor lengths. Unlike the actively mixed CSTR system the tube-in-tube process lacks sufficient mixing and mass transfer. This is evident from the reduced conversion of all three reactions compared to their CSTR counterparts that all produced an average of 70% DFF (see Figure 89). The longer length columns produced the largest quantity of product, whilst the shorter length reactor had a more robust steady-state at lower conversion. Residence time therefore plays a prominent role in passively mixed systems, with the system limited by mass transfer. The 150 cm and 300 cm are comparable, indicating a residence time of 3.6 minutes is sufficient, with longer times having little impact. The foam produced was visibly less fine, with larger bubbles forming naturally from the catalase catalysed decomposition of hydrogen peroxide. This reduction in surface area may further contribute to reduced DFF particulate transport through the reactor, thereby preventing higher conversion.

Table 15 shows the results of testing wider-bore tubing. As mentioned previously the larger bore tubing was used to enhance foam generation, providing a larger formation area. This was essential for a system using compressed air to both provide the oxidant and generate the foam.

Table 15 - Optimisation of GOase catalysed bio-oxidation of HMF to DFF in continuous flow using a wide-bore reactor with a tube-in-tube pre-mixer.

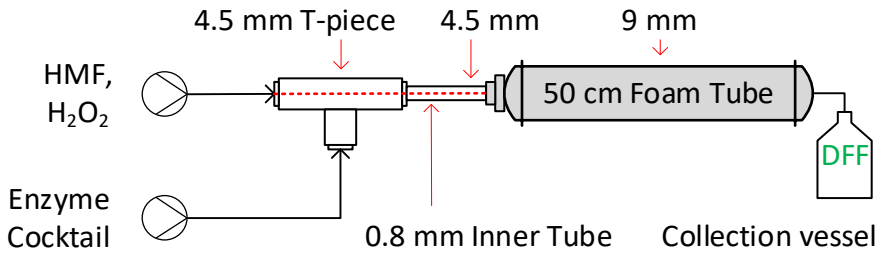

Entry	HMF (mM)	t_{Res} (mins)	Remaining HMF (%) [b]	Conversion (%) [b]			Mass balance (%)
				HMFCA	DFF	FFCA	
1	200	5.0	15.8	0.5	59.6	0.4	-23.7
2[a]	200	3.67	24.0	0.2	49.2	0.2	-26.4

*[a] reaction setup incorporated a steel wire mesh packed tube before the reactor column, [b] determined by HPLC analysis at steady-state. ID = internal diameter, t_{res} = residence time. Reactor tubing was a 50 cm (9.0 mm ID) coiled tube. Enzyme cocktail contains $GOase_{M3\text{-}5}$ (**LOT 2017-1**), catalase, horseradish peroxidase and copper sulphate.*

Table 15 shows two experiments with different the same reactor and different flow rates giving residence times of 5.0 and 3.7 minutes, Entries 1 and 2 and the steady-state data are in Figure 100 and Figure 101 respectively. A higher residence time gave increased conversion of HMF to DFF, forming 10% more product with 9% less HMF leftover. The mesh used in Entry 2 produced a visibly finer foam with a homogenous bubble size distribution. Increased residence time using the mesh would be beneficial, yielding increased conversion.

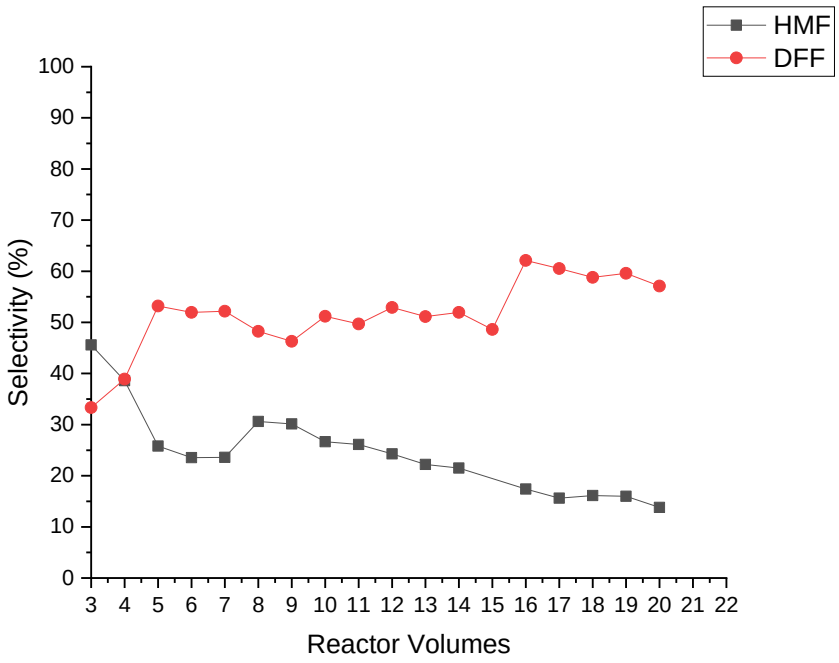

Figure 100 - GOase$_{M3-5}$ catalysed bio-oxidation of 200 mM HMF in continuous flow with a 50 cm (9 mm ID) reactor and a tube-in-tube pre-mixer (Table 15, Entry 1).

Steady-state fluctuates in this reaction, not reaching the ideal conditions. The downward trend observed by HMF indicates a trend of increasing conversion. The opposing upward trend by DFF is visible. Five reactor volumes are required to reach a near steady-state, longer than the narrower tubing. Although the column volumes are similar, it may require more time for the foam to grow and fill the larger tubing. Once filled the foam is then in contact with a greater surface area. Dependent upon which flow regime it's under (high or low-quality), this could drastically alter the flow through the pipe, either hindering or enhancing it.

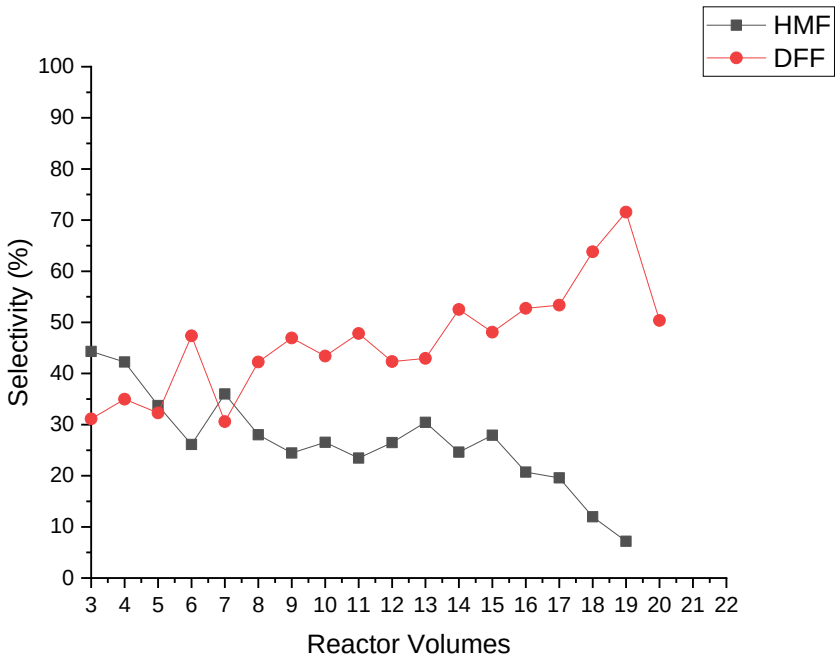

Figure 101 - GOase$_{M3-5}$ catalysed bio-oxidation of 200 mM HMF in continuous flow with a 50 cm (4.5 mm ID) reactor and a tube-in-tube pre-mixer with steel wire packed mesh (Table 15, Entry 2).

The lack of active mixing for the reaction has extended the time taken to reach steady-state. After 20 RV's DFF production is still rising whilst HMF is proportionally declining. The change initially observed at reactor volume 17 is from pump refilling. The system takes roughly 4 RVs to return to its previous rate of conversion, a slight increase in time from the CSTR systems. At the higher flow rate used (2 mL.min^{-1}) conversion of 55% after 20 RV's is an excellent outcome. The effect of the mesh isn't discernible from the tabulated results, however at higher flow rates a finer foam was produced. Inspection of the mesh after reaction completion revealed a large quantity of enzyme residue. The high shear stress produced from forcing the liquid and foam through the mesh may have caused partial foam collapse.

3.2.5 Air sparge pre-mixer

As an alternative to providing the enzyme oxygen from the decomposition of hydrogen peroxide, it was decided to test the use of air. To note, the reaction rate may be 20% of that using pure oxygen due to the partial pressure of oxygen in air. A non-permeable tube-in-tube cross-piece was used as a pre-mixer, installed before the reactor column with an attached air sparge. Its purpose was to generate the foam as the two liquids meet and travel through a steel mesh. The foam was formed by the capture of liquid in the mesh and the rapid flow of air through the tube creating bubbles stabilised by the protein present. The lengths and diameter of reactor varied to ensure a sufficient residence time. Air flow was controlled using a rotameter and kept at either 0.10 $L.min^{-1}$ or 0.04 $L.min^{-1}$. No back-pressure regulators were installed. To ensure the reactions produced a foam without the presence of hydrogen peroxide, a surfactant was added to a number of reactions, listed in Table 17. Four surfactants were chosen, based on their solubility, and tested for their foamability in a buffer solution, the results are visible in Figure 102.

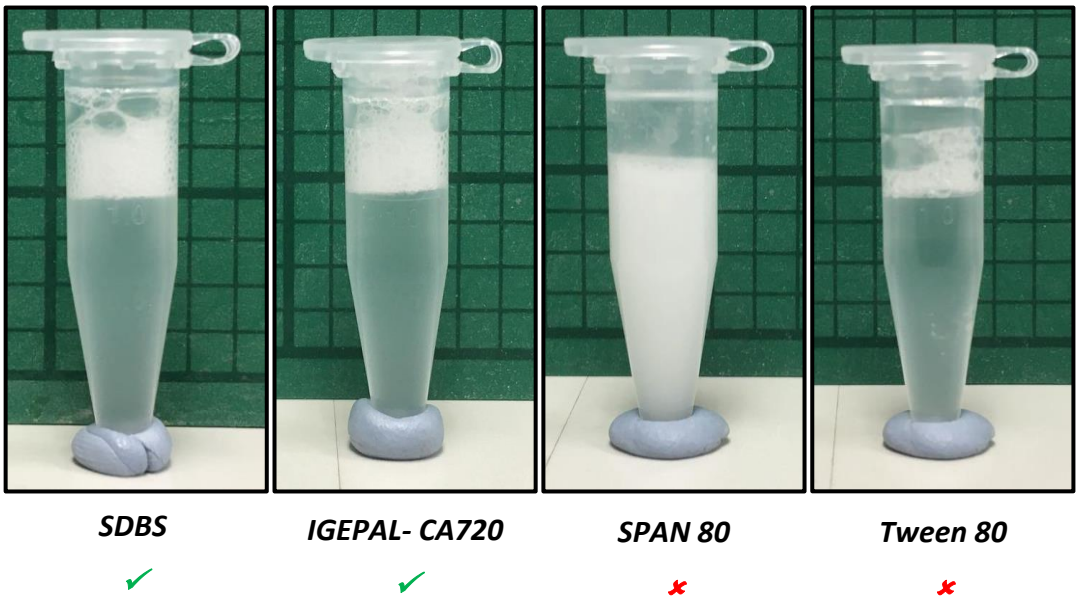

Figure 102 – Comparison of the foamability of different surfactants in 100 mM pH 7.4 potassium phosphate buffer solution at RTP. 0.1% w/v or 0.1% v/v of surfactant added.

The two surfactants that produced a stable foam were sodium dodecylbenzene sulphate (SDBS) and polyoxyethylene-(12)-isooctylphenyl ether (IGEPAL-CA720). Sorbitane monooleate (SPAN 80) produced an emulsion and polyethylene glycol sorbitane monooleate (Tween 80) had poor solubility. Batch reactions using the $GOase_{M3-5}$ system were then completed in triplicate using an incubator shaker, to determine the effect of the surfactant on enzyme activity.

Table 16 - Assay of GOase catalysed bio-oxidation of HMF to DFF in batch using an incubator shaker with added surfactant.

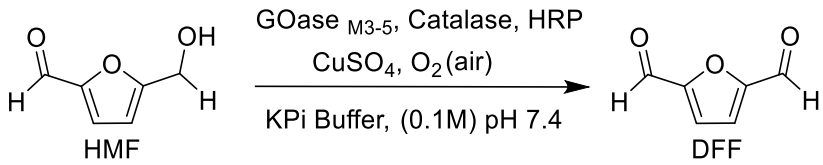

Entry	Addition of Surfactant	Reaction replicates	Remaining HMF (%) [a]	DFF Conversion (%) [a]
18[a]	None	Control	36.7	30.0
19[a]	SDBS	1	37.1	21.4
20[a]	SDBS	2	36.4	21.5
21[a]	SDBS	3	34.6	25.8
-	Average	Average	36.0	22.9
22[b]	IGEPAL	1	27.8	24.2
23[b]	IGEPAL	2	34.2	23.7
24[b]	IGEPAL	3	32.0	27.7
-	Average	Average	31.3	25.2

*[a] Reactions had 0.1% w/v SDBS added to them, [b] Reactions had 0.1% v/v IGEPAL-CA720 added to them, [c] determined by HPLC analysis. Reactions completed in 15 mL falcon tubes in an incubator shaker at 37 °C and 350 rpm using $GOase_{M3-5}$ (**LOT 2018-2).** HRP = horseradish peroxidase, KPi = potassium phosphate. $CuSO_4$ is added to provide the necessary cofactor ions to the active site.*

Both surfactants caused a reduction in DFF product formation, with a slight impact on HMF conversion. The IGEPAL surfactant was notably better, with less HMF remaining and more DFF produced. This was therefore chosen as a suitable surfactant to add to the substrate pump for continuous flow foam reactions.

Table 17 - Optimisation of GOase catalysed bio-oxidation of HMF to DFF in a continuous flow, using a narrow-bore reactor with a tube-in-tube per-mixer, air sparge and steel-wire mesh.

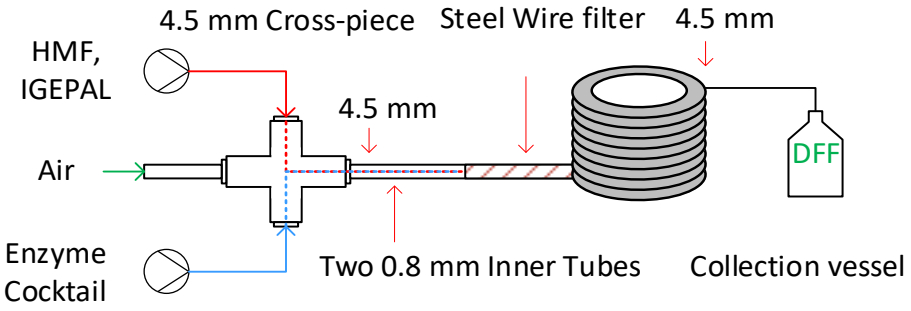

Entry	Air flow ($L.min^{-1}$)	t_{Res} (mins)	Remaining HMF (%) [a]	Conversion (%) [a]			Mass balance (%)
				HMFCA	DFF	FFCA	
1	0.10	0.25	51.7	0.0	7.6	0.1	-40.6
2	0.10	0.25	52.7	0.0	7.3	0.0	-40.0
3	0.04	1.25	55.5	0.0	4.3	0.0	-40.2

*[a] determined by HPLC analysis at steady-state. Reactor tubing was a 150 cm (4.5 mm ID) coiled tube. Enzyme cocktail contains $GOase_{M3\text{-}5}$ (**LOT 2018-2**), catalase, horseradish peroxidase and copper sulphate. All reactions included addition of IGEPAL-CA720 at 1% v/v. t_{res} = residence time.*

Table 17 shows the results of HMF oxidation with GOase using air as the oxygen source. Significantly less DFF was produced than the peroxide-based systems, partly because of the partial pressure of oxygen in air and partly the much shorter residence time, due to higher gas flow rate. Correcting for the oxygen concentration, by multiplying by 5, the conversion would be 20-35% which is still much less than the 85% seen in the peroxide system so may be due to the shorter residence time. The mass balance was very poor but consistently bad at 40%. Increasing the residence time from 0.25 to 1.25 minutes actually produced less DFF, with more fouling observed on the longer 300 cm reactor tubing. Notably, little foam was observed in the tubing; the output was mainly liquid with a small amount of foam bubbles. Entries 1 and 2 are replicates that demonstrate the reproducibility of the process with similar selectivity of all intermediates and products.

In an attempt to overcome these problems, the residence time was increased using a wider bore tube and lower air flow rate, Table 18.

Table 18 - Optimisation of GOase catalysed bio-oxidation of HMF to DFF in continuous flow, using a wide-bore reactor with a tube-in-tube per-mixer, air sparge and steel-wire mesh.

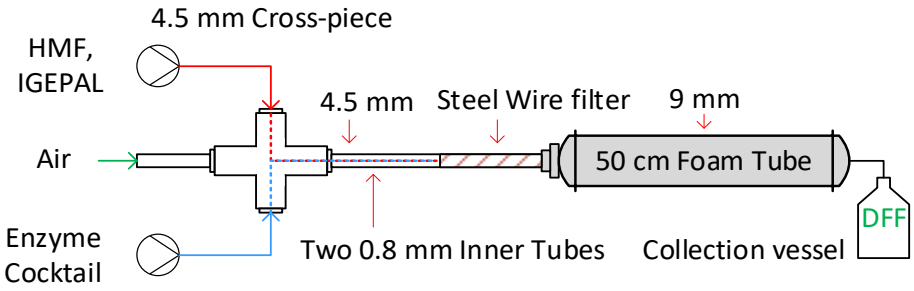

Entry	Air flow ($L.min^{-1}$)	t_{Res} (mins)	Remaining HMF (%) [b]	Conversion (%) [b]			Mass balance (%)
				HMFCA	DFF	FFCA	
1	0.04	0.47	49.3	0.0	8.6	0.0	-42.1
2[a]	0.04	0.47	42.6	0.0	11.1	0.1	-46.2

*[a] reaction used a flow rate of 2 $mL.min^{-1}$, [b] determined by HPLC analysis at steady-state. ID = internal diameter, t_{res} = residence time. Reactor tubing was a 50 cm (9.0 mm ID) horizontal tube. Enzyme cocktail contains $GOase_{M3\text{-}5}$ (**LOT 2018-2**), catalase, horseradish peroxidase and copper sulphate. All reactions included addition of IGEPAL-CA720 at 1% v/v.*

Wider tubing favoured the reaction with up to 11% DFF conversion, compared to long, narrow-bore tubing with 4.3%, Table 17, Entry 3. Less FFCA and no HMFCA were produced under these conditions. Increasing the liquid flow rate produced more DFF whilst having minimal impact on the residence time, Entry 2. At higher liquid flow rates, a finer foam was observed. At a higher pressure the liquid is forced rapidly through the mesh producing a finer foam with a visibly homogenous bubble size distribution. At the lower liquid flow rates, the volume is insufficient to completely coat the mesh, hence a trickling of liquid is observed, with minimal foam.

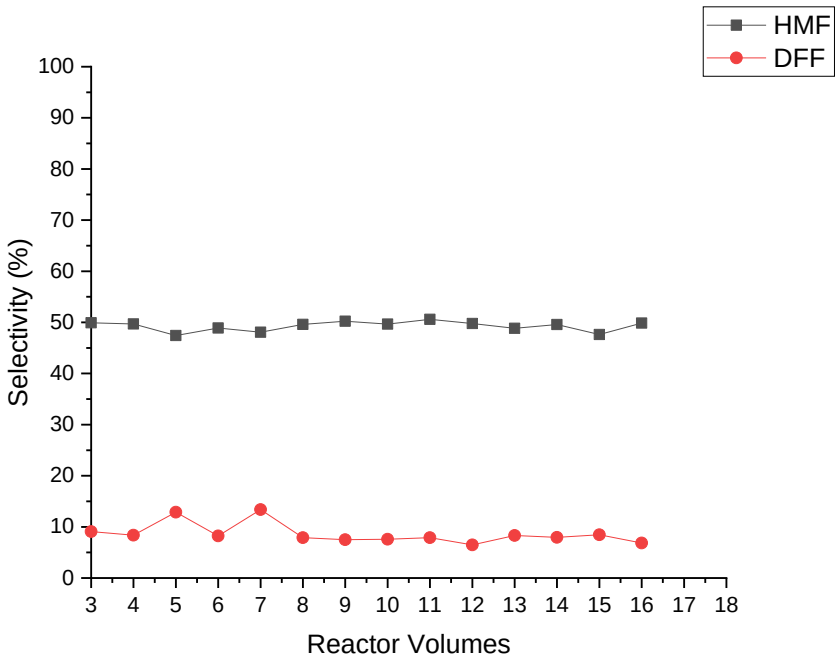

Figure 103 - Reaction profile of the GOase$_{M3\text{-}5}$ catalysed bio-oxidation of 200 mM HMF in continuous flow with a 50 cm (9 mm ID) reactor and a tube-in-tube air sparge, mesh pre-mixer (Table 18, Entry 1).

Although conversion to DFF averages out at 8.6%, this is using compressed air, that contains only 21% oxygen, ~5 times less than the pure oxygen formed from peroxide decomposition, so this would equate to 41% conversion with a residence time of only 0.47 minutes. The productivity of this system would be 21 g.L.$^{-1}$min^{-1} if pure oxygen gas were used. Significant mass loss of 42% is observed. This reaction demonstrated considerable promise; with longer tubing, reduced air flow rate or an increase to 5 bar pressure the conversion would improve.

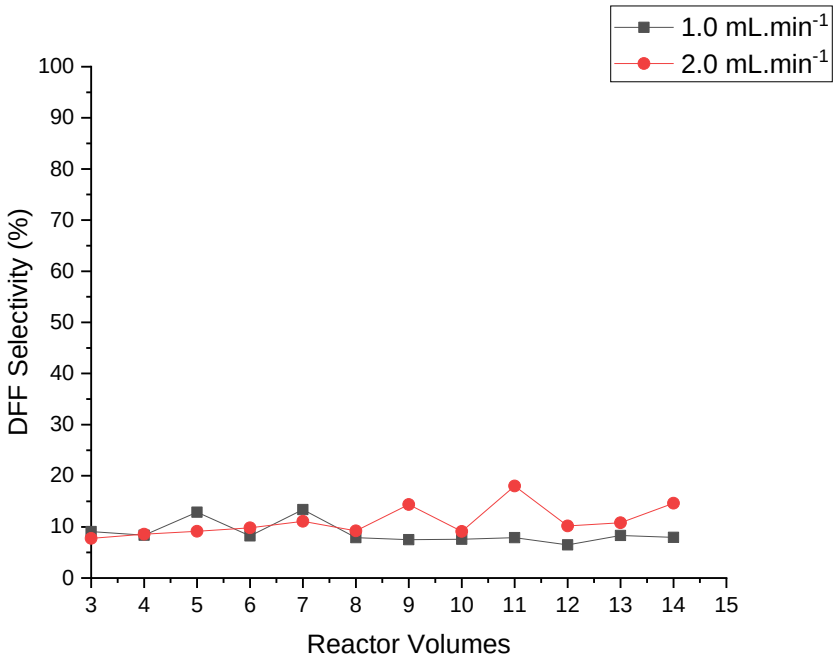

Figure 104 - GOase$_{M3-5}$ catalysed bio-oxidation of 200 mM HMF in continuous flow with a 50 cm (4.5 mm ID) reactor and a tube-in-tube pre-mixer with steel wire packed mesh and air sparge. Use of two liquid flow rates of 1 mL.min^{-1} (Table 18, Entry 1) and 2 mL.min^{-1} (Table 18, Entry 2).

Figure 104 shows a comparison between the DFF conversion at two liquid flow rates, 1.0 and 2.0 mL.min^{-1}, used to form the foam. Variation of the liquid flow rate has little impact on the conversion, with the residence time dominated primarily by the much higher flow rate of air through the system, 0.04 L.min^{-1}, a ratio of 10:1 and 40:1 gas to liquid. Steady-state conversion at the 2.0 mL.min^{-1} flow rate is lower, indicating the residence time was insufficient for substantial conversion to occur. However, foam was of a higher quality enabled by increased coverage of the mesh with liquid, thereby enhancing the production of bubbles. The foams for both systems had relatively large bubble size distribution with a lack of homogeneity.

To provide a longer residence time a different reactor design was used in which the reaction would occur in a continuously gas (air) and liquid fed sparged tank. The DFF solid, and some liquid are transported out of the reactor by the foam, Table 9

Table 19 - Optimisation of GOase catalysed bio-oxidation of HMF to DFF in continuous flow coiled tube, connected to a Drechsel bottle with an air sparge.

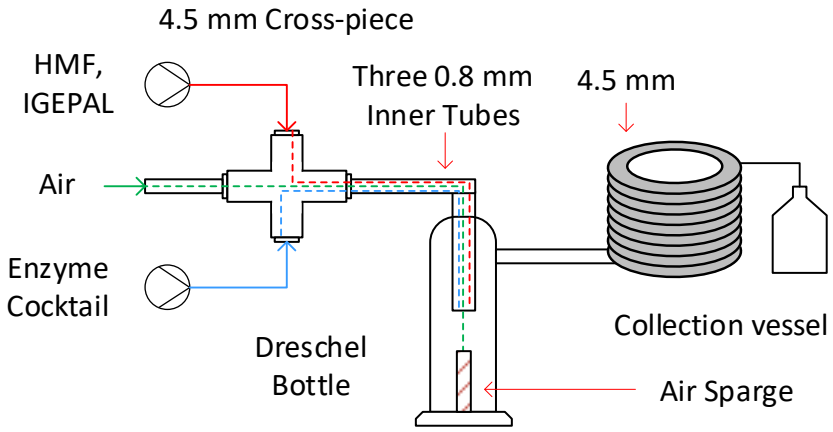

Entry	Air flow (L.min^{-1})	t_{Res} (mins)	Remaining HMF (%) [c]	Conversion (%) [c]			Mass balance (%)
				HMFCA	DFF	FFCA	
1[a]	0.04	1.00	45.9	0.0	5.1	0.0	-49.0
2[b]	0.04	12.00	43.2	0.0	17.4	0.0	-39.4
3[b]	0.10	3.00	42.9	0.0	12.4	0.0	-44.7
4[b]	0.04	12.00	40.5	0.0	20.9	0.1	-38.5

*[a] system used a 15 mL Drechsel bottle without an air filter sparger and batch GOase$_{M3-5}$ (LOT **2017-1**), [b] system used a Drechsel bottle of 250 mL volume with an air filter sparger and batch GOase$_{M3-5}$ (LOT **2018-2**), [c] determined by HPLC analysis at steady-state. Enzyme cocktail contains GOase$_{M3-5}$, catalase, horseradish peroxidase and copper sulphate. All reactions included addition of IGEPAL-CA720 at 1% v/v. Reactor tubing was a 150 cm (4.5 mm ID) coiled tube. t_{res} = residence time.*

The liquid volume in a Drechsel bottle (250 mL volume) was maintained by the enzyme cocktail feed at around 1 mL.min^{-1} and this provided a longer residence time, though has not as yet been defined. With an air flow rate of 0.04 L.min^{-1} 17% conversion to DFF was observed, which would equate to 85% conversion with pure oxygen.

However, a large loss in mass balance was observed, averaging over 40%. This may be due to solid held-up in the reactor, not able to be transported by the foam. Use of an air sparger produced the finest foams, no air sparger saw the formation of large bubbles and a more heterogenous foam, Entry 30. Unlike prior entries the use of $GOase_{M3\text{-}5}$ (**2018-2**) produced more DFF with longer residence times. The shorter, apparent residence time of 1 minute was insufficient for oxygen mass transfer, whilst a higher air flow rate of 0.1 $L.min^{-1}$ gave less conversion, but produced a visually fine foam.

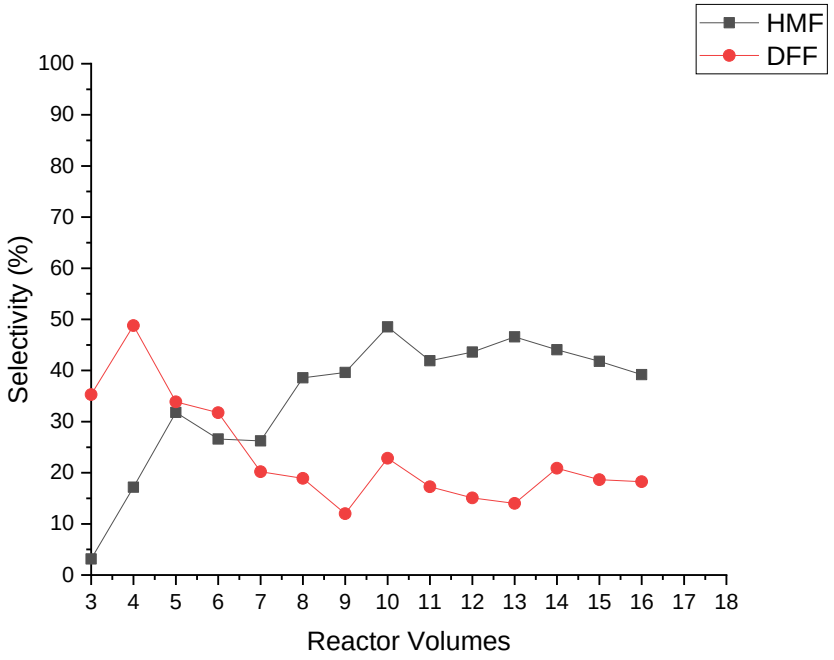

Figure 105 - GOase$_{M3-5}$ catalysed bio-oxidation of 200 mM HMF in continuous flow with a 250 cm Drechsel bottle and a 150 cm (4.5 mm ID) reactor with an attached air filter sparger (Table 19, Entry 2).

Introduction of an air filter sparger improved the foam produced, with a more visibly defined bubble size distribution. The finer foam helped improve mass transfer and particulate transport through the reactor, with bends and junctions subject to considerable fouling, hence the observed mass loss as seen in Figure 108. Use of a stable batch of GOase$_{m3-5}$ could yield conversion similar to that of the peroxide systems. Coupling a longer residence time with improved gas transfer helped initially at improving DFF conversion, however the steady-state conversion fell with time. The higher conversion is linked to the height of the sparger in the bottle; as such the foam and liquid height were further measured. Comparing Entry 2 with Entry 4 demonstrates the reproducibility of the surfactant process, with similar production of all four compounds. Testing the liquid enzyme outflow in an HMF GOase batch reaction gave further conversion showing that all three enzymes were therefore still active. The catalase was included to break down the enzyme generated peroxide.

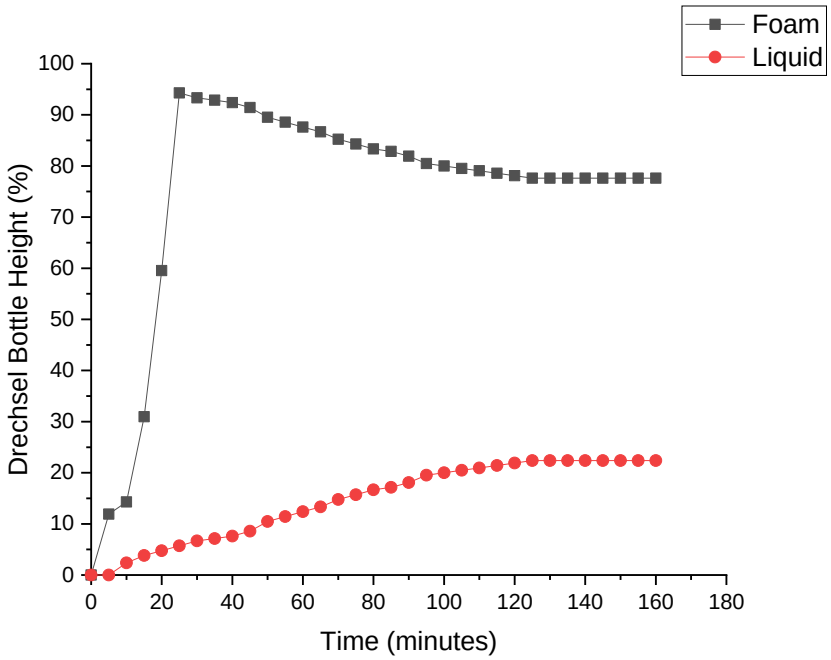

Figure 106 – The formation and height of foam in a 250 mL Drechsel bottle over the course of 3hrs (Table 19, Entry 4). The height of the Drechsel bottle is 210 mm.

Figure 105 shows a graph of the foam and liquid levels in the Drechsel bottle. After 5 minutes rapid formation of the foam begins, taking 25 minutes to reach a maximum of 198 mm in height. The initial lag before formation is due to the height of the sparger in the bottle; it is suspended 10-15 mm up from the base. Solution dropping onto the sparger and forming a film may still foam, however the remainder collects in the bottom and won't foam until the liquid reaches a certain height. This critical height is seen between 15 and 20 minutes when the foam doubles in height from 65 to 125 mm and then further to its maximum. The gradual decline in foam height, along with corresponding liquid increase, reaches a steady-state at 163 mm (Foam) and 47 mm (Liquid) after 125 minutes. This demonstrates that formation of the foam and liquid, takes longer to reach steady-state than the reaction.

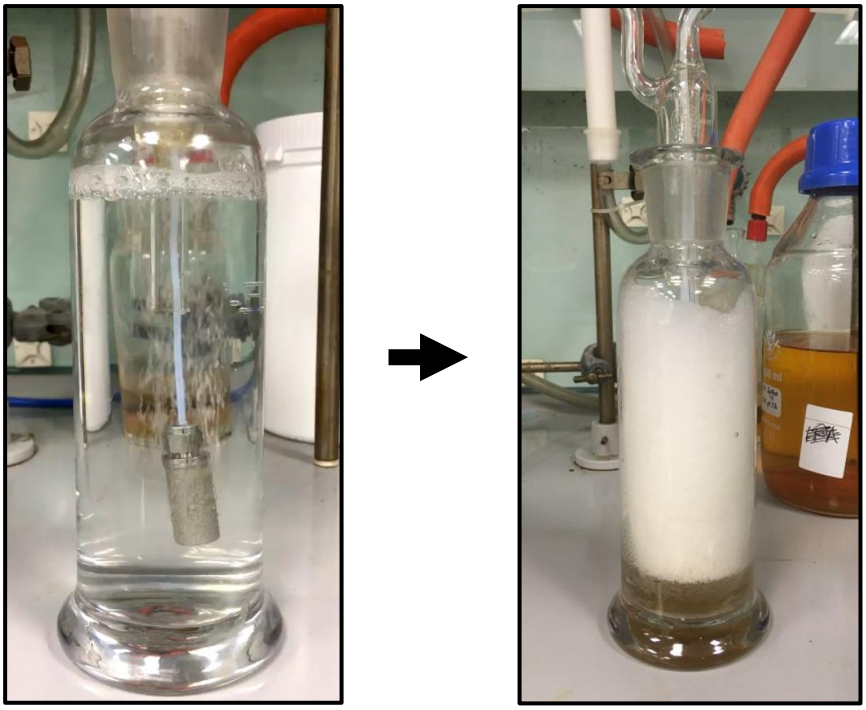

Figure 107: [left] Height of the suspended air filter sparger within the Drechsel bottle; [right] the 250 mL Drechsel bottle being filled with foam during a GOase$_{M3\text{-}5}$ catalysed oxidation of HMF.

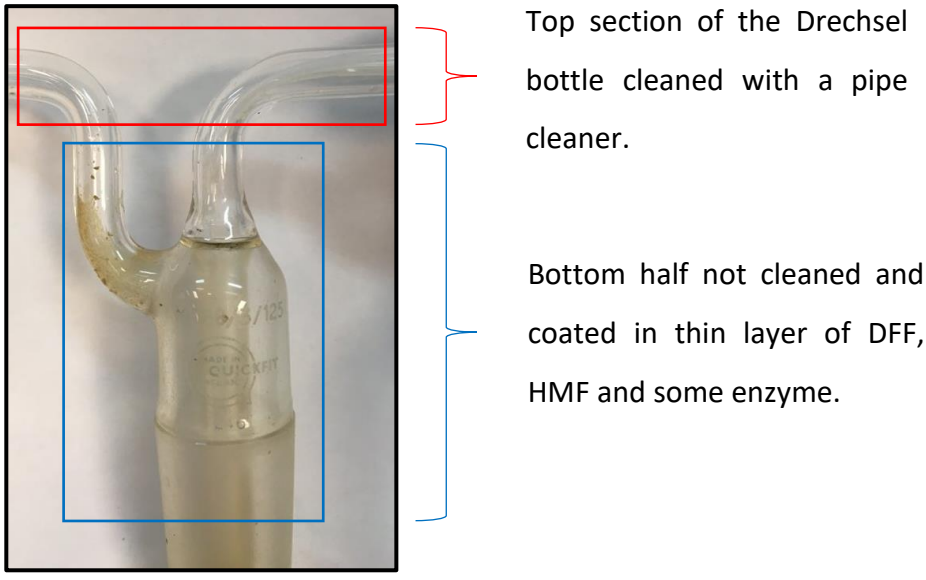

Figure 108 – Top-half of Drechsel bottle after being cleaned with water and a pipe cleaner, indicating build-up of particulate at the joints and tubing bends.

3.2.6 Transport of particulate by an aqueous foam

To determine an approximate quantity of DFF solid transported by the foam a set of experiments were carried out using both the surfactant, and peroxide systems. Foam was collected in 1.5 mL Eppendorf tubes and filled to the top. The weight of foam, and volume of liquid after centrifugation were then taken. The resultant pellet was dried out before being weighed. This pellet represented the mass of insoluble particulate transported by the foam through the reactor system. Samples were completed in quintuplet for a more precise statistical average.

Table 20 – Measurement of foam particulate taken from samples of surfactant and peroxide reactions.

Reaction replicates	**Foam Weight (mg)**	**Centrifuged Liquid Volume (µL)** [c]	**Solid Pellet Weight (mg)**
1[a]	74.9	65.0	0.4
2[a]	73.1	65.0	0.2
3[a]	114.0	100.0	0.4
4[a]	96.2	80.0	0.1
5[a]	127.9	115.0	0.3
6[a]	125.9	120.0	0.4
7[a]	104.2	95.0	0.1
Average	***102.2***	***91.0***	***0.3***
1[b]	365.6	320.0	1.3
2[b]	412.0	375.0	1.5
3[b]	365.2	325.0	1.2
4[b]	406.9	360.0	1.4
5[b]	375.9	330.0	1.4
6[b]	324.4	285.0	1.3
7[b]	333.3	295.0	1.3
Average	***369.1***	***327.0***	***1.3***

*[a] Surfactant base; samples taken from reaction shown in Figure 105, [b] Peroxide based; samples taken from reaction shown in Figure 90, [c] measured using a range of autopipettes to remove the liquid. Samples were both taken from reactions using the lower activity and stability GOase$_{M3\text{-}5}$ (**2018-2**). Samples taken over the course of 10 minutes at steady-state.*

The foam produced by surfactant systems was less dense than the peroxide equivalent, with considerably less solid transported as a result. Although for peroxide systems a larger quantity of liquid is observed in the samples, indicating less foam is produced overall. This demonstrates the efficiency of the drechsel bottle reactor for foam generation, as minimal liquid exits the reactor. The difference in foam produced is visible in Figure 109. The surfactant-based foam has larger bubbles with less packing, whilst the peroxide-based foam is denser with smaller, homogenous bubbles. The latter produces a high surface area foam with increased capacity for carrying insoluble DFF.

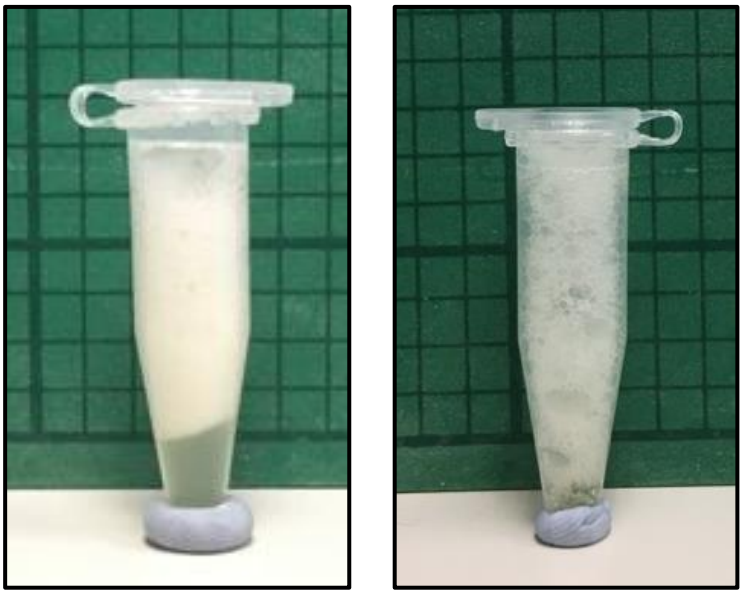

Peroxide Foam ***Surfactant Foam***

Figure 109: [left] Sample of foam produced by the decomposition of hydrogen peroxide; [right] sample of foam produced by the foaming of a surfactant using an air sparge. Both samples were taken from the GOase$_{M3\text{-}5}$ catalysed oxidation of 200 mM HMF.

The quality of the foam produced in the peroxide system is superior, with active mixing by the CSTR likely helping break up large bubbles and prevent collapse by coalescence. Introduction of an active mixer to the drechsel bottle system may provide the necessary adjustment to improve foam quality. Based on the average DFF selectivity for the peroxide system there is roughly 20% solids on the foam.

3.3 Conclusions

Production of large quantities of DFF under aqueous conditions is highly challenging due to its poor solubility. In this work a continuous method for the efficient synthesis of DFF has been explored. With the foundations for continuous flow foam reactions and the transport of insoluble particulate. Initial development explored the complexity of foam residence times, exploring effective techniques for its calculation and measurement. Reactions using an active mixer (CSTR) proved advantageous over passive mixers (tube-in-tube), with a finer foam produced by the physical agitation. The quality of foam created impacted the quantity of insoluble DFF that could be transported through the system. Foams containing a smaller, homogeneous bubble distribution gave higher conversion. Enzyme activity was retained after a reaction allowing for the possibility of reaction recycling to increase conversion. The development of a technique for the purification and extraction of DFF by DCM and celite allowed for quantitative yield determination.

The surfactant reactions using an air sparge had varied success, with controlled selectivity of the products. DFF was the dominant product in all reactions, however at a reduced conversion compared to the peroxide-systems. The highest conversion required a large reactor volume to substantially increase the residence time from >1 minute to <10 minutes. Introduction of a surfactant removed the need for hydrogen peroxide, reducing the cost and environmental impact of the process. Further research using a more stable and active batch of $GOase_{m3\text{-}5}$ would be of significant interest. In particular the generation of foams using an air sparge to ensure a fine and uniform foam. Implementation of this enables the production of DFF in aqueous reactions using compressed air as the oxygen source. Further studies would assist in developing a scalable process to be telescoped to the CAL-B catalysed oxidation of DFF to FDCA. Generating FDCA from HMF in a tandem continuous flow bio-oxidation.

Chapter 4 – Life-cycle assessment for the production of FDCA compared to terephthalic acid

4.1 Introduction

Under the ISO 14040 series of standards, life-cycle assessment consists of four distinct phases: goal and scope definition, life cycle inventory analysis, impact assessment and interpretation. The initial stage lays the foundation for the remaining three to build upon. All the stages interact with one another, particularly interpretation that can result in continuous improvements throughout the analysis.

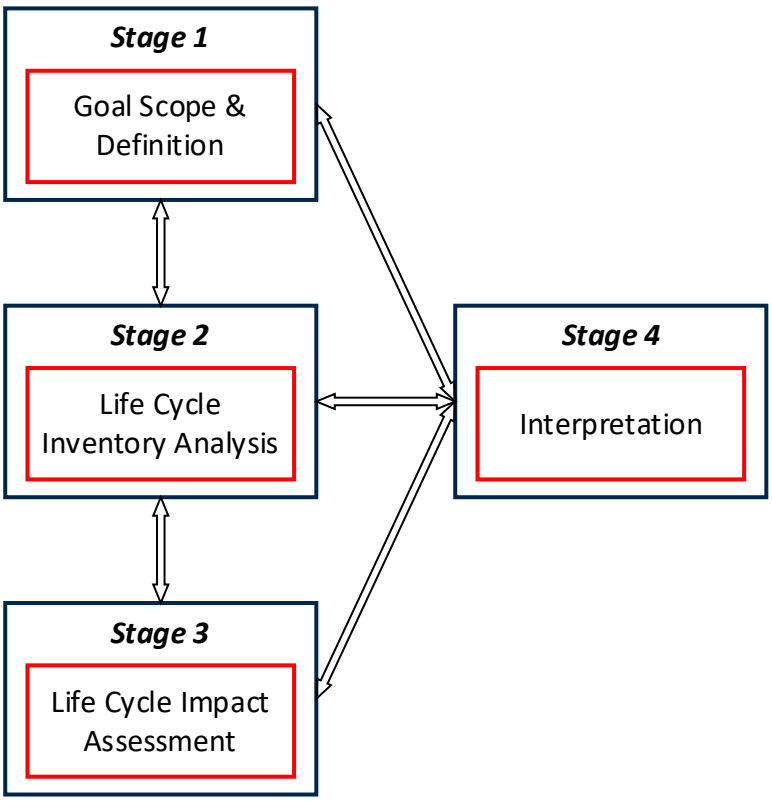

Figure 110 – Framework of a life-cycle assessment as outlined by the ISO 14040 standard. Four distinct phases are present with continuous interaction between them throughout the analysis.

Numerous life-cycle assessment (LCA) studies have been performed on biorefinery systems. The approach isn't infallible, with continued debate surrounding feedstocks and land-use. The discussion regarding first, second and third generation feedstocks taking precedence. Unlike fossil fuel based LCA's the timing of biogenic carbon is up for debate, with the release and capture of carbon occurring continuously throughout, particularly for biodegradable products that may take several years to decompose.

A further complication arises from the multiple high-value products produced, making the choice of functional unit, system boundaries and allocations complex. Determination of a single product is therefore difficult due to the large volume of by-products and waste streams. The functional unit is critical to an LCA, used as the unit of expression for the environmental impact. Given in MJ, kWh or simply as mass (1 kg), these can then be converted to CO_2 – equivalents (CO_2-e) for impacts factors akin to global warming.

When multiple high-value products are produced the environmental impact can be separated for each, using either allocation or systems expansion. For allocation the impact is determined by physical or economic properties of the products. System expansion, preferred by the ISO 14044 standard, includes the effects each product has on other product systems. System expansion requires identification and quantification of all products, which isn't always possible. This approach depends upon multiple assumptions, increasing the uncertainty of the final analysis. For a cradle-to-gate LCA allocation is preferred to narrow the scope of the study, assigning by-products as waste streams rather than including their cradle-to-grave impact.

Work by *Ahlgren et al.* [116] discusses in detail the issue surrounding many LCA techniques, particularly for biorefineries. Their work identified a number of methodological inconsistencies between studies, the report aims and functional unit rarely matched. This was exacerbated by poor documentation for assumptions, making any conclusions highly unreliable. Unfortunately, their report fails to make many comparisons to current fossil fuel based LCA's, a tool useful to analyse shortfalls in the current biorefinery approach. LCA literature for bio-polymers like PEF therefore contain various assumptions about the synthesis process, with most taking mass balance data from articles or patents. Data on the complete synthesis of bio-renewable alternatives is therefore lacking or minimalistic. Particularly for platform chemicals that lack any ready-to-use LCI data. This is evident for the HMF to FDCA process studied in this report, where the compounds and their precursors have no existing LCA or LCI databases.

A more comprehensive study by *Nessi et al.* [118] for the European Commission, investigated a range of petrochemical plastics and their bio-polymer alternatives, focusing primarily on plastic bottles. A Cradle-to-Cradle approach was adopted with the expectation that the bottles would either be landfilled, incinerated or recycled. The study included plastics for production of a bottle from: PET, PEF, HDPE and PLA. For PEF the ethylene glycol was produced from Brazilian sugarcane as a secondary renewable alternative. The FDCA was produced from the oxidation of HMF using potassium permanganate. [159] The HMF was derived from fructose, and the fructose was from corn starch. [159] The report focused primarily on articles and literature rather than current patented processes, with differences between the two, particularly mass yields. Furthermore, corn production has been taken from US sources, when the rest of the LCI data is from Europe, introducing a slight inconsistency in their data acquisition.

An extensive study by Eerhart *et al.*[159] explored the greenhouse gas (GHG) emissions from the production of PEF compared to PET. As with prior studies, LCI data for the PEF process was taken from literature and patents. Notably their assessment incorporated a combined-heat and power (CHP) plant. Although advantageous to GHG emissions, this creates bias in favour of the PEF. Avantium's recently patented process for HMF production from fructose was used. The process begins with the enzymatic isomerisation of glucose to fructose, where the effluent is separated in an ion exchange resin. Pure fructose is solubilised with 95 wt.% methanol and sulphuric acid. The reaction is then heated to 200 °C at 50 bars. The quantity of methanol is controlled to prevent the more stable formation of methoxy methyl furan (MMF), this occurs when methanol is in excess. However, important data to structure an LCA is critically lacking. Stated in equivalents of oxygen required, the quantities of reagents used are not stated. Therefore, Avantium's process cannot be used to generate a robust LCA for HMF production unless more detailed synthesis data is made available.

Recent research by Gomes *et al.* has focused on the downstream processing of PET, particularly how it is recycled. [160] The study focused on three different methods for recycling the bottles in Brazil. The three scenarios were: (1) landfill, (2) recycling for use as textile fibres and (3) recycling for food packaging. As expected, scenario (3) saw the lowest environmental impacts, but the highest land occupation. However, as stated by the authors, no air emissions data was taken into consideration. All three scenarios produce greenhouse gases and that lack of data means the comparison isn't entirely robust.

Production of HMF has been assessed by multiple authors, notably by Lam *et al.* who investigated the production of platform chemicals from valorised food waste. Data was taken from multiple literature sources using a variety of catalyst-solvent systems on a number of different feedstocks. [161] A Cradle-to-Gate approach was taken with a 1 g of food waste feedstock as the functional unit (FU). Electricity was taken into account, calculated from the power and duration of the microwave reactor for this specific route. For chemicals not documented in a database, the authors estimated them according to the EcoInvent method for building life-cycle inventories. [162] Unfortunately, the majority of techniques chosen for HMF production by the authors are infeasible at large scale. The processes are not cost-competitive, especially in comparison to that from Avantium.

FDCA recovery has been detailed by Bello *et al.* [163] Two separate routes have been modelled in Aspen Plus for the separation of FDCA as a faux Cradle-to-Gate approach. Cultivation, extraction of raw materials and production of FDCA are included. The routes use bimetaliic Pd-Au nanoparticles to catalyse the oxidation of HMF, with extraction by either vacuum or crystallisation. [164] Although the approach is limited to the downstream processing in the life-cycle, modelling of large scale- manufacture has been completed. Unlike prior publications the authors have taken into consideration the effects of large-scale production compared to lab-scale. Similar to the above studies the functional unit is mass based (1 $kg.h^{-1}$ of FDCA), with scenarios set out as allocations rather than system expansion.

Since the choice of functional unit for an LCA is distinct, many of these reports cannot be compared, with different units used for each. Although all align with the ISO 14044 standard, some chose only literature sources, others patents and some a mixture of both. Different approaches are also taken in attempts to cover sections of, or the full life-cycle of a product. These discrepancies leave a gap for comparison of modern biorefinery techniques compared to a petroleum process. A direction designed to use patented information supplemented with recent literature values.

The following sections examine two methods used to form FDCA from maize corn. The two processes provide an environmental overview of the impact of FDCA manufacture from bio-renewables. These are compared to a petroleum derived terephthalic acid process, a monomer for the production of PET.

4.2 Product System and System Boundary

4.2.1 Goal and scope

The goal was to analyse and compare the production of FDCA from bio-renewable raw materials with the production of terephthalic acid from petroleum sources. The study investigates the environmental impact of different FDCA production methods, whilst comparing the methods developed in this thesis to an existing literature technique; the Pt/C catalysed oxidation of HMF to FDCA by Davis *et al.*[165] This provides an insight into bio-renewable alternatives and the necessary improvements required for their green manufacture.

4.2.2 Functional unit

For the study undertaken in this section, a functional unit of 1 kg was chosen. This is applicable to 1 kg of FDCA and 1 kg of terephthalic acid. A Cradle-to-gate assessment of FDCA from maize starch using two HMF oxidation techniques has been explored; compared against the production of terephthalic acid from a crude oil mix.

4.2.3 System boundaries & allocation procedures

The products of treatment processes are allocated as waste-producing streams (allocation at the point of substitution). Transport has not been included unless listed as agricultural equipment. As defined in Figure 111 the repeating inputs are electrical and thermal energy for a unit process. Each unit process includes a number of chemicals and raw materials, these have been allocated as processes or as elementary flows if located at the boundary of the study. Environmentally relevant emissions to air, water and land are included for each unit process in the life-cycle (such as CO_2, NO_2, CH_4). The boundary has been specified as cradle-to-gate for FDCA, which include the following operations as seen in Figure 111:

- Harvesting of maize grain.
- Mechanical and thermal treatment to maize starch.
- Enzymatic conversion to glucose then high fructose corn syrup (HFCS).
- Dehydration of fructose to 5-hydroxymethylfurfural (HMF).
- Oxidation of HMF to FDCA by Pt/C or galactose oxidase and CAL-B.

For each unit process the following factors were included in the system boundary, these have been selected based on Europe (EU-28) or Germany (DE) for consistency:

- Input of raw materials and processed chemicals.
- Energy for heating and cooling (thermal conversion from fossil fuels).
- Process and cooling water (ground water from rivers).
- Process steam (thermal conversion from fossil fuels and bioderived heat)
- Harvesting of crops (ploughing, sowing, crop protection and fertilisers).
- Electricity usage (AC consumer mix).
- Conversion and use of land (arable or industrial).
- Use of chemical plants.

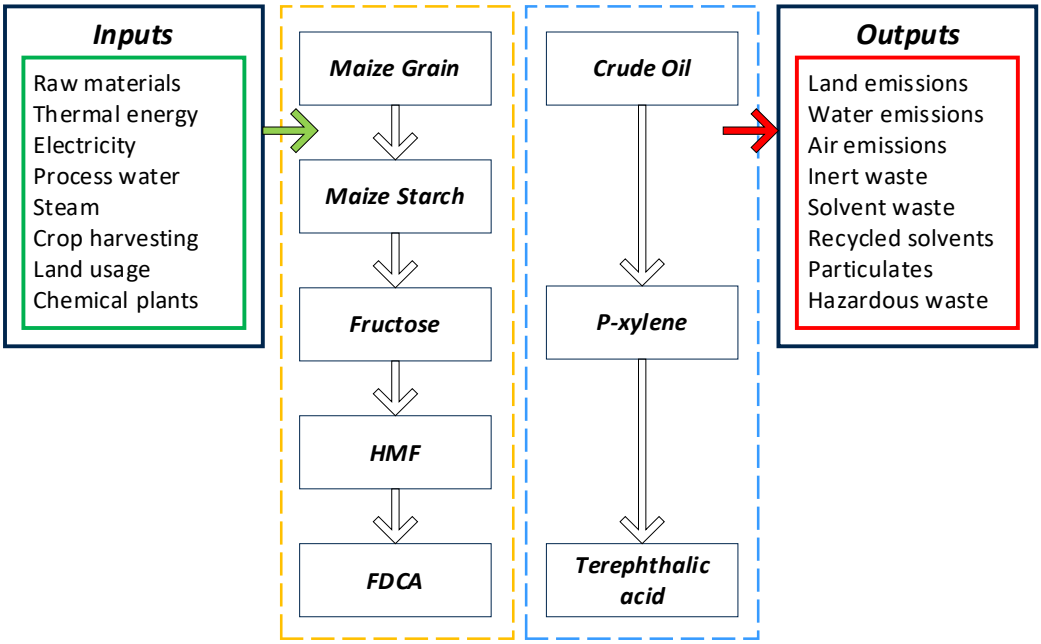

Figure 111: [left] Life Cycle flow diagram for the production of FDCA from maize grain with inputs and outputs; [right] life cycle flow diagram for the production of terephthalic acid from crude oil. Each box within a life-cycle represents a unit process.

4.2.4 Impact categories

The chosen impact categories for this assessment relate strongly to the impact of manufacture demonstrating the impact of a bio-renewable approach. Human and aquatic toxicity have not been included as they were not of interest in this study. Interpretation of results follows a procedure of adjustment, determining areas of critical significance to an Impact Category. As such the following have been chosen as suitable impact categories:

- Global warming potential (GWP 100 years) (kg CO_2 – equivalent).
- Acidification potential (AP) (kg CO_2 – equivalent).
- Eutrophication potential (EP) (kg phosphate – equivalent).
- Ozone layer depletion (ODP) (kg R11 – equivalent).
- Fossil depletion (FD) (kg oil – equivalent).

4.2.4.1 Global warming potential (GWP)

A direct result of climate change is the increase in global average temperature resulting in the melting of ice caps and rising sea levels.[166] In order to quantify this change the rate of energy change per unit area of the globe, measured at the top of the atmosphere was introduced. Known as radiative forcing. Global warming potential was defined by the IPCC and adopted in the Kyoto Protocol as a global-mean radiative forcing of an emission relative to one unit mass of the reference gas CO_2.[166] CML 2001 was developed by the Institute of Environmental Science at Leiden University, the Netherlands.[167] CML methodology restricts quantitative modelling to early stages, in the cause-effect chain, limiting uncertainties.

4.2.4.2 Acidification potential (AP)

This relates to the long-term exposure of ecosystems to acid inputs, resulting in the decline of forests and wildlife depletion.[168] It is caused by the release of protons or corresponding anions such as: SO_2, NO_X, NH_3 and Cl. An approach used, and applied in this work, linked the release of acidic protons and molar mass to estimate the AP of each substance using SO_2 as a reference substance.[168]

4.2.4.3 Eutrophication potential (EP)

The enrichment of aquatic systems with nutrients, resulting in the increased production of algae, phytoplankton and aquatic plants.[168] This reduces the water quality and damages the aquatic ecosystem. The process can occur in both aquatic and terrestrial ecosystems, with the input of surplus N and P. The accumulation of total phosphates is used as an indicator and reference value.[168]

4.2.4.4 Ozone layer depletion (ODP)

Developed by the World Meteorological Organisation (WMO) it evaluates the effects of compounds on the stratosphere ozone.[169] The main compounds identified are halogenated compounds such as CFC's and HCFC's. The impact uses the refrigerant R11 (trichloromonofluoromethane) as a reference compound.[169]

4.2.4.5 Fossil depletion (FD)

Developed by the National Institute for Public Health in the Netherlands, as part of ReCiPe 2016; a harmonised life-cycle assessment method for mid and endpoint level assessments.[170] Fossil resource scarcity as it can also be referred to, converts the energy value of a material or compound into kg oil -equivalent. This allows for the comparison of material consumption between different systems.[170]

4.2.5 GaBi structure

In GaBi a unit process requirement (UPR) is generated as a plan, this plan contains all the inputs and outputs of that single unit process. These inputs and outputs are termed flows and can be elementary or tracked. A tracked flow has all its life-cycle impact assessment (LCIA) data included in the final LCA; hence a unit process (plan) is required for each tracked flow. Conversely, an elementary flow is usually an allocated waste stream or by-product that is included as an input or output, but does not have allocated LCIA data within the scope of the study. This prevents the LCA from stretching too far from the boundaries of the study. Unit processes (plans) generated for elementary flows therefore contain only the inputs and outputs from production.

4.3 Life Cycle Inventory Analysis

Data obtained for the study has come from reliable sources. EcoInvent, GaBi, the Federal National Renewable Energy Laboratory and Scientific journals. Data has been collected from LCA databases available between the years 2000-2014 with a European geographical origin (RER), otherwise a Rest-of-World dataset (RoW) has been used. The Unit Process Requirement (UPR) data has been used to develop LCA's for a variety of chemical manufacturing processes. Technology coverage has been included as conversion of land from agriculture to industrial and the use of chemical plants (in units) as per EcoInvent's inputs from the Technosphere.

Data taken from the databases has been checked thoroughly for robustness, with standard deviations included where possible. Any calculated, estimated or measured results have been stated in GaBi as such, along with their associated assumptions.

4.3.1 Bio-alternative and petrochemical route

In total three systems have been compared: (**1**) the bio-based production of FDCA from the galactose and CAL-B catalysed oxidations of HMF and DFF respectively, (**2**) the metal (Pt/C) catalysed oxidation of HMF to FDCA and (**3**) the petrochemical production of terephthalic acid. Both routes (**1**) and (**2**) share the same raw material feedstock, maize grain. To ensure a high level of consistency of the data; methodological considerations, system boundaries and allocation procedures remain unchanged. Decisions relating to evaluating inputs and outputs are also the same, to ensure a robust outcome for impact categories.

4.3.2 Maize grain

Production of 1 kg maize grain (USA, 2004-2014) with a yield of 9315 kg.ha^{-1} and a moisture content of 14%.[171] Assessment begins from the harvesting of the crop and includes inputs of: seeds, mineral fertilisers, pesticides and irrigation. It has been assumed no organic fertilisers are used. All machine operations and infrastructure have been incorporated. The activity ends at the drying of the grains.

Table 21 – Tracked flows in GaBi for the production of maize grain.

Input/output	**Tracked Flows[a]**	**Quantity**
Input	Ammonia (agrarian)	0.00844 kg
	Ammonium nitrate	0.00489 kg
	Ammonium phosphate	0.00585 kg
	Irrigation water	245.00 kg
	Ground lime	0.0305 kg
	Potassium chloride	0.0719 kg
Output	Maize grain	1 kg

[a] tracked flows in GaBi that are included as individual processes within the unit processes, each containing their own elementary flows. All other inputs are listed as elementary flows and include: herbicides, pesticides, fungicides, insecticides and conversion of arable land by ploughing, cultivating and harrowing. All other outputs are listed as elementary flows and include all the emissions to land, air and water.

4.3.3 Maize starch

Production of 1 kg of maize starch (DE, 2002-2014) from maize grain with an average 14% water content, in-line with the maize corn used.[171] Assessment begins from the mechanical separation of maize grain from harvesting debris and includes inputs of: swelling in process water, milling and desiccation. All machine operations and infrastructure have been incorporated. The activity ends at the drying of the extracted starch.

Table 22 – Tracked flows in GaBi for the production of maize starch

Input/output	**Tracked Flows[a]**	**Quantity**
Input	Maize grain[b]	1.26 kg
	Electrical power	0.707 KWh
	Thermal energy[c]	3.99 MJ
	Process water	1960 kg
Output	Maize starch	1 kg

[a] tracked flows in GaBi that are included as individual processes within the unit processes, each containing their own elementary flows [b] uses maize grain produced from data obtained in 4.3.2 Maize grain [c] thermal energy generated from natural gas in Germany. All other inputs are listed as elementary flows and include: maize grain treatment and the use of chemical plant infrastructure. All other outputs are listed as elementary flows and include all the emissions to land, air and water.

4.3.4 Fructose

Production of 1 kg of glucose (RoW, 2015-2020) has been modified and estimated using the addition of glucose isomerase to produce fructose.[171,172] Initially starch if saccharified at 60 °C with glucoamylase (0.61 kg of enzyme per kg of dry starch). The fermentation process produces 1 kg of glucose syrup, addition of glucose isomerase can convert this into high fructose corn syrup at 42% fructose (HFCS-42). [173] This has been used as the reference point for fructose due its commercial availability.

Table 23 – Tracked flows in GaBi for the production of fructose from HFCS.

Input/output	**Tracked Flows[a]**	**Quantity**
Input	Maize starch[b]	0.9 kg
	Alpha amylase	0.00011 kg
	Glucoamylase	0.00011 kg
	Glucose isomerase	0.00011 kg
	Process water	18.415 kg
	Process steam	0.2 MJ
	Thermal energy[c]	2.15 MJ
Output	Untreated water	0.027 kg
	Fructose[d]	0.42 kg

[a] tracked flows in GaBi that are included as individual processes within the unit processes, each containing their own elementary flows, [b] uses maize starch produced from data obtained in 4.3.3 Maize starch, [c] thermal energy generated from natural gas in Germany, [d] Estimated on 42% average fructose in HFCS, purification not included in this study. All other inputs are listed as elementary flows and include the use of chemical plant infrastructure. All other outputs are listed as elementary flows and include: glucose by-product and all the emissions to land, air and water.

4.3.5 HMF (5-hydroxymethulfurfural)

Production of 4.5g of HMF from 10g of fructose (USA, 2017) has been taken from data supplied by Isola *et al.*[159] and scaled to 1 kg. All chemicals used in the synthesis have been included as individual processes. The process is based on a lab-scale synthesis. The synthesis uses a lithium bromide (LiBr) catalyst with sulphuric acid in dimethylacetamide to dehydrate the fructose. Avantium's route, although significantly greener, is lacking available data to produce a robust LCA from.[174]

Table 24 – Tracked flows in GaBi for the production of HMF.

Input/output	Tracked Flows[a]	Quantity
Input	Fructose[b]	2.2 kg
	Electrical power	1680 KWh
	Ethyl acetate	11.9 kg
	Hexane	1.87 kg
	Lithium bromide	2.2 kg
	Dimethylacetamide	20.7 kg
	Liquid nitrogen	11 kg
	Sodium chloride	44 kg
	Sodium sulphate	2.2 kg
	Sulphuric acid	0.0726 kg
	Deionised water	11 kg
	Sodium silicate (waterglass)	178 kg
Output	Ethyl acetate (recycled)	11.3 kg
	Dimethylacetamide (recycled)	19.7 kg
	Sodium silicate (recycled)	60 kg
	HMF	1 kg

[a] tracked flows in GaBi that are included as individual processes within the unit processes, each containing their own elementary flows, [b] uses purified fructose produced from data obtained in 4.3.4 Fructose.[175] *All inputs are listed in below. Two unlisted outputs include inert chemical waste and emissions to water.*

4.3.6 DFF (Diformylfuran)

Production of 1 kg of DFF has been calculated from a galactose oxidase catalysed bio-oxidation of HMF (Entry 4 - Chapter Three). A continuous flow reaction gave an average conversion of 85% with a residence time of 4 minutes. Electricity for the hotplate stirrer and two pumps was estimated as a scale-out from their technical specifications.[176,177] Production of galactose oxidase and catalase was generated as an estimate from glucoamylase, cellulase and alpha amylase.[172] Purification included several washes with dichloromethane (DCM) and a water recrystallisation, yielding an estimated return of 93% of the DCM after vacuo distillation. DFF yield was constant at 78% after purification and extraction.

Table 25 – Tracked flows in GaBi for the production of DFF.

Input/output	**Tracked Flows[a]**	**Quantity**
Input	HMF[b]	1.36 kg
	Electrical power	0.908 KWh
	Catalase[c]	0.166 kg
	Galactose oxidase[c]	0.0832 kg
	Copper sulphate	0.00193 kg
	Hydrogen peroxide	1.46 kg
	Sodium phosphate	0.716 kg
	Deionised water	50.4 kg
	Dichloromethane	62.9 kg
Output	Dichloromethane (recycled)	59.7 kg
	DFF	1 kg

[a] tracked flows in GaBi that are included as individual processes within the unit processes, each containing their own elementary flows, [b] uses HMF produced from data obtained in 4.3.5 HMF (5-hydroxymethulfurfural), [c] enzyme production has been estimated based on data provided for cellulase, glucoamylase and alpha amylase production.[172] All inputs aside from horseradish peroxidase are listed below. Data for its acquisition is not currently available. All outputs are listed.

4.3.7 FDCA (2,5-furandicarboxylic acid) by $GOase_{M3-5}$ & CAL-B

Production of 1 kg of FDCA has been calculated from a CAL-B catalysed bio-oxidation of DFF from 4.3.6 DFF (Diformylfuran). A batch reaction gave 96% conversion after 24 hours in an incubator shaker at 40°C (Table 6, Entry 1 – Chapter Two). Electricity for the incubator shaker was estimated from its technical specifications and its maximum capacity of vials for simultaneous reactions, a scale-out approach was taken.[178]

Table 26 – Tracked flows in GaBi for the enzymatic production of FDCA.

Input/output	**Tracked Flows[a]**	**Quantity**
Input	DFF[b]	0.857 kg
	Electrical power	1.38 KWh
	CAL-B Lipase[c]	1.47 kg
	T-butanol	119 kg
	Ethyl acetate	138 kg
	Hydrogen peroxide	2.24 kg
Output	CAL-B Lipase (recycled)[d]	0.368 kg
	FDCA	1 kg

[a] tracked flows in GaBi that are included as individual processes within the unit processes, each containing their own elementary flows, [b] uses DFF produced from data obtained in 4.3.6 DFF (Diformylfuran), [c] enzyme production has been estimated based on data provided for cellulase, glucoamylase and alpha amylase production[172], [d] estimated on the ability to recycle the enzyme at least three times. All inputs and outputs are listed below. CAL-B is immobilised on beads and its recycling is estimated on its sustained activity in continuous flow.

4.3.8 FDCA (2,5-furandicarboxylic acid) by Pt/C

Production of 1 kg of FDCA has been calculated from Davis *et.al*.[165] The Pt/C catalysed oxidation of HMF to FDCA in sodium hydroxide, using pressurised oxygen to give a yield of 67% after 6 hours. Catalyst manufacture has not been included due to a lack of available data, instead the quantity of Platinum (from mined sources) has been incorporated at a 3% loading. Product purification and solvent extraction has not been listed by the authors and is thus excluded from this study. Electricity has been estimated using a standard laboratory magnetic stirrer hotplate and a Parr reactor running at 295 K for 6 hrs.[177,179]

Table 27 – Tracked flows in GaBi for the metal catalysed production of FDCA.

Input/output	**Tracked Flows[a]**	**Quantity**
Input	HMF[b]	1.49 kg
	Electrical power	0.766 KWh
	Platinum metal[c]	0.000304 kg
	Gaseous oxygen	1.75 kg
	Sodium hydroxide	0.947 kg
Output	FDCA	1 kg

[a] tracked flows in GaBi that are included as individual processes within the unit processes, each containing their own elementary flows, [b] uses HMF produced from data obtained in 4.3.5 HMF (5-hydroxymethulfurfural), [c] estimated as the proportion of mined platinum metal within the catalyst, not recycled as data not stated in report.[165] *All inputs and outputs are listed in the table below, limited information was available for use within the report. Estimations were therefore not made in regards to emissions or purification steps.*

4.3.9 Crude oil mix

Production of 1 kg of crude oil mix (DE, 2017) to a refinery.[180] Coverage of 95% of the input and output flows. Assessment begins from well drilling and includes inputs of: crude oil production, processing and pipeline transport. Oil mix from Germany has been stated and used in this assessment, as an average sample of commercially available crude oil within in the country. All machine operations and infrastructure have been incorporated. The activity ends at the refinery stage.

The crude is an average mix of conventional crude available in the German market. This is a mix of oil from various EU and on-EU countries, totalling 27 contributors. The refinery products such as Xylene are modelled with a parameterised country-specific refinery model, in this instance DE is used. The refinery model represents the current national standard in refining techniques.

As this is a standard process and elementary flow available on a per country basis in GaBi, the only tracked flow is the output of 1 kg of crude oil mix. All flows within are therefore not tracked and counted as elementary flows to the system.

4.3.10 P-xylene

Production of 1 kg of xylene (RER, 2017) defined by the European plastics industry (Plastics Europe).[171] Catalytic reforming out of naphtha to produce the xylene. Assessment begins from the refining of crude oil and includes inputs of: crude oil fractional distillation, processing and refining. Natural gas is included as hydrogen is required for the desulphurisation of crude. All machine operations and infrastructure have been incorporated. The activity ends at the production of purified xylene (99%). The assessment does not report information on recyclable wastes, inputs of air/nitrogen/oxygen and unspecified CFC/HCFC emissions to air. Catalysts used such as rhodium on silica have been included as elementary flows but are not tracked due to a lack of available data.

Table 28 – Tracked flows in GaBi for the production of xylene.

Input/output	**Tracked Flows[a]**	**Quantity**
Input	Crude oil[b]	0.803 kg
	Natural Gas	0.068 m^3
	Process water	74.8 kg
	Electrical power	0.2047 KWh
Output	Xylene	1 kg

[a] tracked flows in GaBi that are included as individual processes within the unit processes, each containing their own elementary flows, [b] uses crude oil produced from data obtained in 4.3.9 Crude oil mix (available on GaBi). All other inputs are listed as elementary flows and include: hazardous waste incineration, ores/minerals, and the use of chemical plant infrastructure. All other outputs are listed as elementary flows and include all the emissions to land, air and water.

4.3.11 Terephthalic acid

Production of 1 kg of purified terephthalic acid (RER, 2014) defined by the European plastics industry (Plastics Europe).[171] Reaction between xylene and acetic acid. Assessment begins from the reaction between the two compounds and includes inputs of: raw materials, processing and energy input. All machine operations and infrastructure has been estimated. The activity ends at the production of purified terephthalic acid (99%). The assessment does not report information on recyclable parameters relating to Dissolved Organic Carbon (DOC), Total Organic Carbon (TOC) and Chemical Oxygen Demand (COD) as part of emissions to water.

Table 29 – Tracked flows in GaBi for the production of terephthalic acid.

Input/output	**Tracked Flows[a]**	**Quantity**
Input	Xylene[b]	0.661 kg
	Electrical power	0.469 KWh
	Liquid nitrogen	0.0488 kg
	Sodium hydroxide	0.00145 kg
	Process water	0.767 kg
	Process steam	0.64 kg
	Thermal energy[c]	1.63 MJ
Output	Acetic acid	0.05 kg
	Terephthalic acid	1 kg

[a] tracked flows in GaBi that are included as individual processes within the unit processes, each containing their own elementary flows, [b] uses xylene produced from data obtained in 4.3.10 P-xylene, [c] thermal energy generated from natural gas in Germany. All other inputs are listed as elementary flows and include: hazardous waste incineration and the use of chemical plant infrastructure. All other outputs are listed as elementary flows and include: all the emissions to land, air and water and particulates emissions.

4.4 Life Cycle Impact Assessment of FDCA

The results for the LCIA for the production of FDCA by Pt/C and $GOase_{M3-5}$ with CAL-B are presented below. The global warming impact of each cradle-to-gate production from maize grain is first presented, then the remaining impact categories and the largest contributors are discussed.

Production from HMF either enzymatically or by Pt/C has been assigned separate life-cycles with individual plans. The figures below show the full life-cycle used in GaBi for each, along with the quantities required at each stage. The enzymatic route (**1**) Figure 112, this incorporates the galactose oxidase catalysed oxidation of HMF to DFF in continuous liquid foam flow (see Chapter 3), followed by the CAL-B catalysed oxidation of DFF to FDCA in flow (see Chapter 2). The Pt/C route (**2**) Figure 113, includes the platinum carbon catalysed oxidation of HMF to FDCA investigated by Davis *et al.*[165]

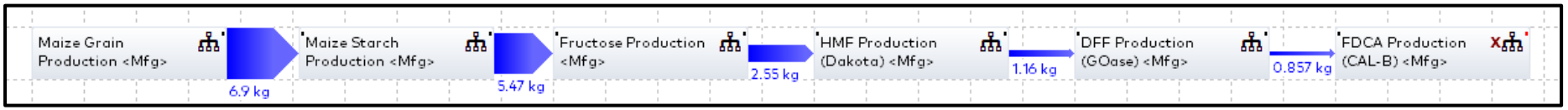

*Figure 112 – Route (**1**) Full life-cycle for the enzymatic catalysed production of FDCA from maize grain as used in GaBi. Each arrow represents the direction of material movement through the system with the quantity of material transferred. 6.9 kg of maize grain produce 1 kg of FDCA.*

*Figure 113 – Route (**2**) Full life-cycle for the Pt/C catalysed production of FDCA from maize grain as used in GaBi. Each arrow represents the direction of material movement through the system with the quantity of material transferred. 8.87kg of maize grain produced 1 kg of FDCA.*

4.4.1 Global warming potential (100 years)

The system used to calculate the global warming potential is (GWP100) CML 2001.

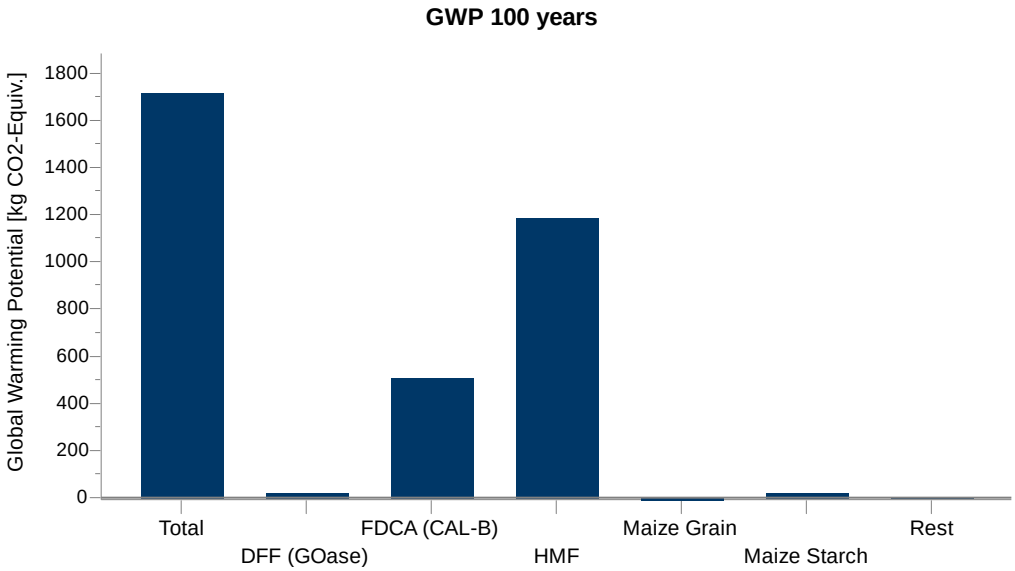

*Figure 114 – Route (**1**) GWP 100 years for the cradle-to-gate production of FDCA from maize grain. The synthesis of HMF to FDCA is done enzymatically using GOase and CAL-B.*

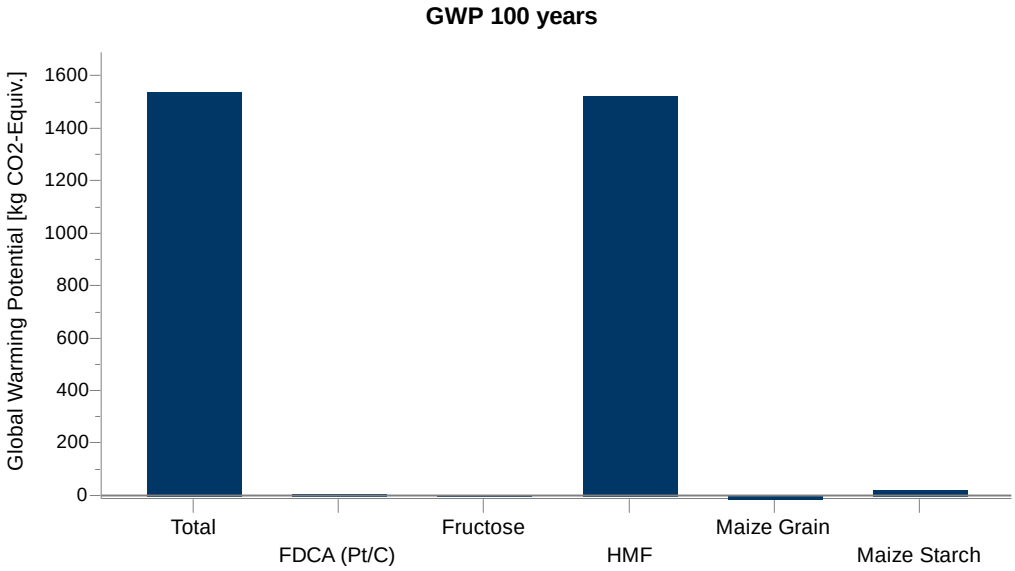

*Figure 115 – Route (**2**) GWP 100 years for the cradle-to-gate production of FDCA from maize grain. The synthesis of HMF to FDCA is done by metal catalysis using Pt/C.*

Without interpretation (adjustment of the LCA) the use of a Pt/C would have a smaller GWP100 impact, producing less CO_2. This however is not an accurate assessment of the metal catalysed process. Minimal information on electricity usage, solvents and product purification has been discussed in the report by Davis *et al*.[165] Inclusion of this information would increase the amount of CO_2 produced. Furthermore, recycling the ethyl acetate/t-butanol solvent system used in route (**1**) to produce FDCA (Figure 114), would lower the impact of this stage considerably. The largest contributor in both scenarios is the production of HMF, dominated heavily by the electrical power use. This is far higher than necessary, taking <1675 KWh to produce 1 kg of HMF. The DFF process on the other hand takes >1 KWh for a 1 kg. The data provided in the report by Isola *et.al* [159] has stated a value of 7.54 kwh for only 4.5 g of HMF, a electricity requirement far greater than what's required for 1 kg of purified terephthalic acid at an industrial scale. Adjustment of this value to a more realistic estimate of 1 kwh per kilo for industrial scale, significantly reduces the GWP100 impact for both processes by 1,000 kg CO_2 – equivalent (see Figure 116).

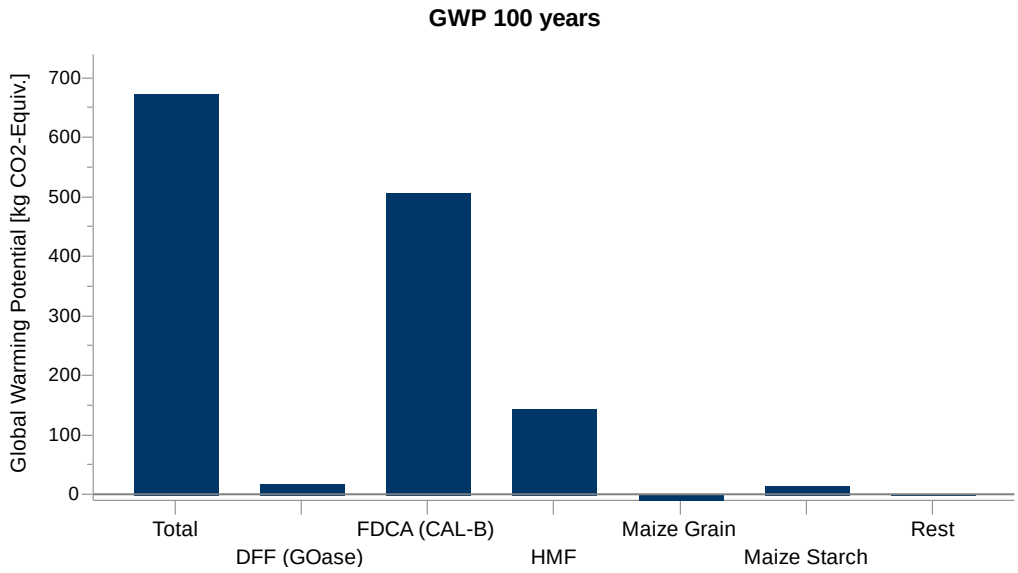

*Figure 116 – Route (**1**) GWP 100 years for the cradle-to-gate production of FDCA from maize grain. Production of HMF has been adjusted to a lower electricity power usage of 1 kWh per 1 kg of HMF.*

The GWP100 impact for the enzymatic and metal catalysed unit process is shown below in Figure 117 and Figure 118 respectively. The impact from DFF production is significant for the enzymatic route (**1**), recycling the solvents would improve the GWP100 impact of the process. The electricity requirement is minor as there's no input of thermal energy. The platinum catalysed process is impacted heavily by the harvesting and growth of maize grain; however, it is lower than route (**1**) at 500 kg CO_2-e

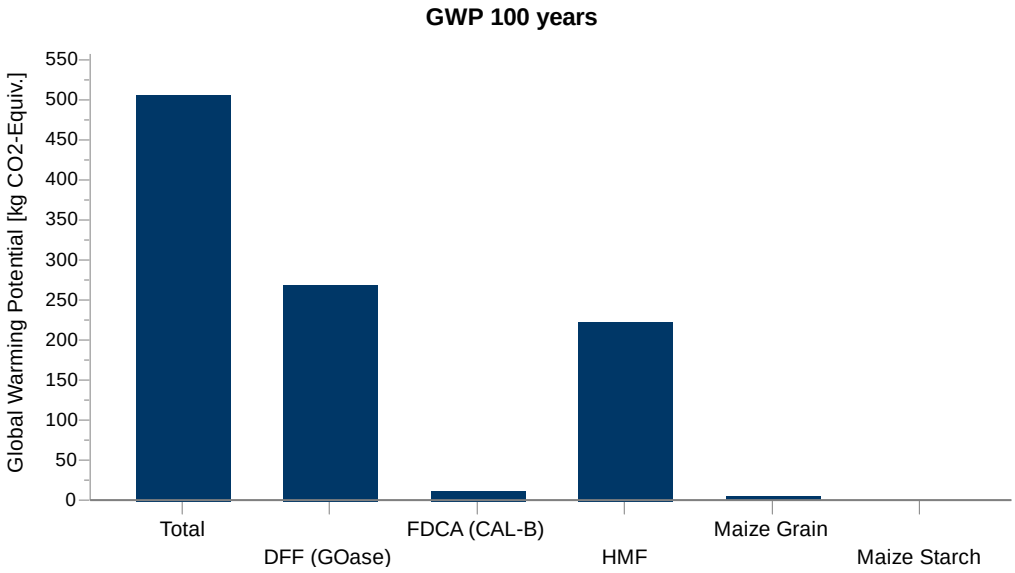

*Figure 117 – Route (**1**) GWP 100 years for the life-cycle of FDCA from HMF. Production of HMF has been adjusted to a lower electricity power usage of 1 kWh per 1 kg of HMF.*

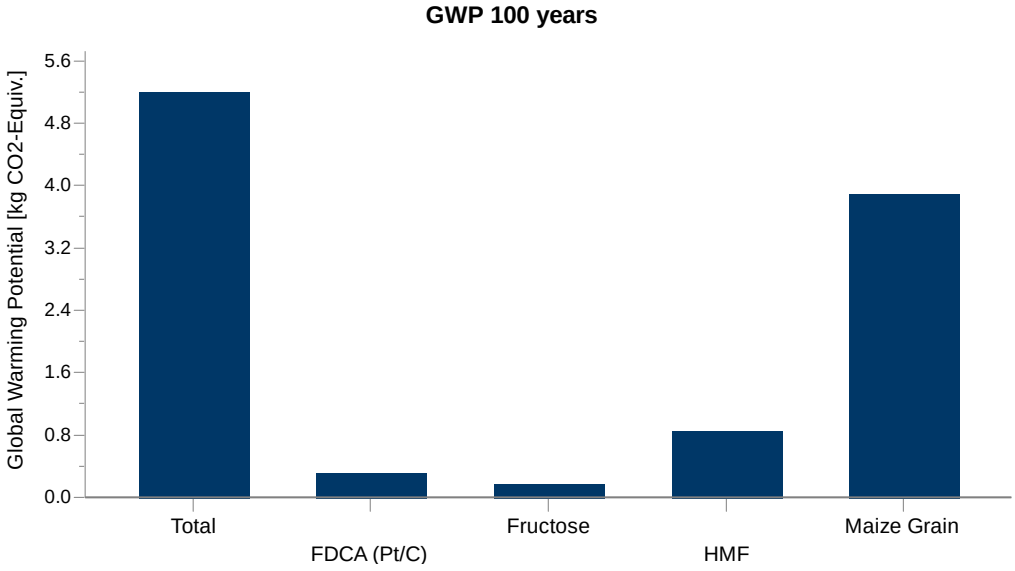

*Figure 118 – Route (**2**) GWP 100 years for the unit-process of FDCA from HMF. Production of HMF has been adjusted to a lower electricity power usage of 1 kWh per 1 kg of HMF.*

4.4.2 Acidification potential (AP)

The system used to calculate acidification potential (AP) is CML 2001. Analysis used an estimate of 1 kWh per 1 kg for HMF.

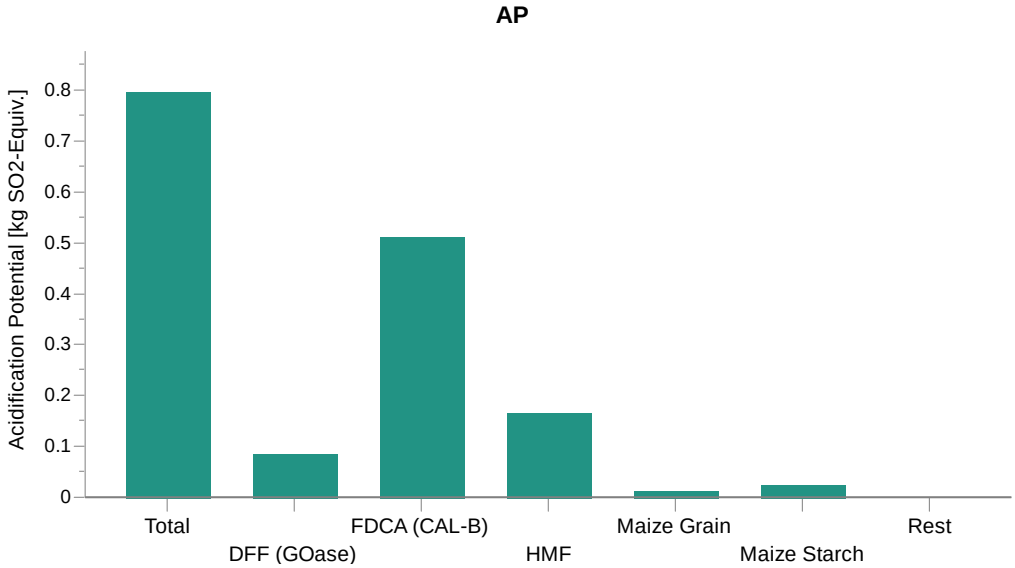

*Figure 119 – Route (**1**) AP for the cradle-to-gate production of FDCA from maize grain. The synthesis of HMF to FDCA is done enzymatically using GOase and CAL-B.*

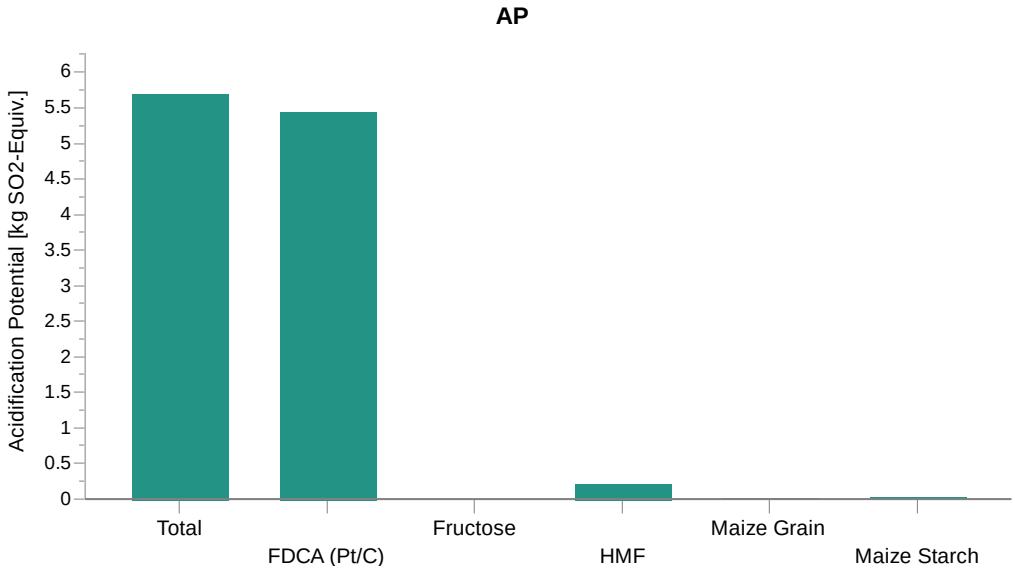

*Figure 120 – Route (**2**) AP for the cradle-to-gate production of FDCA from maize grain. The synthesis of HMF to FDCA is done by metal catalysis using Pt/C.*

Route (**1**) has a smaller AP impact, producing less SO_2. Platinum mining, refining and production contributes to the large AP (5.44 kg SO_2-e) seen in Figure 120. Its impact would further increase with LCA data on catalyst production, a thermally intensive process. High thermal energy processes usually burn coal or oil to generate the heat, both generate sulphur dioxide, the former dependent upon the type of coal (brown, hard etc). As with the GWP100 impact, ethyl acetate and t-butanol production contribute heavily towards the AP for the enzymatic process. At industrial scale these solvents are usually captured by vacuum distillation, enabling roughly 90% of the solvent to be recycled. Addition of solvent recycling for EtOAc and t-butanol, reduces the AP impact for the process by 0.4 kg SO_2 – equivalent (see Figure 121). The highest contributor then becomes the use of dimethylacetamide; solvent for the dehydration of fructose to HMF.

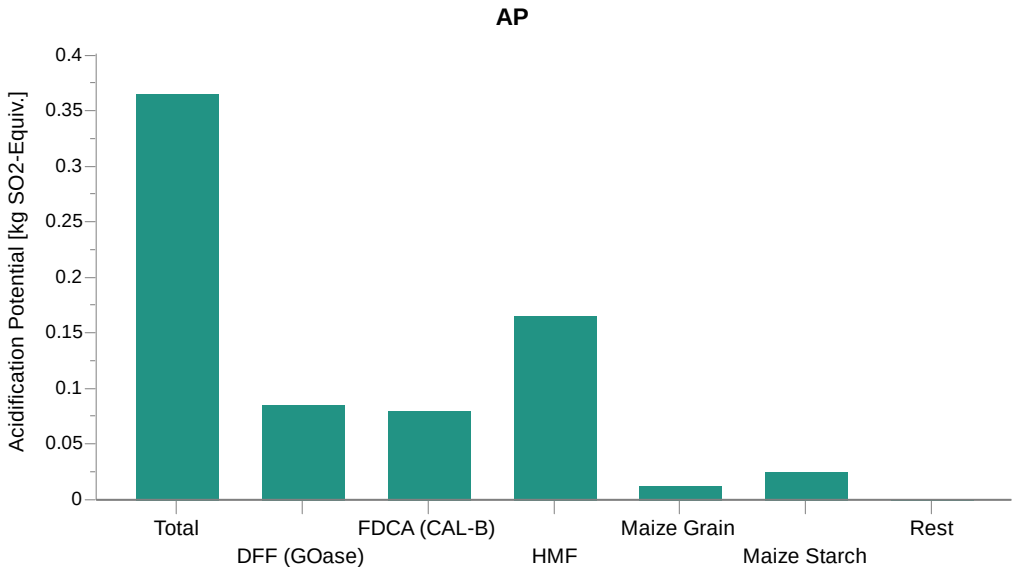

*Figure 121 – Route (**1**) AP for the cradle-to-gate production of FDCA from maize grain. Production of FDCA has been adjusted to include recycling of the two reaction solvents (EtOAc and t-butanol) by 90%.*

4.4.3 Eutrophication potential (EP)

The system used to calculate the eutrophication potential (EP) is CML 2001. Analysis used an estimate of 1 kWh per 1 kg for HMF.

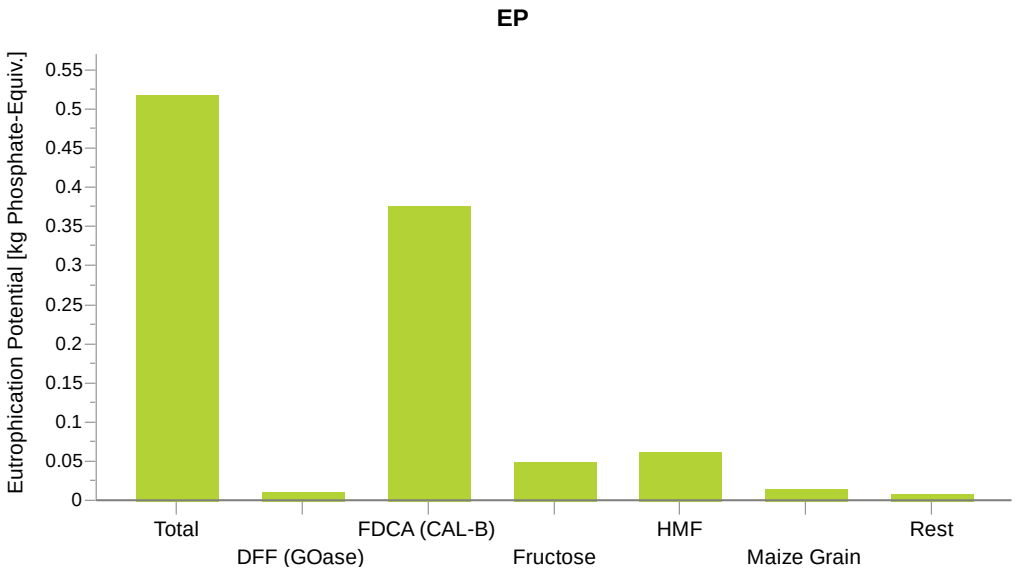

*Figure 122 – Route (**1**) EP for the cradle-to-gate production of FDCA from maize grain. The synthesis of HMF to FDCA is done enzymatically using GOase and CAL-B.*

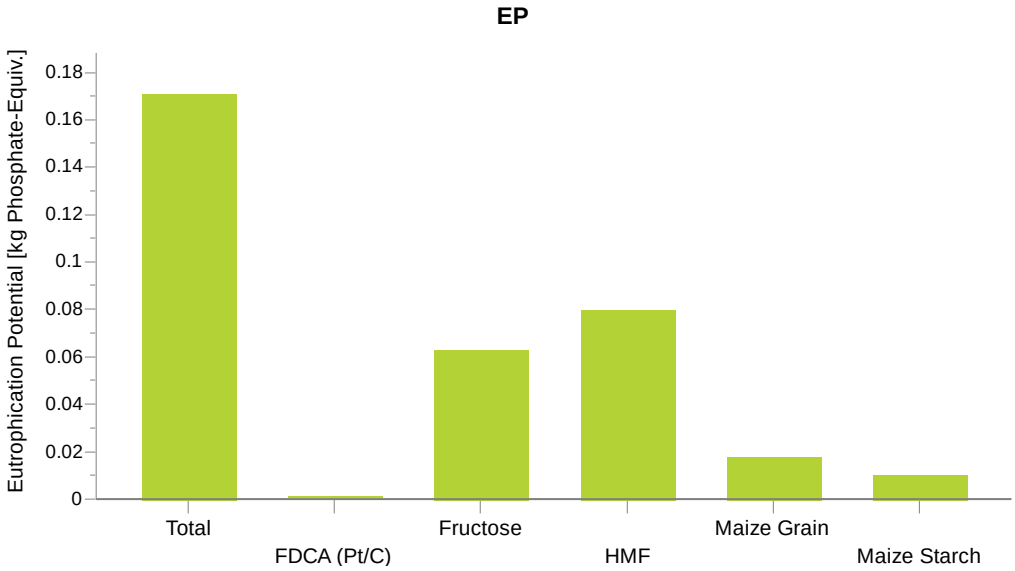

*Figure 123 – Route (**2**) EP for the cradle-to-gate production of FDCA from maize grain. The synthesis of HMF to FDCA is done by metal catalysis using Pt/C.*

The use of a platinum catalysed oxidation to produce FDCA from HMF would have a smaller EP impact, producing less phosphate. Route (**1**) uses a range of solvents that have higher phosphate manufacture emissions: ethyl acetate, t-butanol and hexane. Since no information is available for extraction and purification in route (**2**), these processes could not be included. Therefore, the effect of solvents is lower than expected. The overall impact is low for both systems (<1 kg of phosphate equivalent), whilst for each stage the largest impacting flows are solvents and water/air emissions. For the cradle stage of operation, the use of fertilisers is the main source of phosphates. As noted in (4.4.2 Acidification potential) recycling the solvent system used for the enzymatic synthesis would lower the environmental impact. Addition of solvent recycling for EtOAc and t-butanol, reduces the EP impact for the process by 0.4 kg phosphate – equivalent (see Figure 124). This adjustment aligns the two processes. The platinum catalysed route (**2**) would see an increase upon the addition of downstream processing data. After interpretation of the results, HMF production becomes the highest contributor, as hexane and dimethylacetamide manufacture produce the majority of phosphate emissions.

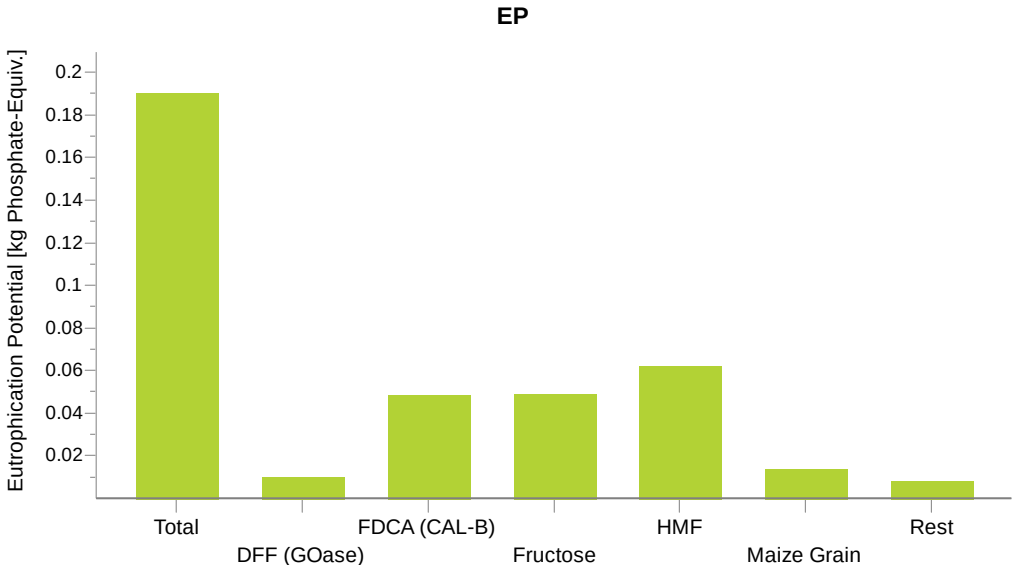

*Figure 124 – Route (**1**) EP for the cradle-to-gate production of FDCA from maize grain. Production of FDCA has been adjusted to include recycling of the two reaction solvents (EtOAc and t-butanol) by 90%.*

4.4.4 Ozone layer depletion potential (ODP)

The system used to calculate the ozone layer depletion potential (ODP) is CML 2001. Analysis used 1 kwh per 1 kg for HMF and the recycling of EtOAc and t-butanol solvents.

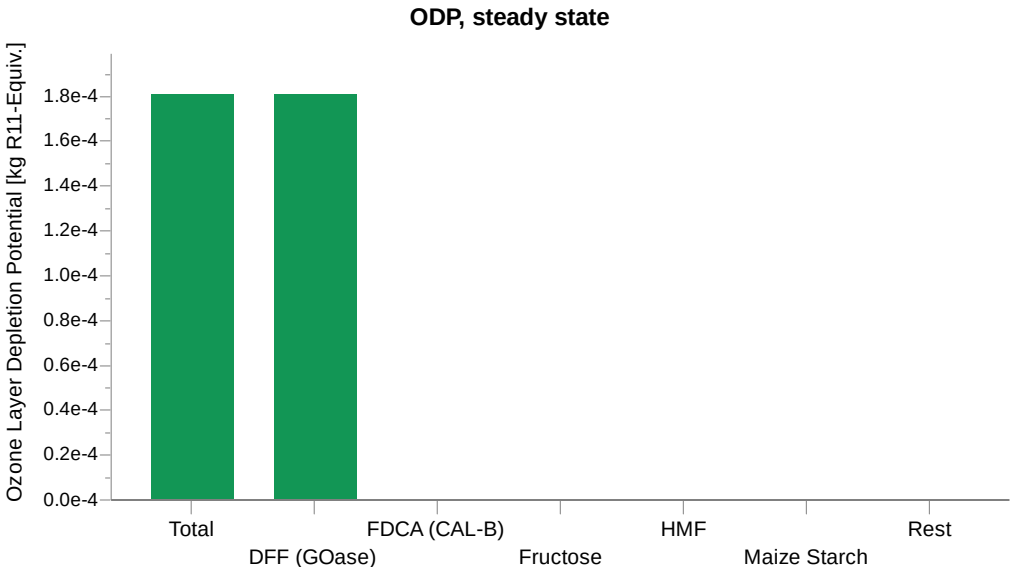

*Figure 125 – Route (**1**) ODP for the cradle-to-gate production of FDCA from maize grain. The synthesis of HMF to FDCA is done enzymatically using GOase and CAL-B.*

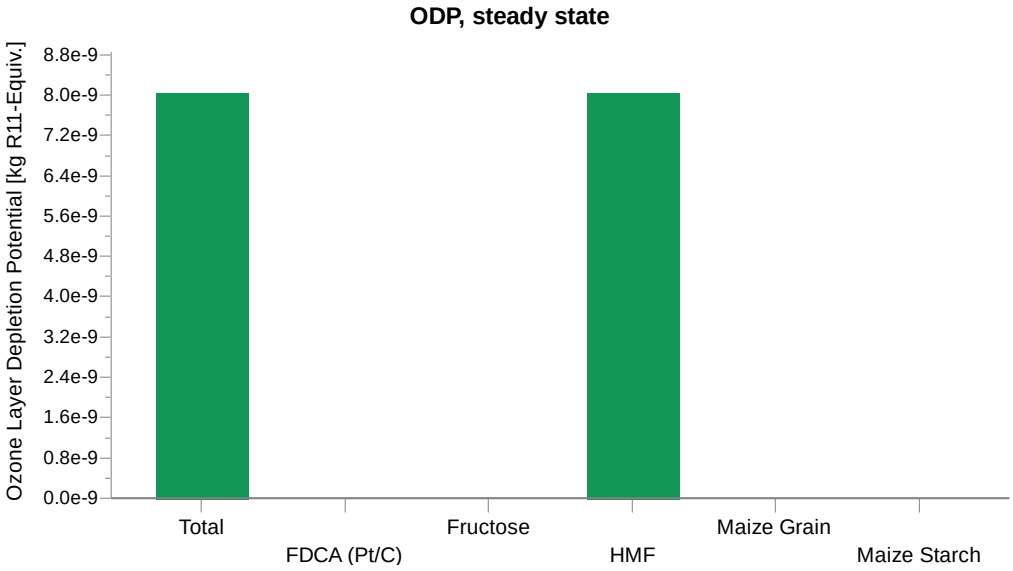

*Figure 126 – Route (**2**) ODP for the cradle-to-gate production of FDCA from maize grain. The synthesis of HMF to FDCA is done by metal catalysis using Pt/C.*

The ozone layer depletion impact for both methods is minimal as neither use CFC (chloroflurocarbon) compounds in their manufacture. Route (**1**) has a larger impact, solely from the use of dichloromethane (DCM). Removal of this chlorinated solvent lowers the impact to an equivalent level seen in route (**2**). Recycling of DCM is already estimated at 90%, captured from vacuum distillation after extraction. For the production of HMF dimethylacetamide is the sole contributor to ODP, substitution for a greener solvent would reduce both impacts. Substitution of DCM with ethyl acetate reduces the ODP impact for route (**1**) by 1.8 x 10^{-4} kg R11 – equivalent (Figure 127) Since route (**2**) requires more HMF to be produced (latter reactions having lower efficiencies), it has a greater impact than route (**1**). After interpretation of the results, HMF production becomes the highest contributor, as lithium bromide manufacture produces the majority of CFC's. Use of an alternative by Avantium would lower this considerably. Their route uses greener chemicals with improved downstream processing to give high yields of HMF.[174]

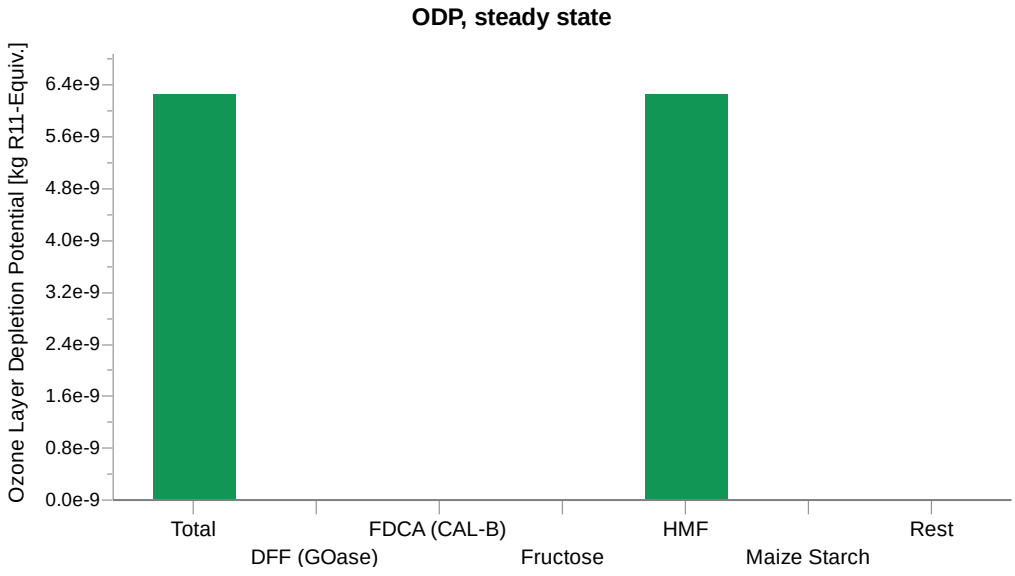

*Figure 127 – Route (**1**) ODP for the cradle-to-gate production of FDCA from maize grain. Production of DFF has been adjusted to substitute ethyl acetate as an extraction solvent, instead of using dichloromethane. A 90% recycling estimate has been included.*

4.4.5 Fossil depletion (FD)

The system used to calculate the fossil depletion (FD) is ReCiPe 2016. Analysis used 1 kWh per 1 kg for HMF, the recycling of EtOAc and t-butanol solvents and substitution of DCM with EtOAc.

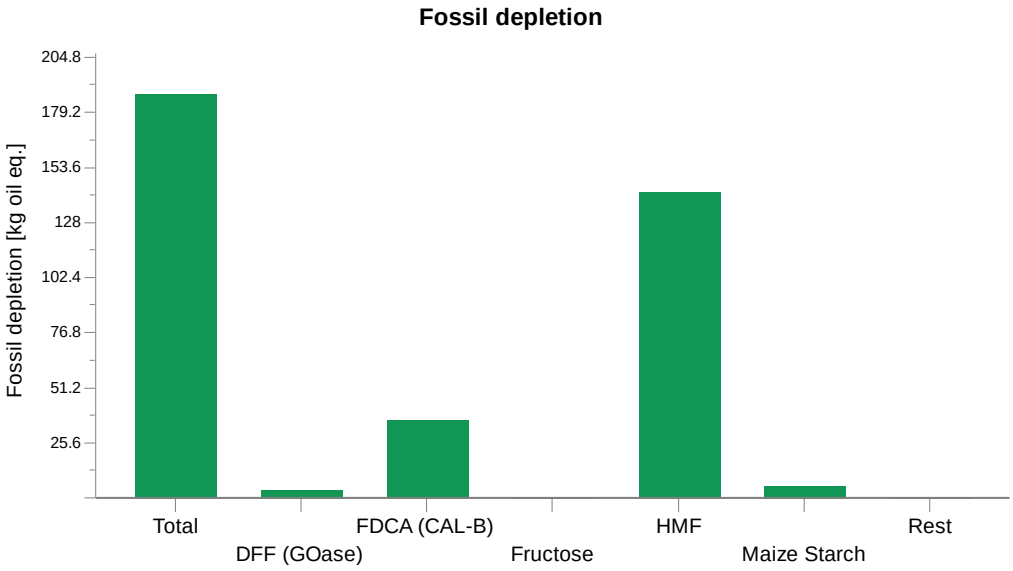

*Figure 128 - Route (**1**) FD for the cradle-to-gate production of FDCA from maize grain. The synthesis of HMF to FDCA is done enzymatically using GOase and CAL-B.*

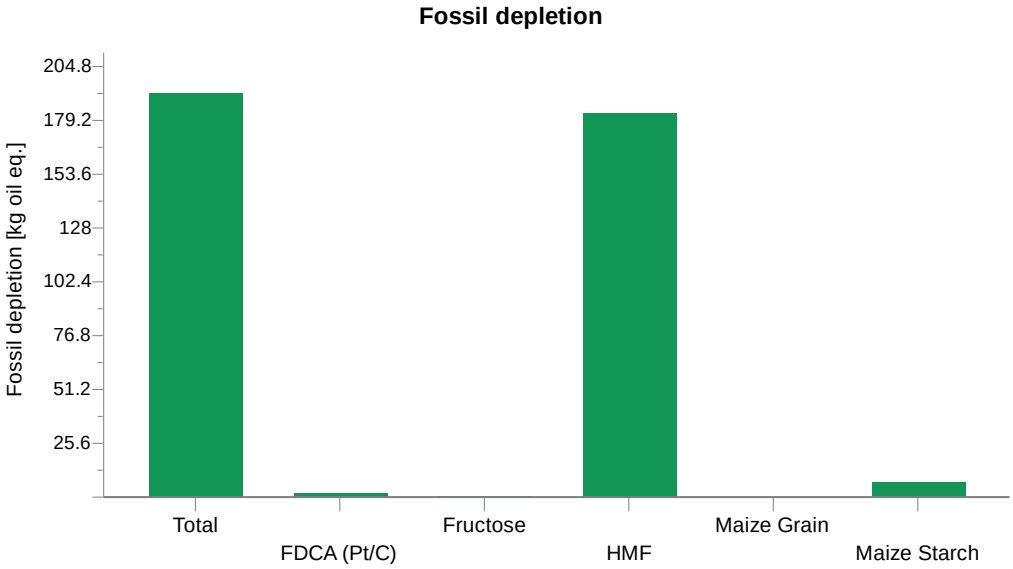

*Figure 129 – Route (**2**) FD for the cradle-to-gate production of FDCA from maize grain. The synthesis of HMF to FDCA is done by metal catalysis using Pt/C.*

The fossil depletion (DF) impact for route (**1**) is slightly lower (188 kg oil-e), using the lower number of resources to produce 1 kg of FDCA. In route (**2**) (192 kg oil-e) production of HMF makes a significant contribution, however the lower efficiency of conversion from HMF to FDCA means more material is required at each stage. A total of 2.55kg of fructose is required for 1 kg of HMF in route (**1**) whilst route (**2**) requires 3.28 kg of fructose, as seen in Figure 113. This is a 28% increase in material usage throughout, that applies to all inputs and outputs from the unit process. The overall FD is not 28% higher as the Pt/C catalysed oxidation is highly efficient for material use; this would change with data on extraction and purification. The highest contributor for both routes (**1** & **2**) is dimethylacetamide, at 96 kg oil - equivalent, roughly half the overall impact.

4.5 Life Cycle Impact Assessment of Terephthalic Acid

The results for the LCIA of the production of terephthalic acid from crude oil are presented below. The global warming impact of the cradle-to-gate production from crude oil mix is first presented, then the remaining impact categories and the largest contributors are discussed.

Production from crude oil, through xylene to produce purified terephthalic acid has been designated into individual plans. The figure below shows the full life-cycle used in GaBi for each, along with the quantities required at each stage.

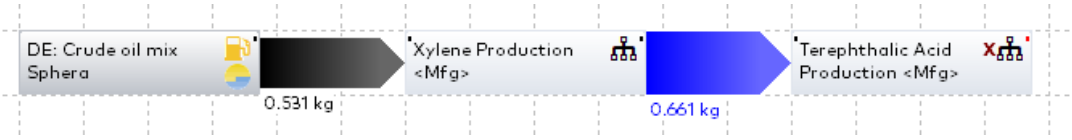

*Figure 130 – Route (**3**) Full life-cycle for the industrial scale production of purified terephthalic acid from a crude oil mix (DE) as used in GaBi. Each arrow represents the direction of material movement through the system with the quantity material transferred. A total of 0.531 kg of crude oil are required to produce 1 kg of terephthalic acid. This only accounts for crude oil used in the primary products of xylene and terephthalic acid.*

4.5.1 Global warming potential (100 Years)

The system used to calculate the global warming potential is (GWP100) CML 2001.

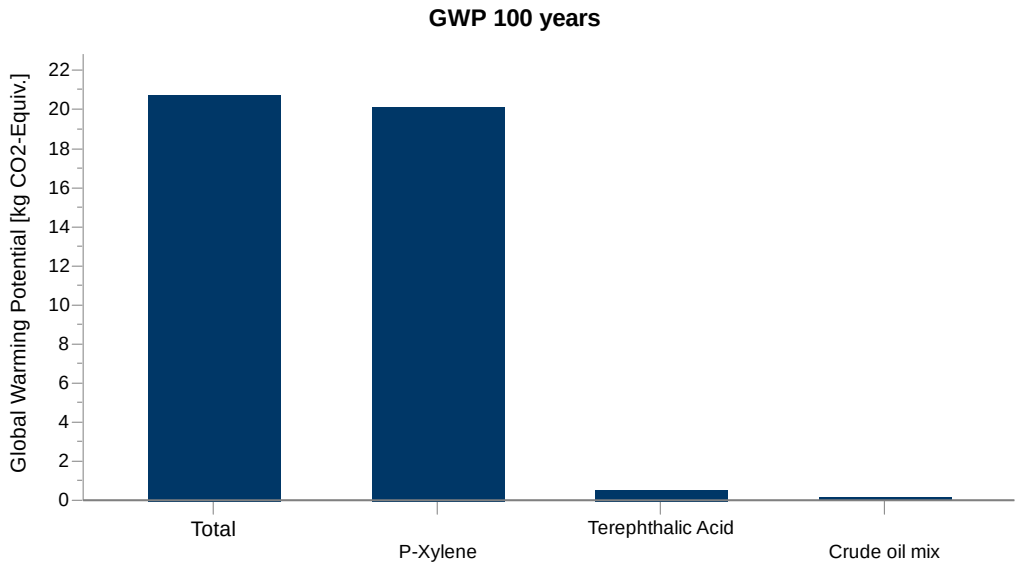

*Figure 131 - Route (**3**) GWP 100 years for the cradle-to-gate production of terephthalic acid from crude oil mix.*

This process has a notably smaller GWP100 impact than routes (**1** & **2**). The enzymatic oxidation (**1**) at 242 kg CO_2-e and the platinum catalysed oxidation (**2**) at 218 kg CO_2-e respectively. A notable difference is the optimisation of a large industrial scale process over a long time period, compared to the extrapolated lab-scale techniques. The current routes for FDCA production would yield a terephthalic acid substitute with a far higher carbon footprint. Aside from the major contribution from natural gas, the major contributors are electricity, water and the extraction of crude oil. The carbon dioxide impact is low for all other unit processes, as petroleum-based products are produced on a massive scale, particularly terephthalic acid for PET production. GaBi uses a crude oil mix of the average oil available in Germany. The composition of all the crudes can vary drastically, with different proportions of naphtha (30-60%). The assumption used by GaBi means this impact would change on a country and supplier basis. An average has been chosen by GaBi to allow for consistent LCA generation.

4.5.2 Acidification potential (AP)

The system used to calculate the acidification potential is (AP) CML 2001.

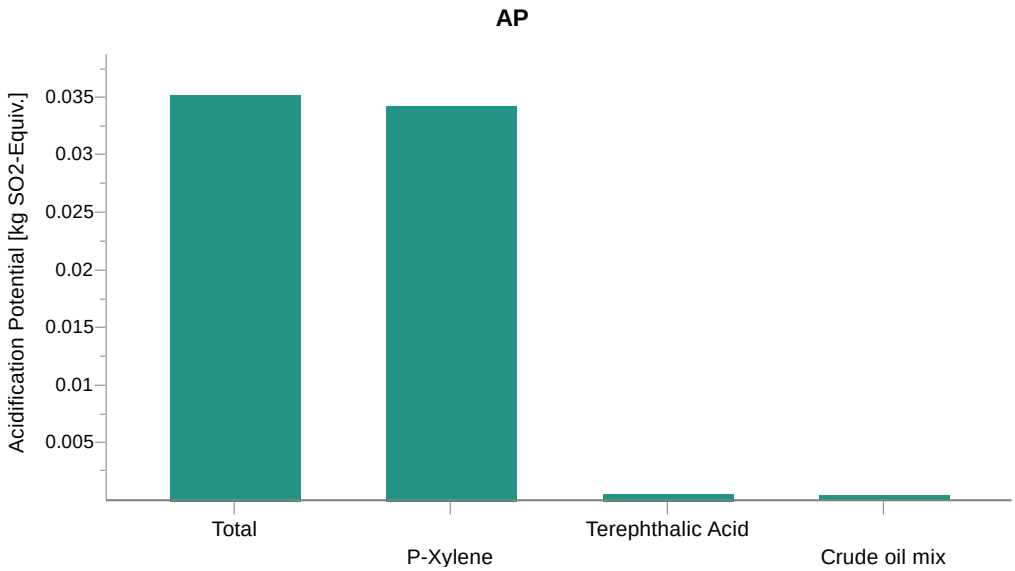

*Figure 132 - Route (**3**) AP for the cradle-to-gate production of terephthalic acid from crude oil mix.*

Similar to the GWP100 impact, AP is lowest for route (**3**). High volume production is more energy efficient than lab-scale with improved recycling instruments and precise emissions monitoring. Further development into up-scaling routes (**1** & **2**) would reduce these lab-scale inefficiencies. Xylene production is the largest contributor to sulphur dioxide emissions, largely through the combustion of refinery gases. Refineries burn a portion of the gases produced, the combustion produces large quantities of sulphur dioxide, an emission present throughout refineries in Europe. The remaining contribution comes from electricity and process water, specific to Germany and different for countries with no coal-fired power plants akin to the UK. Process heat has a low contribution, using refined and cleaned gases. Use of this data limits the study directly to Europe, where refineries conform to air pollution protocols using sophisticated air monitoring systems.

4.5.3 Eutrophication potential (EP)

The system used to calculate the eutrophication potential is (AP) CML 2001.

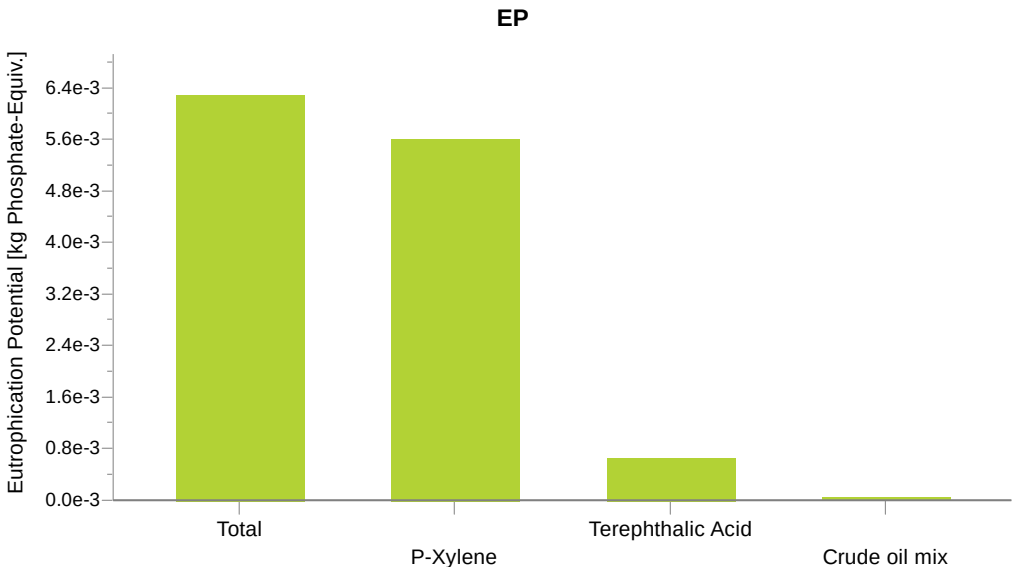

*Figure 133 - Route (**3**) EP for the cradle-to-gate production of terephthalic acid from crude oil mix.*

The EP is lowest for route (**3**). Xylene contributes the majority of the phosphate emission. The highest contributors are the direct emissions of phosphates to land, air and water rather than raw material use. Electricity and process water still have an impact, but are small in comparison at 0.426 x 10^{-3} kg SO_2 – e and 0.350 x 10^{-3} kg SO_2 – e respectively. As seen in (4.5.2 Acidification potential (AP)) the choice of fuel for generating thermal energy impacts the AP. For EP, electricity generation plays a large role, contributing 0.00123 x 10^{-4} kg SO_2 – e. The dataset has limits associated with the composition of natural gas used. As seen with the crude mix, natural gas mix available on GaBi comprises an average mixture of gas from numerous countries. Each gas has different origins, (shale, oil well etc) and therefore different quantities of phosphate compounds. This result is therefore applicable to DE, differing dramatically between countries that source their gas from shale, offshore platforms and ground wells.

4.5.4 Ozone layer depletion (ODP)

The system used to calculate the ozone layer depletion is (ODP) CML 2001.

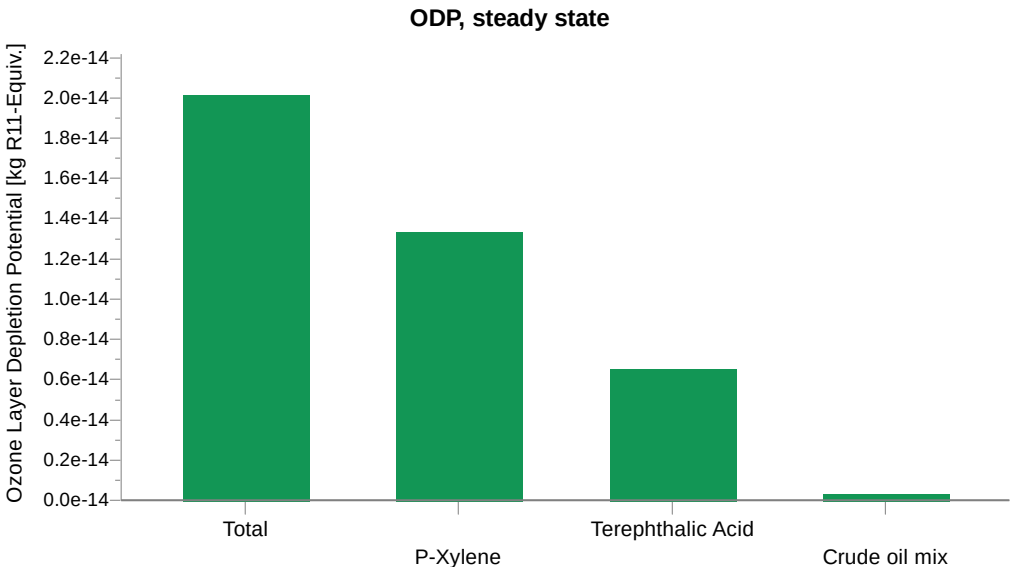

*Figure 134 - Route (**3**) ODP for the cradle-to-gate production of terephthalic acid from crude oil mix.*

As seen in the previous two impact analyses, route (**3**) provides the lowest ODP impact. In Figure 134 xylene production has the largest impact, due to its large natural gas requirement, with each refinement stage producing 25% less CFC's and HCFC's. The major contributors are the use of electricity at 5.95 x 10^{-15} kg R11 – e and process water at 1.46 x 10^{-15} kg R11 – e. The former can be reduced by using renewably generated electricity whilst the latter relies on improved water treatment facilities at refineries. The impact of this production is minimal and follows a similar trend of increasing as product refinement progresses. The database used for this is applicable to European countries that commit to the Montreal protocol to reduce CFC production. However the dataset would show significantly higher levels of CFC's for countries in Asia that contribute to 70% of the worlds current production.[181]

4.5.5 Fossil depletion (FD)

The system used to calculate the fossil depletion (FD) is ReCiPe 2016.

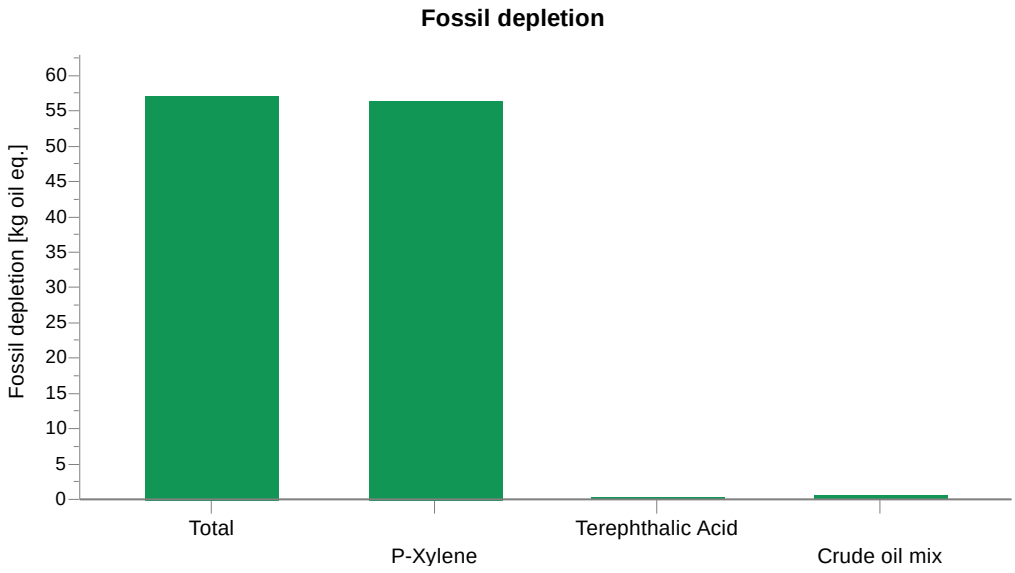

*Figure 135 - Route (**3**) FD for the cradle-to-gate production of terephthalic acid from crude oil mix.*

Production of purified terephthalic acid has been refined by the polymer industry over the decades, yielding a highly efficient process. Furthermore, there are few waste streams, with the majority of by-products having a useful production line. As expected of an industrial process, the amount of material used decreases as the refining progresses, with the largest material requirement set at the raw material (crude oil). Xylene however is similar contributing to ~48% of the total FD. The process has reasonable efficiency, producing 1 kg of terephthalic acid at the cost of 57 kg oil – e. Aside from gas and oil, the remaining inputs contribute equally; electricity and process water. Whilst thermal energy does have an impact, it's contribution is heavily influenced by the combustion of refined gases to generate heat.

4.6 Interpretation

For the purpose of this study a comparison has been made between the enzymatically developed process for the production of FDCA and its petroleum counterpart terephthalic acid. Changes have not been made to the terephthalic acid life-cycle route (**3**) as this is an already refined industrial scale process. Adjustments have been incorporated into route (**1**) based on interpretations made in (4.4 Life Cycle Impact Assessment of FDCA). The GWP100 impact has been compared as this exhibited the largest degree of change. The alterations are summarised in the table below, and included in the results calculation.

*Table 30 – Alterations made during the interpretation stage on the cradle-to-gate enzymatic production of FDCA, route (**1**).*

Unit Process Change	**Original Value**	**Altered value**
Electrical power for HMF production [a]	1680 KWh per 1kg	1 KWh per 1 kg
EtOAc & t-butanol Solvent recycling [b]	0% recycled	90% recycled
Substitution of DCM for EtOAc in extractions [c]	Dichloromethane (63 kg)	Ethyl acetate (45 kg)

[a] original values and changes derived from analysis in 4.4.1 Global warming potential (100 years), alters the electricity requirement to produce 1 kg of HMF, [b] original values and changes derived from analysis in 4.4.2 Acidification potential (AP), alters the recycling of solvents used for the oxidation of DFF to FDCA, [c] original values and changes derived from analysis in 4.4.4 Ozone layer depletion potential (ODP), alters the extraction and purification solvent used for DFF production. Changes are made based on feasible and viable solutions to major impact contributors.

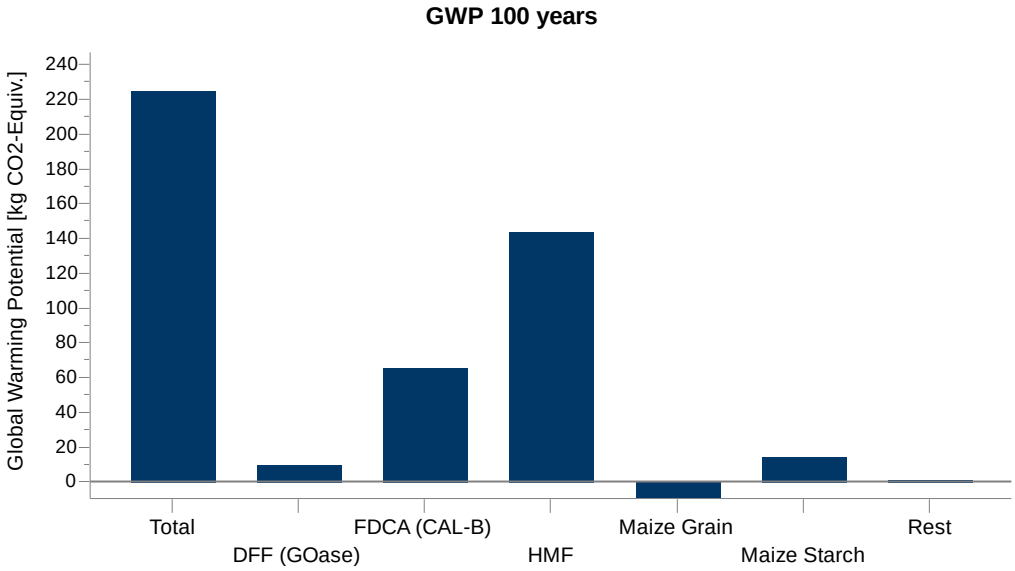

*Figure 136 – Route (**1**) GWP 100 years for the cradle-to-gate production of FDCA from maize grain. Adjustments have been made to unit processes to reduce the largest contributors, as stated in Table 30.*

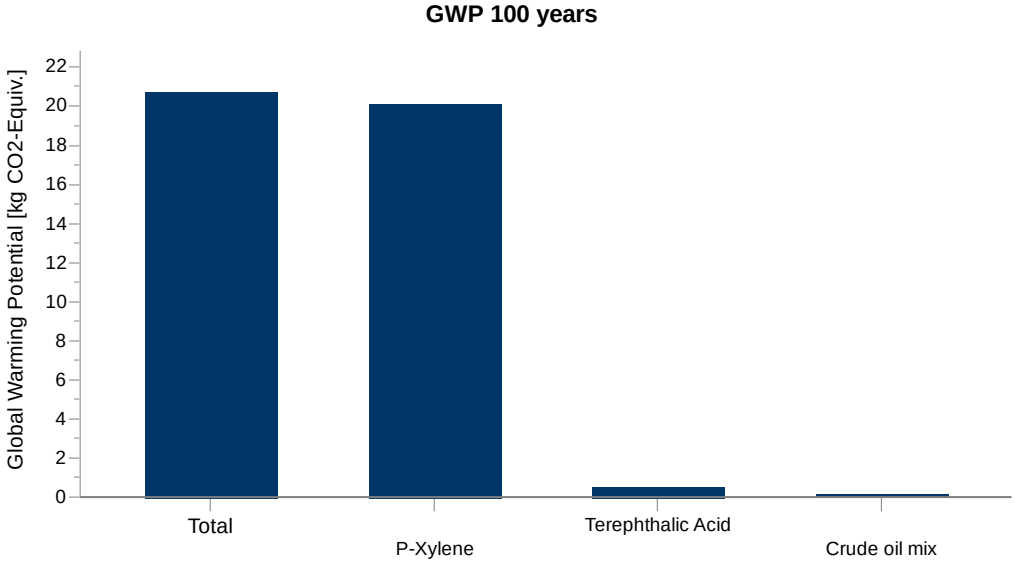

*Figure 137 - Route (**3**) GWP 100 years for the cradle-to-gate production of terephthalic acid from crude oil mix. No adjustments have been made as the process is already optimised at an industrial scale.*

As expected, the reduction is significant for route (**1**), however it is still a factor of 10 higher than route (**3**). Half of the major contribution for route (**1**) comes from the production of HMF, a route lacking necessary process optimisation. The major contributor is the production of sodium silicate (waterglass), used for column chromatography. At large scale more efficient separation techniques such as membrane filtration and distillation are available. LCA data taken from the report on HMF production corresponds to a lab-scale production and its associated inefficiencies. Significant improvement is required for route (**1**) to reduce its environmental impact, improves the efficiency of the process and reduce waste streams. Implementation of the Avantium synthesis route from fructose would further reduce the impact, however the required data is not available in the public domain.

4.6 Conclusions

Industrial scale production of FDCA requires significant process development to reduce its environmental impact. In this work two methods for the efficient cradle-to-gate production of FDCA have been explored. The life-cycle of the bio-renewable enzyme process has been compared against its petroleum analogue, terephthalic acid. A selection of impact categories was allocated based on the importance and interests of the work. Data was taken from reliable databases available at EcoInvent, GaBi and the National Renewable Energy Laboratory, with assumptions stated when necessary. The lack of available detailed data for the platinum catalysed route (**2**) meant a significant reduction in environmental impacts. With the inclusion of product purification, catalyst manufacture and thermal input, the environmental impact would increase. The production of FDCA in route (**1**) would benefit from the inclusion of accurate LCA data pertaining to enzyme production by fermentation for catalase, HRP and galactose oxidase as this required estimation.

For the enzymatic route (**1**), significant reductions in the environmental impact can occur through process optimisation; ethyl acetate extractions, efficient industrial scale equipment, solvent recycling of EtOAc and T-BuOH and the use of Avantium's process for producing HMF.

Terephthalic acid production is highly efficient with a relatively small carbon footprint. The industry has existed for over 40 years, allowing it time to optimise and refine the process. For newly developed bio-renewable processes to compete considerable process development is required. Initially they may have a far greater environmental impact, but continued research helps minimise this. A few simple changes reduced the GWP100 impact of FDCA production (**1**) by over 1500 kg CO_2 – e, continued refinement would yield further reduction. Production of FDCA enzymatically is a greener route than the common Pt/C catalysed alternative, however significant work is required to improve the sustainability of the process.

Chapter 5 - Conclusions and Future Work

The work in this thesis has focused on exploring the techniques of 5-hydroxymethylfurfural (HMF) oxidation and how the technology could be improved to develop an industrial scale process for the production of 2,5-furandicarboxylic acid (FDCA). The main goals were initially: (i) green route for the synthesis of FDCA; (ii) evaluation of enzymatic continuous flow processes for DFF; (iii) evaluation of a continuous liquid foam system for producing diformylfuran (DFF). (iv) life-cycle assessment of the processes to evidence improved sustainability. The thesis has contributed to each of the above areas and demonstrated some new approaches to solving the problems of producing sustainable bioplastic monomers.

Procedures for the oxidation of an alcohol or aldehyde to the respective carboxylic acid are numerous, with a plethora of conditions and capabilities. Work in Chapter 2 discussed suitable techniques for the oxidation of the intermediate DFF to FDCA. Initial work, developing a small selection of suitable oxidisers proved a considerable challenge. The problems of selectivity and conversion were overcome using an approach described in the literature with CAL-B lipase and *tert*-butylhydroperoxide in batch, re-configuring this, and making it safer to operate, as a continuous flow system. This approach provided the optimum product selectivity under conditions suitable for continuous flow. The *in-situ* production of peroxyacetic acid enabled a fast and relatively safe oxidation to occur. At a high product selectivity of 95%, this approach presents a significantly more cost-competitive and environmentally friendly alternative to current FDCA forming reactions. Despite this, the process still required pure DFF substrates to achieve peak efficient oxidation, suffering significant mass imbalance when using an enzyme generated DFF solution. Future work should focus on the improvement of the process and a continuous liquid foam reaction may be a good way to operate this in continuous flow. An optimised continuous process would allow for a telescoped reaction of HMF to DFF to FDCA helping increase the production

efficiency. Further development of the separation and purification of the diacid is essential for an industrially viable process, particularly at the large scale required to compete with the terephthalic acid production.

In Chapter 3, the continuous oxidation of HMF in a liquid foam reactor was developed and operated above the solubility limit of DFF to increase the productivity. Since dialdehyde product has limited solubility in water, all the processes described to date operate below saturation and this results in large quantities of waste and low productivity. A novel continuous liquid foam system was developed to transport the insoluble product particulate through the reactor, bypassing the need to use more hazardous solvents. Several reactors were built to generate a protein stabilised foam *in-situ*, using hydrogen peroxide or air as an oxygen source.

The combination of an aqueous foam and continuous flow reactor produced DFF at a steady 85% conversion, from a fairly concentrate 0.5 M solution of HMF. This is a ten-fold increase on current aqueous conversions reported in the literature. A greener alternative was explored using compressed air instead of peroxide, generating high conversions of DFF in minutes, a significant reduction on the hour-long batch reactions. It was shown that at the end of the reaction the enzymes retain most of their activity, and since the DFF product is a solid, it is easy to envisage product separation and enzyme/liquid recycle. To facilitate a wider uptake of this technology further development of these compressed air reactions is required with optimisation of the mass transfer parameters to increase the conversion of the substrate. Further work would involve application of this process to the DFF to FDCA bio-oxidation, and other complex enzymatic catalysed oxidations.

Life-cycle assessment (LCA) is a complex tool for analysing a product's environmental impact. Each LCA contains numerous assumptions and estimations based on robust available data. The work described in Chapter 4 addressed the impact of FDCA synthesis from the combination of reactions in Chapter 2 and 3, compared to a Pt/C catalysed oxidation and terephthalic acid production. The ability to compare the developed reaction to existing techniques is essential for the development of a sustainable synthesis. The study demonstrated the changes and improvements modern green chemistry must make to compete with the fossil fuel industry. Producing a renewable alternative is a trade-off between a sustainable product, at the cost of a higher environmental impact. Interpretation demonstrated areas of considerable improvement to the enzymatic route, lowering its impact below that of the metal catalysed route. Data for chemicals, enzymes or processes was unavailable or inaccessible, future work would benefit considerably from the access to these and the inclusion of all waste streams, highlighting the areas of efficiency or improvement.

An area of future interest are the derivatives of FDCA, alternatives containing either a thiophene or pyrrole, instead of furan. Pyrrole can be deprotonated, enabling the ring to be broken apart, enhancing its degradation by microorganisms. 1HPDCA has the potential to form a readily biodegradable plastic from bio-renewable sources. Production of 1H-pyrrole-2,5-dicarboxylic acid (1HPDCA) is currently limited to research, with only a brief number of articles mentioning the compound. A patent by Song *et.al* [182] describes a bioplastic containing a combination of thiophene and pyrrole in the polymer backbone. The molecular weight is said to vary drastically, indicating that there is a semblance of flexibility within the polymerisation process. This resilience grants polymer production for numerous applications, giving the product a potentially larger polymer market than FDCA, such as polyethylene which can be high density (HDPE) or low density (LDPE)

In summary, continuous enzymatic oxidations provide a green approach for the synthesis of furan-derivatives under mild conditions, rapidly producing DFF and FDCA in minutes. This thesis has focused on improving current oxidation reactions to further align with the interests of industry, which has been achieved by developing novel continuous foam flow reactors and the *in-situ* generation of oxidisers. Further development studied the environmental impact of each process, highlighting areas of improvement and the benefits over alternative techniques. During this work, areas of interest for future research in the field of enzymatic oxidations in flow have been identified: these include: (i) production off foams for the transport of insoluble particulate; (ii) developing downstream purifications and extractions in flow; (iii) introducing telescoped enzymatic oxidations for a lower environmental impact; (iv) optimisation of the enzymatic catalysed production of FDCA. Furthermore, as all the reactions are suitable for continuous flow, there would be significant interest in the application of enzyme immobilisation for $GOase_{M3\text{-}5}$. As the chemical manufacturing industry strives for greener processes, the move to biotransformation's is inevitable. Therefore, providing a simple and effective technique for high concentration bio-oxidations in continuous flow, will be crucial for the widespread adoption of these processes on an industrial scale.

Chapter 6 – Experimental

6.1 Offline Analytical Equipment

Quantitative analysis was performed using an Agilent 1100 series HPLC instrument with a DAD and the data was processed with Chemstation software. The HPLC was fitted with a BioRad Aminex HPX 87-H reverse-phase column with a 20 µL injection volume (300 mm length, 7.8 mm ID and 9 µm particle size). UV-Vis analysis was performed using an Ocean Insight Flame UV-Vis flow cell spectrometer.

NMR spectroscopy was performed on a Bruker 500 Ultrashield™ NMR Spectrometer (^{1}H at 500 MHz, ^{13}C at 126 MHz) with the appropriate deuterated solvent. Assignment of NMR signals for compounds was done using either Metsrenova or TopSpin software. Chemical shifts in both ^{1}H and ^{13}C NMR spectra are expressed in ppm, reported as singlet (s), doublet (d), triplet (t), quartet (q) and a combination thereof, or multiplet (m). Coupling constant (J) are quoted in Hz, calculated as an average between coupling partners.

Measurement of pH was performed using a Mettler Toledo pH Meter with attached pH probe and confirmed with universal indicator paper supplied by Fisherbrand. The instrument was calibrated before use, using Mettler supplied buffer standards at pH 2, 4.7 and 10. Peroxide tests were completed using potassium iodide starch paper from Macherey-Nagel.

Quantitative HPLC analysis used external calibration on standards of each intermediate and product. Calibrations were repeated any time modifications or changes were made to the HPLC instrument; including but not limited to repairs or equipment shutdown.

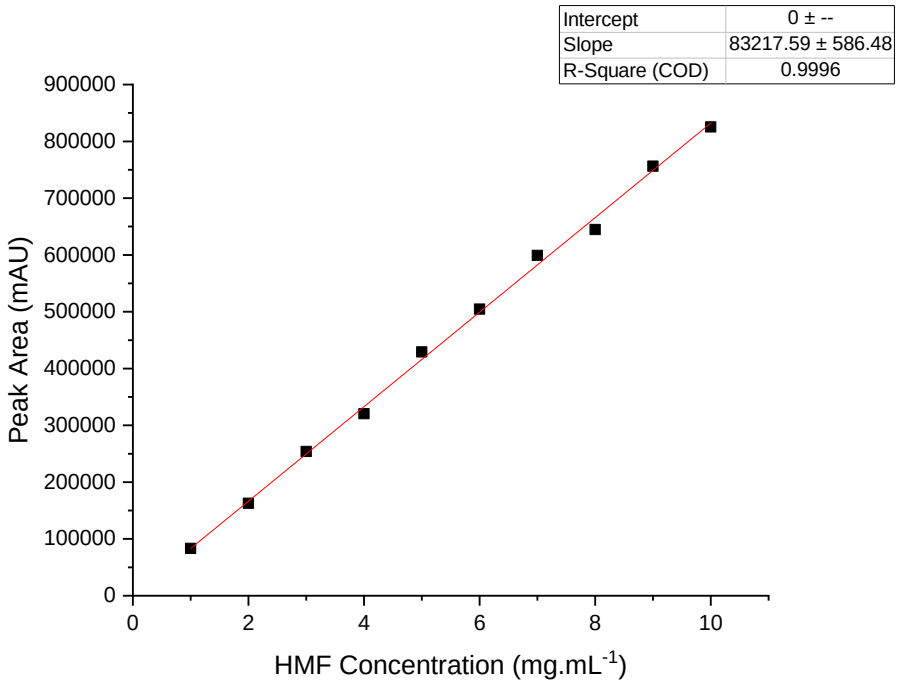

Figure 138 – External calibration curve of HMF on an Agilent 1100 series with a DAD and a BioRad Aminex HPX 87H reverse phase column with a 20 µL injection volume.

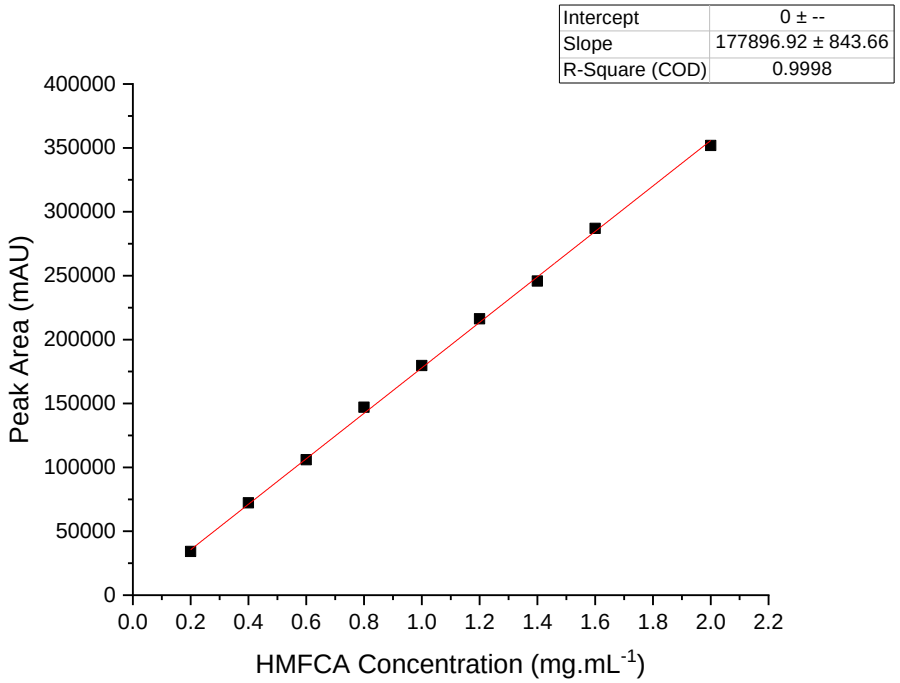

Figure 139 – External calibration curve of HMFCA on an Agilent 1100 series with a DAD and a BioRad Aminex HPX 87H reverse phase column with a 20 µL injection volume.

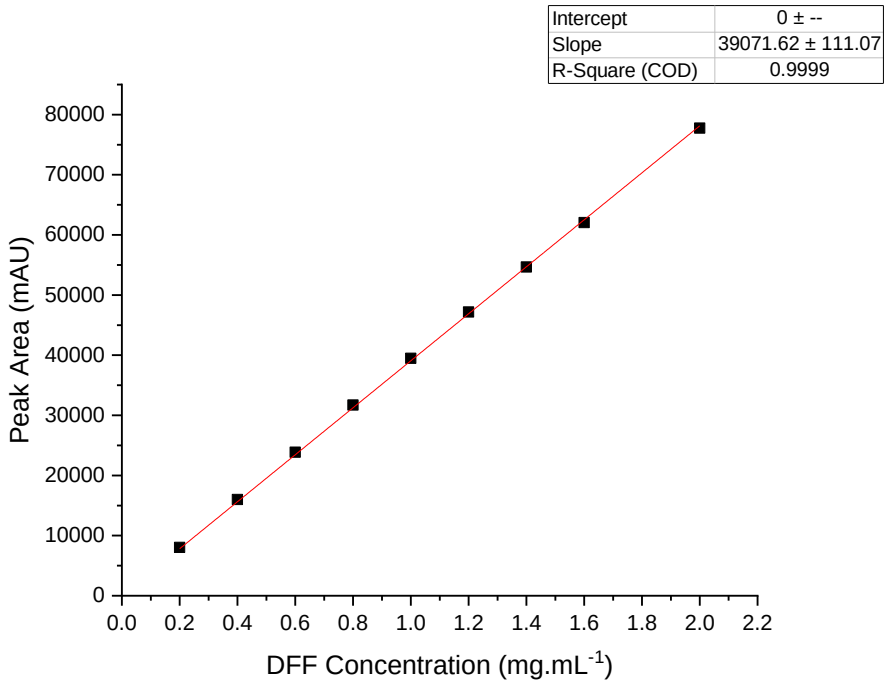

Figure 140 – External calibration curve of DFF on an Agilent 1100 series with a DAD and a BioRad Aminex HPX 87H reverse phase column with a 20 µL injection volume.

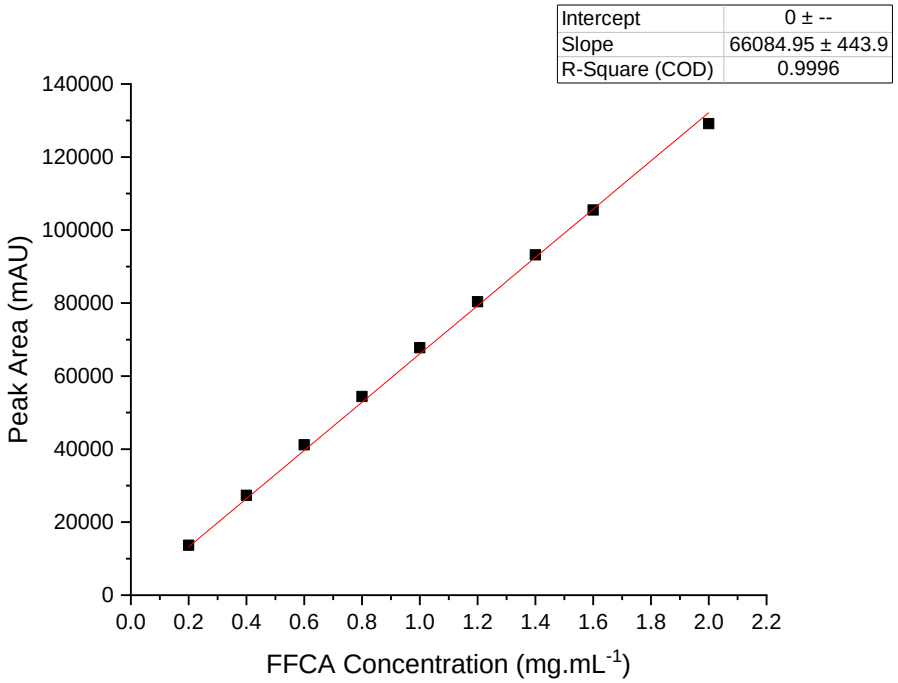

Figure 141 – External calibration curve of FFCA on an Agilent 1100 series with a DAD and a BioRad Aminex HPX 87H reverse phase column with a 20 µL injection volume.

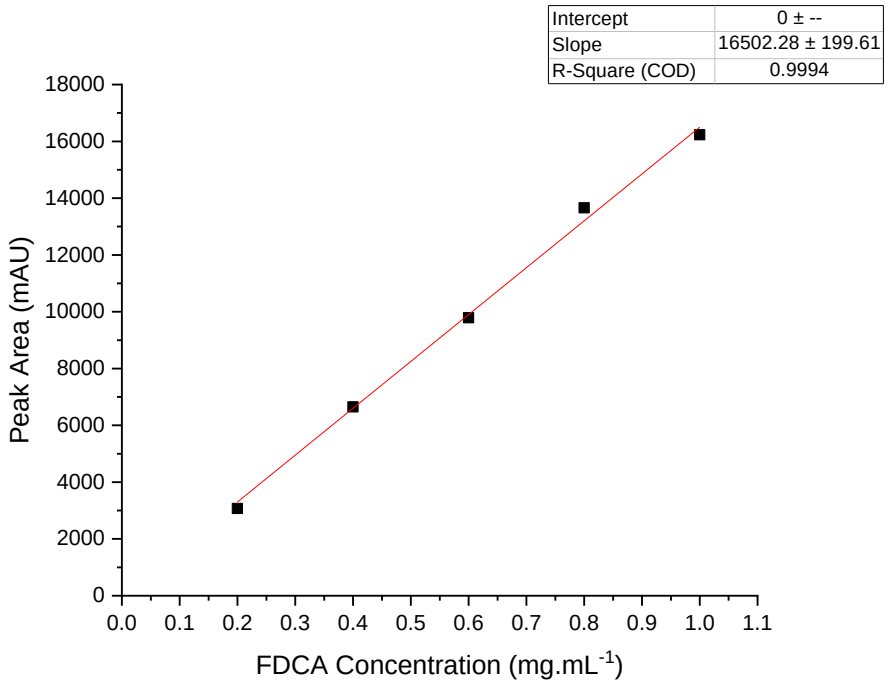

Figure 142 – External calibration curve of FDCA on an Agilent 1100 series with a DAD and a BioRad Aminex HPX 87H reverse phase column with a 20 µL injection volume.

6.2 Incubator Shaker

Batch enzymatic reactions were completed in a SciQuip shaker shown in Figure 143. Reaction flasks (50 mL centrifuge tubes) were kept at a 45° angle using a designated holder. All Falcon tubes were sealed shut for reactions, using the screw-top lids. Hydrogen peroxide was manually added using a P200 or P20 Gilson Scientific Auto-Pipette with disposable tips. The Incubator was set to 37 °C and 500 rpm shaker speed. Sampling was done using a P200 and P1000 Gilson Scientific auto-pipettes into 1.5 mL Eppendorf tubes. A SciQuip Sigma centrifuge separated the denatured enzyme from solution in preparation for chromatographic analysis.

Figure 143 – SciQuip MIDI incubator shaker, the 50mL falcon tube platform was used instead of conical flask holders for reactions. Temperature was set to 37 °C and a shaker speed of 500 rpm. The unit was pre-heated for 15 minutes before use.

6.3 ChemSpeed Automated Reactor System

The automated reactor and sampling system used was a ChemSpeed. Samples were taken at designated intervals with reaction times able to go for a full 24hrs. The instrument is capable of programmed procedures and was therefore tailored for each individual reaction, with a generic structured process built upon each time. Reactors were heated to 37 °C using a Huber oil bath and shaken at 500 rpm for the duration of the procedure. Sampling was completed automatically; a needle taking 50 µL directly from the reaction mixture and diluting it with 900 µL of the appropriate solvent and 50 µL of quenching solution in a 1.5 mL Eppendorf. Reactions were completed using a singular script set up on the ChemSpeed. With a 'master script' being altered each time a new variable was introduced. The script is constructed from individual tasks defined on the indigo tab on the left-hand side. A simple drag and drop approach to add or remove tasks, with sub-sections being created to organise tasks in a control window as shown Figure 144.

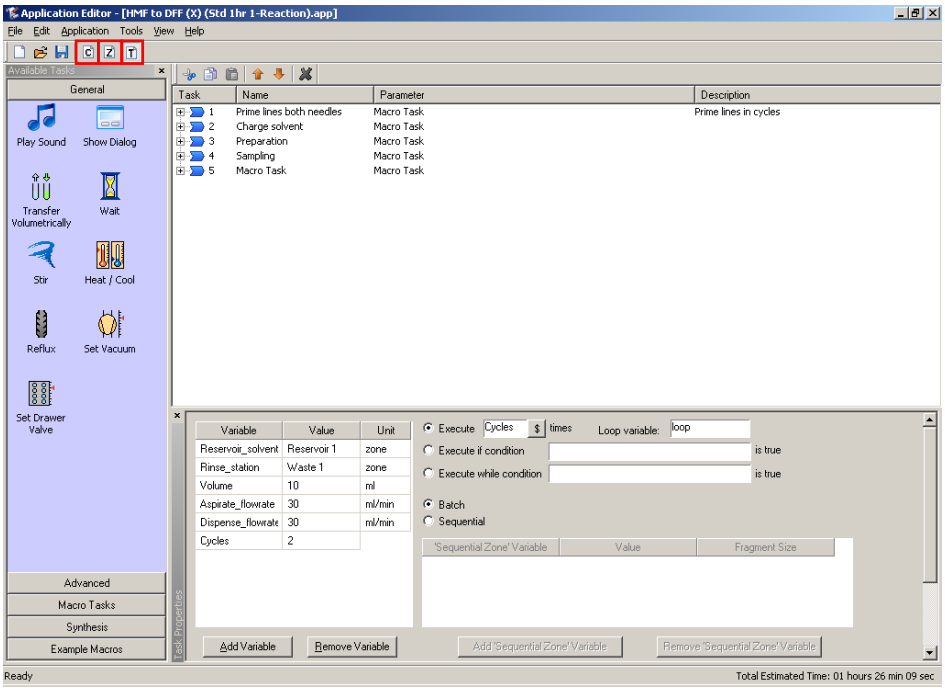

Figure 144 – Automated reactor system software (ChemSpeed) with the master script setup prior to each reaction, allowing modifications for any variable alterations.

6.4 Chapter 2 Procedures

6.4.1 Chemicals

2,5-furandicarboxlyic acid (99%, Sigma Aldrich), 5-hydroxymethylfurfural (98%, Avantium), diformylfuran (99%, Tokyo Chemical Industry), 5-formyl-2-furancarboxylic acid (99%, Sigma Aldrich), 5-hydroxymethyl-2-furancarboxylic acid (99%, TCI), sodium tungstate dihydrate (Fluorochem), methyltrioctylammonium hydrogen sulfate (Sigma Aldrich), hydrogen peroxide (30% w/v in water, Fischer), potassium phosphate monobasic (99%, Sigma Aldrich), potassium phosphate dibasic (99%, Sigma Aldrich), potassium monopersulfate – Oxone™ (99%, Fischer), t-butanol (Fischer Scientific), acetic acid (97%, Fischer), *Candida antarctica B* immobilised on Lewatit VP OC 1600 resin (Novozyme 435, Novozymes), sulphuric acid (98%, Fischer), catalase from bovine Liver 10,000 AU (Pure enzyme, Sigma Aldrich), deuterated water (99%, Sigma Aldrich), sodium deuteroxide (99%, Sigma Aldrich), deuterated sulphuric acid (99%, Sigma Aldrich), Diemthyl Sulfone NMR Standard (99%, Sigma Aldrich), deuterated dimethyl sulfoxide (99%, Sigma Aldrich). galactose oxidase $M_{3\text{-}5}$ mutant Strep tag (CFE, Prozomix).

6.4.2 Synthesis of FDCA from HMF by the Cannizzaro reaction

To a two-necked 25ml round-bottomed flask 5-hydroxymethylfurfural (2.52 g, 20 mmol) and potassium hydroxide (4.48 g, 80 mmol) was added to 5 mL of water. A 50 µL sample of the mixture was taken for a t=0 point using a 200 µL Gilson Auto-pipette and diluted to 1 mL using deionised water in a 1.5 mL Eppendorf. The mixture was then heated to 70 °C and left to stir for 5 minutes before drop-wise addition of hydrogen peroxide (30% w/v) (12.51 mL, 160 mmol) over a 15minute period. Temperature was closely monitored and H_2O_2 stopped if it exceeded 90 °C. 50 µL samples were taken from the reaction every 5 minutes, quenched with catalase (50 µL, 10 $mg.mL^{-1}$) and neutralised with HCl (50 µL, 2 $mol.L^{-1}$). The mixture was then left to cool to 60 °C before neutralising with HCl (5-10 mL, 12 mol L^{-1}).

6.4.3 Synthesis of FDCA from DFF & FFCA by the Cannizzaro reaction

The procedure for this process was identical to that described in (6.4.2 Synthesis of FDCA from HMF by the Cannizzaro reaction), with changes only made to the quantity of each reactant. Quantities of each reagent used are summarised in the table below. The quench and sampling remained the same as the aforementioned procedure for HMF.

Table 31 – Reagent quantities for the Cannizzaro reaction of DFF/FFCA.

Substrate	***Reagent***	***Quantity***	***mmol***
DFF	Diformylfuran	10.0 mg	0.08
	Potassium hydroxide	18.0 mg	0.32
	Hydrogen peroxide [a]	50.0 µL	0.64
	Deionised water	5.0 mL	-
FFCA	5-formyl-2-furancarboxylic acid	3.5 mg	0.25
	Potassium hydroxide	56.0 mg	1.00
	Hydrogen peroxide [a]	156.0 µL	4.00
	Deionised water	25.0 mL	-

[a] hydrogen peroxide used was 30% v/v in concentration, with preparations as described in (6.4.2 Synthesis of FDCA from HMF by the Cannizzaro reaction).

6.4.4 Synthesis of FDCA from $GOase_{M3-5}$ synthesised DFF by the Cannizzaro reaction

The procedure for this process was identical to that described in (6.4.2 Synthesis of FDCA from HMF by the Cannizzaro reaction), with changes only made to the quantity of each reactant. Quantities of each reagent used are as follows: aqueous buffered GOase synthesised diformylfuran (25 mL, average value at 2mg.mL^{-1} DFF, 0.4 mmol), potassium hydroxide (90 mg, 1.6 mmol), hydrogen peroxide (251 µL, 3.2 mmol). Aqueous buffered DFF was acidified with HCl (5 mL, 2 mol.L^{-1}), the solution centrifuged, and the supernatant used in the reaction as the solvent after removal of remnant enzyme. The HCl quench was reduced accordingly. Sampling was unchanged against (6.4.2 Synthesis of FDCA from HMF by the Cannizzaro reaction).

For the ^{1}H NMR, a 3 mL solution of deuterated water was separated into two 1.5 mL Eppendorfs (1.5 mL in each). For the pD 5 the solution was acidified with deuterated sulphuric acid drop-wise and tested using pH 2-5 indicator paper. For the pD 8 the solution was basified with sodium deuteroxide drop-wise and tested using pH 6-9 indicator paper. A 1 mg sample of DFF was measured using a Mettler Toledo 6-figure balance and then dissolved in each sample for ^{1}H NMR analysis.

^{1}H NMR (NaOD, 500 MHz) δ 9.66 (s, 2H), 9.49 (s, 1H), 9.40 (s, 1H), 7.51 (s, 2H), 7.44 (d, 1H), 7.43 (d, 1H), 7.02 (d, 1H), 6.71 (d, 1H), 6.67 (d, 1H), 6.58 (d, 1H), 6.00 (s, 1H), 5.55 (s, 1H) ppm.

^{1}H NMR (D_2SO_4, 500 MHz) δ 9.41 (s, 2H), 7.45 (d, 2H), 6.67 (m, 2H), 6.00 (s, 1H) ppm.

6.4.5 Monophasic aqueous Noyori oxidation

To a three-necked 25 mL round-bottomed flask 5-hydroxymethylfurfural (1 g, 7.9 mmol), sodium tungstate dihydrate (0.05 g, 0.17 mmol) and methyltrioctylammonium hydrogensulfate (0.074 g, 0.16 mmol) were added to 10 mL of water. The mixture was then heated to 90 °C with a condenser, and left stirring for 15 minutes. Hydrogen peroxide (2.9 mL, 37 mmol) was then fed into the reactor over a period of 4 hours. 50 µL samples were taken from the reaction every 60 minutes, quenched with sodium bisulfite (50 µL, 10 $mg.mL^{-1}$) then neutralised with HCl (50 µL, 2 $mol.L^{-1}$).

6.4.6 Biphasic Noyori oxidation

To a three-necked 25 mL round-bottomed flask 5-hydroxymethfylfurfural (1 g, 7.9 mmol), sodium tungstate dihydrate (0.05 g, 0.17 mmol) and methyltrioctylammonium hydrogensulfate (0.074 g, 0.16 mmol) were added to 9 mL of water and 1 mL of toluene. The mixture was then heated to 90 °C with a condenser, and left stirring for 15 minutes. Hydrogen peroxide (2.9 mL, 37 mmol) was then fed into the reactor over a period of 4 hours. 50 µL samples were taken from the reaction every 60 minutes, quenched with sodium bisulfite (50 µL, 10 $mg.mL^{-1}$) then neutralised with HCl (50 µL, 2 $mol.L^{-1}$).

^{1}H NMR (DMSO-d^{6}, 500 MHz) δ 8.30 (s, 2H), 2.34 (S, 2H) ppm. ^{13}C NMR (DMSO-d^{6}, 126 MHz) δ 181, 154, 122 ppm. In agreement with published data.[127]

6.4.7 CAL-B catalysed oxidation

To a 50 mL polypropylene Falcon tube (centrifuge tube) diformylfuran (27.92 mg, 0.22 mmol) or 5-formyl-2-furancarboxylic acid (11.76 mg, 0.084 mmol) and CAL-B (immobilised enzyme, 48 mg) was added to ethyl acetate (5 mL, 51 mmol) and tert-butanol (5 mL, 52 mmol). A 50 µL sample of the mixture was taken for a t=0 point using a 200 µL Gilson Auto-pipette and diluted to 1 mL using deionised water in a 1.5 mL Eppendorf. The tube was then set in a tube rack within a pre-heated incubator shaker at 40 °C. The shaker was set to a stir speed of 500 rpm and an overall run-time of 26 hours. Hydrogen peroxide (30% w/v) (27.5 µL, 0.35 mmol) was added in every hour using a P100 Gilson auto-pipette, totalling (165 µL, 2.12 mmol) after the first 6 hours. 50 µL samples were taken from the reaction every 60 minutes (before H_2O_2 addition) and quenched with catalase (50 µL, 10 $mg.mL^{-1}$) or sodium bisulfite (50 µL, 10 $mg.mL^{-1}$), then neutralised with HCl (50 µL, 2 $mol.L^{-1}$). The reaction was left mixing for 24 hours where it was tested with Starch paper and remnant H_2O_2 neutralised if necessary, using either catalase or sodium bisulfite.

6.4.8 CAL-B catalysed oxidation - solvent & substrate modifications

The procedure for this process was identical to that described in (6.4.7 CAL-B catalysed oxidation), with changes made to the quantity of each reactant and the solvent system. The quench and sampling remained the same as the aforementioned procedure for DFF. Most experiments were completed in an incubator shaker, with the exception of those using the ChemSpeed. Conditions for these remained the same, with the instrument automating addition of H_2O_2. Shaker speed (500 rpm) and temperature (40 °C) were equivalent to the shaker reactions. Reactions in aqueous solvents without CAL-B used equivalent reagent quantities and conditions to those with, hence it has been excluded from the summary table.

Table 32 - Reagent quantities for the lipase-catalysed aqueous/t-butanol oxidation of HMF, DFF and GOase synthesised DFF.

Substrate	***Reagent***	***Quantity***	***mmol***
HMF	5-hydroxymethylfurfural	5.54 mg	0.04
	Acetic acid	1.00 mL	17.5
	t-butanol	1.00 mL	10.5
	Hydrogen peroxide [b]	172 µL	2.2
	Immobilised CAL-B	9.60 mg	-
DFF	Diformylfuran	5.58 mg	0.04
	Acetic acid	1.00 mL	17.5
	t-butanol	1.00 mL	10.5
	Hydrogen peroxide [b]	48.96 µL	0.63
	Immobilised CAL-B	9.60 mg	-
GOase DFF[a]	Aqueous buffered DFF [a]	2.79 mL	0.04
	Acetic acid	1.00 mL	17.5
	t-butanol	1.00 mL	10.5
	Hydrogen peroxide	48.96 µL	0.63
	Immobilised CAL-B	9.60 mg	-

[a] Aqueous solution of DFF from a reaction of HMF catalysed by GOase [b] hydrogen peroxide used was 30% (w/v) in concentration. With preparations as described in (6.4.7 CAL-B catalysed oxidation).

Table 33 - Reagent quantities for the lipase-catalysed aqueous oxidation of HMF, DFF and GOaseM3-5 synthesised DFF.

Substrate	***Reagent***	***Quantity***	***mmol***
HMF	5-hydroxymethylfurfural	5.54 mg	0.04
	Acetic acid	1.00 mL	17.5
	Hydrogen peroxide [b]	172 µL	7.3
	Immobilised CAL-B [c]	9.60 mg	-
DFF	Diformylfuran	5.58 mg	0.04
	Acetic acid	1.00 mL	17.5
	Hydrogen peroxide [b]	48.96 µL	0.63
	Immobilised CAL-B [c]	9.60 mg	-
GOase DFF[a]	Aqueous buffered DFF	2.79 mL	0.04
	Acetic acid	1.00 mL	17.5
	Hydrogen peroxide [b]	48.96 µL	0.63
	Immobilised CAL-B [c]	9.60 mg	-

[a] Aqueous solution of DFF from a reaction of HMF catalysed by GOase [b] hydrogen peroxide used was 30% (w/v) in concentration [c] Candida antarctica B immobilised on polymethacrylate beads. With preparations as described in (6.4.7 CAL-B catalysed oxidation).

6.4.9 Potassium peroxymonosulfate oxidation

To a 50 mL polypropylene Falcon tube (centrifuge tube) diformylfuran (3 mg, 0.02 mmol) and potassium peroxymonosulfate (14.6 mg, 0.09 mmol) was added to 2 mL of water. A 50 µL sample of the mixture was taken for a t=0 point using a 200 µL Gilson Auto-pipette and diluted to 1 mL using deionised water in a 1.5 mL Eppendorf. The tube was then set in a tube rack within a pre-heated incubator shaker at 25 °C. The shaker was set to a stir speed of 500 rpm and an overall run-time of 30 minutes. 50 µL samples were taken from the reaction every 5 minutes and quenched with sodium bisulfite (50 µL, 10 $mg.mL^{-1}$). The reaction was left mixing for 1 hour where it was tested with Starch paper and remnant H_2O_2 neutralised if necessary, using sodium bisulfite.

6.4.10 Potassium peroxymonosulfate substrate modifications

The procedure for this process was identical to that described in the previous section (6.4.9 Potassium peroxymonosulfate oxidation), with changes made to the quantity of each reactant and the solvent system. The quench and sampling remained the same as the aforementioned procedure for DFF. All experiments were completed in an Incubator shaker.

Table 34 - Reagent quantities for the Oxone™ oxidation of HMF, DFF, GOaseM3-5 synthesised DFF and FFCA.

Substrate	***Reagent***	***Quantity***	***mmol***
HMF	5-hydroxymethylfurfural	3.0 mg	0.02
	Potassium peroxymonosulfate	14.6 mg	0.09
	Deionised water	2.0 mL	-
DFF	Diformylfuran	3.0 mg	0.02
	Potassium peroxymonosulfate	14.6 mg	0.09
	Deionised water	2.0 mL	-
FFCA	5-formyl-2-furancarboxcylic acid	3.36 mg	0.02
	Potassium peroxymonosulfate	7.3 mg	0.05
	Deionised water	2.0 mL	-
GOase DFF[a]	Aqueous buffered DFF [a]	2.79 mL	0.04
	Potassium peroxymonosulfate	27.2 mL	0.18

[a] Aqueous solution of DFF from a reaction of HMF catalysed by GOase. with preparations as described in (6.4.8 CAL-B catalysed oxidation - solvent & substrate modifications).

6.4.11 Analytical sampling and setup

HPLC mobile phase was 0.005 mM H_2SO_4 running under isocratic conditions. Method: 100% of acid mobile phase for 55 minutes, flow rate of 0.6 $mL.min^{-1}$. Injection volume 20 µL and column temperature 60 °C. A guard column was included and incorporated into the heating system. 50 µL samples were taken, quenched with either: sodium bisulfite (50 µL, 10 $mg.mL^{-1}$) or catalase (50 µL, 10 $mg.mL^{-1}$), 50 µL of 1 $mol.L^{-1}$ HCl and made up to 1 mL with 850 µL deionised water. The samples were then centrifuged at 14,000 rpm for 5 minutes. The supernatant was then analysed.

6.4.12 Residence time distribution

The residence time distribution (RTD) was measured using a packed column and singular CSTR pre-filled with water pumped using three Jasco PU980 pumps at a flow rate of 0.2 mL.min^{-1} and 2.0 mL.min^{-1}. A pulse of 10% (v/v) red food dye was injected into the tertiary inlet of the first reagent CSTR using a manual valve. The outlet stream was then monitored using an in-line UV-Vis flow cell spectrometer (516 nm), taking a measurement every second.

Table 35 – Tracer absorbance values for the packed column and CSTR at flow rates (FR) of 2.0 mL.min^{-1} and 0.2 mL.min^{-1}.

	Normalised RTD Function $[E(\theta)]$		***Experimental*** $E(t)$	
T_{res}***/sec***	F_R ***2.0 mL.min^{-1}***	F_R ***0.2 mL.min^{-1}***	F_R ***2.0 mL.min^{-1}***	F_R ***0.2 mL.min^{-1}***
20	0.023	0.022	3.83E-04	4.26E-04
21	0.024	0.021	4.02E-04	3.65E-04
22	0.026	0.017	4.25E-04	2.81E-04
23	0.028	0.014	4.84E-04	2.45E-04
24	0.032	0.012	5.55E-04	2.19E-04
25	0.036	0.011	5.85E-04	1.98E-04
26	0.037	0.010	6.03E-04	1.70E-04
27	0.040	0.009	6.71E-04	1.51E-04
28	0.045	0.008	7.83E-04	1.42E-04
29	0.051	0.007	8.52E-04	1.35E-04
30	0.056	0.022	9.35E-04	4.26E-04

T_{res} = residence time in seconds, F_r = flow rate in mL.min^{-1}. The normalised RTD function $[E(\theta)]$ *was calculated by division of each absorbance value by the total area under the absorbance curve. The residence time distribution function* $E(t)$ *was calculated by division of each absorbance value by the average normalised area. Further calculation determined the volume of the packed column.*

6.5 Chapter 3 Procedures

6.5.1 Chemicals

2,5-furandicarboxlyic acid (99%, Sigma Aldrich), 5-hydroxymethylfurfural (98%, Avantium), diformylfuran (99%, Tokyo Chemical Industry), galactose oxidase M_{3-5} mutant Strep tag (CFE, Prozomix), horseradish peroxidase type II 150-250AU (99%, Sigma Aldrich), copper sulphate hydrous (99%, Fischer Scientific), hydrochloric acid (37%, Fischer), hydrogen peroxide (30% w/v in water, Fischer), potassium phosphate monobasic (99%, Sigma Aldrich), potassium phosphate dibasic (99%, Sigma Aldrich), sulphuric acid (98%, Fischer), catalase from bovine liver 10,000 AU (Pure enzyme, Sigma Aldrich), polyoxyethylene (12) isooctylphenyl ether (IGEPAL-CA720, Sigma Aldirch), sodium dodecylbenzene sulphate (SDBS, Sigma Aldrich), sorbitane monooleate (SPAN 80, Sigma Aldrich), polyethylene glycol sorbitane monooleate (Tween 80, Sigma Aldrich).

6.5.2 Continuous stirred tank reactors for the $GOase_{M3-5}$ catalysed oxidation of HMF

To a 250 mL beaker (A) kept on ice, 5-hydroxymethylfurfural was added (2150 g, 17 mmol) and diluted with 40 mL of (0.1 M, pH 7.4) potassium phosphate buffer and 32 mL of hydrogen peroxide (5% w/v, 40 mmol). To a second 250 mL beaker (B) kept on ice galactose oxidase M_{3-5} mutant (132 mg), horseradish peroxidase (1.32 mg), catalase (264 mg) and 1.32 mL of copper sulphate (14.5 mM, 0.02 mmol) were added. The solutions were stirred and left for 10 minutes. Each solution was transferred to a 50 mL glass syringe connected to a (Harvard Apparatus Pump II) syringe pump. The syringe diameter was set to 27.5 mm and a pump rate on each of 0.5 $mL.min^{-1}$ (totalling 1 $mL.min^{-1}$). The two pumps connected to a single CSTR of 2 mL volume, this connected to a coiled tubular reactor of 4.5 mm or 9 mm internal diameter. Steady-state was assumed at 3 reactor volumes, with samples taken every reactor volume.

Samples were centrifuged (foam collapse) before removal of 50 µL of sample. The sample was then quenched with HCl (50 µL, 1 M) and diluted with deionised water (900 µL) before chromatographic analysis. All HMF reactions at 200 mM followed the above reaction scheme, with increases made to quantities when a longer reaction time was required. To ensure HMF concentration remained constant, hydrogen peroxide concentration was increased rather than the volume; the volume of 32 mL remained constant.

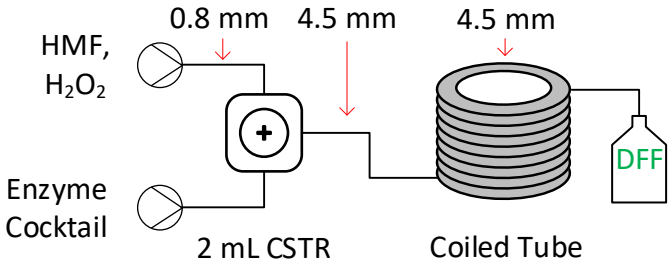

Figure 145 – Galactose oxidase catalysed oxidation in a continuous flow tubular reactor (100, 150 cm and 300 cm coiled tube). A combined flow rate of 1 mL.min^{-1}. Enzyme cocktail contains GOase$_{M3\text{-}5}$, catalase, HRP and $CuSO_4$. HMF mixture also contains hydrogen peroxide.

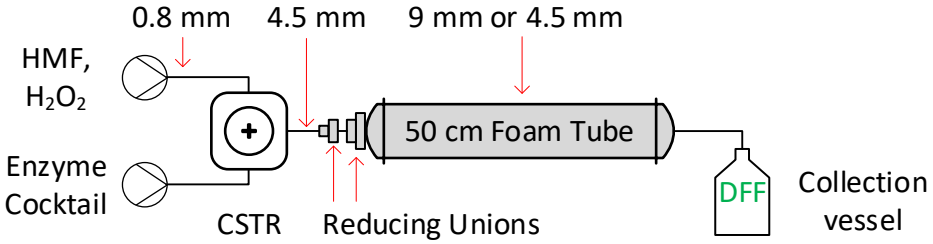

Figure 146 - Galactose oxidase catalysed oxidation in a continuous flow tubular reactor (50 cm 9 mm internal diameter (ID) coiled tube). A combined flow rate of 1 mL.min^{-1}. Enzyme cocktail contains GOase$_{M3\text{-}5}$, catalase, HRP and $CuSO_4$. HMF mixture also contains hydrogen peroxide. Feed piping is 0.8 mm ID, output of CSTR is 4.5 mm ID. This travels through several reducing unions to the 9 mm ID reactor tubing.

Two reactions used reduced HMF concentration, the quantity of each reagent is shown in Table 36.

Table 36 – HMF concentration changes made to the method discussed in 6.4.2 Synthesis of FDCA from HMF by the Cannizzaro reaction.

HMF Concentration (mM)	***Reagent***	***Quantity***	***mmol***
25	5-hydroxymethylfurfural	268.7 mg	2
	Galactose oxidase ($_{M3-5}$)	70 mg	-
	Horseradish peroxidase	0.7 mg	-
	Catalase	70 mg	-
	Hydrogen peroxide (5% w/v)	4 mL	8
	Potassium phosphate buffer [a]	80 mL [b]	-
	Copper sulphate [c]	0.7 mL	-
125	5-hydroxymethylfurfural	1343 mg	11
	Galactose oxidase ($_{M3-5}$)	70 mg	-
	Horseradish peroxidase	0.7 mg	-
	Catalase	70 mg	-
	Hydrogen peroxide (5% w/v)	20 mL	44
	Potassium phosphate buffer [a]	80 mL [b]	-
	Copper sulphate [c]		-

[a] Phosphate buffer had an ionic strength of 100 mM (0.1 mol.L^{-1}) and a pH of 7.4 [b] the combined buffer volume of both feed solutions, each feed used half (40 mL) [c] copper sulphate solution used had a concentration of 14.5 mM.

Analysis of fouling residue used a crude sample extracted from the inner walls of reactor tubing using a pipe cleaner. Remaining un-dissolved solid was filtered out prior to analysis using cotton wool.

^{1}H NMR (DMSO-d^{6}, 500 MHz) δ 9.82 (s, 2H), 7.67 (s, 2H) ppm; ^{13}C NMR (DMSO-d^{6}, 126 MHz) δ 181, 154, 122 ppm. In agreement with published data.[183]

6.5.3 Purification and extraction of DFF

Foam and liquid from the full duration of a continuous flow reaction were taken. The bulk solution was transferred into 50 mL centrifuge (Falcon) tubes and weighed on a balance to ensure equal weight. Tubes were then centrifuged at 5000 rpm for 5 minutes using a SciQuip Sigma large benchtop centrifuge. Each sample was centrifuged twice to ensure complete collapse of the foam, before addition of 2.5mL of 1 M HCl. Tubes were centrifuged twice again to denature the enzyme.

The supernatant was removed and the enzyme pellet discarded. The resultant aqueous solution was then extracted with dichloromethane (3 x 50 mL). The combined organic extracts were washed over Celite ™ using a Buchner funnel and filter paper, then concentrated in *vacuo* to yield diformylfuran as an orange solid (2448 mg, 35%).

^{1}H NMR (DMSO-d^{6}, 500 MHz) δ 9.82 (s, 2H), 7.67 (s, 2H) ppm; ^{13}C NMR (DMSO-d^{6}, 126 MHz) δ 181, 154, 122 ppm. In agreement with published data. [183]

6.5.4 Tandem continuous stirred tank reactors for the $GOase_{M3-5}$ catalysed oxidation of HMF

To a 250 mL beaker (A) kept on ice, 5-hydroxymethylfurfural was added (2150 g, 17 mmol) and diluted with 40 mL of (0.1 M, pH 7.4) potassium phosphate buffer and 32 mL of hydrogen peroxide (5% w/v, 40 mmol). To a second 250 mL beaker (B) kept on ice galactose oxidase M_{3-5} mutant (132 mg), horseradish peroxidase (1.32 mg), catalase (264 mg) and 1.32 mL of copper sulphate (14.5 mM, 0.02 mmol). To a third 250 mL beaker (C) kept on ice galactose oxidase M_{3-5} mutant (33 mg), horseradish peroxidase (0.33 mg) and 0.33 mL of copper sulphate solution (14.5 mM, 0.005 mmol) were added. The solutions were stirred and left for 10 minutes. Each solution was transferred to a 50 mL glass syringe connected to a (Harvard Apparatus Pump II) syringe pump. The syringe diameter was set to 27.5 mm and a pump rate on each of 0.5 $mL.min^{-1}$ (totalling 1 $mL.min^{-1}$). Pumps (A) & (B) connected to a single CSTR of 2 mL volume, this connected to a 300 cm coiled tube of 4.5 mm ID. Pump (C) connected to a 2^{nd} CSTR and a 150 cm coiled tube of 4.5 mm ID. Steady-state was assumed at 3 reactor volumes, with samples taken every reactor volume.

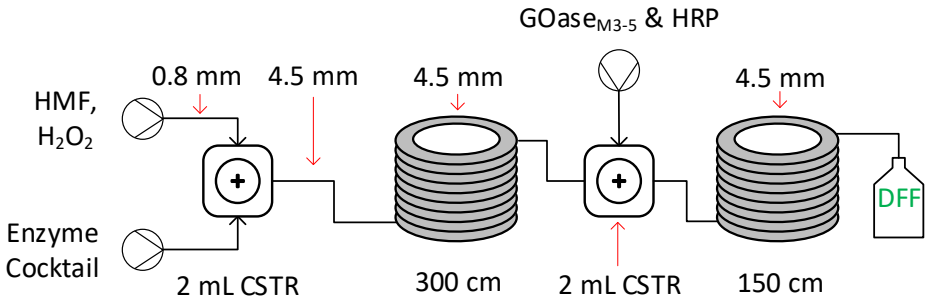

Figure 147 - Galactose oxidase catalysed oxidation in a tandem continuous flow tubular reactor. A 300 cm tube followed by a 2nd CSTR and 150 cm tube. A second enzyme pump containing $GOase_{M3-5}$ and HRP is added at the second CSTR. A combined flow rate of 1.5 $mL.min^{-1}$. Enzyme cocktail contains $GOase_{M3-5}$, catalase, HRP and $CuSO_4$. HMF mixture also contains hydrogen peroxide.

6.5.5 Tube-in-tube mixer for the $GOase_{M3-5}$ catalysed oxidation of HMF

To a 250 mL beaker (A) kept on ice, 5-hydroxymethylfurfural was added (2150 g, 17 mmol) and diluted with 40 mL of (0.1 M, pH 7.4 potassium phosphate buffer and 32 mL of hydrogen peroxide (5% w/v, 40 mM). To a second 250 mL beaker (B) kept on ice galactose oxidase M_{3-5} mutant (132 mg), horseradish peroxidase (1.32 mg), catalase (264 mg) and 1.32 mL of copper sulphate (14.5 mM, 0.02 mmol) were added. The solutions were stirred and left for 10 minutes. Each solution was transferred to a 50 mL glass syringe connected to a (Harvard Apparatus Pump II) syringe pump. The syringe diameter was set to 27.5 mm and a pump rate on each of 0.5 $mL.min^{-1}$ (totalling 1 $mL.min^{-1}$). The two pumps connected to a tube-in-tube mixer, this connected to a coiled tubular reactor of 4.5 mm or 9 mm internal diameter. Steady-state was assumed at 3 reactor volumes, with samples taken every reactor volume.

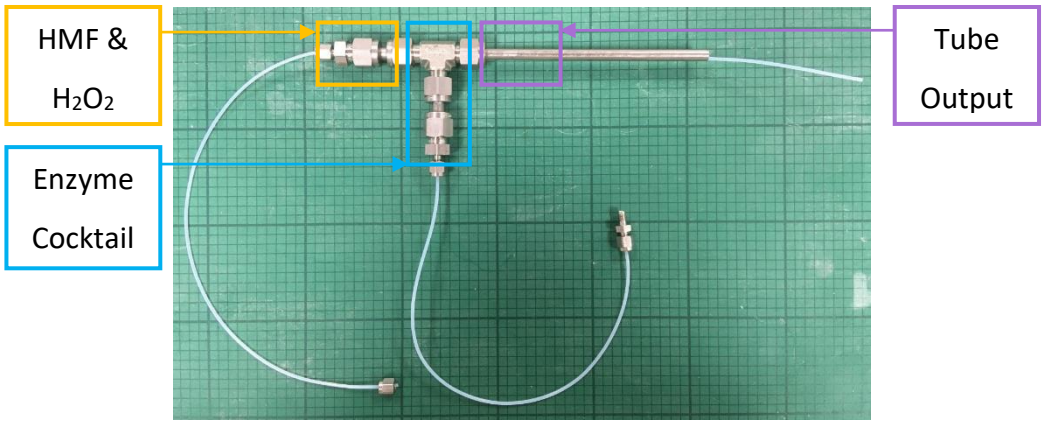

Figure 148 - Tube-in-tube air sparge reactor. The substrate inlet tubing of 0.8 mm ID travels through the T-piece and ends at the reactor connection point. Reactor tubing of varying length and diameter is swaged onto the 4.5 mm steel output tube.

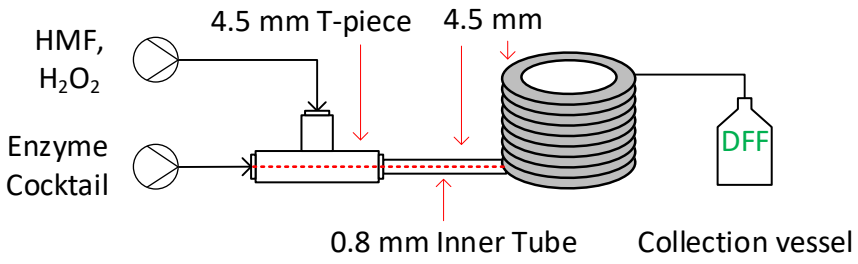

Figure 149 - Galactose oxidase catalysed oxidation in a continuous flow tubular reactor (100 cm, 150 cm and 300 cm long 4.5 mm inner diameter (ID) coiled tube). With prior tube-in-tube reactor to separate the streams of flow until the larger tube. A combined flow rate of 1 mL.min^{-1}. Enzyme cocktail contains GOase$_{M3-5}$, catalase, HRP and $CuSO_4$. HMF mixture also contains hydrogen peroxide. Feed piping is 0.8 mm ID, T-piece and its output is 4.5 mm ID.

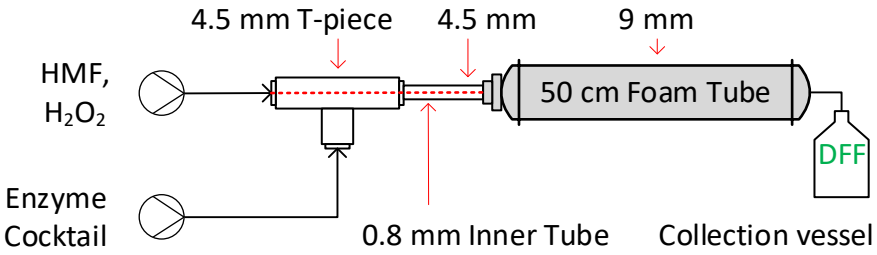

Figure 150 - Galactose oxidase catalysed oxidation in a continuous flow tubular reactor (50 cm 9 mm inner diameter (ID) coiled tube). With prior tube-in-tube reactor to separate the streams of flow until the larger tube. A combined flow rate of 1 mL.min^{-1}. Enzyme cocktail contains GOase$_{M3-5}$, catalase, HRP and $CuSO_4$. HMF mixture also contains hydrogen peroxide. Feed piping is 0.8 mm ID, T-piece and its output is 4.5 mm ID. The two liquid streams converge at the aperture of the 9 mm ID tubing.

6.5.6 Air sparge Tube-in-tube mixer for the $GOase_{M3-5}$ catalysed oxidation of HMF

To a 250 mL beaker (A) kept on ice, 5-hydroxymethylfurfural (2084 g, 16 mmol) and 80 µL (0.1% v/v, 0.12 mmol) IGEPAL-CA720, diluted with 40 mL of (0.1 M, pH 7.4 potassium phosphate buffer. To a second 250 mL beaker (B) kept on ice galactose oxidase M_{3-5} mutant (132 mg), horseradish peroxidase (1.32 mg), catalase (264 mg) and 1.32 mL of copper sulphate (14.5 mM, 0.02 mmol) were added. The solutions were stirred and left for 10 minutes. Each solution was transferred to a 50 mL glass syringe connected to a (Harvard Apparatus Pump II) syringe pump. The syringe diameter was set to 27.5 mm and a pump rate on each of 0.5 $mL.min^{-1}$ (totalling 1 $mL.min^{-1}$). The pumps connected to an air sparge tube-in-tube mixer, and then a tubular reactor of 4.5 mm or 9 mm ID. Steady-state was assumed at 3 reactor volumes. Air flow was maintained using one of two variable flow rotameters (0.4 $L.min^{-1}$ – 5.0 $L.min^{-1}$ or (0.04 $L.min^{-1}$ – 1.00 $L.min^{-1}$), supplied by Key Instruments.

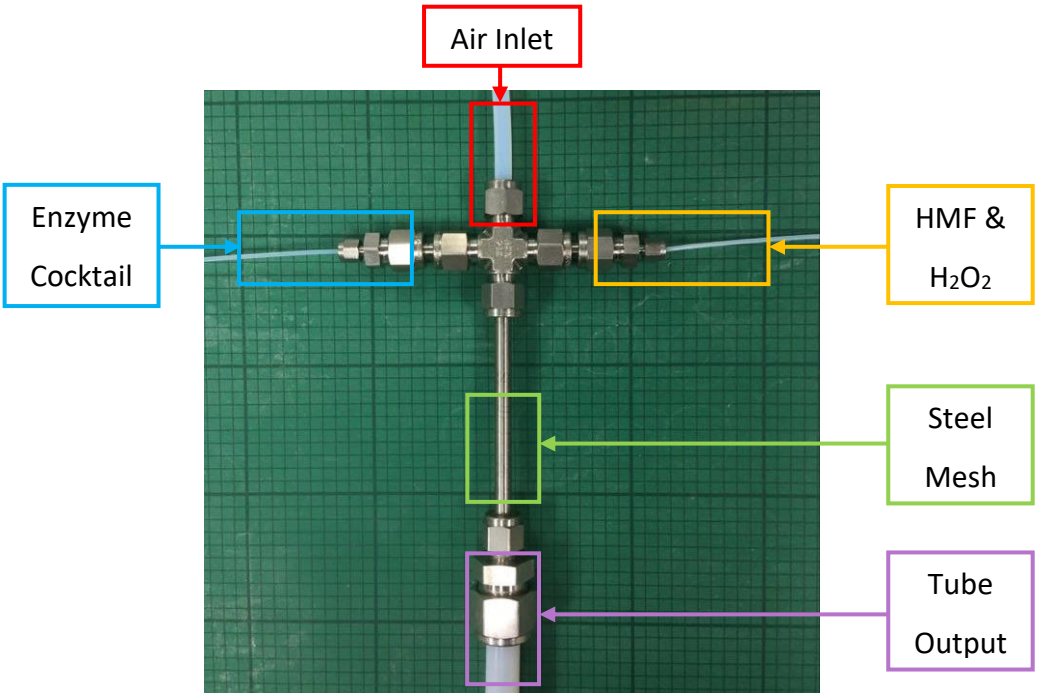

Figure 151 – Tube-in-tube air sparge and mesh reactor. The two solution inlets of 0.8 mm ID tubing travel through the cross-piece and end halfway down the steel exit tube (4.5 mm ID). The remaining half of that tube is packed with steel mesh. Enzyme cocktail contains $GOase_{M3-5}$, catalase, HRP and $CuSO_4$.

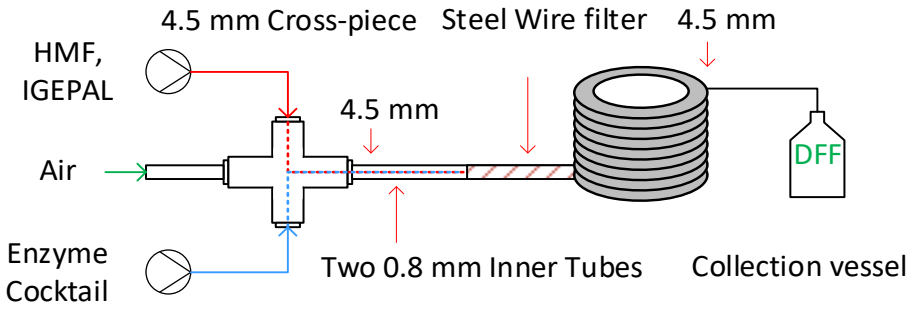

Figure 152 - Galactose oxidase catalysed oxidation in a continuous flow tubular reactor (100 cm-150 cm, 4.5 mm internal diameter (ID) coiled tube). A combined flow rate of 1 mL.min^{-1}. Enzyme cocktail contains GOase$_{M3-5}$, catalase, HRP and $CuSO_4$. Feed piping has a 0.8 mm ID, cross-piece and connected tubing has a 4.5 mm ID. This travels through several reducing unions to the 4.5 mm ID reactor tube.

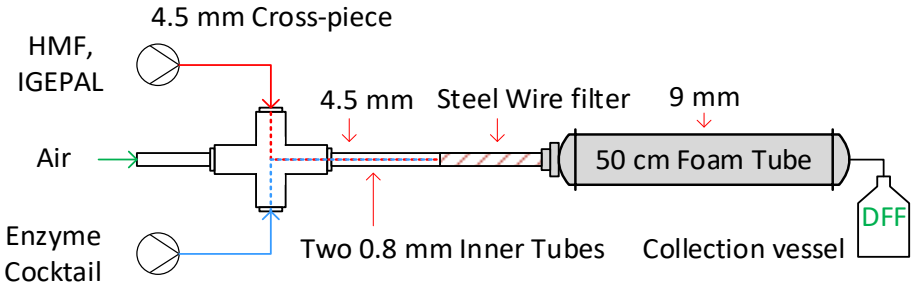

Figure 153 - Galactose oxidase catalysed oxidation in a continuous flow tubular reactor (50 cm 9 mm internal diameter (ID) horizontal tube). A combined flow rate of 1 mL.min^{-1}. Enzyme cocktail contains GOase$_{M3-5}$, catalase, HRP and $CuSO_4$. Feed piping has a 0.8 mm ID, cross-piece and connected tubing has a 4.5 mm ID. This travels through several reducing unions to the 9 mm ID reactor tube.

6.5.7 Drechsel bottle air sparge mixer for the GOase catalysed oxidation of HMF

To a 250 mL beaker (A) kept on ice, 5-hydroxymethylfurfural (2084 g, 16 mmol) and 80 µL (0.1% v/v, 0.12 mmol) IGEPAL-CA720, diluted with 40 mL of (0.1 M, pH 7.4 potassium phosphate buffer. To a second 250 mL beaker (B) kept on ice galactose oxidase $M_{3\text{-}5}$ mutant (132 mg), horseradish peroxidase (1.32 mg), catalase (264 mg) and 1.32 mL of copper sulphate (14.5 mM, 0.02 mmol) were added. The solutions were stirred and left for 10 minutes. Each solution was transferred to a 50 mL glass syringe connected to a (Harvard Apparatus Pump II) syringe pump. The syringe diameter was set to 27.5 mm and a pump rate on each of 0.5 $mL.min^{-1}$ (totalling 1 $mL.min^{-1}$). The pumps connected to an air sparge tube-in-tube mixer, and then a tubular reactor of 4.5 mm or 9 mm ID. Steady-state was assumed at 3 reactor volumes. Air flow was maintained using one of two variable flow rotameters (0.4 $L.min^{-1}$ – 5.0 $L.min^{-1}$ or (0.04 $L.min^{-1}$ – 1.00 $L.min^{-1}$), supplied by Key Instruments. Foam height was measured by eye using a ruler.

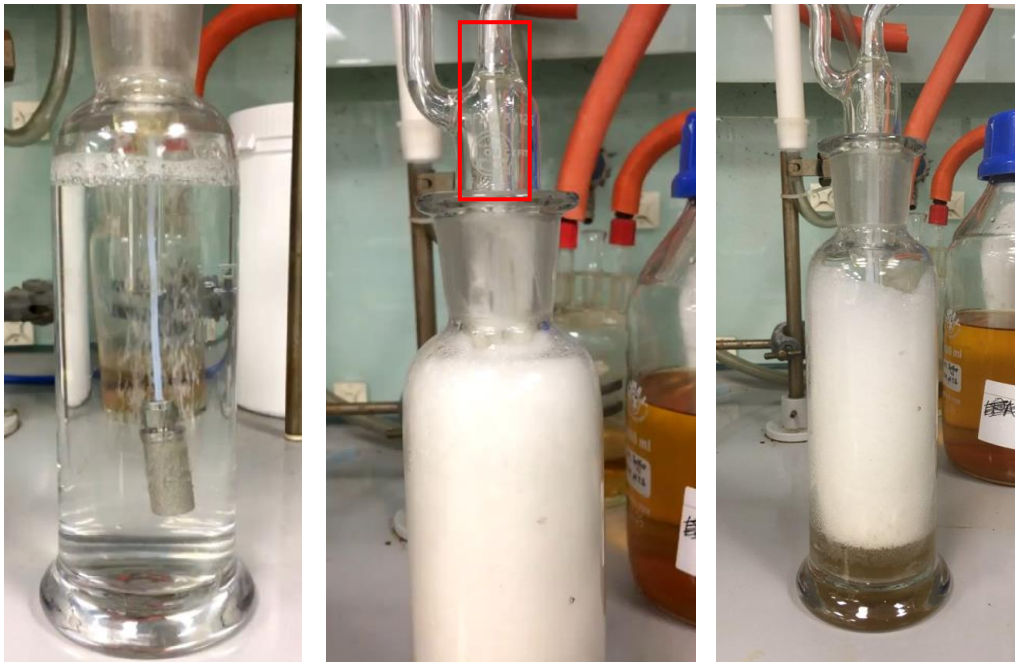

Figure 154 – [left] air sparger suspended in the Drechsel bottle [middle] Drechsel bottle filled with foam and three inner pipes highlighted in red [right] liquid and foam filling the bottle during a GOase catalysed oxidation of HMF to DFF using compressed air.

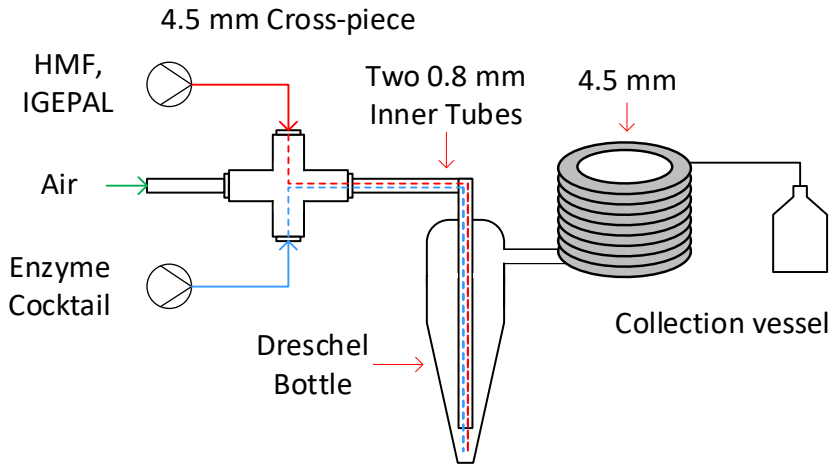

Figure 155 - Galactose oxidase catalysed oxidation in a continuous flow tubular reactor (100 cm-150 cm, 4.5 mm internal diameter (ID) coiled tube) and 15 mL volume Drechsel bottle. A combined flow rate of 1 mL.min^{-1}. Enzyme cocktail contains GOase$_{M3-5}$, catalase, HRP and $CuSO_4$. Feed piping has a 0.8 mm ID, cross-piece and connected tubing has a 4.5 mm ID. This travels through several reducing unions to the 4.5 mm ID reactor tubing. Compressed air travels around the inner tubing and bubbles up through the liquid in the Drechsel bottle.

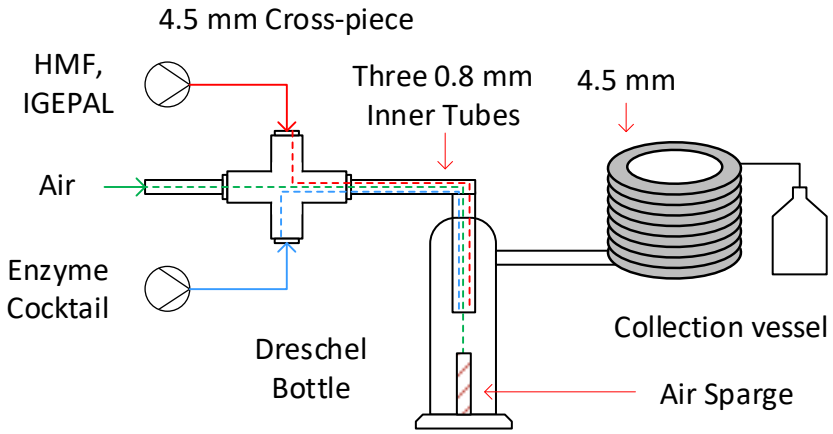

Figure 156 - Galactose oxidase catalysed oxidation in a continuous flow tubular reactor (100 cm-150 cm, 4.5 mm internal diameter (ID) coiled tube) and 250 mL volume Drechsel bottle. A combined flow rate of 1 mL.min^{-1}. Enzyme cocktail contains GOase$_{M3-5}$, catalase, HRP and $CuSO_4$. Feed piping has a 0.8 mm ID, cross-piece and connected tubing has a 4.5 mm ID. This travels through several reducing unions to the 4.5 mm ID reactor tubing. Compressed air travels through an inner tube into an air sparger at the bottom of the Drechsel bottle.

6.5.8 Surfactant assay for $GOase_{M3-5}$ catalysed oxidation of HMF

To a 1.5 mL eppendorf 1 mL of potassium phosphate buffer (0.1 M, pH 7.4) was added. To each eppendorf the following was added:

(1) Sodium dodecylbenzene sulphate (10 mg, 0.03mmol).

(2) Polyoxyethylene (12) isooctylphenyl ether (10 µL, 0.015 mmol).

(3) Sorbitane monooleate (10 mg, 0.02 mmol).

(4) Polyethylene glycol sorbitane monooleate (10 µL, 0.008mmol).

Each eppendorf was then manually shaken for 15 seconds before allowing to rest for a minute. Pictures were taken after 15minutes to ensure sufficient foam stability. The reactions used a batch of galactose oxidase with lower stability and activity (2018).

To a 50 mL beaker (A) kept on ice, 5-hydroxymethylfurfural (2150 g, 17 mmol) and sodium dodecylbenzne sulphate (80mg, 0.23 mmol) then diluted with 40 mL of (0.1 M, pH 7.4) potassium phosphate buffer. To a second 50 mL beaker (B) kept on ice galactose oxidase M_{3-5} mutant (132 mg), horseradish peroxidase (1.32 mg), catalase (264 mg) and 1.32 mL of copper sulphate (14.5 mM, 0.02 mmol) were added. The solutions were stirred and left for 10 minutes. In a 15 mL centrifuge (falcon) tube 5 mL of solution (A) and (B) were mixed and placed in an incubator shaker at 37 °C and 350 rpm for 2 hours. The reaction was run in triplicate.

To a 50 mL beaker (C) kept on ice, 5-hydroxymethylfurfural (2150 g, 17 mmol) and polyoxyethylene (12) isooctylphenyl ether (80 µL, 0.12 mmol) then diluted with 40 mL of (0.1 M, pH 7.4) potassium phosphate buffer. To a second 50 mL beaker (D) kept on ice galactose oxidase M_{3-5} mutant (132 mg), horseradish peroxidase (1.32 mg), catalase (264 mg) and 1.32 mL of copper sulphate (14.5 mM, 0.02 mmol) were added. The solutions were stirred and left for 10 minutes. In a 15 mL centrifuge (falcon) tube 5 mL of solution (C) and (D) were mixed and placed in an incubator shaker at 37 °C and 350 rpm for 2 hours. The reaction was run in triplicate.

To ensure secondary enzymes were at optimum efficiency, a control reaction was run in tandem and undertaken using the following procedure. To a 50 mL beaker (E) kept on ice, 5-hydroxymethylfurfural (2150 g, 17 mmol) was diluted with 40 mL of (0.1 M, pH 7.4) potassium phosphate buffer. To a second 50 mL beaker (F) kept on ice galactose oxidase $M_{3\text{-}5}$ mutant (132 mg), horse radish peroxidase (1.32 mg), catalase (264 mg) and 1.32 mL of copper sulphate (14.5 mM, 0.02 mmol) were added. The solutions were stirred and left for 10 minutes. In a 15 mL centrifuge (Falcon) tube 5 mL of solution (E) and (F) were mixed and placed in an incubator shaker at 37 °C and 350 rpm for 2 hours.

From all reactions 50 µL samples were taken, acidified with 50 µL of 1 M HCl and made up to 1 mL with 900 µL deionised water. The samples were then centrifuged at 14,000 rpm for 5 minutes and the supernatant analysed by HPLC to determine product selectivity.

6.5.9 Particulate transport by an aqueous foam

For a peroxide system, samples were taken from a reaction completed under conditions stated in (6.5.2 Continuous stirred tank reactors for the GOaseM3-5 catalysed oxidation of HMF). Eppendorf's were filled with foam and weighed. Samples were centrifuged at 15,000 rpm for 5 minutes to collapse the foam. The supernatant was removed using several Gilson pipettes (P200, P100 and P20). The solid remaining was left to air dry for 2 hours, then its weight measured.

For a surfactant system, samples were taken from a reaction completed under conditions stated in (6.5.6 Air sparge Tube-in-tube mixer for the $GOase_{M3-5}$ catalysed oxidation of HMF). Eppendorf's were filled with foam and weighed. Samples were centrifuged at 15,000 rpm for 5 minutes to collapse the foam. The supernatant was removed using several Gilson pipettes (P200, P100 and P20). The solid remaining was left to air dry for 2 hours, then its weight measured.

6.5.10 Galactose oxidase batch activity (2017 & 2018)

To a 250 mL beaker (A) kept on ice, 5-hydroxymethylfurfural was added (2150 g, 17 mmol) and diluted with 40 mL of (0.1 M, pH 7.4) potassium phosphate buffer and 32 mL of hydrogen peroxide (5% w/v, 40 mmol). To a second 250 mL beaker (B) kept on ice galactose oxidase M_{3-5} mutant (132 mg), horseradish peroxidase (1.32 mg), catalase (264 mg) and 1.32 mL of copper sulphate (14.5 mM, 0.02 mmol) were added. The solutions were stirred and left for 10 minutes. Each solution was transferred to a 50 mL glass syringe connected to a (Harvard Apparatus Pump II) syringe pump. The syringe diameter was set to 27.5 mm and a pump rate on each of 0.5 $mL.min^{-1}$ (totalling 1 $mL.min^{-1}$). The two pumps connected to a single CSTR of 2 mL volume, this connected to a 150 cm coiled tubular reactor of 4.5 mm internal diameter.

6.5.11 Reaction recycling

Three 1mL samples were taken from the collection vessel of a continuous flow reaction and placed in Eppendorf's. Samples were placed in an incubator shaker at 37 °C and 350 rpm for 2 hours to react. A 50 µL sample of each was acidified, centrifuged and the supernatant analysed by HPLC to determine if further conversion had occurred.

6.5.12 Analytical sampling and setup

HPLC mobile phase was 0.005 M H_2SO_4 running under isocratic conditions. Method: 100% of acid mobile phase for 50 minutes, flow rate of 0.6 $mL.min^{-1}$. Injection volume 20 µL and column temperature 60 °C. A guard column was included and incorporated into the heating system. 50 µL samples were taken, acidified with 50 µL of 1 M HCl and made up to 1 mL with 900 µL deionised water. The samples were then centrifuged at 14,000 rpm for 5 minutes and the supernatant analysed.

6.5.13 Residence time distribution

The residence time distribution (RTD) was measured using a premixing CSTR and a 1m long tubular coiled reactor pre-filled with the protein-stabilised foam using two Harvard Apparatus Pump II syringe pumps at a flow rate of 1 mL.min^{-1}. A pulse of 10% (v/v) red food dye was injected into the tertiary inlet of the CSTR using a manual valve. Samples of the outlet stream were collected in 15 second intervals. Each sample was treated with 50 µL of 1 M HCl and then centrifuged to collapse the foam. Samples were then diluted further by a factor of 10 to ensure accurate measurement, before transfer to a crystal cuvette for spectrographic analysis on the UV-Vis for 10 seconds. Results were taken at the optimal dye absorbance of 516 nm.

Table 37 – Tracer absorbance values for the tubular column and CSTR at a flow rate (FR) of 1 mL.min^{-1}.

	Normalised RTD Function $[E(\theta)]$	***Experimental*** $E(t)$
T_{res}***/sec***	F_R ***1.0 mL.min^{-1}***	F_R ***1.0 mL.min^{-1}***
120	0.0058	0.0015
135	0.0053	0.0010
150	0.0048	0.0012
165	0.0077	0.0024
180	0.1096	0.0492
195	0.4031	0.1405
210	0.5741	0.1296
225	0.5551	0.1316
240	0.5906	0.1463
255	0.6146	0.1429
270	0.4728	0.0796

T_{res} = residence time in seconds, F_r = flow rate in mL.min^{-1}. The normalised RTD function $[E(\theta)]$ was calculated by division of each absorbance value by the total area under the absorbance curve. The residence time distribution function $E(t)$ was calculated by division of each absorbance value by the average normalised area.

6.6 Chapter 4 Procedures

6.6.1 Life-cycle assessment

Data used in the work was acquired from EcoInvent, GaBi and the National Renewable Energy Laboratory (LCA commons). Any data taken from EcoInvent was under allocation at the point of substitution, and taken from the 2014 database (EcoInvent 3.1). Data was transcribed from the Unit Process Requirements (UPR) report into GaBi where applicable. Elementary flows that had no defined object in GaBi were added in as such, with no associated data. Any chemicals missing from the GaBi database were added in as processes with elementary flows, data taken from EcoInvent as a UPR. A functional unit of 1 kg was fixed throughout all process and plan development, being fixed on the product of each unit process.

6.6.2 Developed unit processes

Most chemicals used were lacking a usable process listed in GaBi, as such the data was taken from EcoInvent and used to generate a (u-so) unit process, single operation or (u-bb) unit process, black-box. U-so applied to data with sufficient emissions, waste and elementary flows listed in a reliable database. U-bb applied to data that contained numerous assumptions, estimations or calculations based on limited data. When stated, any standard deviations values were included in the inputs and outputs.

Unit processes were developed as “production/manufacturing” plans in GaBi and saved as both a plan and a process. Most processes used a number of repeating inputs that were kept constant throughout, these have been listed in (Table 38). For ease of data access, Germany and Europe were chosen as the most suitable candidates due to the wide availability of data for the two regions. Any direct energy inputs used were a consumer mix, this includes electricity, oil, natural gas and process water.

Table 38 – Repeated inputs used to develop individual unit processes for the LCA of cradle-to-gate manufacture of FDCA and terephthalic acid.

Input [a]	***Country***	***Comments***
Thermal energy (gas)	DE or EU-28	Gas production mix
Thermal energy (coal)	DE	Hard coal
Process water	DE or EU-28	From surface or ground
Process steam	DE or EU-28	From natural gas (90%)
Electricity	DE or EU-28	Grid mix (AC)
Natural gas	DE or EU-28	Production mix
Crude oil	DE	Crude oil mix (43 $MJ.kg^{-1}$)
Naphtha	DE	At refinery (44 $MJ.kg^{-1}$)

[a] chosen inputs were available and listed in GaBi under the appropriate energy database.

All unit processes developed for the work are listed in (Table 39). These have been generated from various databases and transcribed into GaBi. The table includes all individual unit processes developed and excludes the large generated plans created for the life-cycle (maize grain, maize starch, HMF, xylene etc).

Table 39 – Unit processes for the cradle-to-gate LCA of FDCA and terephthalic acid.

Unit Process	***Location***	***Process used in***	***Database [b]***
Alpha amylase	USA	Fructose	LCA Commons
Aluminium oxide	EU	Methanol	EcoInvent
Bromine	EU	Lithium Bromide	EcoInvent
Butanol	EU	FDCA [c]	EcoInvent
CAL-B lipase	USA	FDCA [c]	LCA Commons [a]
Catalase	USA	DFF [c]	LCA Commons [a]
Copper oxide	EU	Copper sulphate	EcoInvent
Copper sulphate	EU	DFF [c]	EcoInvent
Dichloromethane	EU	DFF [c]	EcoInvent
Dimethylacetamide	EU	HMF	EcoInvent
Dimethylamine	EU	Dimethylacetamide	EcoInvent
Ethyl acetate	EU	HMF, DFF & FDCA [c]	EcoInvent
Galactose oxidase	USA	DFF [c]	LCA Commons [a]
Glucoamylase	USA	Fructose	LCA Commons
Glucose isomerase	USA	Fructose	LCA Commons [a]
Hexane	EU	HMF	EcoInvent
Lithium bromide	EU	HMF	EcoInvent
Lithium hydroxide	EU	Lithium bromide	EcoInvent
Methanol	EU	Dimethylamine	EcoInvent
Platinum	RU	FDCA [d]	EcoInvent
Sodium carbonate	EU	Sodium phosphate	EcoInvent
Sodium phosphate	EU	DFF	EcoInvent
Sodium silicate	EU	HMF	EcoInvent
Sodium sulphate	EU	HMF	EcoInvent

[a] estimated from the production data of cellulase, glucoamylase and alpha amylase [b] all unit processes used available elementary flows from GaBi, some listed in Table 38 [c] enzymatic oxidation route of HMF to FDCA [d] Pt/C catalysed oxidation of HMF to FDCA. These have been generated as individual unit processes with elementary flows

An example of a developed unit process for lithium bromide production is shown in Figure 157. The black cogs refer to generated processes, shown for “Bromine Production” and “Lithium Hydroxide Production”. Processes with no GaBi symbol (blue and yellow circle) are manually rather than procedurally generated. Each of these processes were created as a unit process, allowing for a complete life-cycle in accordance with ISO 14040.

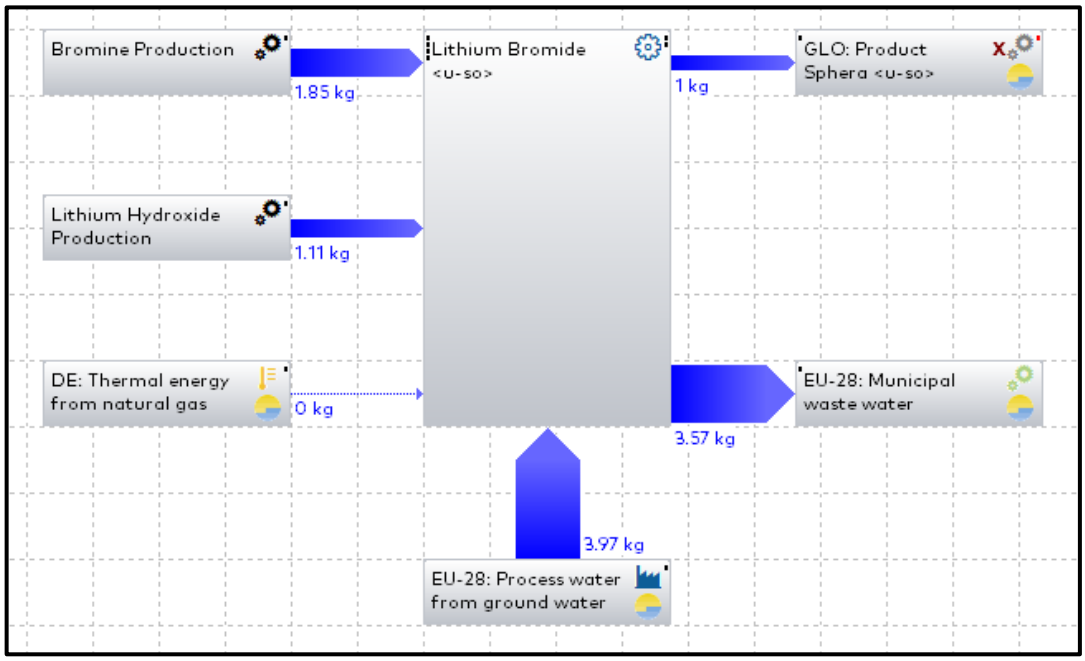

Figure 157 – Manually generated unit process for the production of 1 kg of lithium Bromide, data taken from EcoInvent.

The Unit processes generated for lithium hydroxide and bromine are shown in Figure 158 and Figure 159 respectively. The functional unit is 1 kg and is fixed to the output of product, shown by the “GLO: Product” flow. Thermal energy and electricity are stated as MJ or KWh respectively, conversion to kg is done at the results calculation stage, hence quantity is listed at 0 kg for these inputs.

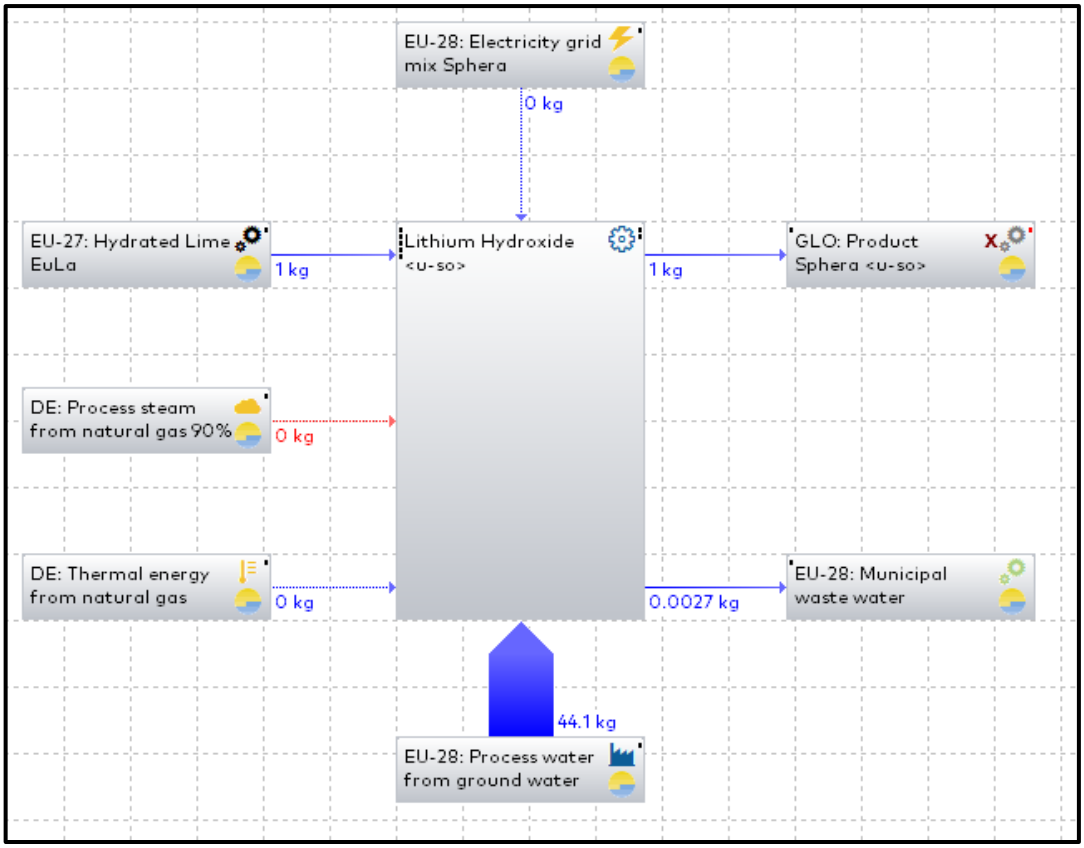

Figure 158 – Manually generated unit process for the production of 1 kg of lithium hydroxide*, data taken from EcoInvent.*

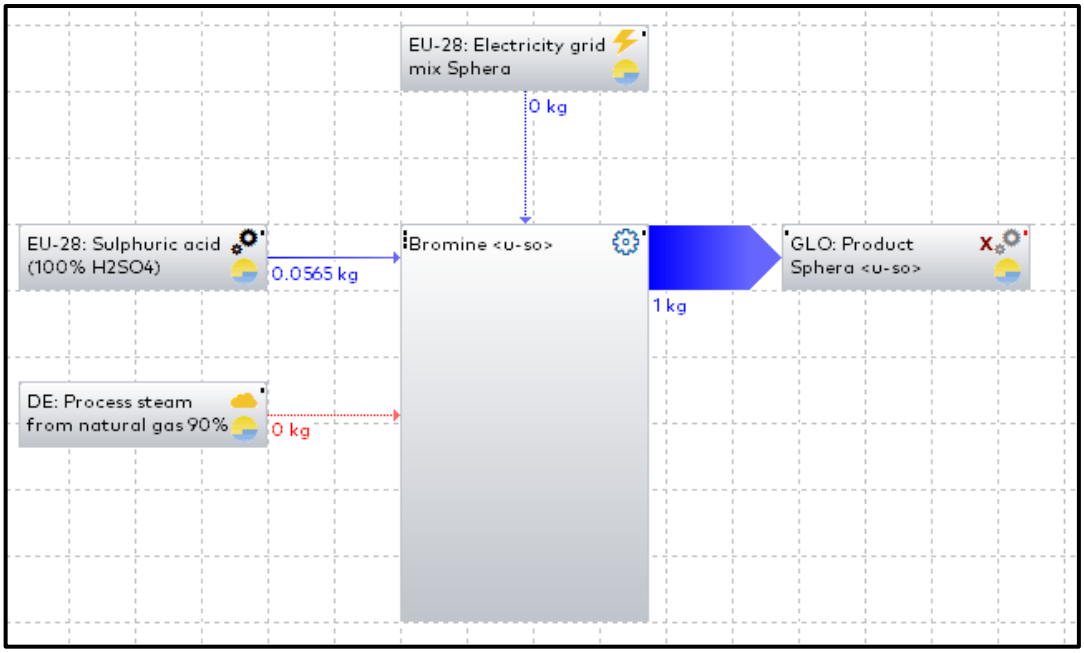

Figure 159 – Manually generated unit process for the production of 1 kg of bromine, data taken from EcoInvent.

6.6.3 Maize grain

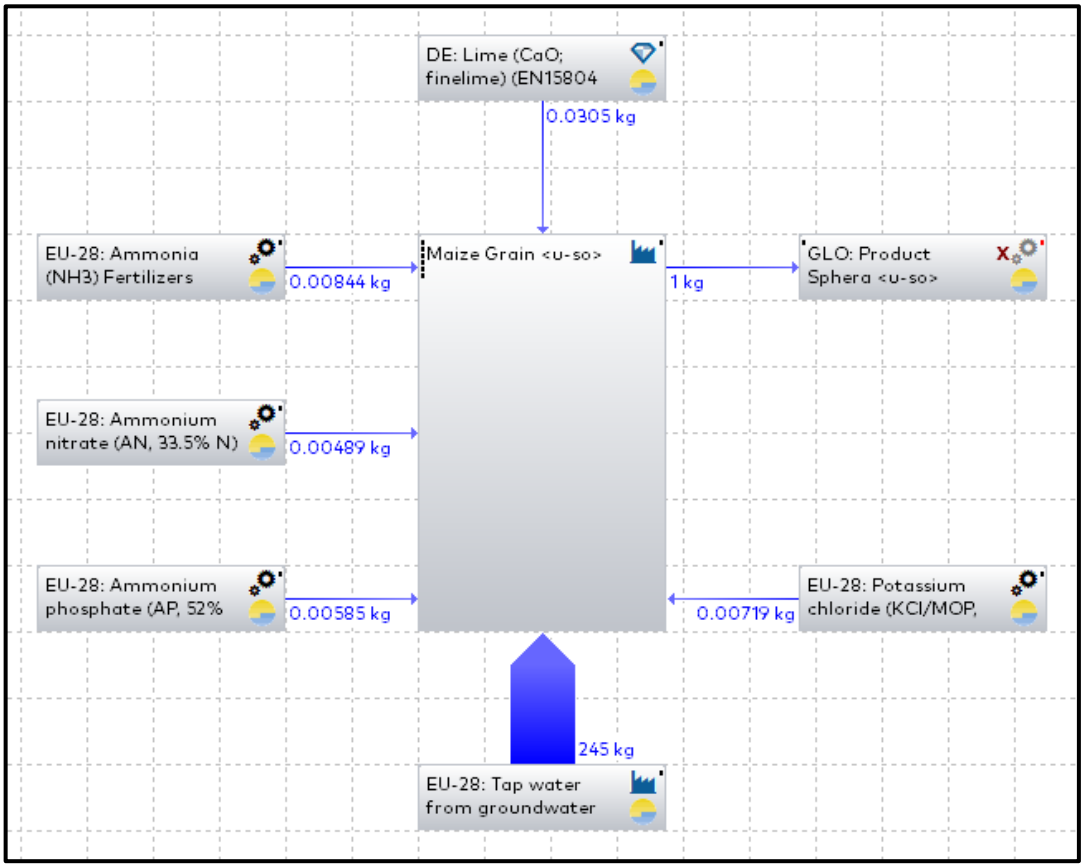

Figure 160 - Manually generated unit process for the production of 1 kg of maize grain (RoW), data taken from EcoInvent. Tracked flows are shown as unit processes with the transfer or material or energy, whilst all remaining inputs and outputs are elementary flows. Includes any interpretation changes made.

6.6.4 Maize starch

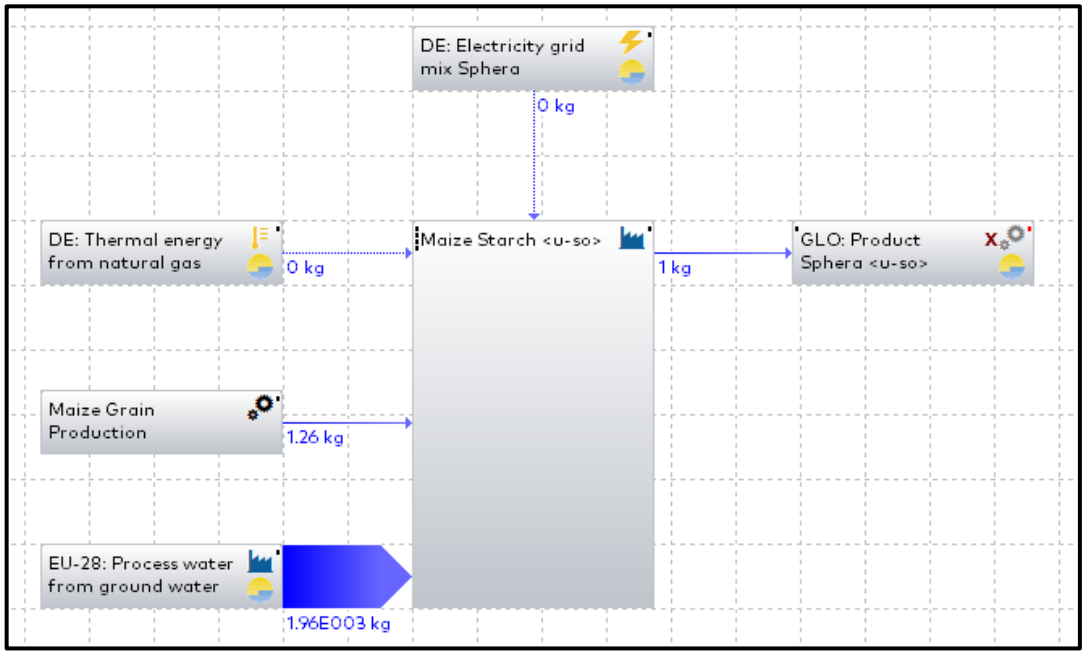

Figure 161 - Manually generated unit process for the production of 1 kg of maize starch (RoW), data taken from EcoInvent. Tracked flows are shown as unit processes with the transfer or material or energy, whilst all remaining inputs and outputs are elementary flows. Includes any interpretation changes made.

Inputs

Flows	Quantities	Amount	Units	Tra	Standar	Origin	Comment
Electricity [Electric power]	**Energy (net ca**	**0.254**	**MJ**	**X**	**1 %**	**Literature**	
Maize [Materials from renewabl	**Mass**	**1.26**	**kg**	**X**	**1 %**	**Literature**	
Thermal energy from natural ga	**Energy (net ca**	**3.99**	**MJ**	**X**	**1 %**	**Literature**	
Water (tap water) [Operating m	**Mass**	**1.96E003**	**kg**	**X**	**1 %**	**Literature**	
CH: treatment, maize starch productic	Volume	-0.000691	m3		1 %	Literature	
RER: chemical plant, organics [organic	Number of pieces	4E-010	pcs.		3 %	Literature	
Flows							

Outputs

Flows	Quantities	Amount	Units	Tra	Standar	Origin	Comment
Maize Starch [Materials from rei	**Mass**	**1**	**kg**	**X**	**0 %**	**Literature**	
Processed water to river [Other emiss	Mass	0.127	kg		1 %	Literature	
Water vapour [Inorganic emissions to	Mass	1.14	kg		1 %	Literature	
Flows							

Figure 162 – Example of inputs and outputs for the production of 1 kg of maize starch (RoW). Tracked inputs and outputs are highlighted in bold whilst the remainder are listed as elementary flows.

6.6.5 Fructose

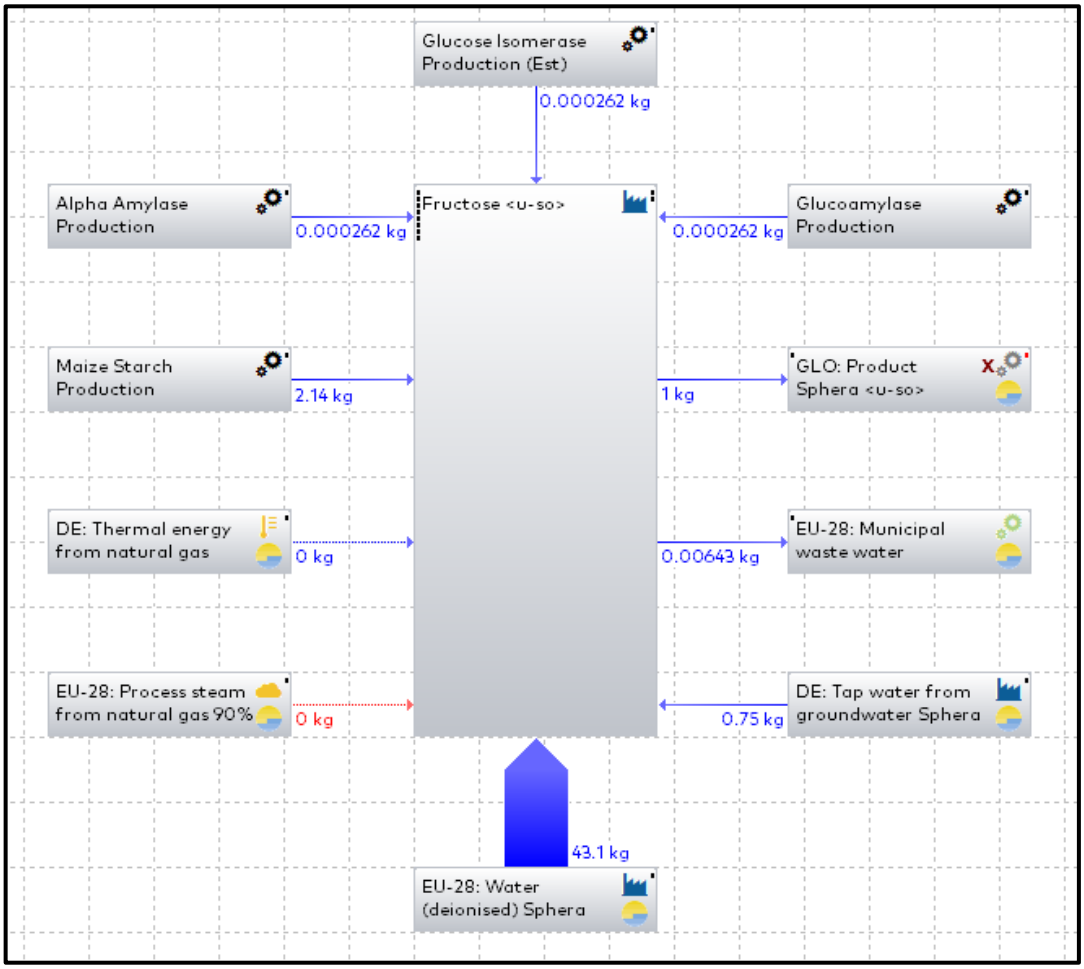

Figure 163 - Manually generated unit process for the production of 1 kg of fructose (EU), data taken from EcoInvent. Tracked flows are shown as unit processes with the transfer or material or energy, whilst all remaining inputs and outputs are elementary flows. Includes any interpretation changes made.

6.6.6 HMF (5-hydroxymethylfurfural)

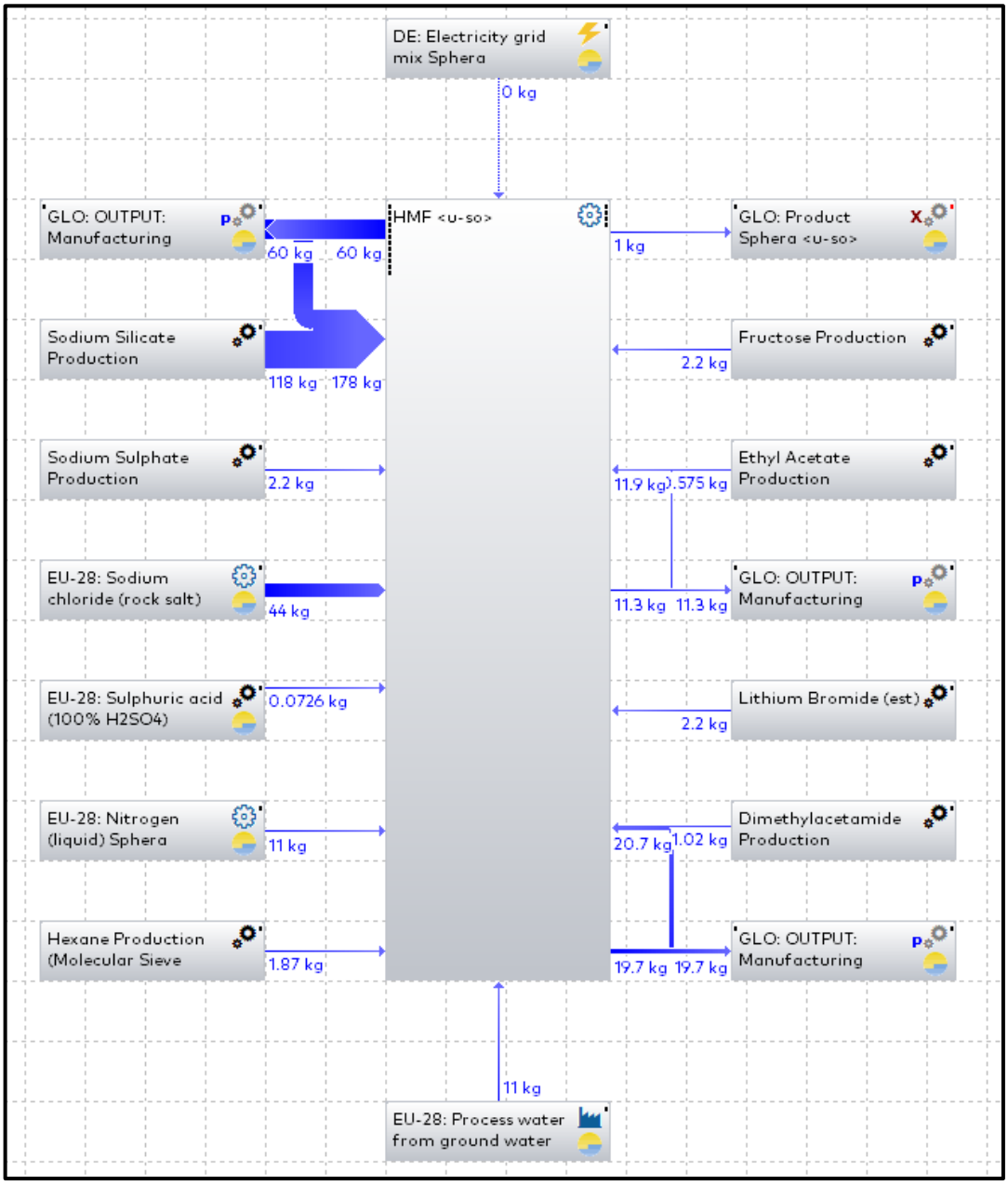

Figure 164 - Manually generated unit process for the production of 1 kg of HMF (EU), data taken from EcoInvent. Tracked flows are shown as unit processes with the transfer or material or energy, whilst all remaining inputs and outputs are elementary flows. Includes any interpretation changes made. GLO: OUTPUT manufacturing refers to a standardised recycling with 5% loss of material and is an output elementary flow.

6.6.7 DFF (Diformylfuran)

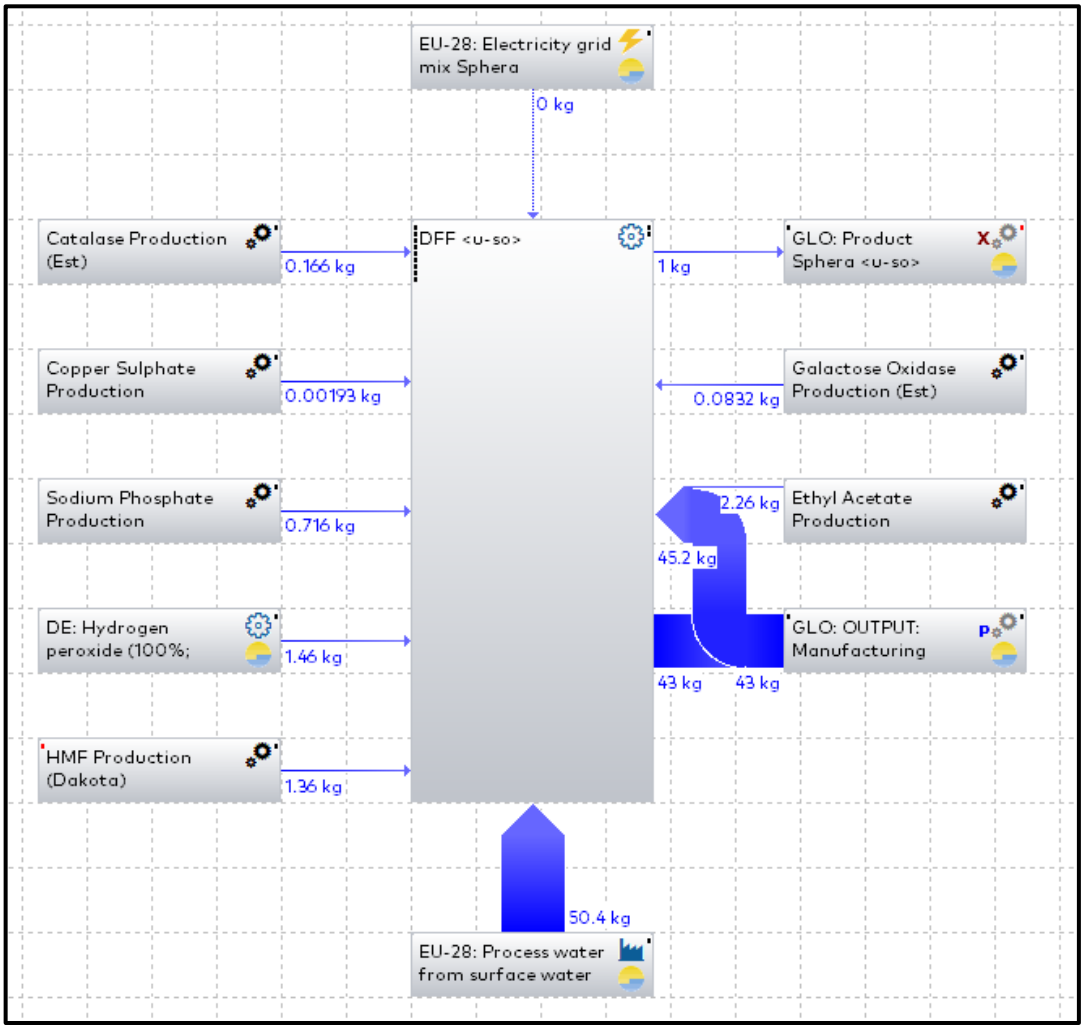

Figure 165 - Manually generated unit process for the production of 1 kg of DFF (EU), data taken from EcoInvent. Tracked flows are shown as unit processes with the transfer or material or energy, whilst all remaining inputs and outputs are elementary flows. Includes any interpretation changes made. GLO: OUTPUT manufacturing refers to a standardised recycling with 5% loss of material and is an output elementary flow. Horseradish peroxidase has not been included due to insufficient data. Sodium phosphate has been used as a substitute for potassium phosphate.

6.6.8 FDCA (2,5-furandicarboxylic acid) by CAL-B lipase

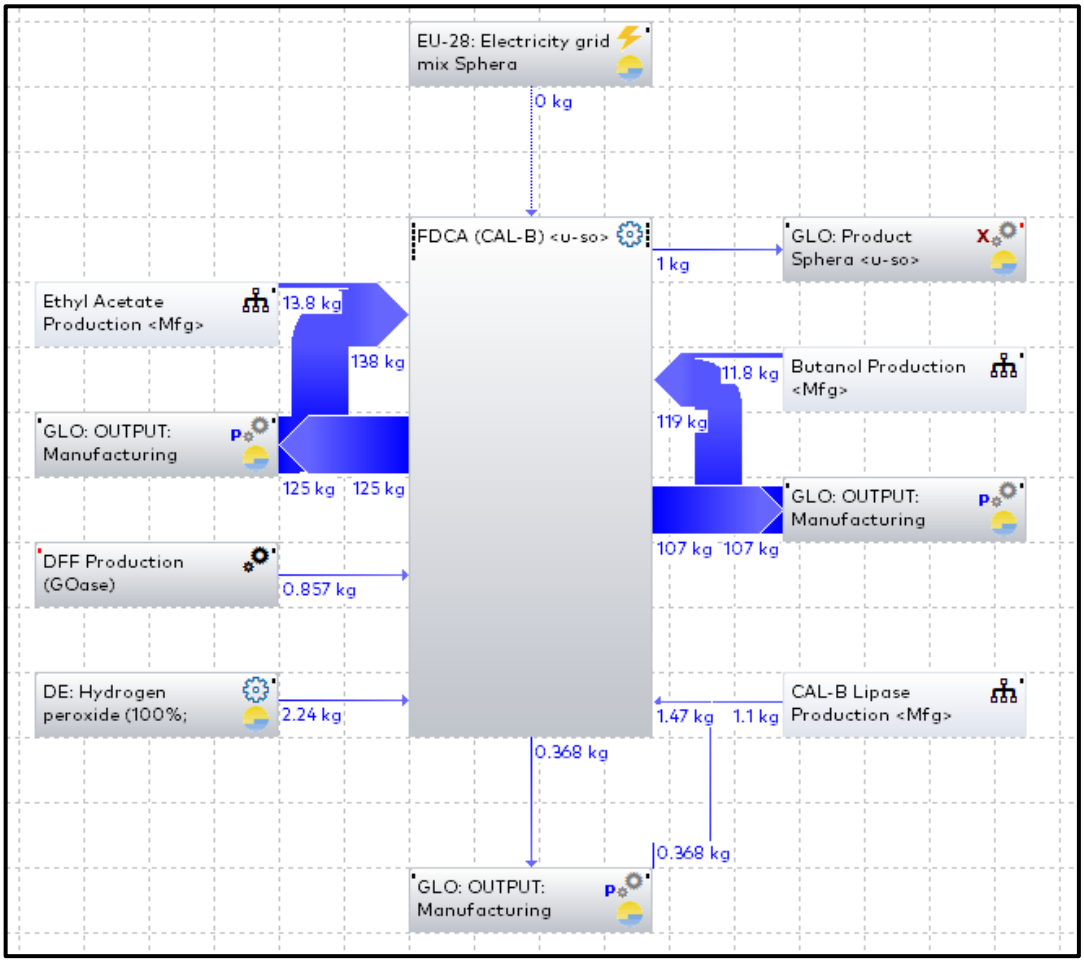

Figure 166 - Manually generated unit process for the production of 1 kg of FDCA by CAL-B (EU), data taken from EcoInvent. Tracked flows are shown as unit processes with the transfer or material or energy, whilst all remaining inputs and outputs are elementary flows. Includes any interpretation changes made. GLO: OUTPUT manufacturing refers to a standardised recycling with 5% loss of material and is an output elementary flow.

6.6.9 FDCA (2,5-furandicarboxylic acid) by Pt/C

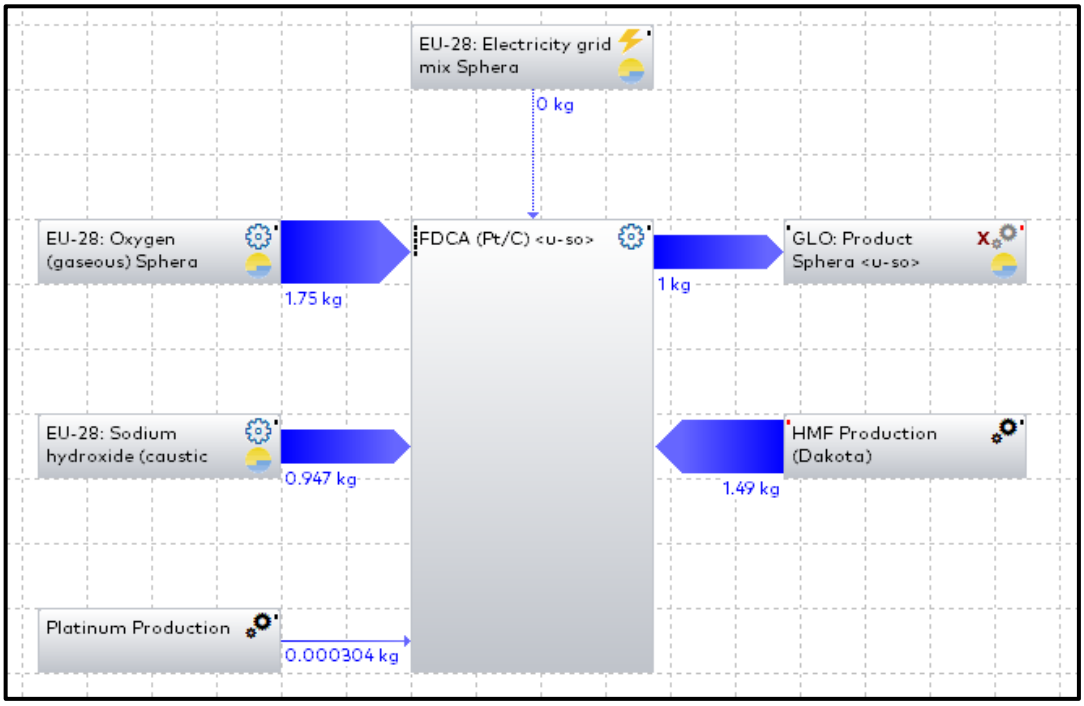

Figure 167 - Manually generated unit process for the production of 1 kg of FDCA by Pt/C (EU), data taken from EcoInvent. Tracked flows are shown as unit processes with the transfer or material or energy, whilst all remaining inputs and outputs are elementary flows. Includes any interpretation changes made. Platinum production refers to the quantity of platinum required as a weight value and does not include information of catalyst production.

6.6.10 Xylene

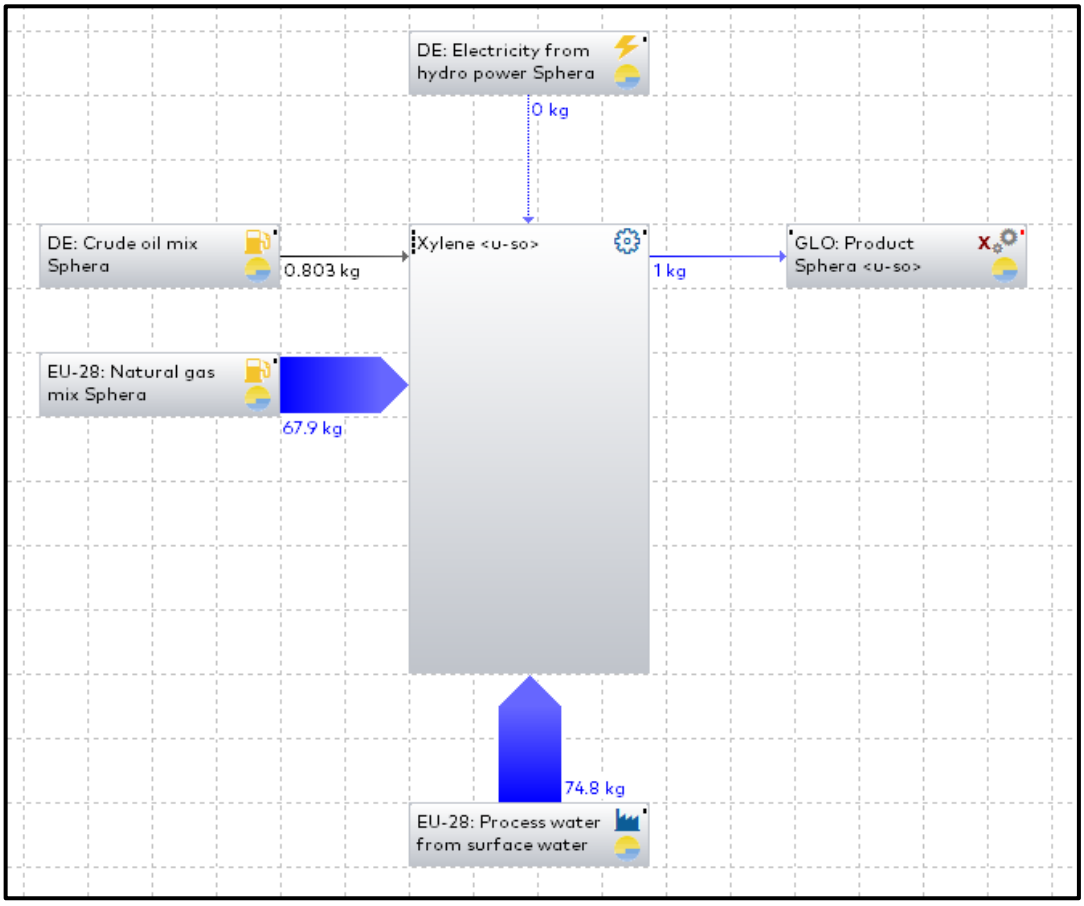

Figure 168 - Manually generated unit process for the production of 1 kg of xylene (EU), data taken from EcoInvent. Tracked flows are shown as unit processes with the transfer or material or energy, whilst all remaining inputs and outputs are elementary flows. Includes any interpretation changes made.

6.6.11 Terephthalic acid

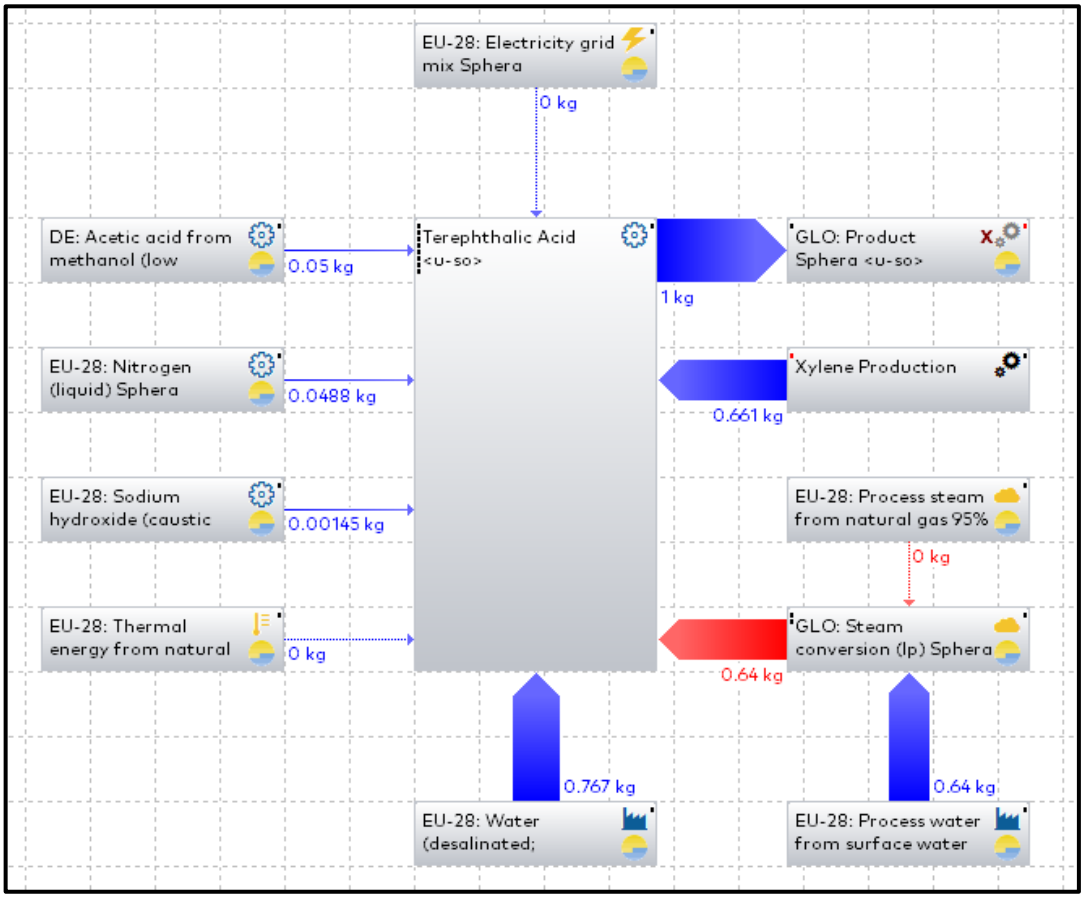

Figure 169 - Manually generated unit process for the production of 1 kg of terephthalic acid (EU), data taken from EcoInvent. Tracked flows are shown as unit processes with the transfer or material or energy, whilst all remaining inputs and outputs are elementary flows. Includes any interpretation changes made. GLO: Steam is an input flow converting water (in kg) and steam from natural gas (in MJ) into process steam in kg.

References

1 United Nations (UN), World Population Projection, https://www.un.org/development/desa/en/news/population/world-population-prospects-2017.html, (accessed 6 April 2018).

2 S. Somani and H. Koenig, *Global Trends in Renewable Energy*, Singapore, 2016.

3 A. U. B. Queiroz and F. P. Collares-Queiroz, *Polym. Rev.*, 2009, **49**, 65–78.

4 M. Anderson, PlantBottle, http://www.coca-colacompany.com/plantbottle-technology, (accessed 6 April 2018).

5 J.-V. Bomtempo, F. Chaves Alves and F. de Almeida Oroski, *Faraday Discuss.*, 2017, **202**, 213–225.

6 U. T. Bornscheuer, G. W. Huisman, R. J. Kazlauskas, S. Lutz, J. C. Moore and K. Robins, *Nature*, 2012, **485**, 185–194.

7 T. Werpy and G. Petersen, *Top Value Added Chemicals From Biomass*, 2004.

8 A. Gandini and M. N. Belgacem, *Prog. Polym. Sci.*, 1997, **22**, 1203–1379.

9 A. Gandini and M. N. Belgacem, in *Monomers, Polymers and Composites from Renewable Resources*, eds. M. N. Belgacem and A. Gandini, Elsevier Ltd., First., 2008, pp. 115–152.

10 C. Moreau, M. N. Belgacem and A. Gandini, *Top. Catal.*, 2004, **27**, 11–30.

11 R.-J. Van Putten, J. C. Van Der Waal, E. De Jong, C. B. Rasrendra, H. J. Heeres and J. G. De Vries, *Chem. Rev.*, 2013, **113**, 1499–1597.

12 US Pat., US4977283A, 1990.

13 US Pat., US2015336090, 2015.

14 AT. Pat., WO2017097843, 2017.

15 US Pat., US2017298039, 2017.

16 US Pat., WO2017083297, 2017.

17 US Pat., US2014295508, 2014.

18 US Pat., US2017305873, 2017.

19 US Pat., WO2017106591, 2017.

20 US Pat., US2015119588, 2015.

21 BR. Pat., WO2015054756, 2015.

22 CN. Pat., CN106458949, 2017.

23 US Pat., US2017157530, 2017.

24 US Pat., US2017260154, 2017.

25 MY. Pat., MY159836, 2017.

26 NL. Pat., WO2016195500, 2016.

27 MX. Pat., MX2015011912, 2015.

28 FR. Pat., EP2944632, 2015.

29 US Pat., WO2016168233, 2016.

30 JP. Pat., JP2011084540, 2011.

31 US Pat., US2014343305, 2014.

32 N. V. Bhagavan and C.-E. Ha, in *Essentials of medical biochemistry : with clinical cases*, eds. N. V. Bhagavan and C.-E. Ha, Elsevier/Academic Press, First., 2011, pp. 39–46.

33 S. M. McKenna, S. Leimkühler, S. Herter, N. J. Turner and A. J. Carnell, *Green Chem.*, 2015, **17**, 3271–3275.

34 N. J. Turner, *Chem. Rev.*, 2011, **111**, 4073–4087.

35 F. Escalettes and N. J. Turner, *ChemBioChem*, 2008, **9**, 857–860.

36 A. Badalyan, M. Neumann-Schaal, S. Leimkühler and U. Wollenberger, *Electroanalysis*, 2013, **25**, 101–108.

37 J. Carro, P. Ferreira, L. Rodríguez, A. Prieto, A. Serrano, B. Balcells, A. Ardá, J. Jiménez-Barbero, A. Gutiérrez, R. Ullrich, M. Hofrichter and A. T. Martínez, *FEBS J.*, 2015, **282**, 3218–3229.

38 A. T. Pedersen, W. R. Birmingham, G. Rehn, S. J. Charnock, N. J. Turner and J. M. Woodley, *Org. Process Res. Dev.*, 2015, **19**, 1580–1589.

39 J. W. Whittaker, *Arch. Biochem. Biophys.*, 2005, **433**, 227–239.

40 P. J. Kersten, *Proc. Natl. Acad. Sci. U. S. A.*, 1990, **87**, 2936–40.

41 C. G. Saysell, T. Barna, C. D. Borman, A. J. Baron, M. J. McPherson and A. G. Sykes, *JBIC J. Biol. Inorg. Chem.*, 1997, **2**, 702–709.

42 KR. Pat., KR20170116051, 2017.

43 CA. Pat., CA2979587, 2016.

44 US Pat., US2017050944, 2017.

45 M. P. J. Van Deurzen, F. Van Rantwijk and & R. A. Sheldon, *J. Carbohydr. Chem.*, 1997, **16**, 299–309.

46 M. Sajid, X. Zhao and D. Liu, *Green Chem.*, 2018, **20**, 5427–5453.

47 A. Kundys, E. Białecka-Florjańczyk, A. Fabiszewska and J. Małajowicz, *J. Polym. Environ.*, 2018, **26**, 396–407.

48 B. Stauch, S. J. Fisher and M. Cianci, *J. Lipid Res.*, 2015, **56**, 2348–2358.

49 C. N. Schutz and A. Warshel, *Proteins Struct. Funct. Bioinforma.*, 2004, **55**, 711–723.

50 D. Méndez-Sánchez, N. Ríos-Lombardía, V. Gotor and V. Gotor-Fernández, *Tetrahedron*, 2014, **70**, 1144–1148.

51 F. Björkling, H. Frykman, S. E. Godtfredsen and O. Kirk, *Tetrahedron*, 1992, **48**, 4587–4592.

52 B. G. Payne and H. P. Williams, *J. Am. Chem. Soc*, 1947, **69**, 551.

53 K. Sato, M. Aoki, M. Ogawa, T. Hashimoto and R. Noyori, *J. Org. Chem.*, 1996, **61**, 8310–8311.

54 R. Noyori, M. Aoki and K. Sato, *Chem. Commun.*, 2003, **34**, 1977–1986.

55 S. Khodabakhshi and M. Baghernejad, *J. Chinese Chem. Soc.*, 2014, **61**, 521–524.

56 S. Cannizzaro, *Ann. der Chemie und Pharm.*, 1853, **88**, 129–130.

57 M. M. Mojtahedi, E. Akbarzadeh, R. Sharifi and M. S. Abaee, *Org. Lett.*, 2007, **9**, 2791–2793.

58 M. Creighton, Everything you Need to Know About The World's Most Useful Plastic (PET and Polyester), https://www.creativemechanisms.com/blog/everything-about-polyethylene-terephthalate-pet-polyester, (accessed 4 September 2017).

59 M. Creighton, The Eleven Most Important Types of Plastic, https://www.creativemechanisms.com/blog/eleven-most-important-plastics, (accessed 4 September 2017).

60 R. Geyer, J. R. Jambeck and K. L. Law, *Sci. Adv.*, 2017, **3**, 25–29.

61 T. U. Gerngross and S. C. Slater, *Sci. Am.*, 2000, **283**, 36–41.

62 L. Lim.T, R. Auras and M. Rubino, *Prog. Polym. Sci.*, 2008, **33**, 820–852.

63 R. Ghoreishi and G. J. Suppes, *RSC Adv.*, 2015, **5**, 68361–68368.

64 A. M. Al-sabagh, F. Z. Yehia, G. Eshaq, A. M. Rabie and A. E. Elmetwally, *Egypt. J. Pet.*, 2016, **25**, 53–64.

65 A. Rudin and P. Choi, in *The Elements of Polymer Science & Engineering*, eds. A. Rudin and P. Choi, Academic Press, Third., 2013, pp. 521–535.

66 A. Ciesielski, *An introduction to rubber technology*, Rapra Technology Ltd, First., 1999.

67 J. Lovett and F. Bie De, *Sustainable Sourcing of Feedstocks for Bioplastics*, Amsterdam, 2016.

68 M. Azeem, F. Batool, N. Iqbal and Haq-ul-Ikram, in *Algal Based Polymers, Blends, and Composites*, eds. K. Z. Mahmood, M. Zuber and M. Ali, Elsevier, First., 2017, pp. 1–31.

69 F. Cherubini, *Energy Convers. Manag.*, 2010, **51**, 1412–1421.

70 R. A. Sheldon, *Green Chem.*, 2014, **16**, 950–963.

71 M. J. John and R. D. Anandjiwala, *Polym. Compos.*, 2008, **29**, 187–207.

72 X. Lu, M. Q. Zhang, M. Z. Rong, D. L. Yue and G. C. Yang, *Compos. Sci. Technol.*, 2004, **64**, 1301–1310.

73 I. K. M. Yu and D. C. W. Tsang, *Bioresour. Technol.*, 2017, **238**, 716–732.

74 C. Wu, *Marketing Production and Financial Analysis of FDCA*, Worcester, 2019.

75 A. Gandini, A. J. D. Silvestre, C. P. Neto, A. F. Sousa and M. Gomes, *J. Polym. Sci. Part A Polym. Chem.*, 2009, **47**, 295–298.

76 A. Gandini, T. M. Lacerda, A. J. F. Carvalho and E. Trovatti, *Chem. Rev.*, 2016, **116**, 1637–1669.

77 Greenpeace Phillipines, *Vol. II Identifying the World's Top Corporate Plastic Polluters Executive Summary*, Manila, 2019.

78 O. Levenspiel, *Chemical Reaction Engineering*, John Wiley & Sons, Inc., Oregon City, Third., 2016.

79 C. J. Mallia and I. R. Baxendale, *Org. Process Res. Dev.*, 2016, **20**, 327–260.

80 P. Angeli and A. Gavriilidis, *Mech. Eng. Sci.*, 2008, **222**, 737–751.

81 A. Gü, M. Jhunjhunwala, M. Thalmann, M. A. Schmidt and K. F. Jensen, *Langmuir*, 2005, **21**, 1547–1555.

82 R. L. Hartman, J. P. McMullen and K. F. Jensen, *Angew. Chemie Int. Ed.*, 2011, **50**, 7502–7519.

83 A. Woitalka, S. Kuhn and K. F. Jensen, *Chem. Eng. Sci.*, 2014, **116**, 1–8.

84 D. G. Retzlolf, P. C.-K. Chan and M.-S. Razavi, *Mathl Compur. Model.*, 1990, **14**, 400–405.

85 J. J. Douglas, M. J. Sevrin and C. R. J. Stephenson, *Org. Process Res. Dev.*, 2016, **20**, 1134–1147.

86 E. J. Horn, B. R. Rosen and P. S. Baran, *ACS Cent. Sci.*, 2016, **2**, 302–308.

87 S. V Ley, *Catal. Sci. Technol*, 2014, **6**, 4676.

88 S. Oka and E. Anthony, *Fluidized Bed Combustion*, CRC Press, First., 2003, vol. 1.

89 C. O. Kappe, *Angew. Chemie Int. Ed.*, 2004, **43**, 6250–6284.

90 R. Munirathinam, J. Huskens and W. Verboom, *Adv. Synth. Catal.*, 2015, **357**, 1093–1123.

91 A. Tanimu, S. Jaenicke and K. Alhooshani, *Chem. Eng. J.*, 2017, **327**, 792–821.

92 R. Karande, A. Schmid and K. Buehler, *Langmuir*, 2010, **26**, 9152–9159.

93 R. Karande, A. Schmid and K. Buehler, *Adv. Synth. Catal.*, 2011, **353**, 2511–2521.

94 Y. Watanabe, Y. Shimada, A. Sugihara, H. Noda, H. Fukuda and Y. Tominaga, *J. Am. Oil Chem. Soc.*, 2000, **77**, 355–360.

95 C. Ortiz, M. Luján Ferreira, O. Barbosa, J. C. S dos Santos, R. C. Rodrigues, Á. Berenguer-Murcia, L. E. Briand and R. Fernandez-Lafuente, *Catal. Sci. Technol*, 2019, **9**, 2380–2420.

96 C. A. A. Adarme, R. A. C. Leão, S. P. de Souza, I. Itabaiana, R. O. M. A. de Souza and C. M. Rezende, *Mol. Catal.*, 2018, **453**, 39–46.

97 B. Grabner, A. K. Schweiger, K. Gavric, R. Kourist and H. Gruber-Woelfler, *React. Chem. Eng.*, 2020, **5**, 263–269.

98 R. Yuryev, S. Strompen and A. Liese, *Beilstein J. Org. Chem.*, 2011, **7**, 1449–1467.

99 L. Tamborini, D. Romano, A. Pinto, A. Bertolani, F. Molinari and P. Conti, *J. Mol. Catal. B Enzym.*, 2012, **84**, 78–82.

100 E. Jones, K. McClean, S. Housden, G. Gasparini and I. Archer, *Chem. Eng. Res. Des.*, 2012, **90**, 726–731.

101 G. Gasparini, I. Archer, E. Jones and R. Ashe, *Org. Process Res. Dev.*, 2012, **16**, 1013–1016.

102 I. Cantat, S. Cohen-Addad, F. Elias, F. Graner, R. Höhler, O. Pitois, F. Rouyer, A. Saint-Jalmes and S. Cox, *Foams: Structure and Dynamics*, Oxford University Press, Oxford, First., 2013.

103 R. J. Pugh, *Adv. Colloid Interface Sci.*, 1996, **64**, 67–142.

104 V. Carrier and A. Colin, *Langmuir*, 2003, **19**, 4535–4538.

105 K. Scientific, Foam, https://www.kruss-scientific.com/services/education-theory/glossary/foam/.

106 S. Abbott, *Surfactant Science: Principles and Practice*, Ipswich, 2015.

107 D. Langevin, *Comptes Rendus - Mec.*, 2017, **345**, 47–55.

108 P. Walstra, *Chem. Eng. Sci.*, 1993, **48**, 333–349.

109 Z. Derikvand and M. Riazi, *J. Mol. Liq.*, 2016, **224**, 1311–1318.

110 S. Sriniv, R. Riniv, R. Rinivasan, A. Asan, D. D. Damodaran and A. Amodaran, *J. Food Sci.*, 2005, **70**, 54–66.

111 B. . Binks, *Curr. Opin. Colloid Interface Sci.*, 2002, **7**, 21–41.

112 T. N. Hunter, R. J. Pugh, G. V. Franks and G. J. Jameson, *Adv. Colloid Interface Sci.*, 2008, **137**, 57–81.

113 V. S. Erasov, M. Y. Pletnev and B. V. Pokidko, *Colloid J.*, 2015, **77**, 614–621.

114 Z. A. AlYousef, M. A. Almobarky and D. S. Schechter, *J. Colloid Interface Sci.*, 2018, **511**, 365–373.

115 A. K. Suresh, T. Sridhar and O. E. Potter, *AIChE J.*, 1985, **30**, 315–322.

116 S. Ahlgren, A. Björklund, A. Ekman, H. Karlsson, J. Berlin, P. Börjesson, T. Ekvall, G. Finnveden, M. Janssen and I. Strid, *LCA of biorefineries identification of key issues and methodological recommendations*, 2013.

117 A. D. La Rosa, G. Recca, J. Summerscales, A. Latteri, G. Cozzo and G. Cicala, *J. Clean. Prod.*, 2014, **74**, 135–144.

118 S. Nessi, C. Bulgheroni, A. Konti, T. Sinkko, D. Tonini and R. Pant, *Comparative Life-Cycle Assessment of Alternative Feedstock for Plastics Production*, 2020.

119 J. B. Binder and R. T. Raines, *J. Am. Chem. Soc.*, 2009, **131**, 1979–1985.

120 J. M. R. Gallo and M. A. Trapp, *J. Braz. Chem. Soc.*, 2017, **28**, 1586–1607.

121 A. Morão and F. de Bie, *J. Polym. Environ.*, 2019, **27**, 2523–2539.

122 J. Sadhukhan, K. S. Ng and E. M. Hernandez, *Biorefineries and Chemical Processes*, 2014.

123 M. R. Chapman, S. C. Cosgrove, N. J. Turner, N. Kapur and A. J. Blacker, *Angew. Chemie Int. Ed.*, 2018, **57**, 10535–10539.

124 R. Gandhari, P. P. Maddukuri and T. K. Vinod, *J. Chem. Educ.*, 2007, **84**, 852–854.

125 J. Meyer, D. Holtmann, M. B. Ansorge-Schumacher, M. Kraume and A. Drews, *Biochem. Eng. J.*, 2017, **118**, 34–40.

126 S. Zhang and L. Zhang, *Polish J. Chem. Technol.*, 2017, **19**, 11–16.

127 T. S. A. Heugebaert, C. V. Stevens and C. O. Kappe, *ChemSusChem*, 2015, **8**, 1648–1651.

128 A. M. C. Afonso, R. N. Candeias, P. D. Simão, F. A. Trindade, A. S. J. Coelho, B. Tan and R. Franzén, *Supplementary information for Comprehensive Organic Chemistry Experiments for the Laboratory Classroom The Cannizzaro Reaction Synthesis of p-chlorobenzylalcohol and p-chlorobenzoic acd*, 2017.

129 Ł. Janczewski, M. Walczak, J. Frączyk, Z. J. Kamiński and B. Kolesińska, *Synth. Commun.*, 2019, **49**, 3290–3300.

130 A. Basso and S. Serban, *Mol. Catal.*, 2019, **479**, 110607.

131 L. Cao, in *Carrier-bound Immobilized Enzymes: Principles, Application and Design*, ed. L. Cao, Wiley-VCH Verlag GmbH & Co. KGaA, First., 2006, p. 30.

132 Y. Z. Qin, Y. M. Li, M. H. Zong, H. Wu and N. Li, *Green Chem. Commun.*, 2015, **17**, 3718–3722.

133 J. Meyer-Waßewitz, D. Holtmann, M. B. Ansorge-Schumacher, M. Kraume and A. Drews, *Biochem. Eng. J.*, 2017, **126**, 68–77.

134 C. Aouf, E. Durand, J. Lecomte, M. C. Figueroa-Espinoza, E. Dubreucq, H. Fulcrand and P. Villeneuve, *Green Chem.*, 2014, **16**, 1740–1754.

135 C. Wiles, M. J. Hammond and P. Watts, *Beilstein J. Org. Chem.*, 2009, **5**, 1–12.

136 J. Meyer, A. E. W. Horst, M. Steinhagen, D. Holtmann, M. B. Ansorge-Schumacher, M. Kraume and A. Drews, *Eng. Life Sci.*, 2017, **17**, 759–767.

137 A. Narsaiah, Venkat, *Synlett*, 2002, **44**, 1178–1179.

138 B. R. Travis, M. Sivakumar, G. O. Hollist and B. Borhan, *Org. Lett.*, 2003, **5**, 1031–1034.

139 J. R. Kennedy and M. A. Stock, *J. Org. Chem.*, 1960, **25**, 1901–1906.

140 M. Fukushima and K. Tatsumi, *Environ. Sci. Technol.*, 2005, **39**, 9337–9342.

141 M. Fukushima and K. Tatsumi, *J. Hazard. Mater.*, 2007, **144**, 222–228.

142 BRENDA, Information of Galactose Oxidase, https://www.brenda-enzymes.org/enzyme.php?ecno=1.1.3.9#KM VALUE [mM], (accessed 20 May 2021).

143 E. Vignati, R. Piazza and T. P. Lockhart, *Langmuir*, 2003, **19**, 6650–6656.

144 J. M. Woodley, *Trends Biotechnol.*, 2008, **26**, 321–327.

145 R. M. Lindeque and J. M. Woodley, *Org. Process Res. Dev.*, 2020, **24**, 2055–2063.

146 R. M. Lindeque and J. M. Woodley, *Catalysts*, 2019, **9**, 262–279.

147 A. K. Liedtke, F. Bornette, R. Philippe and C. De Bellefon, *Chem. Eng. J.*, 2013, **227**, 174–181.

148 Z. Peng, S. Gai, M. Barma, M. M. Rahman, B. Moghtaderi and E. Doroodchi, *Chem. Eng. J.*, 2021, **405**, 126646.

149 G. A. Okpobiri and C. U. Ikoku, *Energy Resour. Technol.*, 1983, **105**, 542–553.

150 B. Haffner, Y. Khidas and O. Pitois, *J. Colloid Interface Sci.*, 2015, **458**, 200–208.

151 Y. Yang, Z. Fang, X. Chen, W. Zhang, Y. Xie, Y. Chen, Z. Liu and W. Yuan, *Front. Pharmacol.*, 2017, **8**, 1–20.

152 B. P. Binks and T. S. Horozov, *Angew. Chemie - Int. Ed.*, 2005, **44**, 3722–3725.

153 K. Golemanov, S. Tcholakova, N. D. Denkov, K. P. Ananthapadmanabhan and A. Lips, *Phys. Rev. E - Stat. Nonlinear, Soft Matter Phys.*, 2008, **78**, 051405.

154 N. D. Denkov, V. Subramanian, D. Gurovich and A. Lips, *Colloids Surfaces A Physicochem. Eng. Asp.*, 2005, **263**, 129–145.

155 N. D. Denkov, S. Tcholakova, K. Golemanov, K. P. Ananthpadmanabhan and A. Lips,

Soft Matter, 2009, **5**, 3389–3408.

156 Y. Yu, Z. A. Soukup and S. Saraji, *Colloids Surfaces A Physicochem. Eng. Asp.*, 2019, **578**, 123548.

157 R. N. Gajbhiye and S. I. Kam, *Chem. Eng. Sci.*, 2011, **66**, 1536–1549.

158 Prozomix, Prozomix, http://www.prozomix.com/home, (accessed 27 October 2017).

159 C. Isola, H. L. Sieverding, R. Raghunathan, M. P. Sibi, D. C. Webster, J. Sivaguru and J. J. Stone, *J. Clean. Prod.*, 2017, **142**, 2935–2944.

160 T. S. Gomes, L. L. Y. Visconte and E. B. A. V. Pacheco, *J. Polym. Environ.*, 2017, **27**, 533–548.

161 C. M. Lam, I. K. M. Yu, S. C. Hsu and D. C. W. Tsang, *J. Clean. Prod.*, 2018, **199**, 840–848.

162 H. Althaus, M. Chudacoff, R. Hischier, N. Jungbluth, M. Osses, A. Primas and S. Hellweg, *Life Cycle Inventories of Chemicals.*, Zürich, 2007.

163 S. Bello, P. Méndez-Trelles, E. Rodil, G. Feijoo and M. T. Moreira, *Sep. Purif. Technol.*, 2020, **233**, 116056.

164 A. Lolli, S. Albonetti, L. Utili, R. Amadori, F. Ospitali, C. Lucarelli and F. Cavani, *Appl. Catal. A Gen.*, 2015, **504**, 408–419.

165 S. E. Davis, L. R. Houk, E. C. Tamargo, A. K. Datye and R. J. Davis, *Catal. Today*, 2011, **160**, 55–60.

166 R. H. Moss, J. A. Edmonds, K. A. Hibbard, M. R. Manning, S. K. Rose, D. P. Van Vuuren, T. R. Carter, S. Emori, M. Kainuma, T. Kram, G. A. Meehl, J. F. B. Mitchell, N. Nakicenovic, K. Riahi, S. J. Smith, R. J. Stouffer, A. M. Thomson, J. P. Weyant and T. J. Wilbanks, *Nature*, 2010, **463**, 747–756.

167 H. D. Brujin, R. V. Duin, M. A. J. Hujibregts, J. B. Guinee, M. Gorree, R. Heijungs, G. Huppes, R. Kleijn, A. D. Koning, L. V. Oers, A. W. Sleeswijik, S. Suh and H. A. Udo De Haes, *Handbook on Life Cycle Assessment*, Springer, Leiden, Seventh., 2002.

168 A. A. Jensen, J. Elkington, K. Christiansen, L. Hoffmann, B. T. Møller, A. Schmidt and F. van Dijk, *Life Cycle Assessment (LCA) - A guide to approaches, experiences and information sources*, 1997.

169 J. Daniel, G. Velders, A. Douglass, P. Forster, D. Hauglustaine, I. Isaksen, L. Kujipers, A. McCulloch and T. Wallington, *Scientific Assessment of Ozone Depletion: 2006*, 2007.

170 M. Huijbregts, Z. J. N. Steinmann, P. M. F. M. Elshout, G. Stam, F. Verones, M. D. M.

Vieira, M. Zijp and R. van Zelm, *ReCiPe 2016 - A harmonized life cycle impact assessment method at midpoint and endpoint level. Report I: Characterization*, 2016.

171 EcoInvent, EcoInvent, https://v31.ecoquery.ecoinvent.org/Home/Index, (accessed 2 February 2021).

172 Novozyme, Natl. Renew. Energy Lab., https://www.lcacommons.gov/lca-collaboration/National_Renewable_Energy_Laboratory/USLCI_2021_Q1_v1/datasets/Processes/31-33: Manufacturing/3251: Basic Chemical Manufacturing, (accessed 9 March 2021).

173 F. Kis, N. Maravić, S. Kertesz and Z. I. Šereš, *Analecta Tech. Szeged.*, 2019, **13**, 28–39.

174 C. J. Van Der Waal, E. Mazoyer, J. H. Baars and G. M. Gruter, in *Liquid Phase Aerobic Oxidation Catalysis*, eds. S. S and L. P. Alsters, Wiley-VCH Verlag GmbH & Co. KGaA, 2016, pp. 311–319.

175 C. Isola, H. L. Sieverding, R. Raghunathan, M. P. Sibi and C. Dean, *J. Clean. Prod.*, 2017, **142**, 2935–2944.

176 Harvard Apparatus, Model '11' Plus Syring Pump User's Manual, https://conquerscientific.com/wp-content/product-images/2011/08/11plusmanualpdf.pdf, (accessed 26 February 2021).

177 Akribis Scientific Limited, Basic Magnetic Hotplate Stirrer, https://www.akribis.co.uk/ika-rct-basic-magnetic-hotplate-stirrer, (accessed 26 February 2021).

178 SciQuip, Benchtop incubator Shakers, https://www.sciquip.co.uk/sciquip-benchtop-incubated-shakers.html.

179 P. Instrument, Series 4590 Micro Stirred Reactors, https://www.parrinst.com/products/stirred-reactors/series-4590-micro-stirred-reactors/specifications/.

180 GaBi, GaBi LCA Database, http://www.gabi-software.com/databases/gabi-databases/, (accessed 2 February 2021).

181 United Nations, *Illegal Trade in Ozone Depleting Substances*, Nairobi, 2012.

182 KR. Pat., KR 2014074023, 2014, 1–33.

183 Q. Girka, B. Estrine, N. Hoffmann, J. Le Bras and J. Muzart, *React. Chem. Eng.*, 2016, **1**, 176–182.